CHITOSAN-BASED POLYMERIC DYES: SYNTHESIS, CHARACTERIZATION, AND APPLICATIONS AS pH-INDICATIVE MATERIALS

JONGJIT CHALITANGKOON

A THESIS SUBMITTED IN PARTIAL FULFILLMENT OF THE REQUIREMENT FOR THE DEGREE OF DOCTOR OF PHILOSOPHY IN APPLIED CHEMISTRY

DEPARTMENT OF CHEMISTRY SCHOOL OF SCIENCE
KING MONGKUT'S INSTITUTE OF TECHNOLOGY LADKRABANG

2023

KMITL-2023-SC-D-012-020

Thesis Title	Chitosan-Based Polymeric Dyes: Synthesis, Characterization, and Applications as pH-Indicative Materials
Student Name	Jongjit Chalitangkoon
Student ID	59605003
Degree	Doctor of Philosophy (Applied Chemistry)
Department	Chemistry
Year	2023
Thesis Advisor	Assoc. Prof. Dr. Pathavuth Monvisade

Abstract

This study focused on the synthesis of chitosan-based polymeric dyes (CSPDs) using the Mannich reaction with phenolphthalein (PHP), phenol red (PR), and rosolic acid (RA) as reagents. The synthesized derivatives were characterized and confirmed using various analytical techniques. The %DS of CS-g-PHPs varied depending on the formaldehyde and PHP contents. CS-g-PHPs exhibited solubility in acidic, strong alkaline, and alkaline/urea conditions. CS-g-PR and CS-g-RA were successfully synthesized using a lower feed ratio to prevent insoluble product formation. The derivatives exhibited non-toxicity towards cells, indicating potential biocompatibility. CSPDs were used to create pH-dependent color-changing films, which showed resistance to dye leaching, indicating strong attachment to the CS matrix. To enhance water solubility, two methods were employed: attaching dyes to carboxyethyl chitosan (CECS) and carboxyethylation of CSPDs. The latter method resulted in successful modification for all CSPDs, providing solubility across a wide pH range. To demonstrate the application of WCSPDs, PR-AA was incorporated into hydrogel films with CECS, SA and PAM using covalent and electrostatic crosslinking, making them suitable for smart wound dressings. The films exhibited stability at pH 5.5, increased swelling at pH 7.4, and dissolution at pH 8.5. The CECS-to-SA ratio affected the swelling degree, and double crosslinking reduced swelling. The films showed color changes and discrimination shades in the pH range of 4-10, making them suitable for monitoring wound status. Incorporating a model drug, diclofenac (DCF), demonstrated controlled

release profiles influenced by film composition and buffer pH solutions. The films exhibited suitable mechanical properties for artificial skin and were non-toxic to human skin fibroblast cells. Overall, this research presents a simple and effective approach to synthesize chitosan-based polymeric dyes with pH-indicative properties. These derivatives offer versatility in pH sensing and stimuli-responsive applications, with potential uses in biomaterials, food packaging, and the biomedical field.

Keywords : Carboxyethylation, Chitosan-based polymeric dyes, pH-dependent coloring, pH-sensitive dyes, Mannich reaction, Smart wound dressing

Acknowledgements

The author wishes to express sincere gratitude to her advisor, Assoc. Prof. Dr. Pathavuth Monvisade, for his unwavering support, invaluable guidance, and dedication throughout her Ph.D. journey. His mentorship has been instrumental in shaping her academic growth and research endeavors.

The author extends heartfelt appreciation to Assoc. Prof. Dr. Taweechai Amornsakchai, Asst. Prof. Dr. Chonlada Ritvirulh, Asst. Prof. Dr. Suparat Rukchonlatee, and Assoc. Prof. Dr. Karoon Sadorn, the esteemed members of her committee, for their valuable insights, meticulous feedback, and constructive criticism, which have significantly enhanced the quality of her work.

Profuse thanks are extended to Assoc. Prof. Johan Foster for graciously hosting the author's research at UBC, Canada. His profound expertise, generous support, and genuine kindness have enriched her academic experience in immeasurable ways.

The author gratefully acknowledges the financial support provided by the Royal Golden Jubilee Ph.D. Program, Thailand Research Fund (RGJ 19).

Special gratitude is expressed to the members of the Polymer Synthesis and Functional Materials Research Unit (PSFMU) for their unwavering assistance, invaluable guidance, and collaborative spirit throughout her Ph.D. journey. Their expertise, camaraderie, and shared commitment to excellence have been indispensable.

The author conveys profound appreciation to all those who have contributed to her academic journey. Their collaboration, mentorship, assistance, and encouragement have been paramount to her growth and success.

Last but not least, to her beloved family, the author expresses immeasurable gratitude for their unwavering support, boundless love, and constant encouragement. Their sacrifices, understanding, and belief in her abilities have been the cornerstone of her achievements. She is forever grateful for their presence in her life and their belief in her dreams.

Jongjit Chalitangkoon

Table of contents

Table of contents (cont.)

Table of contents (cont.)

Table of contents (cont.)

List of tables

List of tables (cont.)

List of figures

List of figures (cont.)

List of figures (cont.)

List of figures (cont.)

List of figures (cont.)

List of figures (cont.)

Abbreviations

CS	Chitosan
CSPD	Chitosan-based polymeric dye
WCSPD	Water-soluble chitosan-based polymeric dye
CECS	Carboxyethylchitosan
PHP	Phenolphthalein
PR	Phenol red
RA	Rosolic acid
AA	Acrylic acid
βCD	β-Cyclodextrin
βCD-DA	β-Cyclodextrin dialdehyde
PAM	Polyacrylamide
GDL	D-glucono-δ-lactone
DCF	Diclofenac sodium salt
DMF	*N*, *N*-Dimethylformamide
FTIR	Fourier transform infrared spectrophotometer
NMR	Nuclear magnetic resonance spectrometer
HSQC	Heteronuclear single quantum coherence spectroscopy
DEPT	Distortionless enhancement by polarization transfer
UV-vis	UV-Vis spectrophotometer
SEM	Scanning electron microscope
XRD	X-ray diffractometer
CI	Crystalline index

Chapter 1
Introduction

1.1 Research Motivation

Dye-containing polymers have gained significant attention across various industries, including painting, textile dyeing, medicine, and chemical analysis [1]. These polymers incorporate sensitive dyes that exhibit remarkable color changes in response to external stimuli, such as pH, temperature, or mechanical force. This unique property has paved the way for the development of sensing polymers with diverse applications, including metal detection [2], intelligent food packaging [3] and health monitoring [4, 5]. Conventional methods of integrating dyes into polymers typically involve non-covalent interactions or covalent attachments [1]. However, these approaches have limitations, such as potential dye migration when using direct mixing or adsorption methods. On the other hand, grafting reactions often involve complex synthesis processes, leading to slow production rates and increased costs. Therefore, there is a need for a simpler approach to synthesize dye-grafted polymers, known as polymeric dyes. These polymeric dyes hold great promise by combining the advantages of dyes and polymers, including enhanced thermal and chemical stability, superior color fastness, excellent biocompatibility, and enhanced safety [6, 7].

Chitosan (CS), derived from partially deacetylated chitin, is a natural cationic polysaccharide that possesses numerous attractive properties such as non-toxicity, biocompatibility, biodegradability, antimicrobial activity, and wound healing capacity. These properties make CS versatile for various industries, including biomedical, cosmetic, food, agriculture, and textiles [8]. The presence of reactive amino and hydroxyl groups in CS has led to interest in chemical modifications to enhance its properties and explore its potential versatility. In the context of dye-grafted CS, there have been reports of grafting pH-sensitive dyes onto CS. For instance, CS grafted with Rose Bengal and Methyl Red *via* an amide linkage has been utilized to fabricate colorimetric nanofibers for biomedical applications [9]. These nanofibers exhibit pH-dependent color changes in both aqueous and gaseous media with minimal dye leaching, suggesting potential applications in wound management.

Among various grafting reactions, the Mannich reaction offers an attractive one-pot synthesis method to modify CS side chains with phenolic compounds possessing free ortho positions [10-13]. However, no evidence of dye grafting onto CS using this reaction has been discovered. In this study, pH-indicative dyes with free ortho positions in the phenol group, such as phenolphthalein (PHP), phenol red (PR), and rosolic acid (RA), were employed to graft onto CS through the Mannich reaction, resulting in chitosan-based polymeric dyes (CSPDs). It was expected that the newly formed chemical bond at the ortho position would not disrupt the chromophore of these dyes. The resulting derivatives were structurally characterized, and their pH-induced color changes in the form of blend films were investigated.

Despite possessing several desirable properties, CS's limited solubility in neutral or basic media poses a challenge for practical applications. To overcome this issue, various methods have been developed to create water-soluble chitosan derivatives. Among these methods, carboxyalkylation using the Michael reaction with water-soluble acryl reagents has shown promise [14, 15]. The resulting water-soluble chitosan derivatives exhibit improved solubility in neutral and basic media, along with enhanced biomedical properties [16-18]. This provides opportunities for their use in neutral aqueous media and their direct blending with anionic polymers without unintended gelation, allowing for greater flexibility in material design. Therefore, to enhance the water solubility of CSPDs, carboxyethylation through the Michael reaction was employed to obtain water-soluble CSPDs (WCSPDs). The structure and coloring properties of WCSPDs were thoroughly investigated.

To demonstrate the practical application of the synthesized polymeric dyes, a WCSPD with a PR moiety (PR-AA) was designed as a smart wound dressing for monitoring wound status. Changes in wound pH can serve as an indicator of wound status, providing insights into the progress or potential infection [19, 20]. The hydrogel was prepared by combining PR-AA with sodium alginate (SA) and polyacrylamide (PAM), along with the addition of D-glucono-δ-lactone (GDL) as a pH modifier and β-cyclodextrin dialdehyde (βCD-DA) as a covalent crosslinker. Additionally, diclofenac sodium salt (DCF) was incorporated as a model drug to enable drug release within the hydrogel films. The prepared hydrogel films were investigated for their pH-responsive color change, morphology, swelling behavior, and drug release characteristics.

1.2 Objectives of the study

1) To synthesize and characterize CSPDs and WCSPDs

2) To prepare and study properties of CSPDs-based films and WCSPDs-based hydrogel films

3) To demonstrate the potential application of hydrogels based on PR-AA for wound monitoring applications

1.3 Scopes of the study

1) CSPDs were synthesized by Mannich reaction of chitosan and pH-indicative dyes (i.e., PHP, PR, and RA).

2) Water-soluble chitosan (Carboxyethylchitosan: CECS) was synthesized by Michael reaction of chitosan with acrylic acid.

3) WCSPDs were synthesized by two methods as follows:

- Grafting dye onto CECS through Mannich reaction.
- Modifying CSPDs with acrylic acid through Michael addition reaction.

4) The synthesized chitosan derivatives were characterized by ^{1}H-NMR, FT-IR, UV-Vis, XRD, and were tested cytotoxicity.

5) βCD-DA was synthesized by oxidation β-cyclodextrin with sodium periodate and the aldehyde content was characterized.

6) The CSPDs were blended with CS to prepare pH-sensing films, and the color response of the films were investigated.

7) The polyelectrolyte hydrogel film of AA-PR, SA, and PAM was fabricated by adding GDL and βCD-DA.

8) The morphology, swelling behavior, and drug release behavior of the hydrogel films were investigated.

1.4 Benefits of the study

Obtain new chitosan-based pH-indicative polymeric dyes with potential pH-sensing applications such as wound monitoring.

Chapter 2

Theory and Literature Reviews

2.1 Stimuli-responsive polymers [21, 22]

Stimuli-responsive systems containing polymers involve a dramatic physicochemical change caused by stimuli (Figure 2.1). The activated systems produce observable or detectable micro- or nanoscale changes, such as morphology, molecular bond rearrangement/cleavage, and molecular motion, which can induce changes in their macroscopic properties such as color, shape, and functionality [22]. They can be created using a responsive polymer or by combining a responsive compound and a polymer that serves as a template or carrier. Because of the versatile selection of backbone and functional groups, stimuli-responsive polymers can be tailored and engineered into a variety of forms, such as particles (micelles, micro/nanogels, vesicles, and hybrid particles), films (polymer brushes, layer-by-layer polymer films, and porous membranes), and bulk gels (hydrogels, organogels, and metallogels) [23]. Many multidisciplinary efforts have been carried out and reported over the years to optimize the functionality of stimuli-responsive polymers and to explore new and innovative applications.

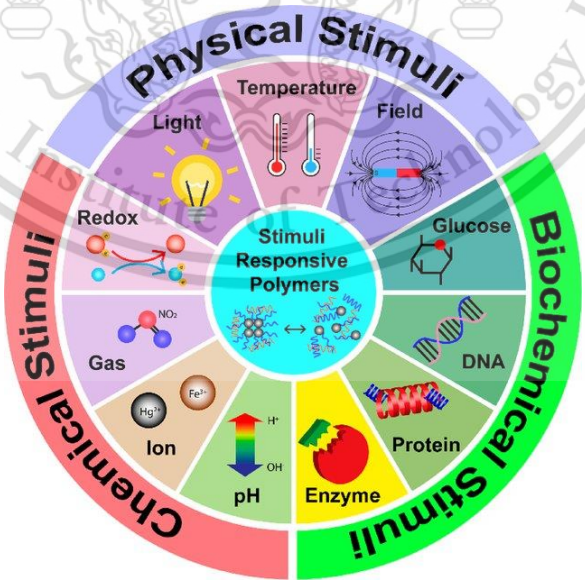

Figure 2.1 Classification of stimuli of stimuli-responsive polymers [24]

2.1.1 Temperature responsive polymers

Temperature-responsive polymers have received a lot of attention in bioengineering and biotechnology applications because certain diseases exhibit temperature changes [25]. These polymers typically have a critical solution temperature that causes intramolecular and intermolecular electrostatic and hydrophobic interactions to be disrupted, resulting in chain collapse or expansion (a volume phase transition). Various temperature-responsive polymers have been reported such as poly(*N*-isopropylacrylamide) (PNiPAAm) [26], poly(*N*-vinylcaprolactam) (PNVC) [27], poly (L-lactic acid)-poly(ethylene glycol)-poly(L-lactic acid) (PLLA-PEG-PLLA) triblock copolymers [28], and poly (ethylene oxide)-poly(propylene oxide)-poly (ethylene oxide) (PEO–PPO–PEO) copolymers [29].

2.1.2 Electro-responsive polymers

Electrical stimuli are widely used in research and applications because they allow for precise control of the magnitude of the current, the duration of an electrical pulse, or the interval between pulses. Conducting polymers, such as polythiophene or sulphonated polystyrene, are examples of electrically responsive polymers that can respond to an external field by swelling, shrinking, or bending. Furthermore, because electric stimuli are used to trigger drug release with pH regulation, they could be considered a derivative of pH-responsive delivery systems [30, 31].

2.1.3 Photo-responsive polymers

Light can be used directly on the polymer surface or delivered to remote locations via optical fibers. The wavelength of the laser should ideally be tuned to the so-called biologically ‘friendly' window [32], the near-infrared part of the spectrum, which is less harmful and penetrates deeper into tissues than visible light. In this case, the light is absorbed minimally by cells/tissue but maximally by the polymers. Light-sensitive chromophores, such as azobenzene groups [33, 34], spiropyran groups [35, 36], or nitrobenzyl groups [37, 38], are present in the majority of photo-responsive polymers.

2.1.4 pH-responsive polymers

Because pH changes occur in a variety of specific or pathological compartments, pH is an important parameter for biomedical applications. For example, the pH of the stomach (pH = 1–3) to the intestine (pH = 5–8) changes along the gastrointestinal tract, the pH change in chronic wounds is found between 5.4 and 7.4, [39] and tumor tissue is acidic extracellularly [40]. pH responsive polymers require the presence of ionizable, weak acidic or basic moieties that attach to a hydrophobic backbone, such as polyelectrolytes. When coiled chains are ionized, the electrostatic repulsions of the generated charges (anions or cations) cause them to extend dramatically. Furthermore, another typical pH responsive polymer exhibits protonation/deprotonation by distributing the charge over the ionizable groups of molecules, such as carboxyl or amino groups. pH responsive polymers including chitosan [41], gelatin [42], albumin [43] and poly(acrylic acid) (PAAc)/chitosan IPN [44] have been reported.

2.1.5 Redox-responsive polymers

Polymers with labile groups offer an advantageous opportunity for the development of redox-responsive biodegradable or bioerodible systems. Disulfide groups, which cleave to thiol groups in a reducing environment, have also been used to induce redox responsiveness [45]. The gel made from PNiPAAm bonded ruthenium *tris*(*2,2′*-bipyridine) [$Ru(bpy)_3$] was found to exhibit a periodic swelling-deswelling change, similar to a heart muscle cell, due to the periodic redox change of $Ru(bpy)_3$, resulting in altering the hydrophobic and hydrophilic properties of the polymer chains [46].

2.1.6 Glucose responsive polymers

For glucose responsive polymers, glucose oxidase (GOx) is conjugated to a smart, pH-sensitive polymer. When GOx converts glucose to gluconic acid, causing a pH shift in the environment, the volume of the pH sensitive polymer changes [47, 48]. In this way, drastic changes in polymer conformation are controlled by the body's glucose level, which has a significant impact on enzyme activity and substrate access.

Smart materials that respond to more than one stimulus at the same time have been extensively researched to combine diagnostics and therapy by monitoring multiple physiological changes at the same time. Furthermore, multiple external stimuli systems are being sought for a variety of new functions and properties to aid in the development of biomimetic systems with long-term stability and durability. Up to now, stimuli responsive polymers have been designed and synthesized in a variety of forms that are used in a wide range of applications such as sensors, controlled drug delivery, artificial muscles, and actuators [49].

2.2 Dye-containing polymers [1]

Natural and synthetic dyes are fascinating compounds because they play important roles in technical and industrial applications such as dyeing textiles, laser dyes and dyes for organic light emitting diodes (OLEDs), liquid crystal (LC) displays, optical data storage, and fluorescent labeling. Furthermore, some dyes are sensitive to external stimuli such as pH and light, allowing them to be used as optical sensors. Improvements in dyeing efficiency or photochemical/photophysical properties, as well as a focus on eco-friendly procedures, reduced toxicity, and lower production costs, are currently in high demand. Combining dyes and polymeric materials with controllable properties like solubility, stability, and toxicity is a promising approach to meeting these requirements. The dye can form covalent or non-covalent bonds with polymers as discussed below.

2.2.1 Non-covalent attachment

Sugar-based polymers (oligo-/polysaccharides) derived from natural sources, such as starch, cellulose, and chitosan, can form dipolar interactions with suitable substrates due to the presence of several polar substituents. Figure 2.2 shows schematic illustration of the non-covalent dye binding to polymeric materials. For example, starch and β-cyclodextrin polymers exhibited adsorption of anionic azo dyes with sulfonate moieties *via* the formation of hydrogen bonds between polymer hydroxyl and amine groups and the sulfonate moieties of azo dyes [50]. Furthermore, cyclodextrins have been shown to form inclusion complexes with a variety of azo dyes, and the formation of host-guest complexes was expected to contribute to the dye sorption of corresponding cyclodextrin-based polymers.

Furthermore, it has been reported that at pH 8, the carboxylate moieties of β-cyclodextrin crosslinked carboxymethyl cellulose formed electrostatic interactions with cationic dyes (basic dyes: Astrazon Blue, Crystal Violet, and Rhodamine B) [51].

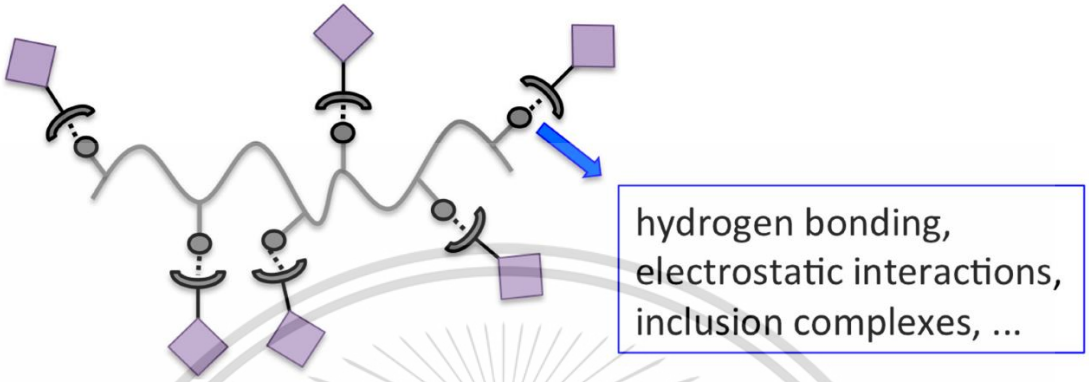

Figure 2.2 Non-covalent dye binding to polymers [1]

Hydrophilic groups in synthetic polymers like poly(acrylic acid-co-acylamide), poly(methyl methacrylate) (PMMA), and poly(vinyl alcohol) (PVA) can form electrostatic interactions, hydrogen bonds, and dipole–dipole interactions with charged dyes. For instance, perylene derivatives (*N,N'-bis*-(2-(1-piperazino)ethyl)-3,4,9,10-perylenetetracarboxylic acid diimide dichloride) were dispersed in poly(vinyl alcohol) (PVA) matrices. It shows shifting emission/absorption spectra caused by temperature dependent formation of dye aggregates [52]. In the case of apolar matrices such as poly(ethylene), special techniques such as melt-extrusion are required to prevent phase separation of both compounds due to the lack of polymer–dye interactions [53]. Hydrophobically modified perylene derivatives were dispersed into linear low-density poly(ethylene) (LLDPE) matrices *via* melt processing. The optical properties of the films were demonstrated by mechanical stimuli responsiveness, which is strongly dependent on the compactness of perylene aggregates provided by the various molecular structures of dyes [54]. Figure 2.3 depicts another example of mechano-responsive films made from various dyes.

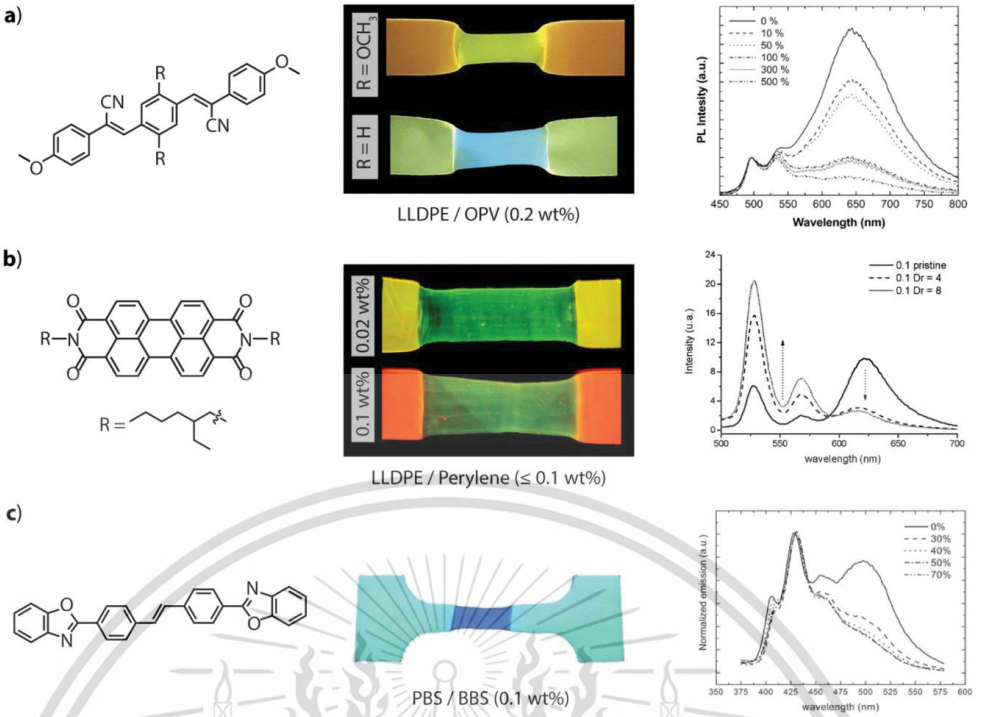

Figure 2.3 The mechanochromism upon tensile deformation under UV illumination and the emission spectra for blended films: a) cyano-substituted oligo(*p*-phenylene vinylene derivatives with LLDPE, b) perylene dye with LLDPE, and c) bis(ben-zoxazolyl)stilbene with poly(1,4-butylene succinate) (PBS) [55]

2.2.2 Covalent attachment

2.2.2.1 Polymerization of colored monomers

In this method, the dye molecule is converted into radically polymerizable derivatives and then (co)polymerized. The overall procedure is depicted in Figure 2.4. Methyl methacrylate monomer was commonly used as a comonomer in the preparation of such solid dye materials because the resulting polymers exhibit excellent transparency in the spectral range of interest.

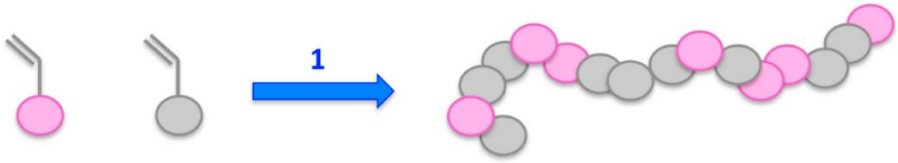

Figure 2.4 Preparation of polymeric dyes *via* co-polymerization of colored monomers [1]

As shown in Figure 2.5, methacrylate-based azo dye monomer was prepared by three steps [56]. To begin, tyramine (**1**) was methacrylated at room temperature with methacrylic anhydride (**2**), then diazotated with 3-aminopyridine (**4**) to yield *N*-(4-hydroxy-3-(pyridin-3-yldiazenyl)phen-ethyl)methacrylamide (**5**). The azo dye monomer was then copolymerized with *N*,*N*-dimethylacrylamide (**6**) as an initiator, yielding a water-soluble polymer bearing an azo dye (**7**). The authors noticed that adding $CuSO_4$ to a water/methanol mixture changed the color of copolymer (**7**) from orange to red, and that this could be reversed by adding γ-CD later.

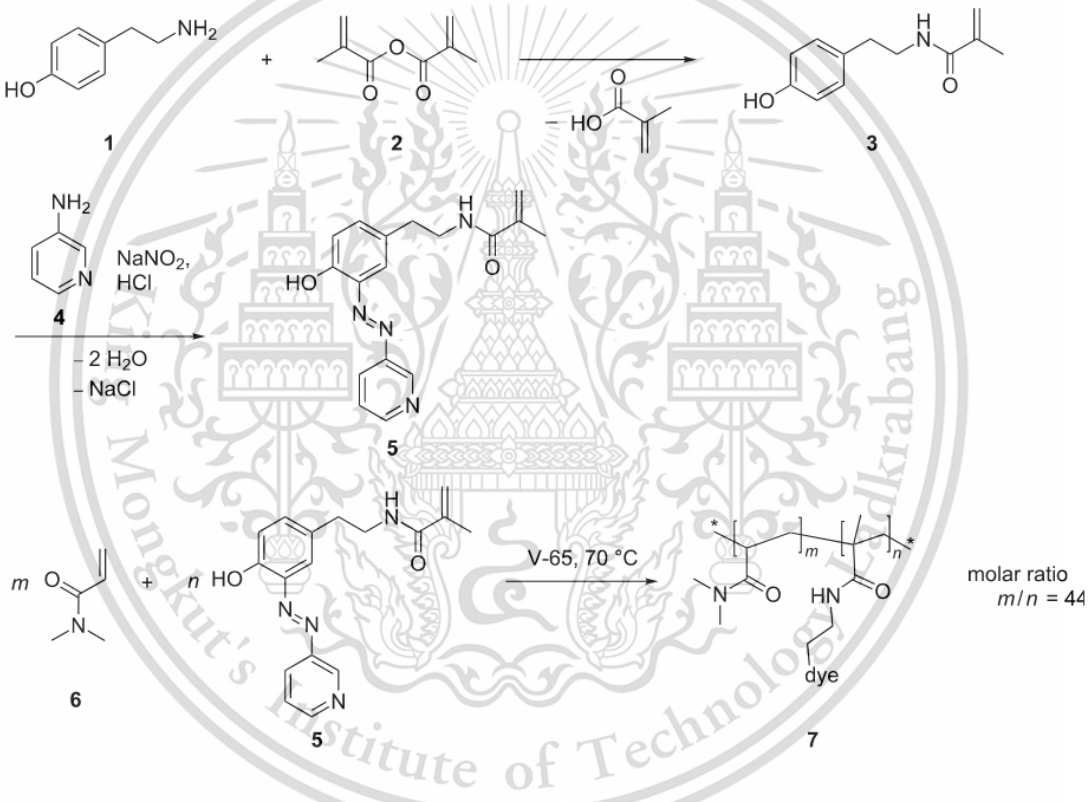

Figure 2.5 Synthesis of *N*-(4-hydroxy-3-(pyridin-3-yldiazenyl)phenethyl) methacrylamide (**5**) and preparation of its water-soluble copolymer (**7**) [56]

Irie and Kungwatchakun synthesized a photo-mechanical transducer gel by copolymerizing acrylamide, *N*,*N*-methylenebisacrylamide, and vinyl monomer-substituted triphenylmethane leuco derivatives (leucohydroxide or leucocyanide) [57]. When the gels were exposed to UV-light, they exhibited a significant reversible deformation, which can be attributed to the light-induced dissociation of the leuco-

derivatives (Figure 2.6). Furthermore, the presence of triphenylmethyl cations caused colorization in gels; after 5 minutes of UV irradiation, the color changed from pale green to deep green, and after several hours in the dark, it returned to the initial pale green.

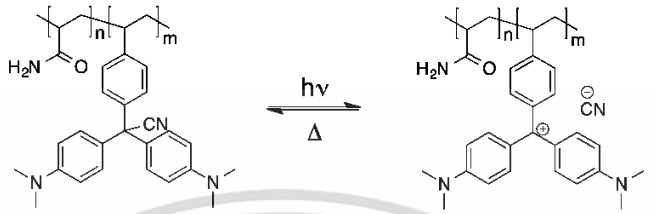

Figure 2.6 Dissociation of triphenylmethane leucocyanide upon UV radiation [1]

2.2.2.2 Polycondensation

Several studies have demonstrated the enormous potential of polycondensation. Figure 2.7 depicts the general procedure of polycondensation. By interfacial polycondensation reactions, several azo dyes and an anthraquinone dye were used to react with sebacoyl chloride [58]. When compared to the visible spectra of monomer dyes, the polymers had the same maximum absorption in visible spectra, but the absorption shifted as the solvent systems changed.

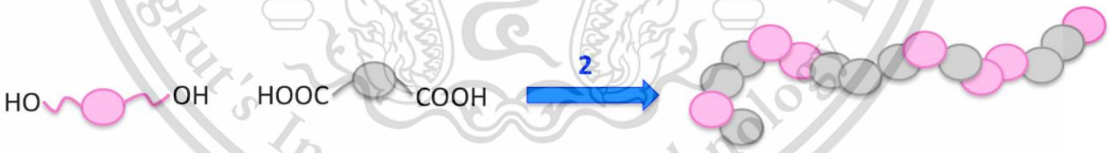

Figure 2.7 Polycondensation for the preparation of dye-containing polymers [1]

The incorporation of phenolphthalein into polymers via polycondensation has demonstrated that such materials have enormous potential. Figure 2.8 shows an example of some materials obtained by reacting the dye with hydroxyl group bearing compounds, such as poly(ether ether ketones), poly(phosphate ester), and poly(ether sulfone). These polymers have been used to create separation membranes with ion exchange properties, as well as flame retardant resins [59-61].

Another example of phenolphthalein-based materials was the creation of polymeric materials in which the pH sensitivity of molecule was preserved [62]. Under Sonogashira–Hagihara cross-coupling condensation reaction, the tetrabromo-derivative of phenolphthalein reacted with 1,4-diethynylbenzene, resulting in pH-switchable porous microporous networks. The color of the material transitioned from yellow orange in the lactone form (N1) to dark yellow-greenish in the salt form (Na-N1) (Figure 2.9). This results in materials that are suitable to produce size selective gas separation materials.

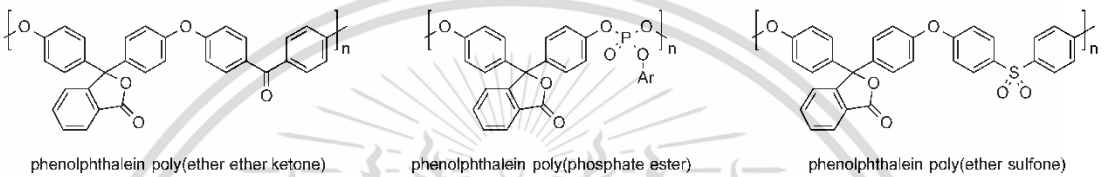

Figure 2.8 Examples of phenolphthalein-containing polymers obtained from polycondensation reactions [1]

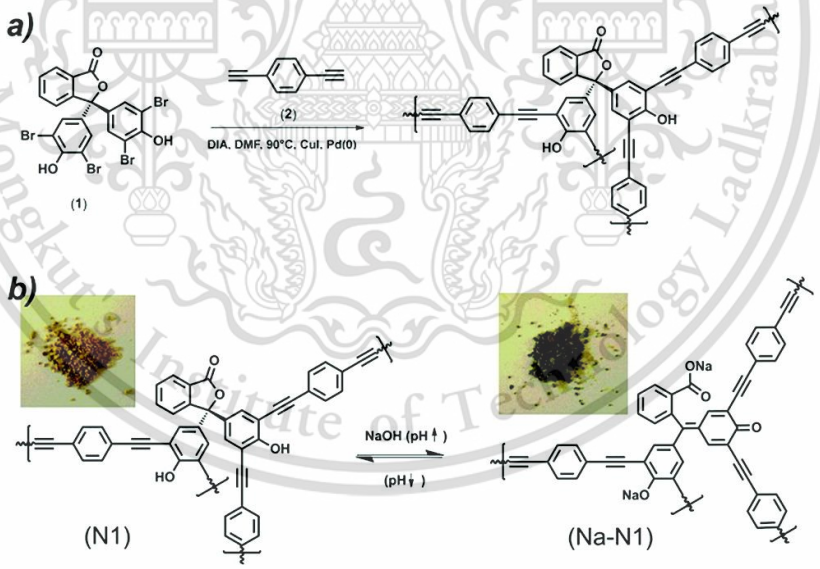

Figure 2.9 Synthetic reaction of phenolphthalein networks (N1) (a) and pH-response of network N1 and its sodium salt form (Na-N1) (b) [62]

2.2.2.3 Polymer attachment of dye molecules

This method necessitates the use of a polymeric backbone with functional side groups that can easily react with the functional groups of small

molecules, which can be dyes or building blocks (Figure 2.10). These building blocks enable the stepwise reaction, which includes the attachment of a chromophore. Depending on the dye structure and the nature of the reactive side group, the chromophoric system can be altered after this attachment.

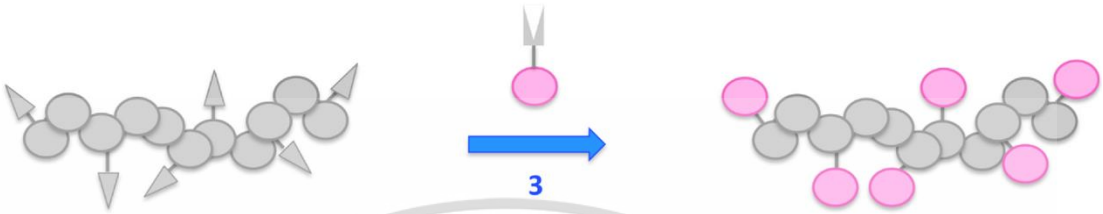

Figure 2.10 Attachment of dye molecules onto polymer [1]

There are numerous techniques for attaching azo dyes to polymer. Even though nucleophilic building blocks can be used to tether polyelectrophiles and then convert them to azo dyes, crosslinking compounds remain a major issue. Dawson et al. described four steps for attaching azo dyes to poly(vinylamine) [63]. The polymer undergoes a Schotten-Baumann reaction with *p*-acetamidobenzene sulfonylchloride in aqueous tetrahydrofuran in the first step. The polymeric sulfanilamide was then produced by hydrolysis in hydrochloric acid. Following diazotization, the polymeric diazonium ions were coupled with sodium *2*-naphthol-*6*-sulfonate. Figure 2.11 depicts the polymeric azo dye reaction pathway.

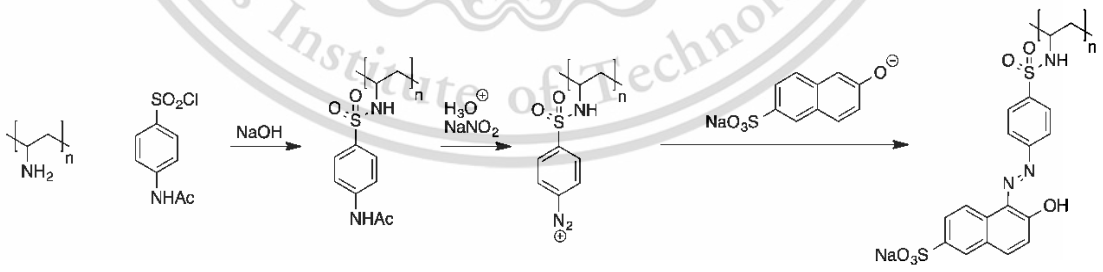

Figure 2.11 Stepwise attachment of an azo dye to poly(vinylamine) [63]

In addition, poly(vinylamine) can be used as starting material for the attachment of anthraquinone dyes [64]. Under Ullmann condensation conditions, 1-bromoanthraquinone derivatives were combined with poly(vinylamine) to produce

intensely colored polymers (Figure 2.12). Due to the low solubility of some anthraquinone derivatives, the polymeric dye was highly hydrophobic. However, the presence of vinyl sulfonate in the copolymer allowed it to be soluble in aqueous media.

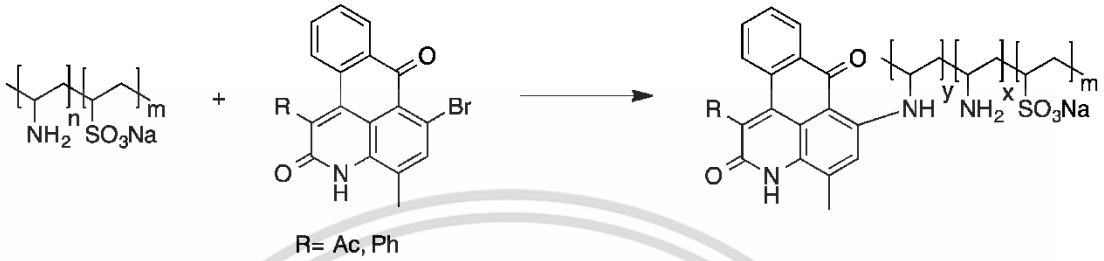

Figure 2.12 Reaction of poly(vinylamine) and an anthraquinone dye [64]

2.2.3 Applications

Polymer-linked dyes are gaining popularity due to their low toxicity and recyclability. In textile dyeing, they also exhibit high color fastness. Dye-containing polymers have thus been used not only in painting and textile dyeing, but also in medicine, optical sensors in chemical research and analysis. Non-toxic dye derivatives have been used inside the human body for medical applications; polymer-linked dyes are an excellent choice. For example, polymeric rylene dyes suitable for staining cellular membranes were obtained by modifying perylene-dicarboxmonoimide, perylene-tetracarboxdiimide, and benzoylterrylen-3,4-dicarboximid with a single poly(ethylene oxide) chain [65]. These polymeric materials exhibited high fluorescence in nonpolar solvents but much lower fluorescence in polar solvents, suggesting that they could be used in sensitive fluorescent probes.

Furthermore, polymer-attached dyes have been reported to be used in the treatment of rheumatoid arthritis. Ebbesen *et al*. used RAFT polymerization with a novel azide-containing methacrylamide monomer to create a copolymer of *N*-(2-hydroxypropyl)methacrylamide and *N*-(3-azidopropyl)methacrylamide, which was then post-modified with fluorescence dye *via* an azide-alkyne click reaction. The synthesized polymeric dye was used as a fluorescence dye (ATTO 680) to track the body. In a murine model of rheumatoid arthritis, it accumulated significantly in

inflamed joints. Moreover, for high molecular weight polymers (54 kDa), it could retain in the blood after 24 h and had excellent bioavailability [66, 67].

Methacrylated anthraquinone dyes were used to create artificial iris implants. Colored dye derivatives (blue, green, and red) were copolymerized with 2-hydroxyethylmethacrylate, tetrahydrofurfuryl methacrylate, and ethylene glycol dimethacrylate as a crosslinker to produce duroplast materials with high resistance to aggressive biological media. Dye diffusion from colored materials was not observed due to covalent modification. Almost any color can be created by combining different anthraquinone monomers in different ratios and concentrations. Following that, the copolymerized material was sharpened for iris implants, as shown in Figure 2.13 [68].

Figure 2.13 Broad color spectrum of mixed anthraquinone monomers (a) and the resulting sharpened blank of polymerized anthraquinone derivatives (b), modified from [68]

Dyes that could change color due to chromophore changes caused by external stimuli were used as indicator dyes for colorimetric sensors. The sensors' benefits include ease of reading with the naked eye, quick detection, high sensitivity, and selectivity [69]. Dye incorporation into polymer as a support matrix, blending with hydrogen bonding, van der Waals forces, and dipole–dipole interactions, and functionalization through covalent linkage are all possible. Many synthetic dyes have been reported as pH-indicator dyes that are used for colorimetric pH sensors, including bromothymol blue, bromophenol blue, bromocresol purple, bromocresol green, methyl red, methyl orange, methyl yellow, and phenol red. For example, the colorimetric sensor based on cotton fabric for sweat pH and lactate detection has been reported [4]. The fabric was treated with three layers of chitosan, sodium

carboxymethyl cellulose, and indicator dye. The sweat pH sensing element was made up of methyl orange and bromocresol green, and the lactate sensor was made up of lactate oxidase (Figure 2.14a). The color of sensing fabrics shifted from red to blue as pH (1-14) increased, and purple intensity increased as lactate level increased (0-25 mM) (Figure 2.14b). This sensor was successfully applied to three human volunteers and was able to differentiate their fitness and potential muscle fatigue. The findings indicated that these non-invasive sensors have a high potential for incorporation into items such as bedsheets, pajamas, shirts, tights, wristbands, and headbands, as well as integration with wearable devices for real-time monitoring of human health and athletic performance.

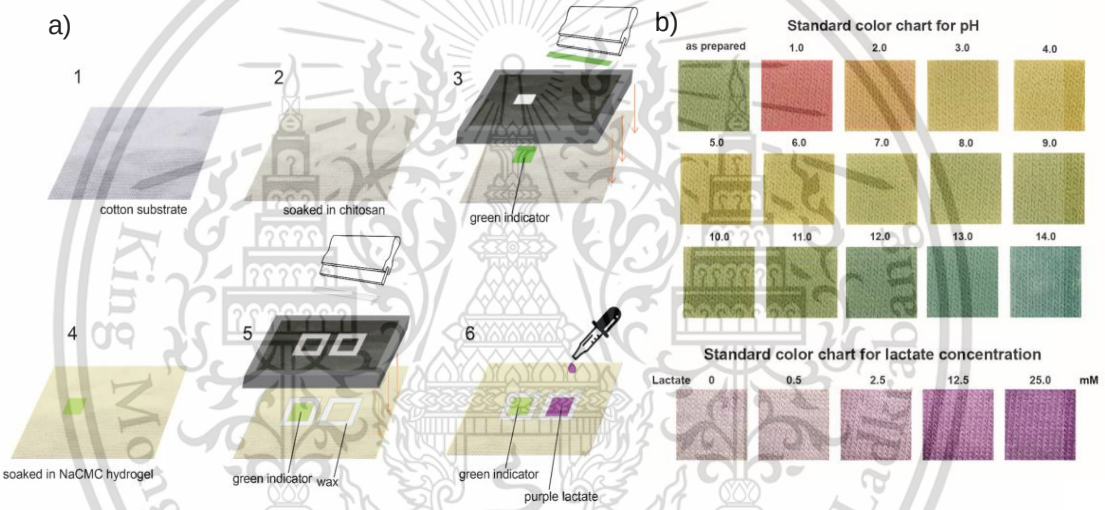

Figure 2.14 Fabrication process of textile based colorimetric sensor (a) and the standard color charts of the resulting textile for sweat pH and lactate detection (b), adapted from [4]

Besides monitoring sweat pH, pH-sensitive dyes are employed for smart wound dressing which can detect wound status for chronic or infected wounds [5]. This type of sensor could not only be observed visually, but the color parameters from image capture by smartphone application (iDerm) could also be analyzed, allowing antibiotic release *via* thermo-responsive drug carriers to be controlled during infection (Figure 2.15).

In the food industry, indicator dyes have been developed as intelligent food packaging that can provide information about food freshness based on substances

released from foods such as pH, carbon dioxide (CO_2), and sulfur compounds. With concerns about the toxicity of synthetic dyes, dye extracted from natural sources such as anthocyanin, curcumin, and green tea extracts have recently been studied. For instance, Nopwinyuwong *et al*. developed a "chemical barcode" from a pH colorimetric indicator that detects CO_2 changes as a spoilage of golden drop, an intermediate-moisture Thai dessert. The label was created by casting an indicator coating onto nylon/LLDPE film, with the indicator solution being an ethanol solution made by combining bromothymol blue and methyl red. Changes in label color from bright light green to orange-red correlate with microbial growth patterns in dessert samples, allowing for real-time spoilage monitoring (Figure 2.16) [70].

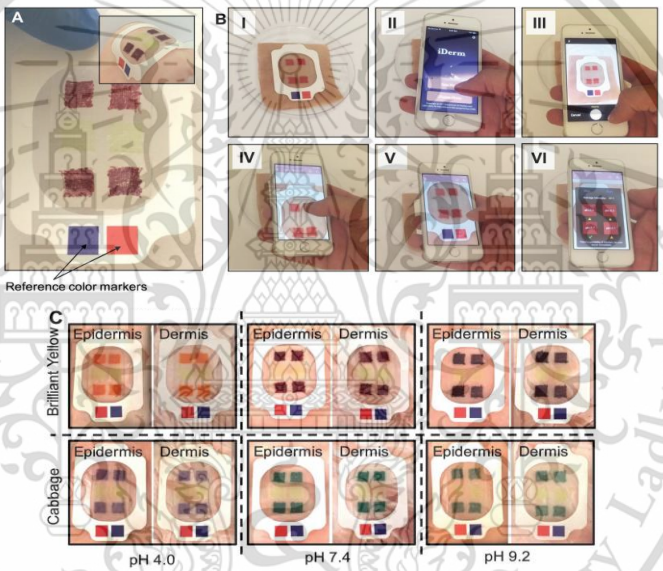

Figure 2.15 Colorimetric pH sensor based on hydrogel dressing (a), demonstrating image capture processing using iDerm (b) and images of the dressings placed on the pig skin sprayed with different pH values (c), adapted from [5]

In terms of dye-functionalized polymers for colorimetric sensors, this is a strategy to solve the dye migration problem, even if suitable functional groups of dye are required. Sui and coworkers recently developed an acidochromic dye-bound cellulose (ARC)/poly(vinyl alcohol) (PVA)-based pH sensor film for food monitoring [3]. The ARC was created by reacting regenerated cellulose with the acidochromic dye, 1-hydroxy-4-[4-(ethylsulfurate sulfonyl)-phenylazo]-naphthalene

(HESPN) (Figure 2.17a). When the pH sensor was immersed in solutions with pH values of 7, 10, and 12, the color of the sensor changed from yellow to brick-red to purple. The pH sensor also had excellent leakage resistance in both acidic and basic solutions (Figure 2.17b). When applied to spoiled shrimp, the pH sensor's color changed from yellow to brown after 24 h at room temperature (Figure 2.17c).

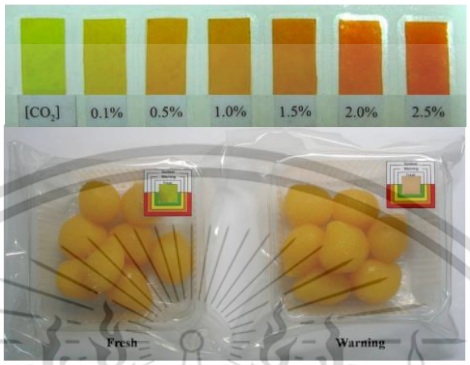

Figure 2.16 Color change of indicator label responding CO_2 (Upper side); packaged golden drop with food spoilage indicator label (Bottom side), adapted from [70]

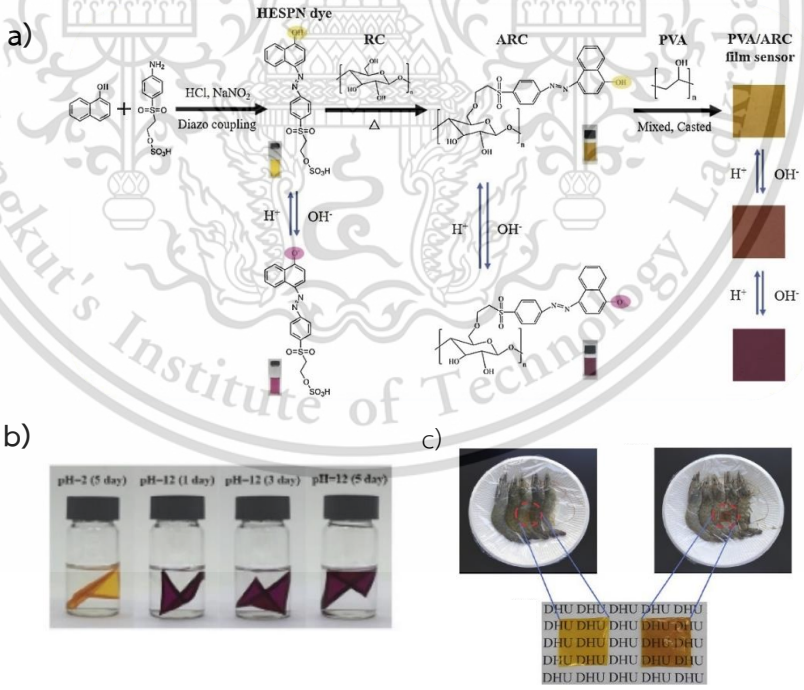

Figure 2.17 Preparation of PVA/ARC pH film sensor (a), optical images of the film sensor immersed in acid-base solutions (b) and optical images of the film placed on shrimp before and after spoilage (c), adapted from [3]

Another study reported a fast, portable, and simple-to-use Au^{+3} sensors made of poly(sodium-4-styrenesulfonate) (PSS)-modified rhodamine B derivative (Rho) spray coated onto the surface of indium tin oxide (ITO) and filtered paper [2]. The polymeric sensors displayed "Off–On" fluorescence with Au^{+3} and could be reversed by rinsing with EDTA solution (Figure 2.18). Furthermore, polymeric dye-based sensors for detecting other chemicals in water, such as cyanide [71], volatile organic compounds (VOCs) [72], organic solvents [73], trinitrotoluene [74], and heavy metal ions [75, 76], have been developed.

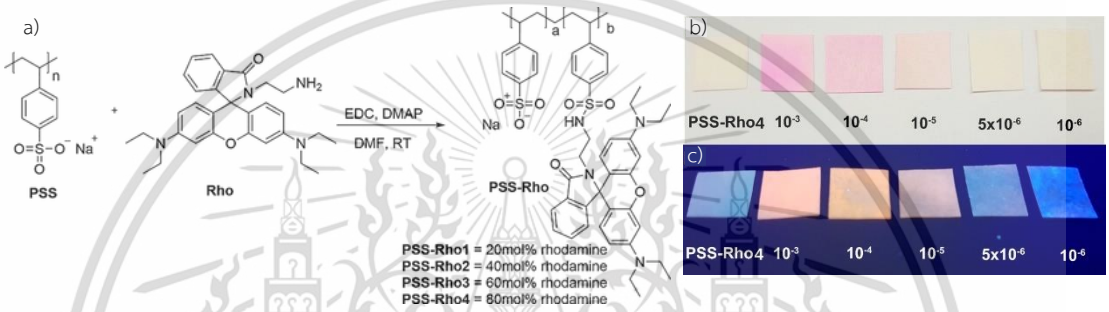

Figure 2.18 Synthetic pathways of rhodamine-based modified PSS (PSS-Rho) (a) and PSS-Rho4-filtered paper after treatment with different concentration of Au^{3+} ions under normal light (b), and under fluorescence light (c), adapted from [2]

From the literature reviews, dye-containing polymers have been applied to colorimetric sensors for many fields. However, because they are mostly made of synthetic polymers that go through multiple step reactions and use a lot of solvent, they may contain toxic residue. The goal of this research is thus to develop a polymeric dye with stimuli responsive properties from chitosan, a polysaccharide derived from natural sources.

2.3 Chitosan [8]

Chitosan is a cationic polysaccharide obtained by partial deacetylation of chitin. Chitin is one of the most abundant natural polymers after cellulose. The chitosan structure consists of D-glucosamine linked to *N*-acetyl D-glucosamine by β-1,4-glycosidic bonds [77]. The chemical structure of chitosan was shown in Figure

2.19. The physicochemical and biological properties of chitosan are determined by the degree of deacetylation (DD). When the DD of chitin exceeds about 50%, it exhibits acid solubility and is referred to as chitosan. The reactive amino groups at C2 atoms and the hydroxyl groups at C3 and C6 atoms of glucosamine units on chitosan have interesting properties such as biocompatibility, biodegradability, low toxicity, antimicrobial activity, and low immunogenicity.

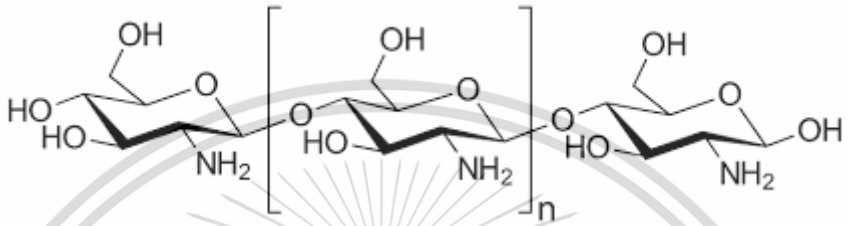

Figure 2.19 Chemical structure of chitosan

2.3.1 Source and production

Chitosan is derived from the deacetylation of chitin extracted from crustacean exoskeletons, insect cuticles, and fungi cell walls. The increased consumption of shellfish, as well as the expansion of aquaculture, resulted in an increase in shellfish waste. As a result, shrimp, prawn, and crab wastes are now the primary source of chitosan production, producing chitosan with molecular weights ranging from 1 to 2 MDa [78]. Mycelium waste from fermentation processes remains untapped for production due to low quantities for significant production [79].

Chitosan is mainly produced by the USA, Thailand, Australia, Japan, Norway, India, and Poland. The exoskeleton of a crustacean is used as the raw material for commercial chitosan production (shellfish waste). Generally, the conventional method of chitosan production is based on chemical extraction, which includes four basic steps: demineralization, deproteinization, discoloration, and deacetylation. These treatments, however, influence random cleavage of the chitin backbone and random deacetylation, resulting in unsatisfactory products. The biological method has proven to be appealing due to its high-quality products, low cost, and environmentally friendly process. This method demineralizes with lactic acid and deproteinizes with proteases. [80]. The schematic of chitosan production is displayed in Figure 2.20.

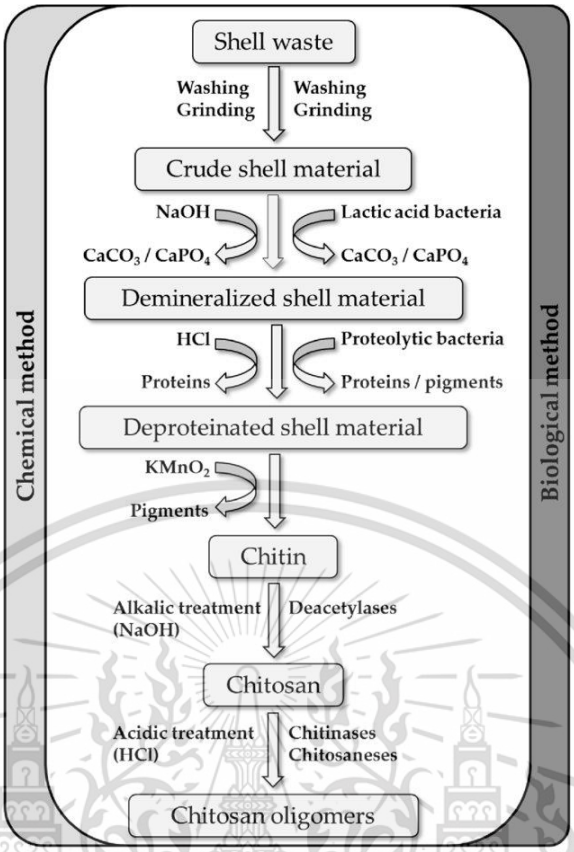

Figure 2.20 Chitosan and chitosan oligomers productions by chemical and biological methods [81]

2.3.2 Properties of chitosan

2.3.2.1 Solubility

Because of the crystalline structure formed by strong hydrogen bonds between the acetyl groups of *N*-acetyl-D-glucosamine units on chitin chains, chitin is insoluble in conventional solvents. When chitin is deacetylated to chitosan, the *N*-amino-D-glucosamine units of chitosan exhibit hydrophilicity and positively charges in acid solution, resulting in swelling and dissolution [82]. Chitosan solubility is determined by the amount of protonated amino groups in the chitosan and the degree of deacetylation. Chitosan has a pKa of about 6.3, indicating that the amine groups can be protonated at low pH to form a water-soluble cationic polysaccharide. Chitosan precipitates or chitosan gel are formed because of the insolubility of quaternary nitrogen salts of chitosan at pH greater than 6. The pH transition of chitosan solubility occurs between 6 and 6.5. Organic acids such as acetic, formic, and lactic acids are used as chitosan solvents; however, 1% acetic acid or 0.1M acetic

acid solutions are the most commonly used solvents for chitosan dissolution. [83]. Furthermore, chitosan is soluble in 1% hydrochloric acid and dilute nitric acid but not in sulfuric or phosphoric acids. Obviously, the molecular weight, ionic concentration, and the use of acids for protonation are all factors in chitosan solubility.

In term of the dissolution of chitin and chitosan, inorganic solvents such as dimethylacetamide (DMAc)/LiCl and $CaCl_2$/MeOH, and ionic liquids such as 1-butyl-3-methylimidazolium chloride (BminCl), alkyl imidazolium chloride ([AMIM]Cl), alkyl imidazolium dimethyl phosphate ([MMIM] [Me_2PO_4]) and 1-allyl-3-methyl-imidazolium acetate ([AMIM]Ac) have been reported. However, these solvents have some drawbacks such as corrosiveness, volatility, toxicity, pollution depolymerization and high cost [82]. Moreover, alkali/urea systems (e.g., NaOH/urea, LiOH/urea, and LiOH/KOH/urea) can be used to dissolve chitin and chitosan *via* freeze-thawing process [84-86]. Even though alkali is traditionally used as a coagulant, the intramolecular and intermolecular hydrogen bonds of chitosan are broken by alkali medium at low temperatures. Urea hydrates, acting as the host molecule, form inclusion complexes with chitosan/alkali, resulting in a stable solution, which is similar to the mechanism of cellulose dissolution [87]. The system's chitin/chitosan solutions are more stable than the acetic acid-dissolved solution. [85]. Furthermore, the system is temperature sensitive, forming gel as the temperature rises due to the loss of stability of inclusion complexes at high temperatures [88, 89]. This system has also been used as solvent for hydrogel fabrications with cellulose [90] or anionic polymer [91-93], and modification of chitosan such as quaternization [94-96], etherification [97], and acylation Michael reaction [98].

2.3.2.2 Biodegradability

Chitosan can be degraded *in vivo* by several enzymes, including chitinases, chitosanases, and chitin deacetylase, but lysozymes, a non-specific enzyme found in mammalian tissues, have received the most attention. The processes produce non-toxic products with lower molecular weight (oligosaccharides), which can then be incorporated or excreted to glycosaminoglycans and glycoproteins [99]. Chitosan can also be degraded in vitro using methods such as oxidation, chemical, and enzymatic hydrolysis, which is used

to prepare low molecular water-soluble chitosan [100]. The degradation mechanism involves random depolymerization (cleavage of glycosidic linkages) followed by deacetylation (hydrolysis of *N*-acetyl linkages), resulting in a decrease in molecular weight and an increase in the degree of deacetylation. Degradation rate of chitosan depends on molecular weight and degree of deacetylation: the low molecular chitosan and degree of deacetylation increase the degradation rate while the high molecular chitosan and degree of deacetylation is expected low degradation [101]. Moreover, the biodegradability of chitosan can be altered chemically. For example, the degradation rates of chitosan conjugates with mercaptonicotinic acid are higher than those of thioglycolic acid conjugated chitosan, demonstrating the strong effects of thiol group contents and ligand type [102].

2.3.2.3 Biocompatibility

Despite the fact that gastrointestinal enzymes can partially degrade chitosan and chitin, they are not bioavailable. Chitosan has an LD50 value of ~16g/kg, which is comparable to glucose values in mouse assays. [103]. According to Schipper's report, chitosan has dose-dependent toxicity with a degree of deacetylation less than 35%, and low toxicity with a degree of deacetylation greater than 35% [104]. The *in vitro* cytocompatibility of chitosan is reported to be higher than chitin. Because of the presence of positively charged amino groups in its structure, chitosan can interact with cells more effectively, improving biocompatibility [99, 105]. The safety of chitosan on foods and drugs has approved by Food and Drug Administration (FDA). However, very few chitosan applications, particularly biomedical applications, have been approved [106, 107].

2.3.2.4 Antimicrobial activity

Chitosan has recognized to exhibit antimicrobial activity against bacteria, fungi, and yeasts [108]. Chitosan frequently inhibits bacterial growth more effectively than fungi growth [109, 110]. Chitosan is considered to have antibacterial activities against both Gram-positive and Gram-negative bacteria. However, there is still debate over whether chitosan's antibacterial activity is more effective against Gram-negative bacteria or not [111]. There are many factors of chitosan affected antimicrobial activity, including pH of media, molecular weight, concentration of

chitosan, degree of deacetylation, type of microorganism, source of chitosan [108]. The pH media of chitosan is critical for this property because its amino groups can transform into positively charged ions that can interfere with microorganism cell membranes. Hence, the chitosan in acidic medium (pH<6.5) only shows the antimicrobial activity. Furthermore, the antimicrobial activity mechanism has been proposed in several ways, including: hydrolysis products from chitosan diffuse into cell and then interact with microbial DNA, inhibiting mRNA and protein synthesis, chitosan can interact with nutrients and essential metals, and chitosan covered on microbial cell inhibits diffusion of nutrients as well as oxygen permeation (for aerobic bacteria) [108].

2.3.2.5 Wound healing property

Chitosan has good biological properties and can speed up wound healing by enhancing the functions of polymorphonuclear neutrophils, macrophages, and fibroblasts or osteoblasts, as well as promoting reepithelialization [112]. Gastric acids in the stomach can be neutralized by the amino groups of chitosan, which is used to treat peptic ulcer disease [113]. Moreover, positively charged chitosan can interact with the cell membrane supporting the reorganization of the epithelial tight junctions [114]. The effects of chitosan on wound healing properties include molecular weight, degree of deacetylation, and chitosan state [112]. Chitosan has been developed for wound dressing in a variety of forms, including films, hydrogels, membranes, and porous matrixes. The dressings demonstrate the ability to treat various wound types with several benefits such as maintaining a moist wound environment, preferably through water permeation, preventing infection, and enhancing wound healing, particularly in burns. In addition, chitosan derivatives have been developed to improve their biological properties such as anticoagulant, increased solubility, cellular uptake, controlled drug delivery, in order to create a wound dressing with effective wound healing [115, 116].

2.3.3 Characterization of chitosan

2.3.3.1 Degree of deacetylation (DD) [117]

Chitosan properties are influenced by the degree of deacetylation (DD), which is determined by the proportion of D-glucosamine and *N*-acetyl-D-glucosamine.

To determine the DD of chitosan, various techniques such as elemental analysis, titration, hydrolytic method, IR spectroscopy, ^{1}H-NMR spectroscopy, and so on are used.

- ***Elemental analysis***

The DD of chitosan can be calculated using carbon and nitrogen mass percentages measured with an elemental analyzer, as shown in equation 2.1. The carbon to nitrogen (C/N) ratios range from 5.145 in completely deacetylated chitosan ($C_6H_{11}O_4N$ as repeating unit) to 6.861 in chitin ($C_8H_{13}O_5N$ as repeating unit). The percentages of N in fully *N*-deacetylated chitosan and fully *N*-acetylated chitin are 8.7 and 6.9 percent, respectively [118, 119].

$$\%DD = \left(1 - \frac{\frac{C}{N} - 5.145}{6.861 - 5.145}\right) \times 100\% \quad (2.1)$$

The nitrogen content of samples with varying DA (degree of acetylation) has relatively small changes, therefore the results obtained from this technique, especially when contaminants are present, are not precise. This technique was used to define chitosan as having more than 7% nitrogen content and chitin as having less than 7% nitrogen content [120].

- ***Potentiometric titration***

Among the non-NMR methods, potentiometric titration is the most consistent and robust technique. However, some of the drawbacks are that measurement is time consuming and labor intensive and solutions of known precisely concentrations are needed [121]. In detail, a known amount of chitosan is dissolved in a known volume of standard HCl solution and titrated against a known volume of standard NaOH solution. The titration curve of pH versus NaOH titration volume is plotted and two inflection points of the curve are found: the first corresponds to neutralization of HCl, and the second to neutralization of the chitosan ammonium ions (Figure 2.21). To determine DD, the amine content of chitosan (NH_2%) is calculated from the consumed NaOH volume (equation 2.2). The

obtained value is then divided by theoretical NH_2% content (9.94%), as follows the equation 2.3.

$$NH_2\% = \frac{(C_1V_1 - C_2V_2) - 0.016}{M} \times 100 \quad (2.2)$$

$$DD\% = \frac{NH_2\%}{9.94\%} \times 100 \quad (2.3)$$

where, C_1 is HCl concentration (mol/L), C_2 is NaOH concentration (mol/L), V_1 is volume of HCl solution (mL), V_2 is volume of NaOH solution (mL), M is the chitosan weight (g), X is the first inflection point (mL), and Y is the second inflection point (mL).

The DD% can also be calculated using the following equation 2.4.

$$DD\% = \left[2.03 \left(\frac{(V_2 - V_1)}{m + 0.0042(V_2 - V_1)} \right) \right] \quad (2.4)$$

where, m is weight of sample(g). V_1 and V_2 are the NaOH volumes corresponding to the deflection points (mL).

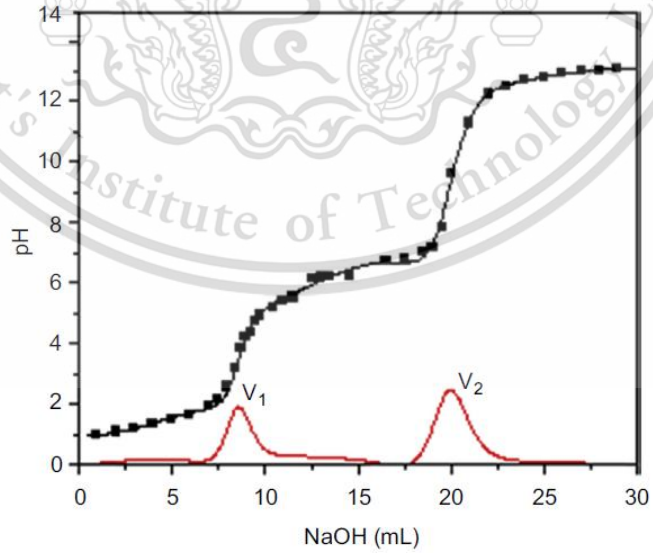

Figure 2.21 Potentiometric titration curve of chitosan [117]

- *Fourier transform infrared spectroscopy (FTIR)*

FTIR is a one of techniques for determining the DD of chitosan. It employs two absorption bands: a characteristic band (probe band) that represents the amide group of *N*-acetyl-D-glucosamine residues, and a reference band that represents a group that is present in both monomers (D-glucosamine and *N*-acetyl-D-glucosamine) [121]. The peaks at 1652 and 3450 cm^{-1}, correspond to the amide I and hydroxyl groups of chitosan, respectively, are the most used probe and reference bands (Figure 2.22) [122-124]. The DD can be calculated using these absorption bands, as following equation 2.5.

$$DD\% = 100 - \frac{A_{1652}}{A_{3450}} \times 115 \quad (2.5)$$

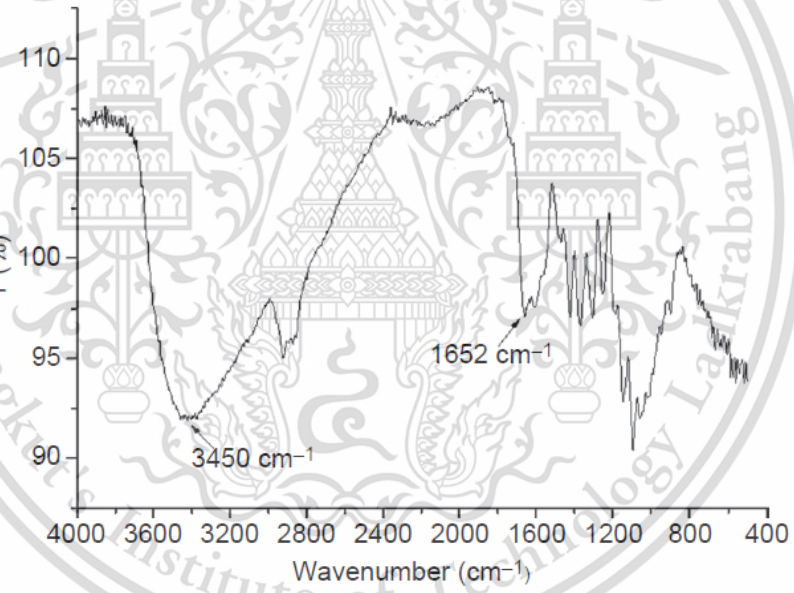

Figure 2.22 Typical FTIR spectra of chitosan [117]

The benefits of determining DD using the FTIR method include a quick reaction, the use of inexpensive chemicals, the use of widely available equipment, and the absence of sample purity or dissolution requirements. FTIR, however, is typically used only for rough estimation of DD, and it must be used with caution. Furthermore, humidity may affect the absorbance of some peaks, and impurity peaks may overlap with chitosan signals.

- *^{1}H-NMR spectroscopy*

The most accurate method for determining DD percentage is ^{1}H-NMR spectroscopy. A known amount of chitosan is dissolved in deuterated aqueous solutions, and spectra ranging from 0 to 6 ppm are measured (Figure 2.23) [125]. To calculate the percentage of DD, the integrals (I) of the *N*-acetyl group peak areas at 2.05 ppm (H-Ac, $-CH_3$) and 3.15 ppm (H at C2, H_2) are used in the following equation 2.6.

$$DD\% = \left\{1 - \left(\frac{I_{CH_3}/3}{I_{H2}}\right)\right\} \times 100 \quad (2.6)$$

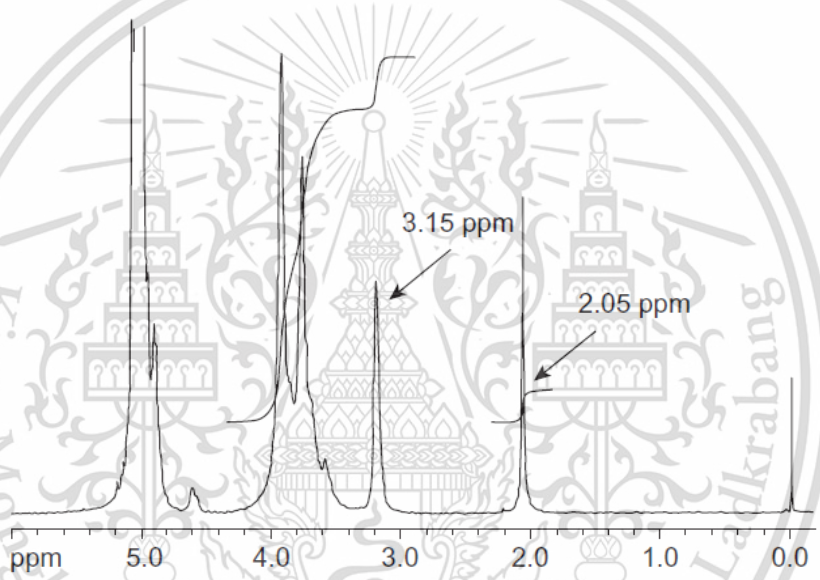

Figure 2.23 ^{1}H-NMR spectra of chitosan [117]

Various proton signals, as listed in Table 2.1, can be used to calculate the DD. For example, the integrals of the peaks of proton H1 of the deacetylated monomer (H1-D) and the three protons of the acetyl group (H-Ac) are used to calculate the percentage of DD as following equation 2.7.

Table 2.1 Chemical shifts for proton in CD_3COOD/D_2O or DCl/D_2O solution at 65°C [117]

Type of proton	Position (δ, ppm)
H_1 (H_1 of GluNAc or H-1(A))	4.62–4.85
H_1 (H_1 of $GluNH_2$ or H-1(D))	4.85–4.97
H_2 (H_2 of $GluNH_2$ or H-2(D))	3.18–3.24
H_2 (H_2 of GluNAc or H-2(A))	3.38–3.65
H_3 (H_3 of $GluNH_2$ or H-3(D))	3.52–3.87
H_3 (H_3 of GluNAc or H-3(A))	3.52–3.65
H_3, H_4, H_5, H_6, $H_{6'}$	3.74–4.34
$HN–COCH_3$ or H-Ac	1.95–2.09

$$DD\% = \left(\frac{H1\text{-}D}{H1\text{-}D + H\text{-}Ac/3} \right) \times 100 \quad (2.7)$$

The percentage of DD can also be calculated using the signal from protons H_2, H_3, H_4, H_5, H_6, $H_{6'}$ ($H_{2\text{-}6}$) of both monomers and the peak of acetyl group (H-Ac) as following equation 2.8.

$$DD\% = \left(1 - \left(\frac{H\text{-}Ac/3}{H_{2\text{-}6}/6} \right) \right) \times 100 \quad (2.8)$$

When the DD is less than 90%, the H1 protons of both deacetylated and acetylated monomers (H1-D, H1-A) are used to calculate the percentage of DD as shown in equation 2.9.

$$DD\% = \left(\frac{H1\text{-}D}{H1\text{-}D + H1\text{-}A} \right) \times 100 \quad (2.9)$$

Compared to other methods, this technique is the most reliable, rapid, simple and accurate. However, the requirement for trained staffs, expensive apparatus and chemicals, as well as the limited chitosan solubility, are limitations [125].

2.3.3.2 Crystallinity

The crystalline isolated chitin and chitosan is determined using XRD analysis. As shown in Figure 2.24, two major crystalline reflection peaks for α-chitin are at 9.6 degrees (020 plane) and 19.6 degrees (110 plane), β-chitin at 9.1 degrees (020 plane) and 20.3 degrees (110 plane), and γ-chitin at 9.6 degrees (020 plane) and 19.8 degrees (110 plane) [126, 127]. The crystallinity of chitin was reduced after it was transformed to chitosan, and a strong reflection at 9-10° was observed due to the incorporation of bound water molecules into the crystal lattice. Despite a slight decrease in crystallinity percentage, the chitin bands were sharper than the chitosan bands.

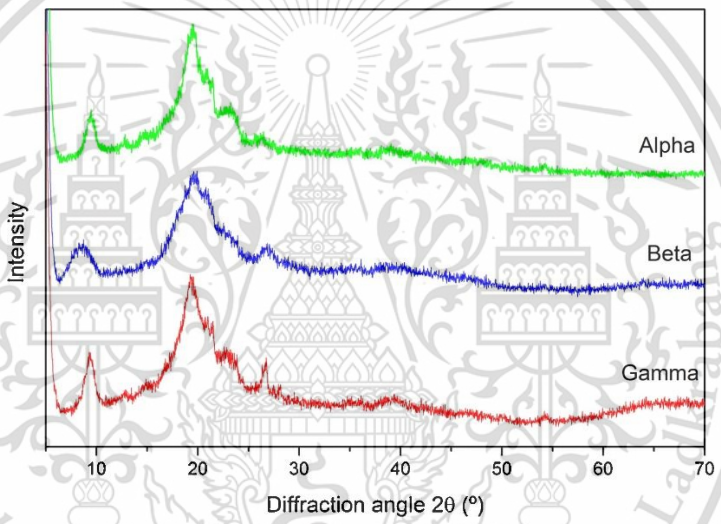

Figure 2.24 XRD spectra: α-, β-,and γ-chitin [126]

For crystallinity of chitosan with various DD, Zhang *et al*. reported that the maximum intensity peak at the (020) reflection decreased with increasing DD and moved to a higher angle. With an increase in DD, the second intensive peak at the (110) reflection also decreased (Figure 2.25). Furthermore, they discovered a linear relationship between CrI_{020} from XRD and the calibrated DD value, implying that XRD could be used to determine the DD of chitin and chitosan [128].

After mathematically modifying the peaks with the Lorentzian function, the crystalline index (CrI) of chitosan can be calculated from 110 phase judged based on polysaccharide diffraction studies [129]. CrI_{110} was calculated using Klug and Alexander's equation, as shown in Equation 2.10, based on the maximum intensity

levels at 110 lattices (I_{110} prior to 20° corresponding to maximum intensity), and at 16° (amorphous diffraction) [130].

$$CrI_{110} = \frac{I_{110} - I_{am}}{I_{110}} \times 100 \quad (2.10)$$

where CrI_{110} is crystallinity index at 110 phase, I_{110} is maximum intensity at around 20°, and I_{am} is amorphous diffraction at 16°.

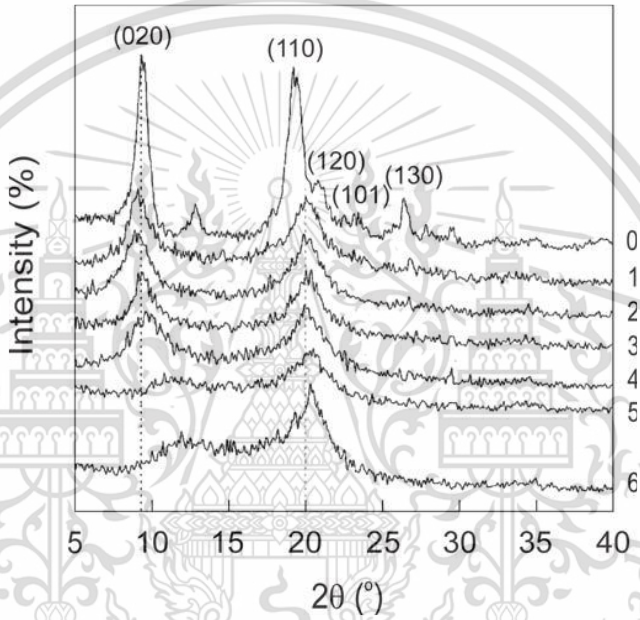

Figure 2.25 Comparison of X-ray powder diffractograms of chitin and chitosan with different DD. The number (0–6) mean different DD (%): 0-16.9, 1-59.4, 2-63.5, 3-58.7, 4-71.4, 5-87.0, 6-92.8 [128]

2.3.4 Modification of chitosan

Chitosan is an attractive material due to its interesting properties. However, these functions are hampered by the fact that chitosan is insoluble in water, not acid resistant, and has poor mechanical properties. The chemical modification of chitosan is a critical step toward a breakthrough in utilization. Chitosan is an amenable molecule with amino and hydroxyl groups that can be grafted with other species without affecting the degree of polymerization of chitosan [131]. Currently, the modified chitosans with a variety of functional groups have been widely reported

[132, 133]. It not only improved the physical and chemical properties of chitosan, but it also created unique properties, resulting in expanded applications.

2.3.4.1 Quaternized chitosan and N-alkyl chitosan

Quaternization of amino groups in chitosan is an attempt to address the issue of poor water solubility and permeability at high pH. (e.g., the intestine and colon) [134]. *N*,*N*,*N*-trimethyl chitosan chloride (TMC), a quaternized derivative, shows high solubility in a broader pH and concentration and it can be used as absorption enhancer for test drugs such as buserelin, octreotide acetate, 9-desglycinamide-8-arginine vasopressin, fluorescein-isothiocyanate dextran (FD4, MW4400), mannitol, and so on [135]. It was found that the mucoadhesive properties is enhanced with degree of quaternization (DQ). Moreover, quaternized chitosan possesses the antibacterial activity, biocompatibility, biodegradability, non-toxicity, thus, it has been widely used in biomedical fields such as insulin delivery, filler fiber in wound dressing, and so on [136-139].

In general, nucleophilic substitution with iodomethane in an alkaline solution of *N*-methyl pyrrolidinone (NMP) was used to create quaternized chitosan derivatives. Domard *et al.* reported TMC synthesis with iodomethane at 36°C for 3 h as seen in Figure 2.26 [140]. They found that derivatives with DQ greater than 25% are soluble in water, and the highest DQ of 64% was obtained by repeating quaternization. The iodide counterion was replaced with chloride, which improved their stability. The reaction occurred not only at the amino groups, but also at the hydroxyl groups of chitosan [141]. Furthermore, TMC prepared by repeating quaternization is poorly soluble in water, where the DQ is greater than 85%, due to a number of O-methylation reactions [142].

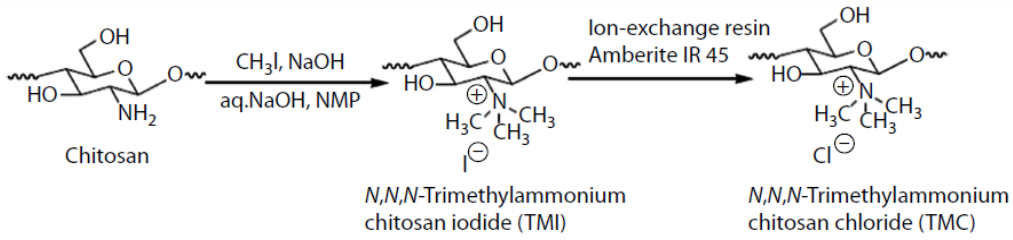

Figure 2.26 Synthesis of TMC [140]

Quaternization of chitosan can also be used glycidyl trimethylammonium chloride (GTMAC) as a quarternizing agent, due to the presence of a quaternary ammonium group itself. This reaction is selective for chitosan amino groups and has a longer side chain than TMC. Daly and Manuszak-Guerrini reported the synthesis of *N*-(2-hydroxy) propyl-3-trimethylammonium chitosan chloride under basic conditions using a commercially available Quat-188 salt, 3-chloro-2-hydroxypropyl trimethyl ammonium chloride [143]. Quat-188 produced the epoxide group which reacted with amino groups and hydroxy groups of chitosan *via* a nucleophilic substitution pathway to introduce the quaternary ammonium substituent, as shown in Figure 2.27.

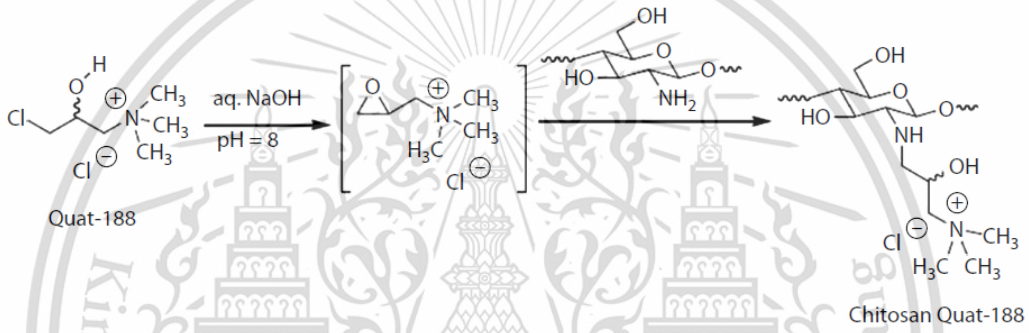

Figure 2.27 Synthesis of quaternized chitosan with 3-chloro-2-hydroxypropyl trimethylammonium chloride (Quat-188) [143]

2.3.4.2 Acyl chitosan

The reaction of chitosan with organic acids and their derivatives (such as anhydride and acyl chloride) in a specific medium (such as aqueous acetic acid/methanol, pyridine, pyridine/chloroform, trichloroacetic acid/dichloroethane, ethanol/methanol mixture, methanol/formamide, or DMA–LiCl) is known as acylation [144]. According to the different activity of functional groups of chitosan, amino group (C2–NH_2) > primary hydroxy group (C6–OH) > secondary hydroxyl group (C3–OH), the aliphatic or aromatic acyl groups could be controlled by the introduced position chain which is at amino (*N*-acylation) [145, 146], hydroxyl (*O*-acylation) [147], or both groups (*N,O*-acylation) [148]. The acylation process breaks down the hydrogen bonds between chitosan molecules, reducing crystallinity and increasing

water solubility. Acylated chitosans with hydrophobic side chains generally improve the properties of assembly polymers, broadening their application range.

The reaction pathway of *N*-acylated chitosan is displayed in Figure 2.28. The derivatives with various side chains such as oleic, linoleic, elaidoic, erucoyl, phthaloyl, p-nitrobenzoyl and cinnamoyl were successfully synthesized with randomly distributions [149-151]. Cyclic acid anhydrides (such as succinic, maleic, glutaric, itaconic, phthalic, cis-1,2,3,6-tetrahydrophthalic, 5-norbornyl-endo- 2,3-dicarboxylic, cis-1,2-cyclohexyl dicarboxylic, trimellitic anhydride, (2-octen-1-yl) succinic, citraconic, trimellitic, pyromellitic) could be used as acylating agents by ring-opening reactions which offered *N*-carboxyacyl chitosan [152, 153]. For lactone molecule, the acylated chitosan poses hydroxylacyl chitosan [154]. Moreover, selective *N*-acylated chitosan could be synthesized by coupling reaction with organic acid using 1-ethyl-3-(3-dimethyl-aminopropyl)-1-carbodiimide hydrochloride (EDC) and *N*-hydroxysuccinimide (NHS) as coupling agents [155, 156]. *N*-acylated chitosan derivatives exhibit enhanced biocompatibility, anticoagulability, blood compatibility, and anti-inflammatory in human body, thus, they can be employed as a drug carrier for sustainable release in pharmaceutical fields [157].

To prepare *O*-acylated chitosan, the ammonium group must be protected using solvents such as trifluoroacetic acid or methanesulfonic acid [158-160]. As shown in Figure 2.29, methanesulfonic acid (MSA) can act as both a solvent and a catalyst in the reaction. Comparing with water-solubility of *N*-acylated chitosan [161, 162], the formation of ester linkage in *O*-acylated chitosan provides organo-solubility such as pyridine and chloroform [160]. Furthermore, it shows ability of enzymatic hydrolysis such as lipase and glycosidases (breaking of glycoside linkage of chitosan derivatives) [131].

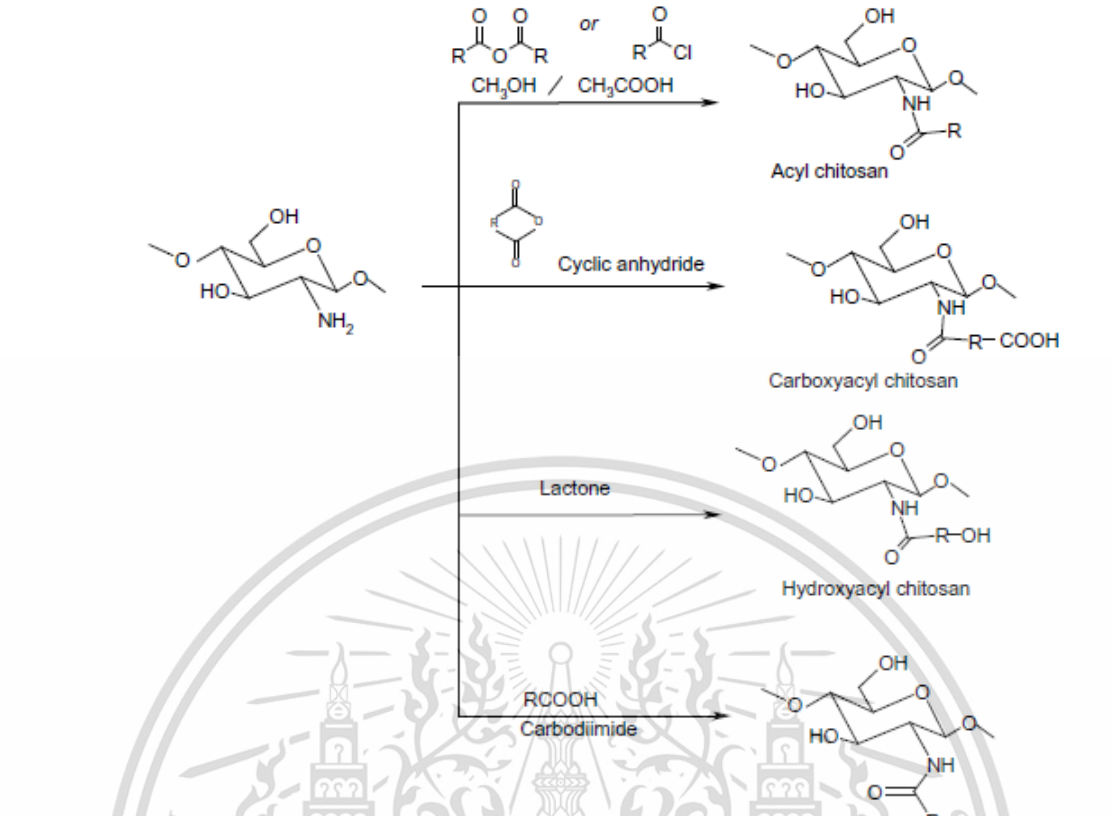

Figure 2.28 Synthesis of *N*-acylated chitosan [131]

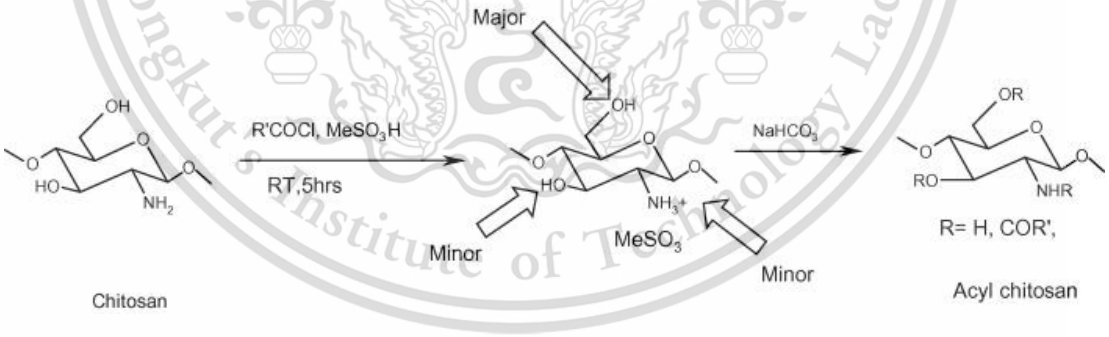

Figure 2.29 Synthesis of *O*-acylated chitosan [131]

2.3.4.3 Hydroxyalkyl chitosan

Hydroxyalkyl chitosans are prepared by reacting chitosan with epoxides (such as ethylene oxide, propylene oxide, butylene oxide and glycidol). The reaction took place primarily at the amino (*N*-hydroxyalkyl chitosan) or hydroxyl (*O*-hydroxyalkyl chitosan) groups, or possibly both. The substitution ratio is affected by

the catalyst (NaOH or HCl) and the temperature. The synthesis of hydroxyalkyl chitosan with certain conditions is illustrated in Figure 2.30. For instance, *N*-hydroxypropylation can be achieved without any catalyst. Acid catalysis produces mostly *N*- but some *O*-alkylation products, whereas alkaline catalysis produces O-alkylation oligomers at temperatures above 40°C [163, 164].

O-hydroxyethylchitosan (glycol chitosan) is prepared by reaction with 2-chloroethanol in alkaline medium [165]. Glycol chitosan exhibits good water-solubility and self-assembly properties in aqueous media. It was prepared to nanoparticles for drug carrier (paclitaxel and doxorubicin) [166, 167]. In addition, it was used to starting molecule to synthesize other chitosan derivatives with hydrophobic molecules such as cholanic acid [168-175], fluorescein isothiocyanate [176, 177], palmytoil, hexadecyl [178], N-acetyl histidine [179], bile acid [180], and farnesal [181] for biomedical applications, as listed in Table 2.2.

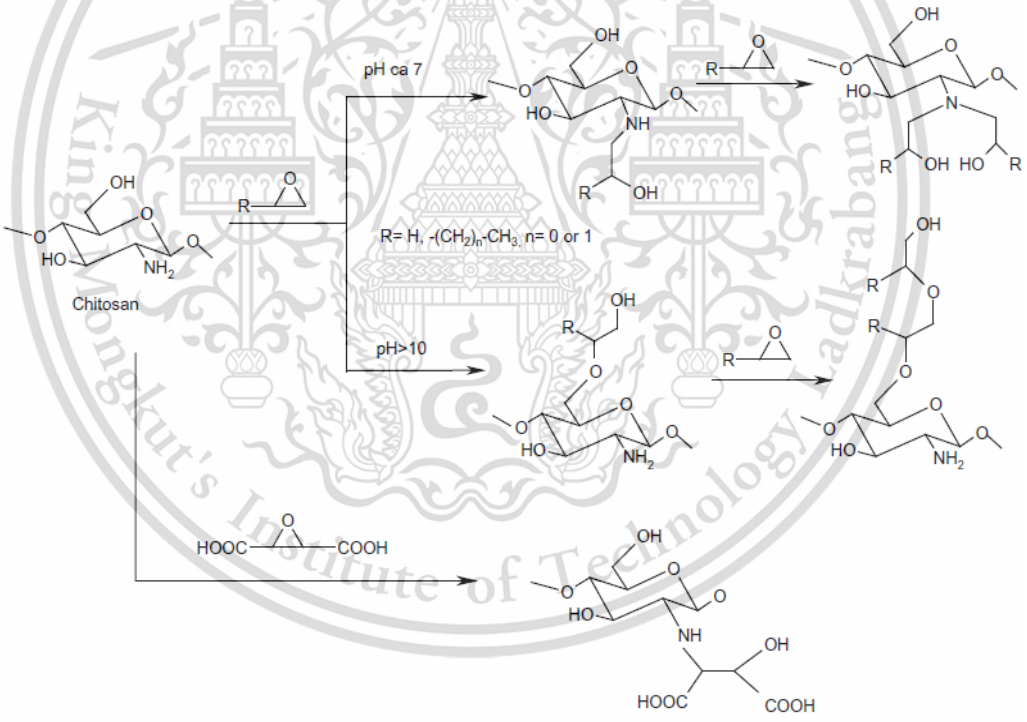

Figure 2.30 Synthesis of hydroxyalkyl chitosan from reacting of epoxide [131]

Table 2.2 Applications of glycol chitosan-based derivatives

Hydrophobic moiety	Application	Ref.
Cholanic acid	Cell targeting, drug delivery (Paclitaxel, peptides, docetaxel, camptothecin, cisplatin) Gene delivery	[168-175]
Fluorescein isothiocyanate	Biodistribution studies in drug delivery, morphological studies	[176, 177]
Palmitoyl, hexadecyl	Gene delivery	[178]
N-acetyl-histidine	Intra-cytoplasmatic drug delivery	[179]
Bile acid	Drug delivery	[180]
Farnesal	Drug delivery	[181]

2.3.4.4 Carboxyalkyl chitosan

Carboxyalkylation of chitosan is a reaction that introduces acidic groups on the backbone resulting in amphoteric polyelectrolytes (that contain both cationic and anionic fixed charges). The derivatives with varying degrees of substitution and charge densities exhibit a flexible controlled pH-dependent behavior that is appealing for the design of pH-responsive materials. Carboxyalkyl chitosan can be synthesized by different reaction conditions as shown in Figure 2.31. Carboxymethyl chitosan is the most common derivative, obtained by reacting monochloroacetic acid under various conditions to obtain selective *N*- and *O*- carboxymethyl chitosan. [182, 183]. In addition, glyoxylic acid is used to selectively form imine bonds at amino groups of chitosan, followed by reductive amination to achieve *N*-carboxymethyl chitosan [184]. Carboxymethyl chitosan has not only water solubility, but also unique properties such as cell adhesion, moisture absorption–retention, antimicrobial properties, and emulsion stabilizing properties [185]. So, it has been widely used in biomedical fields including wound healing [186, 187], tissue engineering [188, 189], drug delivery [190, 191], bioimaging [192, 193] and cosmetics [194, 195].

Sashiwa *et al*. reported the modification of chitosan by Michael reaction with acrylic acid to obtain *N*-carboxylethyl chitosan [14]. Acrylic acid was used as both an acid for dissolving chitosan and a reagent in the reaction. The derivative has good water solubility and biodegradability. Chitosan modified with various acryl reagents e.g., hydroxyethyl acrylate, hydroxypropyl acrylate, acrylamide, acrylonitrile,

PEG-acrylate, and [2-(acryloyloxy)ethyl]trimethylammonium chloride was also described [196]. The results showed the only modified chitosan with acrylic acid ester had good solubility in water. In addition, *N*-carboxyethyl chitosan ethyl ester, which is easily hydrolyzed to free acid, could be used as an intermediate for the substitution of various hydrophilic amines to obtain hydroxyalkyl amines and diamines, without the need for protecting groups [197].

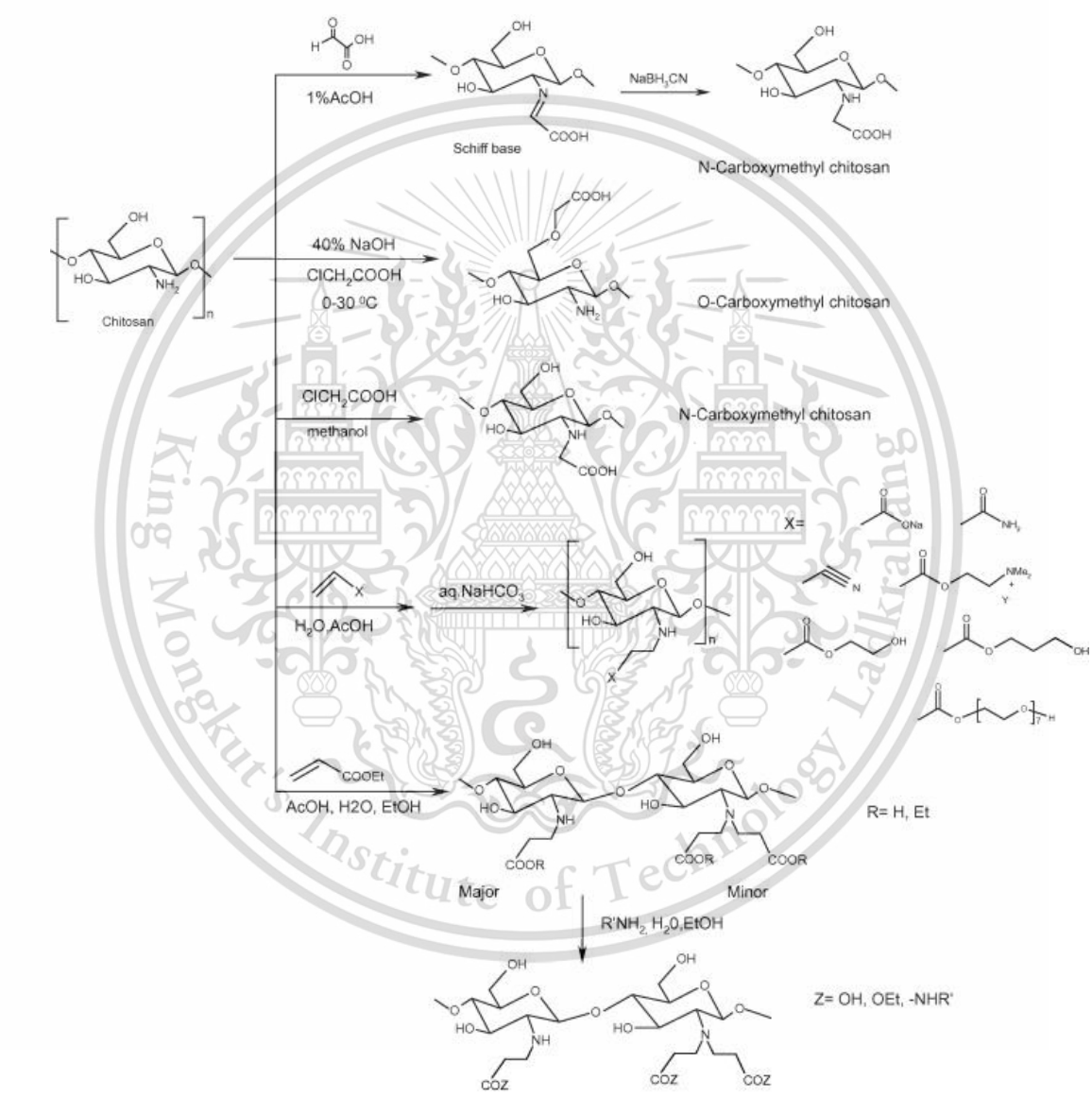

Figure 2.31 Carboxylation of chitosan [131]

2.3.4.5 Thiolated chitosan

Thiolated chitosans or thiomers are chitosan derivatives with thiol functional groups. The derivatives, chitosan–cysteine [198], chitosan–thioglycolic acid

[199], chitosan–4-thiobutylamidine [200], and chitosan–thioethylamidine [201] conjugate, have been reported as shown in Figure 2.32. To bear sulfhydryl groups, the carboxylic groups of cysteine and thioglycolic acid were covalently attached to the amino group of chitosan through the formation of an amide bond using a water-soluble carbodiimide, EDC [198, 199]. The pH condition < 5 was conducted to avoid disulfide formation by oxidation.

The presence of a thiol group on the backbone of chitosan allowed it to have mucoadhesive, permeability, efflux pump inhibiting, antioxidative, and radical scavenging properties [202]. However, pH-dependent reactivity of the derivatives is limited for the physiological intestinal pH due to pKa range of alkyl thiols of 8–10. A pH-independent thiomer derived from 6-Mercaptonicotinic acid (6-MNA) has been developed [203]. Thiol (S–H) and thione (C=S), two tautomeric forms of 6-MNA, can react with a disulfide bond as both a nucleophile and a proton donor, forming disulfide bonds even in the absence of thiolate anions. This derivative exhibited excellent *in situ* gelling properties *via* disulfide bonds without the use of additional oxidizing agents and had a wide pH-reactivity range of 3-6.8. This property has potential for drug delivery applications requiring *in situ* gelation where specific pH such as the vagina. Moreover, the advantages of thiolated chitosan are complexation of metal ions as well as adjustable crosslinking and swelling behavior which applied various fields including pharmaceutical and medical science, wastewater treatment and impregnation of textiles.

2.3.4.6 Chitosan sulfate

Chitosan can be sulfated with a variety of reagents such as concentrated sulfuric acid, oleum, sulfurtrioxide, sulfurtrioxide/pyridine, sulfurtrioxide/trimethylamine, sulfur trioxide/sulfur dioxide, chlorosulfonic acid–sulfuric acid, and others. Examples of sulfating reagents and reaction positions are as shown in Table 2.3. The derivative is attractive in biomedical fields due to its heparin-like structure and anticoagulant and hemagglutination inhibition activities [204-206]. It also has antisclerotic, antiviral, anti-HIV, antibacterial, antioxidant, and enzyme inhibition properties [207-211]. Because of their polyelectrolyte properties, chitosan sulfates can be used as drug carriers in the form of micelles or microcapsules. [212-215]. Additionally, chitosan sulfates have high sorption capacities, which is beneficial for metal ion recovery [216].

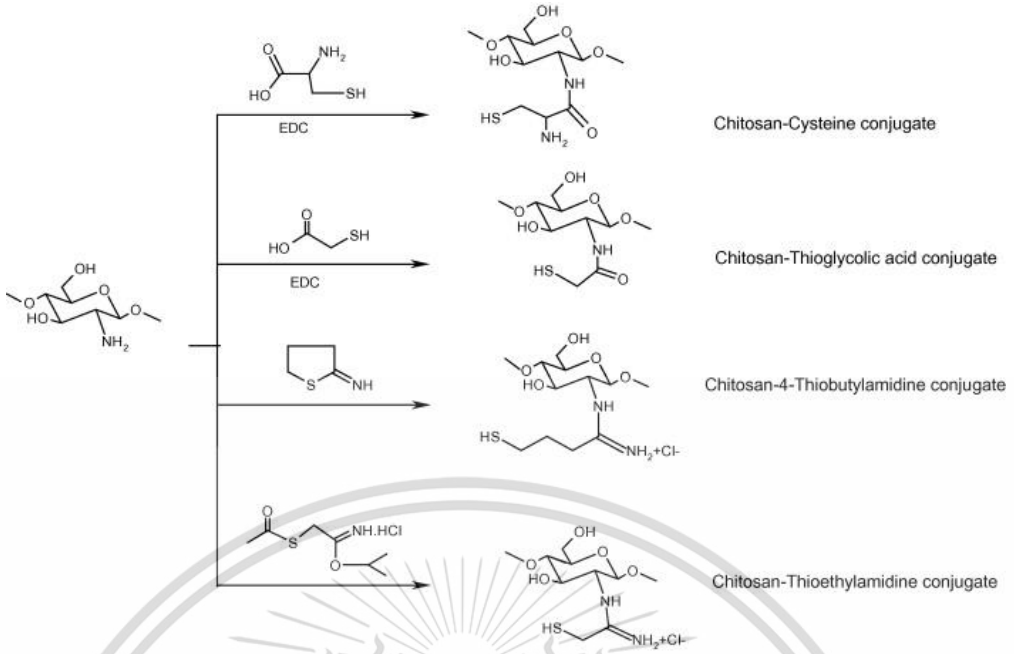

Figure 2.32 Synthesis of thiolated chitosan [131]

Table 2.3 Sulfating reagents and reaction positions of chitosan or chitosan derivatives

Chitosan/chitosan derivatives	**Sulfating reagents**	**Reaction media**	**Sulfating positions**	**Ref.**
Chitosan	Concentrated sulfuric acid	-	O-6, O-3, and N-2	[217]
Low-molecular-weight chitosan	Oleum	Dimethylformamide	O-6 and O-3	[218]
Chitosan	Me_3N-SO_3	Water/Na_2CO_3	O-6, O-3, and N-2	[219]
Chitosan	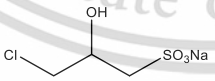	Water	N-2	[220]
Chitosan	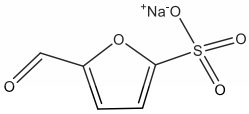	Water	N-2	[216]
6-*O*-tritylchitosan	SO_3-pyridine	Pyridine	O-3 and N-2	[208]
N-mPEG-*N*-octyl chitosan	$ClSO_3H$	DMF	O-6, O-3, and N-2	[221]
Chitosan		8:1 (v/v) acetonitrile/water	N-2	[222]

2.3.4.7 Other chitosan derivatives

As with the water-soluble chitosan example above, chitosan can be grafted with other molecules such as cyclodextrins, dyes, and polyphenol compounds *via* various reactions to produce chitosan derivatives with desired properties. The example of other derivatives is discussed further below.

Cyclodextrins (CDs) are cyclic oligosaccharides that can form complexes with various hydrophobic guests, allowing hydrophobic drugs to be solubilized, stabilized, and transported. Thus, cyclodextrin-linked chitosans have been developed to combine the unique characteristics of both chitosan and cyclodextrin which gained interest in drug delivery system, cosmetics, and analytical chemistry [223]. There are various methods for connecting cyclodextrin and chitosan (Figure 2.33). For example, CD-linked chitosan was prepared by reductive *N*-alkylation of 2-O-formylmethyl-CD could form the host–guest complex with *p*-nitrophenol [224] and 4-*tert*-butyl benzoic acid [225] as well as supramolecular assemblies with adamantane-grafted chitosan [226]. The derivative also showed mucoadhesive features [227].

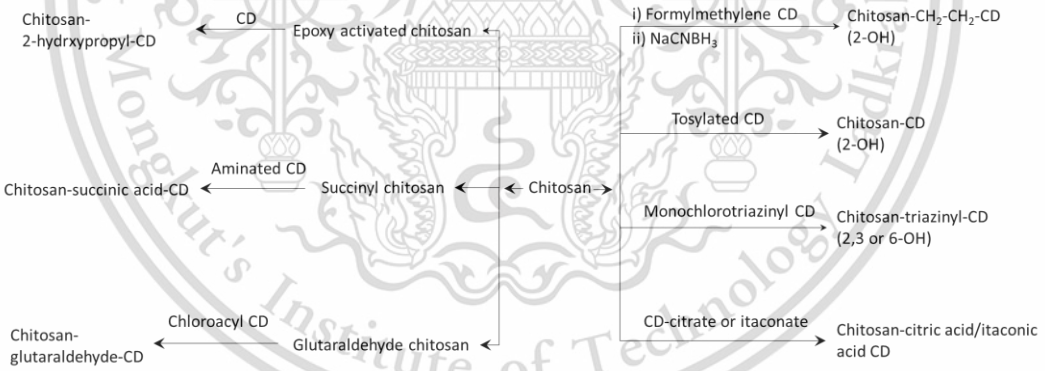

Figure 2.33 Various methods for cyclodextrin-linked chitosan synthesis [131]

Crown ethers have specific molecular structures with high selectivity of complexing metal ions. The synergistic effects of high molecular weight will increase the complexing capacity and selectivity of crown ether-bound chitosans with metal ions. Tang *et al*. reported crown-ether bound chitosan *via* Schiff's-base reaction followed by reduction with sodium borohydride (Figure 2.34). The derivative had not

only good adsorption capacities for Pd^{2+}, Au^{3+}, and Ag^{+} ions, but also high selectivity for the adsorption of Pd^{2+} ions in the presence of Cu^{2+} and Hg^{2+} ions [228].

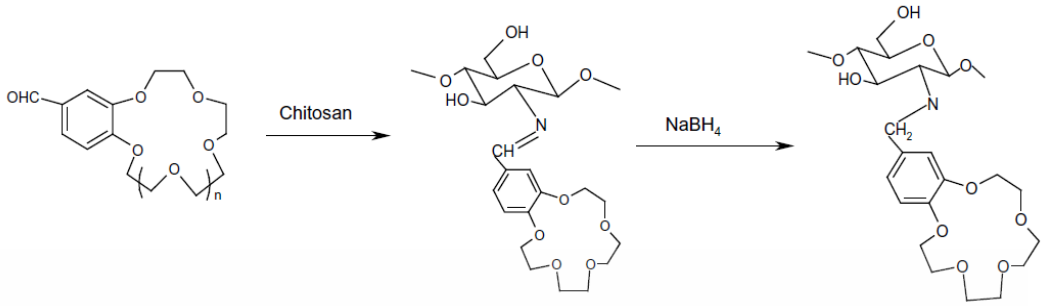

Figure 2.34 Reaction of crown ether-bound chitosan [131]

After cyclodextrins and crown ethers, calixarenes have proven to be an excellent complex capability for ions, organic molecules etc. The first synthesis of calixarene-modified chitosan was reported by Li *et al*. (Figure 2.35). These derivatives showed good adsorption properties for Ag^{+} and Hg^{2+} ions, compared to original chitosan. Despite being insoluble in organic solvents, they can be easily powdered, making them easier to use as an adsorbent than chitosan [229].

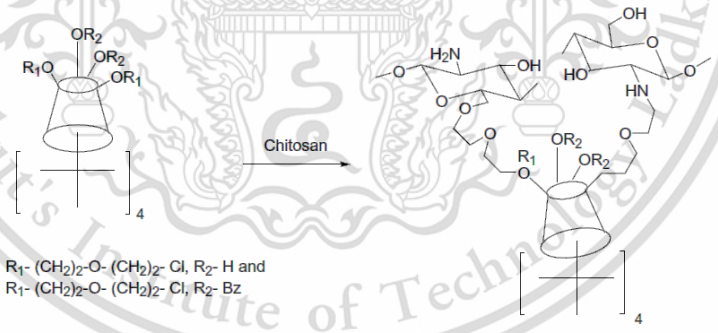

Figure 2.35 Reaction of calixarene-bound chitosan [131]

Polyphenol-chitosan conjugates have gained popularity in recent decades among food industry and biomedicine researchers due to their physicochemical and biological properties, such as increased water solubility and antioxidant activity, which vary and depend on the specific polyphenol and position of conjugation [230]. Polyphenols can be introduced into chitosan using a variety of methods, including activated ester-mediated modification. Woranuch and Yoksan

used a carbodiimide-mediated coupling reaction to attach ferulic acid to chitosan at the C-2 position, as shown in Figure 2.36. EDC activated the carboxyl group to form an *O*-acylisourea intermediate, which was then coupled with the amine of chitosan to yield amide bonds and release isourea as a by-product. When compared to chitosan, the grafted products had a 10% lower crystallinity, were water soluble, and had a higher radical scavenging activity (55%) [231]. Rui *et al*. reported chlorogenic acid-chitosan conjugate by coupling free carboxyl group of chlorogenic acid to amino group of chitosan using 1-ethyl-3-(3-dimethylaminopropyl)-carbodiimide (EDAC). Their increased solubility in distilled water, 1% acetic acid solution (v/v) or 50% ethanol solution (v/v) containing 0.5% acetic acid were found. They also inhibited lipid peroxidation more effectively than free chlorogenic acid [232]. These bioactive polymers have been proposed as having broad potential applications in functional foods.

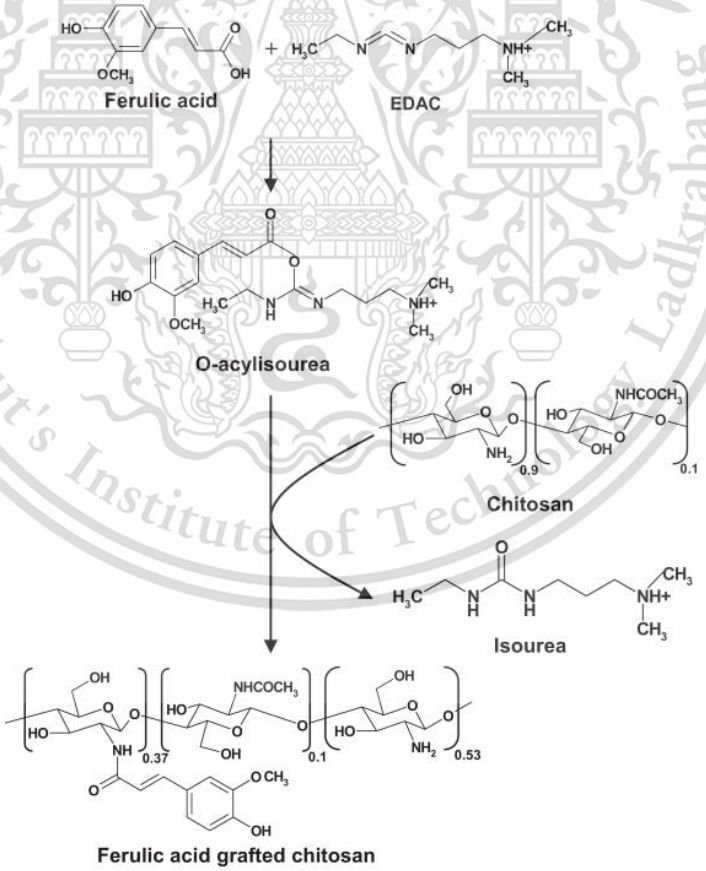

Figure 2.36 Synthesis of ferulic acid grafted chitosan [231]

The Mannich reaction, in addition to the coupling reaction, has been used to selectively graft phenolic compounds to the amino groups of chitosan. Shigemasa and coworkers described a Mannich reaction in methanol of phenolic substrates with formaldehyde and amines. They discovered that the reaction with secondary amines produced the regioselective aminomethylation of 2,4-dihydroxybenzoyl compounds at the C-3 position whereas the reaction with primary amines produced 1,3-benzoxazine derivatives from a subsequent cyclization step. Despite the primary amino groups of chitosan, the cyclic compound was not found from this reaction, obtaining chitosan derivative with benzyl side chain [10]. They also used this reaction to produce chitosan derivatives from 2,4-dihydroxybenzoyl derivatives (Figure 2.37). The chitosan derivatives demonstrated good chitosanase degradability as well as improved solubility in methanol and 2-methoxyethanol. It effectively blocked UVA light, particularly the derivative with phenolic benzophenone side chain, and thus could be used in UV protective coatings [11].

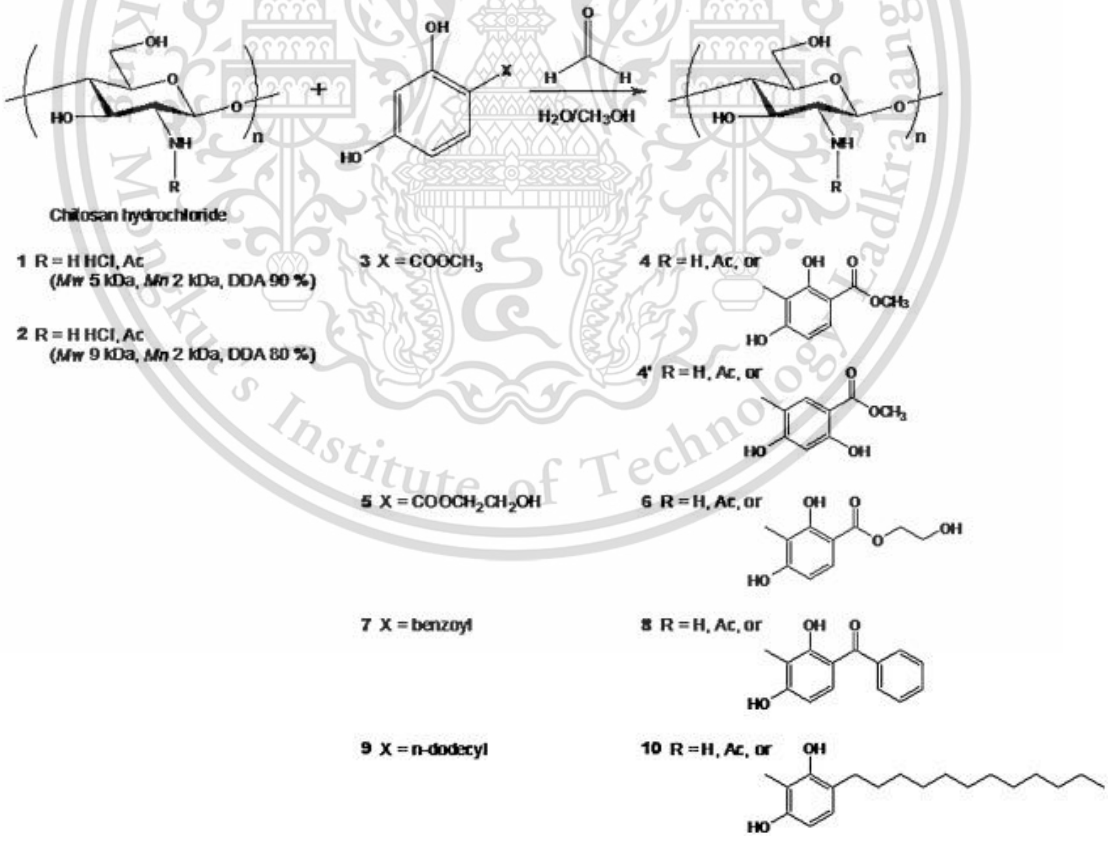

Figure 2.37 Synthesis of chitosan derivatives with 2,4-dihydroxybenzoyl derivatives *via* Mannich reaction [11]

Yu *et al*. also reported the Mannich reaction involving 2.4-dihydoxy-benzophenone and carboxymethyl chitosan hydrochloride to produce multiple-derivatized chitosan. The obtained products were water soluble and the increased molar substitution values could enhance the moisture-retention property and photostability. Because of their high ultraviolet absorption and excellent moisture retention, the grafted products have been suggested as sunscreen ingredients in cosmetic products [13].

Beyki *et al*. reported 8-hydroxyquinoline, a versatile chelating agent for metal separation, anchored onto chitosan *via* the Mannich reaction and prepared to magnetic cobalt imprinted biopolymer by combining with γ-Fe_2O_3 magnetic nanoparticles. Epichlorohydrin was used to link the polymer shell to the magnetic core. After three cycles of sorption and desorption, the biosorbent was stable and repeatable. It also demonstrated highly selective cobalt adsorption in the presence of competing ions [12].

Dye-grafted chitosan was created with the advantages of both dyes and chitosan, such as thermal and chemical stability, good color fastness, biocompatibility, and improved human safety. Two synthetic azo edible colorants, Sunset yellow and Allura red, grafted onto *O*-carboxymethyl chitosan, *via* a chlorosulfonylation in a $SOCl_2$/*N*,*N*-Dimethylformamide chlorination system and a Schotten-Baumann reaction in water/tetrahydrofuran solvent, has been reported by Lv *et al*. [7] The reaction is displayed in Figure 2.38. The highest grafting degree of the two edible colorants could reach up to 29.1% and 33.3%, respectively. The grafted products visibly inhibited the reduction of edible colorant by nicotinamide adenine dinucleotide (NADH) when compared to the colorants alone. This decreased the possibility of non-enzymatic degradation of food dyes in the human stomach and avoided gastrointestinal tract adsorption, thereby improving human safety [7, 233].

Lv and coworkers also reported four polymeric dyes derived from Ullmann condensation of brominated anthraquinone derivatives onto *O*-carboxymethyl chitosan (Figure 2.39). The electronic property and planarity of the substituent group in anthraquinone derivatives clearly affected the adsorption wavelength of prepared polymeric dyes. The polymeric dyes with an electron-donating group and higher planarity exhibited a longer adsorption wavelength and a

darker color. Moreover, the four prepared polymeric dyes were low cytotoxicity on human liver cell lines (LO2) with IC_{50} values more than 7.6 g/L [6].

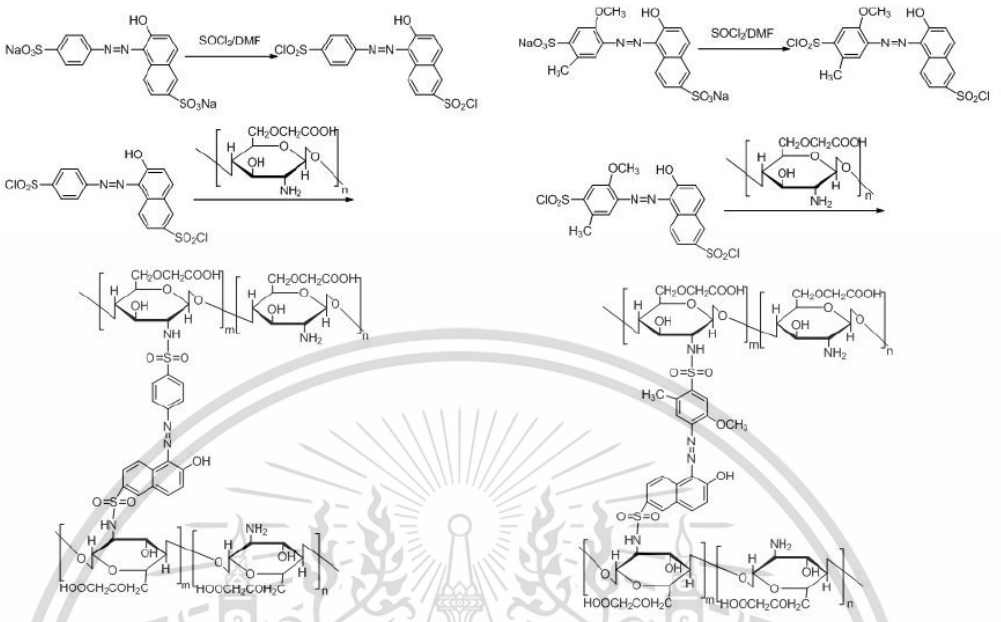

Figure 2.38 Synthesis of dye-grafted chitosan: Sunset yellow (left) and Allura red (right) [7]

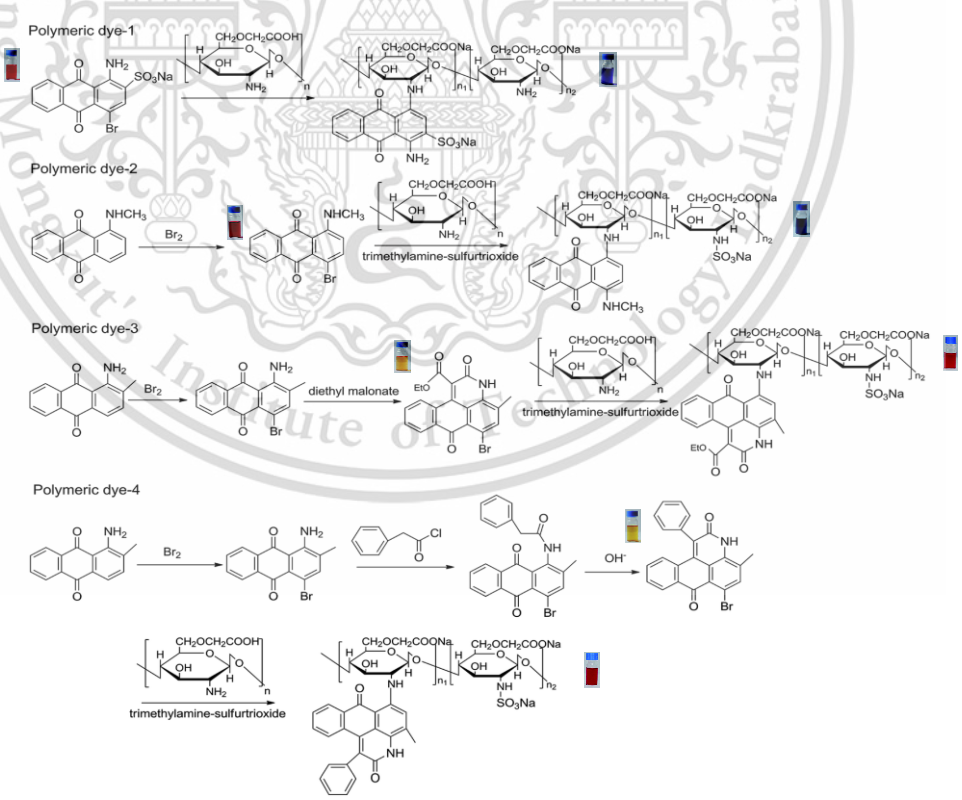

Figure 2.39 Synthetic route of polymeric dyes and color of dyes and polymeric dyes, modified from [6]

Schoolaert *et al*. fabricated halochromic nanofibrous sensors from a blend electrospinning of Methyl Red and Rose Bengal grafted chitosan/poly(ε-caprolactone). Chitosan was modified with carboxyl groups of the dye using coupling reagent to form amide linkages (Figure 2.40) [9]. Because the grafting reaction did not harm the halochromic mechanism of dye, the prepared dye-containing fabrics responded to pH-changes in both aqueous and gaseous media with minimal dye-leaching, allowing it to retain pH sensitivity and color change, similar to the free dyes (Figure 2.41). According to this study, the covalent dye-modification combined with electrospinning, provided a universal method for versatile dye functionalization, resulting in a stable halochromic nanofibrous material for related applications such as protective clothing, agriculture, and wound management.

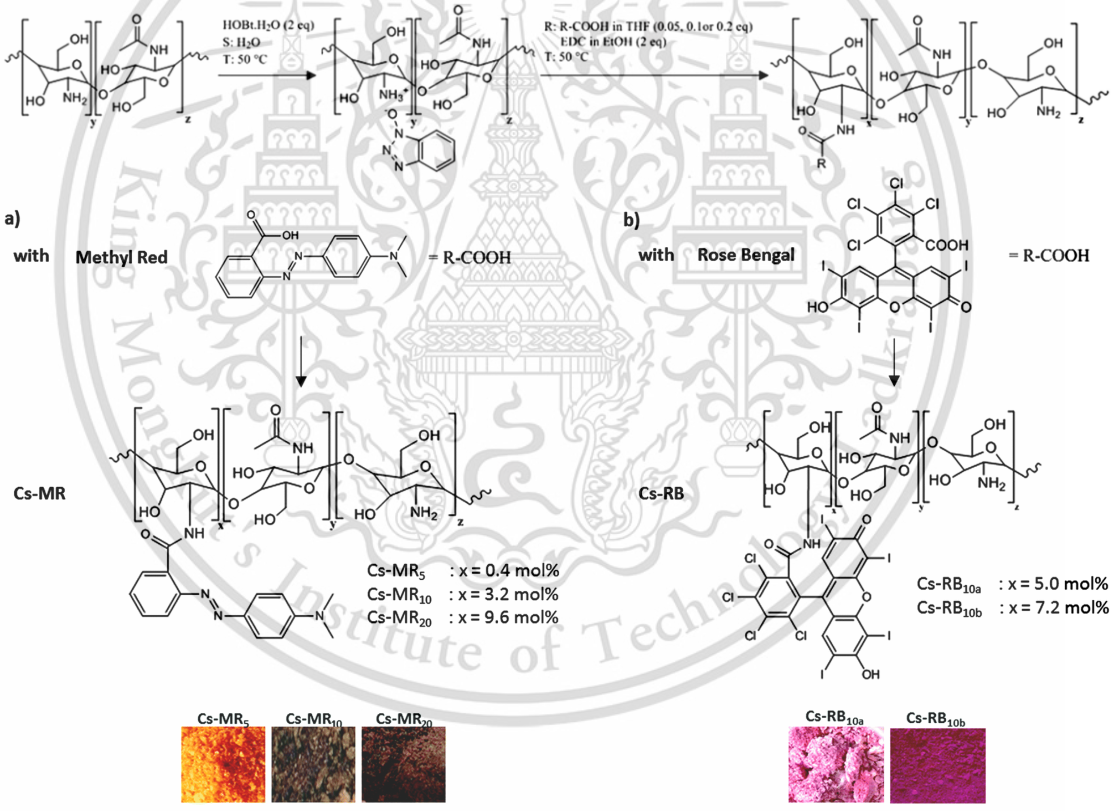

Figure 2.40 Synthetic route for modification of chitosan with a dye possessing a functional carboxyl-group (R-COOH): Methyl red (a) and Rose Bengal (b) [9]

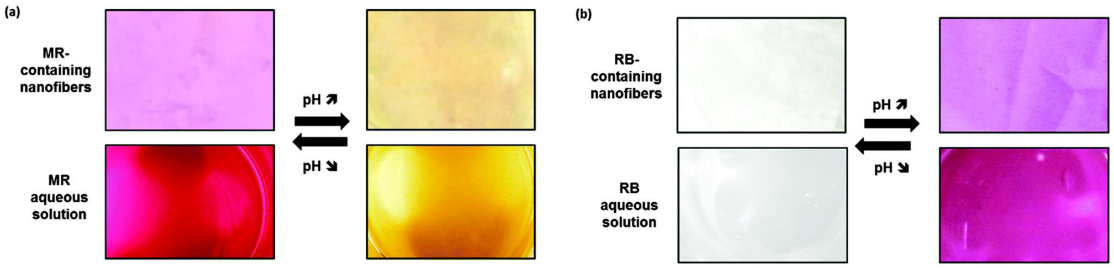

Figure 2.41 Color change with pH of dye-incorporated within a nanofibrous structure and dye solutions: Methyl red (a) and Rose Bengal (b), modified from [9]

2.3.5 Chitosan-based materials

Because of their numerous advantages, chitosan and its derivatives can be processed into a variety of physical forms, including hydrogels, nanofibers, membranes, beads, nanofibers, nanoparticles, microparticles, scaffolds, and sponge-like structures (Figure 2.42). In general, they are combined with synthetic/natural polymers through a chemical reaction with a crosslinker, the functional groups on modified chitosan, hydrogen bonding, hydrophobic association, and electrostatic interactions to improve desired properties [234]. For chemical crosslinkers, linear and aromatic dialdehydes, epoxies, and organic acids can be used. Table 2.4 contains a list of some common chitosan crosslinking compounds. Even though some of them, such as glutaraldehyde, formaldehyde, and epichlorohydrin, are widely used, they may leave a toxic residue in the prepared materials. As a result, a bio-based crosslinker that is both safe and simple to make is gaining popularity. Citric acid, for example, can crosslink by forming amide or ester bonds when heated to high temperatures, as well as by forming ionic interactions with positively charged amino groups of chitosan [235, 236]. Moreover, dialdehyde compounds obtained by oxidizing polysaccharide or modified aldehyde groups to the end chains of polyethylene oxide have recently been extensively developed, resulting in the creation of novel smart materials with mimic functions such as self-healing, injectable, and sol-gel properties [237].

Because of its polycationic nature, chitosan can form polyelectrolyte complexes (PECs) through electrostatic interactions with polyanionic polymers such as alginate, hyaluronic acid, pectin, carrageenan, carboxymethyl cellulose, dextran sulfate, and others [238]. For example, water-soluble chitosan, carboxymethyl

chitosan, can form PEC hydrogels with alginate by adjusting the pH of the mixture to 4-6, which is between the pKa values of their amino and carboxyl groups. The hydrogels formed after being exposed to an acetic acid atmosphere and demonstrated pH-responsive ability, making them suitable for site-specific drug delivery [239]. Moreover, glucono-δ-lactone, a slowly proton release agent, was used to induce the gelation process of the PEC systems [240-243].

Generally, chitosan-based materials are used in a variety of industries due to their required properties, including the food industry, chemical industry, textile industry, medicine, functional materials, and agriculture, as shown in Table 2.5.

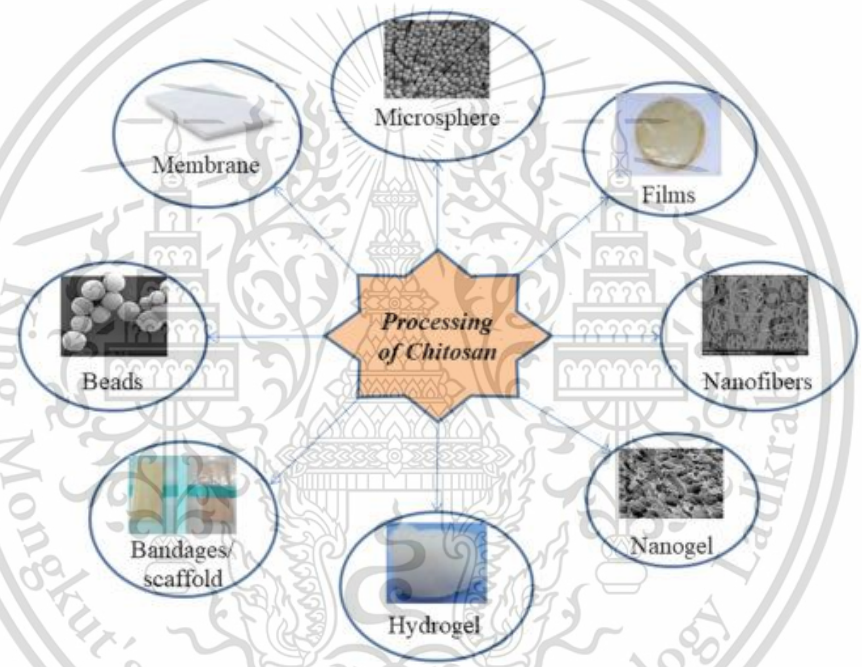

Figure 2.42 Physical forms of chitosan [244]

Table 2.4 Crosslinking agents used with chitosan and bonding type with chitosan

Class	Compound	Bond type	Forms	Applications	Ref.
Aldehydes	Glutaraldehyde	Schiff base, Michael type adduct	- Scaffolds - Films	- Tissue engineering - Wound dressing	[245, 246]
	Glyoxal	Schiff base	- Beads	- Dye removal	[247]
	Oxidized dextran	Schiff base	- Hydrogels	- Tissue engineering	[248, 249]
	Oxidized β-cyclodextrin	Schiff base	- Hydrogels	- Drug delivery	[250]
	Oxidized nanocellulose	Schiff base	- Films	- Food packaging	[251]
	Oxidized xanthan gum	Schiff base	- Hydrogels	- Drug delivery	[252, 253]
	Oxidized sodium alginate	Schiff base	- Scaffolds - Hydrogels	- Tissue engineering - Drug delivery	[186, 254-256]
	Dibenzaldehyde-terminated poly(ethylene glycol)	Schiff base	- Hydrogels	- Drug delivery - Tissue engineering	[257-259]
Epoxies	Epichlorohydrin	Ether, secondary amine	- Membrane - Beads	- Sensors - Heavy metal removal	[137, 260]
	Poly (ethylene) glycol diglycidyl ether	Ether, secondary amine	- Scaffolds - Membranes	- Wound dressing - Lithium batteries	[261, 262]
Organic acids	Citric acid	Ionic, amide	- Fibers - Films	- Drug delivery - Food packaging	[235, 236]
	Oxalic acid	Ionic	- Hydrogels	- Dye removal	[263]
Others	Genipin	Covalent	- Hydrogels	- Drug delivery	[264]
	Tripolyphosphate	Ionic	- Nanoparticles	- Drug delivery	[265]

Table 2.5 Application and related properties of chitosan and its derivatives [133]

Fields	**Example of application**	**Properties**
Food industry	Food packaging preservation	Film-forming property and antibacterial property
	Food preservative	Antibacterial properties
	Beverage clarifier	Flocculation
Chemical industry	Wastewater treatment	Flocculation and chelating and adsorbing property
	Mask and cosmetic creams	Moisture absorption and water retention properties
	Mouthwash	Antibacterial activity
Textile industry	Fiber	Antibacterial and anti-wrinkle
	Dyeing and fixing	Physical adsorption and film-forming property
	Coatings	Film-forming property and antibacterial property
Medicine	Drug carrier	Film-forming, antioxidant, antitumor and biocompatibility
	Wound dressings	Anti-inflammatory and antibacterial properties
	Tissue Engineering	Proliferative, hemostatic, and antibacterial properties
Functional materials	Artificially simulate enzyme	Catalysis
	Liquid crystal materials	Optical and film-forming property
Agriculture	Protect seed	Film-forming property and antibacterial property
	Improve soil	Adsorption and bacteriostatic activity
	Improve crops	Immune and bacteriostatic properties

2.4 Dyes

The hydroxytriarylmethane dye family was studied in this study due to the effect of pH on the chromophore. These dyes are anionic dyes that contain phenolic or quinonoid oxygen atoms in at least two of the carbocyclic rings attached to the central carbon. Subcategories of hydroxytriarylmethane dyes include simple hydroxyarylmethanes, phthaleins, and sulfonphthaleins [266].

2.4.1 Phenolphthalein

Phenolphthalein (PHP) is a well-known acid-base indicator in the phthalein dye class, synthesized through a condensation reaction between phenol and phthalic anhydride (Figure 2.43). PHP is an odorless, white, or yellow-white powder. When the pH is higher than 8.2, PHP changes color from colorless to pink. PHP is used in a variety of applications due to its indicative property in the basic state, including pH sensors [267], halochromic fiber [268], carbonation testing in concrete [269], corrosion sensing coating [270], and colorimetric biodetection [271]. Although PHP can be used as a laxative in medicine, it has been discovered that it has long-term carcinogenic activity [272, 273].

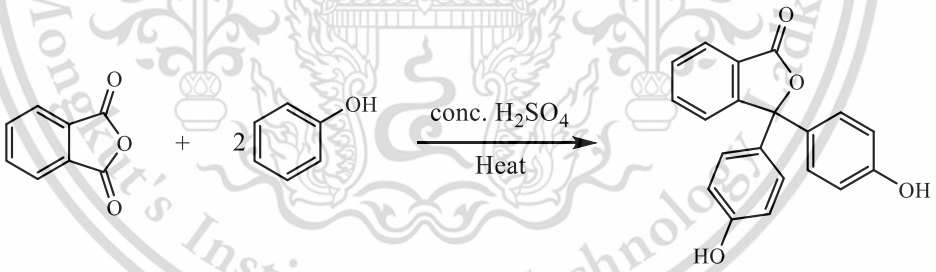

Figure 2.43 Synthesis of phenolphthalein

Furthermore, PHP can form inclusion complexes with β-cyclodextrin. At pH 10.5, the ionized PHP is forced into its lactone structure while the phenolic groups protonate, resulting in a colorless solution (Figure 2.44) [274]. This distinct property has been used to determine the amount of β-cyclodextrin [275] as well as to create multifunctional stimuli-responsive supramolecular materials *via* host-guest interactions as crosslinking points [276].

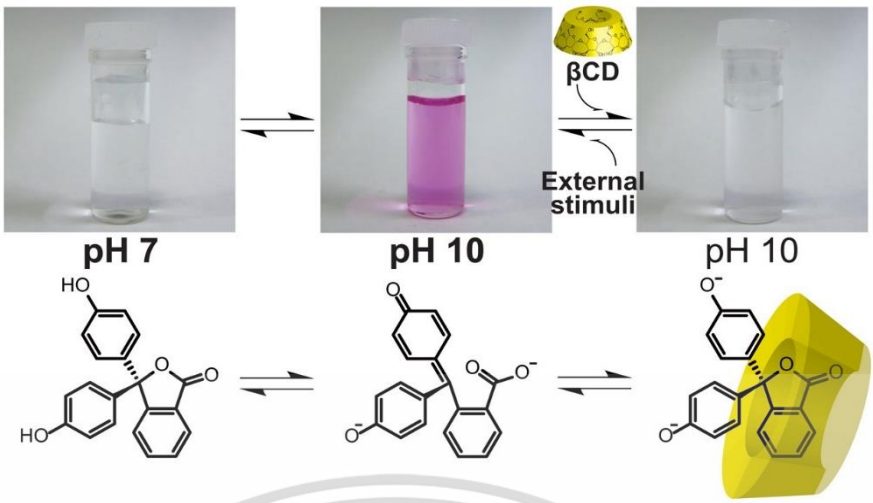

Figure 2.44 pH-dependent color reaction of PHP with β-cyclodextrin [276]

Because there was a free ortho position on the phenol groups, the Mannich reaction was used to attach PHP to the polymer matrix. Zhang *et al*., for example, reported halochromic fiber made by aminating polyacrylonitrile fibers and then immobilizing phenolphthalein using the Mannich reaction [268]. With a pH greater than 10.1, the fibers changed color from pale yellow to violet in a short response time (1 s when soaked in a 20%wt NaOH aqueous solution) (Figure 2.45). The modified fibers did not fade after 300 recyclings, indicating good stability. The authors suggested that the fibers be used for strong alkalinity indicators for skin protection.

Figure 2.45 The modified fiber immersed in various saturated aqueous solutions of (a) $NaHCO_3$, (b) Na_2CO_3, (c) $Ca(OH)_2$, (d) Na_2SiO_3, (e) Na_3PO_4, and 30 wt% aqueous solutions of (f) KOH, and (g) NaOH [268]

2.4.2 Phenol red

Phenol red (PR), also known as phenolsulfonphthalein, is a pH indicator dye that can be made by reacting saccharin and phenol in a single pot, with sulfuric acid acting as a condensing agent (Figure 2.46) [277]. Over a pH range of 6.8 to 8.2, its color gradually changes from yellow to red. When the pH rises above 8.2, PR turns a bright pink (fuchsia) color. The compound exists as zwitterions in crystalline form and in solution under very acidic conditions (low pH), with the sulfate group having a negative charge and the ketene group carrying an additional proton.

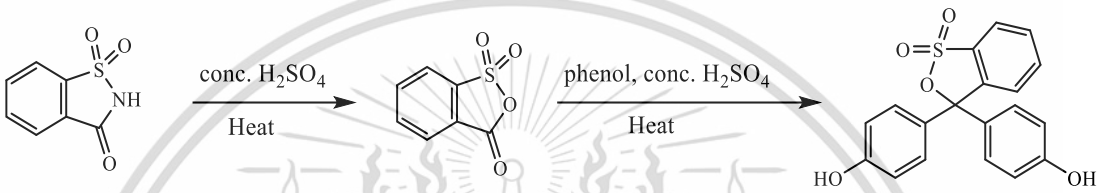

Figure 2.46 Synthesis of phenol red (phenolsulfonphthalein)

PR is widely used in biology, especially indicator for cell culture media. It is, however, removed from some media formulations due to its structural similarity to nonsteroidal estrogen, which induces weak estrogenic activity on breast cancer cells [278]. Furthermore, PR has been reported to be used in photoreceptors, fuel cells, antibacterial agents, display devices, and other applications. [279]. Several studies on the fabrication of pH sensors containing PR *via* adsorption, covalent bonding, or entrapment have been published. However, dye leakage through adsorption and entrapment of PR was discovered in the sensors prepared using the sol-gel process [280, 281]. For covalent binding method, formaldehyde was used to create covalent bonds between phenol red and polyvinyl alcohol (PVA) membranes [282]. These sensors showed fast response times (2–50 s) and long-term stability (at least 3 months). Furthermore, PR was modified with methacrylate and copolymerized with alginate/polyacrylamide to create a colorimetric hydrogel patch for smart wound dressings [283]. The patch changed color in a similar way to free dye, which is used to detect chronic or infected wounds (Figure 2.47).

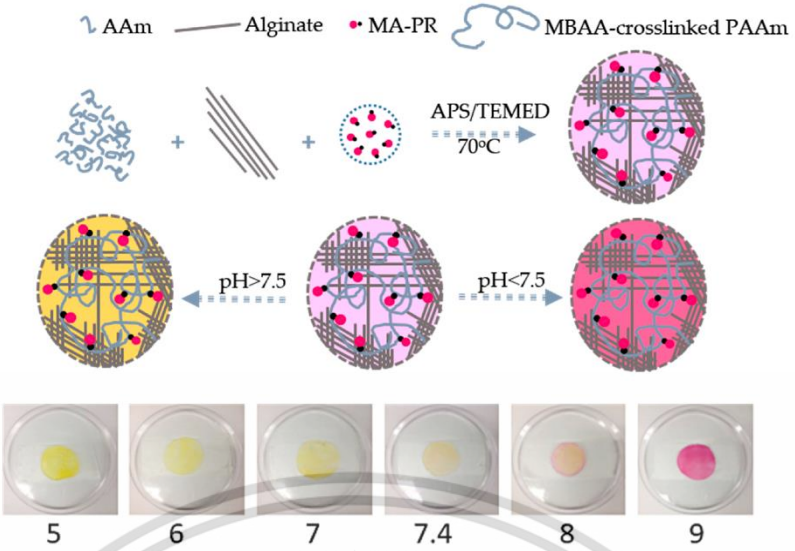

Figure 2.47 Preparation hydrogel patches from methacrylated phenol red (MA-PR), alginate and acrylamide (AAm), and the colorimetric transition of the hydrogel patch in buffer solutions (pH 5-9) [283]

2.4.3 Rosolic acid

Rosolic acid (RA) is a triphenylmethane-based pH indicator. RA can be made by heating phenol and oxalic acid in the presence of concentrated sulfuric acid (Figure 2.48). It transitions from yellow to red at a pH of 6.6-8.0.

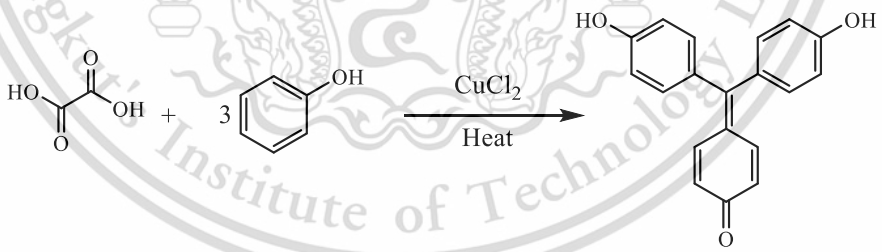

Figure 2.48 Synthesis of rosolic acid

In various countries, RA is used to detect acid neutralizers in milk. Positive results were observed in pink-colored milk samples containing the adulterant sodium hydroxide (Figure 2.49) [284]. Moreover, it has a wide range of chemical, industrial, and medical applications, including lithium batteries, semiconductors, printing materials, thermochromic materials, corrosion inhibitors, antireflective coatings, and

so on [279]. In terms of pH sensors, RA was used in chemosensor arrays developed as artificial sensory systems, similar to other synthetic pH indicator dyes [285, 286]. Attaching RA to polymers for pH sensors, on the other hand, has not been discovered.

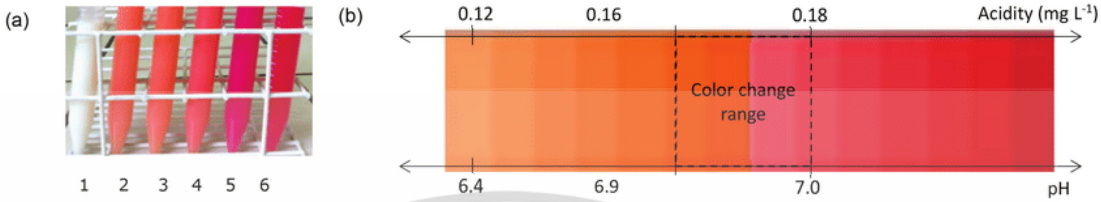

Figure 2.49 Colors observation in the rosolic acid test for the detection of different acid neutralizers in milk (a), and color scale correlated acidity and pH values (b) [284]

According to the literature, these dyes (e.g., PHP, PR, and RA) were chosen for this study due to their pH-indicative properties that are relevant in the physiological pH range. In addition, the free ortho position of phenol groups found in these dyes was expected to allow them to bind with amino-containing polymers, particularly chitosan, *via* the Mannich reaction, resulting in polymeric dyes that still change color when pH is changed.

Chapter 3

Research methodology

3.1 Materials

- Chitosan (CS), Eland Co., Ltd., Analytical grade
- Acrylic acid (AA), Sigma-Aldrich Co., Ltd., Analytical grade
- Phenolphthalein (PHP), Carlo-Erba Reagents, Analytical grade
- Phenol red (PR), Acros Organics Co., Ltd., Analytical grade
- Rosolic acid (RA), Acros Organics Co., Ltd., Analytical grade
- Formaldehyde (HCHO), Carlo-Erba Reagents, Analytical grade
- β-Cyclodextrin (βCD), Wako chemical Co., Ltd., Analytical grade
- Polyacrylamide (PAM) (Mw > 5,000,000), BDH Laboratory, Analytical grade
- D-glucono-δ-lactone (GDL), Merck Millipore Ltd., Analytical grade
- Sodium alginate (SA: M_w 1296 kDa), Acros Organics Co., Ltd., Analytical grade
- Sodium periodate ($NaIO_4$), Acros Organics Co., Ltd., Analytical grade
- Ethylene glycol (EG), Carlo-Erba Reagents, Analytical grade
- Acetic acid (AcOH), Carlo-Erba Reagents, Analytical grade
- Sodium hydroxide (NaOH), Carlo-Erba Reagents, Analytical grade
- Ethanol (EtOH), Carlo-Erba Reagents, Analytical grade
- *N*, *N*-Dimethylformamide (DMF), Carlo-Erba Reagents, Analytical grade
- Isopropanol (*i*-PrOH), Zen Point, Commercial grade
- Acetone ($(CH_3)_2CO$), Zen Point, Commercial grade
- Potassium hydroxide (KOH), Acros Organics Co., Ltd., Analytical grade
- Lithium hydroxide (LiOH), Acros Organics Co., Ltd., Analytical grade
- Urea (NH_2CONH_2), Carlo-Erba Reagents, Analytical grade
- Concentrated hydrochloric acid (HCl), Carlo Erba Reagents, Analytical grade
- Calcium chloride dihydrate ($CaCl_2 \cdot 2H_2O$), Merck Millipore Ltd., Analytical grade
- Sodium carbonate (Na_2CO_3), Carlo-Erba Reagents, Analytical grade
- Hydroxylamine hydrochloride, Carlo-Erba Reagents, Analytical grade
- Potassium hydrogen phthalate (KHP), Carlo-Erba Reagents, Analytical grade
- Citric acid ($C_6H_8O_7$), Carlo-Erba Reagents, Analytical grade

- Potassium phosphate monobasic (KH_2PO_4), Carlo-Erba Reagents, Analytical grade
- Sodium tetraborate decahydrate ($Na_2B_4O_7{\cdot}10H_2O$), Carlo-Erba Reagents, Analytical grade
- Sodium bicarbonate ($NaHCO_3$), Carlo-Erba Reagents, Analytical grade
- Potassium chloride (KCl), Carlo-Erba Reagents, Analytical grade
- Tris(hydroxymethyl)aminomethane ($H_2NC(CH_2OH)_3$), Carlo-Erba Reagents, Analytical grade
- Phosphate buffered saline tablets, Merck Millipore Ltd., Analytical grade
- Diclofenac sodium salt (DCF) Sigma-Aldrich Co., Ltd., Analytical grade
- Potassium bromide (KBr), Carlo-Erba Reagents, Spectroscopic grade
- Tetramethylsilane (TMS), Sigma Aldrich Co., Ltd., Analytical grade
- Deuterium oxide (D_2O), Cambridge Isotope Laboratories, NMR spectroscopy grade
- Dimethyl sulfoxide-d_6 (DMSO-d_6), Cambridge Isotope Laboratories, NMR spectroscopy grade
- Trifluoroacetic acid (TFA), Sigma-Aldrich Co., Ltd., Analytical grade
- Keratinocyte cell line (HaCat) Sigma Aldrich Co., Ltd., Analytical grade
- Dulbecco's modified Eagle's medium (DMEM), Sigma Aldrich Co., Ltd., Analytical grade
- Fetal bovine serum (FBS), Sigma Aldrich Co., Ltd., Analytical grade
- Methylthiazolyldiphenyl-tetrazolium bromide (MTT), Sigma Aldrich Co., Ltd., Analytical grade

3.2 Apparatus

- Fourier transform infrared spectrophotometer (FTIR), Perkin Elmer Inc., Spectrum GX
- Nuclear magnetic resonance spectrometer (NMR), JEOL Co. Ltd., JNM-ECZ-500R/S1
- X-ray diffractometer (XRD), RIGAKU Ltd., Smartlab SE
- Scanning electron microscope (SEM), FEI Co. Ltd., QUANTA 250
- UV-Vis spectrophotometer (UV-Vis), Lab Tech Co. Ltd., BlueStar B
- Colorimeter, Hunter Associates Laboratory, Inc., HunterLab MiniScan XE Plus

- Petri dish, Hycon, K1004
- Hotplate, IKA® Works (Thailand) Co. Ltd., HS-5
- Thermostat, IKA® Works (Thailand) Co. Ltd., Euro-ST B
- Water bath, Thermo Fisher Scientific Co., Ltd., Isotemp
- Microplate reader, Thermo Fisher Scientific Co., Ltd., Multiskan GO
- Balance, Denver Instrument, TC-254
- Dessicator, Thai Pure Science Co., Ltd.
- Oven, Thermo Fisher Scientific Co., Ltd., Isotemp
- pH-meter, Eutech Instruments Pte. Ltd., pH 700
- Micropipette, Scilogex, LLC, Autoclavable Pipettor 200-1000 µL
- Freezer, Liebherr, LGT 2325
- Freeze dryer, ScanLaf A/S Company, CoolSafe™
- Dialysis tube membrane (14,000 cutoff), Sigma-Aldrich Co., Ltd.
- Magnetic bar
- Glassware

3.3 Experiment

3.3.1 Preparation of Carboxyethylchitosan (CECS)

Carboxyethylchitosan (CECS) was prepared *via* a Michael addition reaction of acrylic acid and chitosan, as described by Sashiwa *et al*. [14] with slight modification. In brief, 6 g chitosan was dissolved in 600 mL distilled water containing 4.65 g acrylic acid. The molar ratio of amine group (-NH_2) to carboxylic acid group (-COOH) was 1:2. The solution was stirred constantly at 60°C for 2 days. Afterward, 2.5 M NaOH aqueous solution was added to the solution to adjust the pH to 10–12. The obtained mixture was dialyzed against distilled water for 2 days and then lyophilized to obtain CECS.

3.3.2 Preparation of chitosan-based polymeric dyes (CSPDs)

CSPDs were synthesized by the Mannich reaction of chitosan, formaldehyde, and dye containing phenol groups (PHP, PR, and RA). In brief, 1 g chitosan was dissolved in 100 mL of 1% w/v acetic acid. The 50 mL dye dissolved in DMF, and formaldehyde was then added to the solution. The amount of dye and formaldehyde were prescribed as follows in Table 3.1. The mixture was heated at

60°C for 24 h with vigorously stirring. After that, 0.5M NaOH solution was added dropwise into the mixture to precipitate obtained polymers. The product was collected by filtration and washing with ethanol. Subsequently, the precipitate was purified in two methods:

1. The precipitates were dissolved in 1% acetic acid solution, dialyzed in distilled water for 7 days and then lyophilized.
2. The precipitates obtained were dispersed in distilled water overnight. They were then redissolved in 1% acetic acid solution and subjected to centrifugation at 6000 rpm for 10 minutes to remove any remaining dye residues. The precipitates were washed repeatedly until the filtrate became clear. Finally, the CSPD was obtained by drying the precipitates at 60°C.

Table 3.1 Feed ratios of CSPDs

Formula	CS (g)	Formaldehyde (g)	Type of dyes			Mole ratio*	Purification method**
			PHP (g)	PR (g)	RA (g)		
CS-g-PHP (F1)	1	0.214	0.839	-	-	1:0.5:0.5	1
CS-g-PHP (F2)	1	0.429	0.839	-	-	1:1:0.5	1
CS-g-PHP (F3)	1	0.429	1.679	-	-	1:1:1	1
CS-g-PHP (F4)	1	0.858	1.679	-	-	1:2:1	1
CS-g-PHP (P1)	1	0.214	0.839	-	-	1:0.5:0.5	2
CS-g-PR	1	0.043	-	0.934	-	1:0.1:0.5	2
CS-g-RA	1	0.043	-	-	0.766	1:0.1:0.5	2

*Mole ratios were calculated from amino groups of CS: formaldehyde: dye.

**For CS-g-PHP, method 1 was designated for “F” and method 2 was designated for “P”.

3.3.3 Preparation of water-soluble polymeric dyes (WCSPDs)

Water-soluble polymeric dyes (WCSPDs) were achieved from two methods, i.e., grafting dye onto CECS through Mannich reaction and modifying CSPDs with acrylic acid through Michael addition reaction.

Method 1: Dye-grafted CECS

The products were obtained by grafting dyes onto CECS *via* Mannich reaction. In detail, 2 g CECS was dissolved in distilled water (200 mL). The dye solution (in 100 mL DMF) and formaldehyde were added into the clear solution and stirred at 60°C for 24 h. Subsequently, the reaction was poured into the excess isopropanol. The precipitate was filtrated and redissolved in distilled water (200 mL). The solution was dialyzed against distilled water for 3 days and then lyophilized to obtain the product. The feed ratios are shown in Table 3.2.

Table 3.2 Feed ratios of WCSPDs by method 1

Formula	CECS (g)	Formaldehyde (g)	Type of dyes		Mole ratio*
			PHP (g)	RA (g)	
AA-P1	1	0.117	0.458	-	1:0.5:0.5
AA-P2	1	0.234	0.458	-	1:1:0.5
AA-P3	1	0.234	0.916	-	1:1:1
AA-P4	1	0.468	0.916	-	1:2:1
AA-RA	1	0.023	-	0.417	1:0.1:0.5

*Mole ratios were calculated from amino groups of CECS: formaldehyde: dye.

Method 2: Acrylic acid grafted CSPDs

The method was carried out through the Michael addition reaction, similar to CECS synthesis described in section 3.3.1. In brief, the amount of acrylic acid was dissolved in 200 mL of distilled water. Then, 2 g of CSPD was added to the solution and stirred until it completely dissolved. The reaction was then heated at 60°C for 2 days. Subsequently, the pH of solution was adjusted to 10–12 by adding 2.5 M NaOH. The mixture was purified by dialysis against distilled water for 3 days. The product was dried by lyophilization. The feed ratios are shown in Table 3.3.

3.3.4 Preparation of β-cyclodextrin dialdehyde (βCD-DA)

β-cyclodextrin dialdehyde (βCD-DA) was prepared by oxidizing β-cyclodextrin (βCD) with sodium periodate adapting from the procedure of Lou *et al* [250]. Briefly, βCD (9.08 g) was dissolved in 200 mL distilled water. The amount of sodium periodate was then added into the solution. The reaction was stirred at room temperature in the dark for 0.5 h. After that, the prescribed amount of ethylene glycol and calcium chloride was added to quenching reaction, and the calcium iodate precipitate was obtained. Filtration was used to remove the precipitate. The filtrate was then treated with 10% w/v solution of sodium carbonate before being filtered to remove the calcium carbonate precipitate. The obtained solution was then precipitated into excess acetone. The βCD-DA was obtained by filtration and drying at 60°C.

Table 3.3 Feed ratios of WCSPDs by method 2

Formula	CSPDs (g)			AA (g)
	P1	CS-g-PR	CS-g-RA	
P1-AA	2	-	-	1.638
PR-AA	-	2	-	1.506
RA-AA	-	-	2	1.597

3.3.5 Characterization

- **Solubility test**

Solubility of modified polymers was evaluated at desired temperature at a concentration of 1% w/v in various solvents: distilled water, 1% w/v acetic acid, 1% w/v citric acid, 0.1M HCl, 1.5M NaOH, 1.5M KOH, and 1.5M LiOH. The solubility of CSPDs was also established in LiOH/urea/H_2O solution in weight ratio of 4.8:8:87.2 *via* freeze (-40°C)–thawing (room temperature) process at least twice.

- **FTIR spectroscopy**

FTIR spectra of the products were obtained using the potassium bromide (KBr) technique. FTIR spectra were scanned against an air background at wavenumber ranging from 4000 to 400 cm^{-1} with resolution of 4.0 cm^{-1}.

- **^{1}H NMR spectroscopy**

^{1}H NMR spectra were recorded at 500 MHz with tetramethylsilane (TMS) as internal standard. For CS and CSPDs, CF_3COOH/D_2O was utilized as the solvent, while D_2O was used for CECS and WCSPDs.

The structure of chitosan is shown in Figure 3.1. Degree of deacetylation percentage (%DD) of chitosan was calculated as following equation 3.1.

$$\%DD = 100 - \left(\frac{H_7/3}{H_{2-6}/3} \times 100 \right) \quad (3.1)$$

where H_7 is the integral area of acetyl protons (–COCH_3) of chitosan at about 1.86 ppm and $H_{2\text{-}6}$ is the integral area of chitosan proton at about 3.2-3.8 ppm.

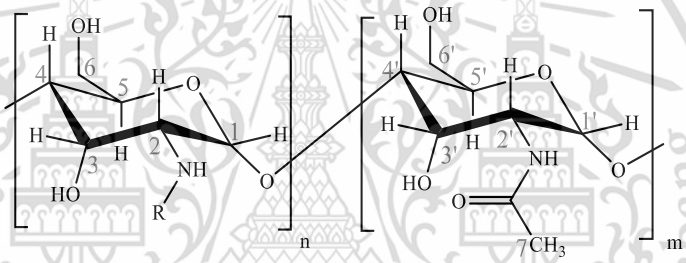

Figure 3.1 Structure of chitosan

In the case of CECS, its structure is presented in Figure 3.2. The degree of substitution percentage of acrylic acid grafted onto chitosan (%DS_{AA}) was calculated as follows equation 3.2.

$$\%DS_{AA} = (1 - DD) \times \frac{3}{2} \times \frac{H_b}{H_7} \times 100 \quad (3.2)$$

where H_b is the integral area of monomer moiety protons (-CH_2-CO-) at about 2.30 ppm, H_7 is the integral area of acetyl protons (–COCH_3) of chitosan at about 1.86 ppm.

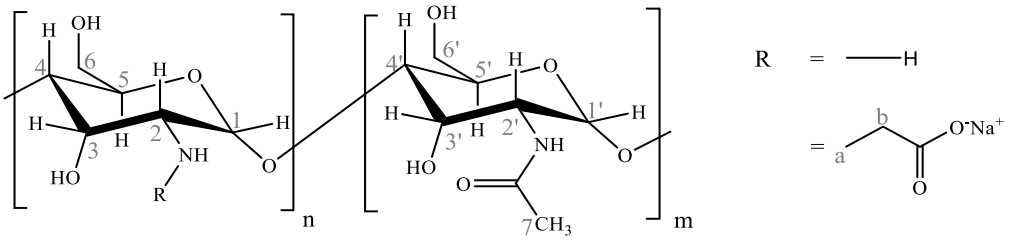

Figure 3.2 Structures of CECS

For CSPDs, their structures are shown in Figure 3.3. The degree of substitution percentage (%DS_{DYE}) of the polymeric dyes was calculated using equation 3.3.

$$\%DS_{DYE} = (1-DD)\times\frac{3}{11}\times\frac{H_{Ar}}{H_7}\times 100 \qquad (3.3)$$

where H_{Ar} is the integral area of aromatic protons of dye at δ 6.7-7.9 ppm, H_7 is the integral area of acetyl protons (–COCH_3) of chitosan at about 1.86 ppm.

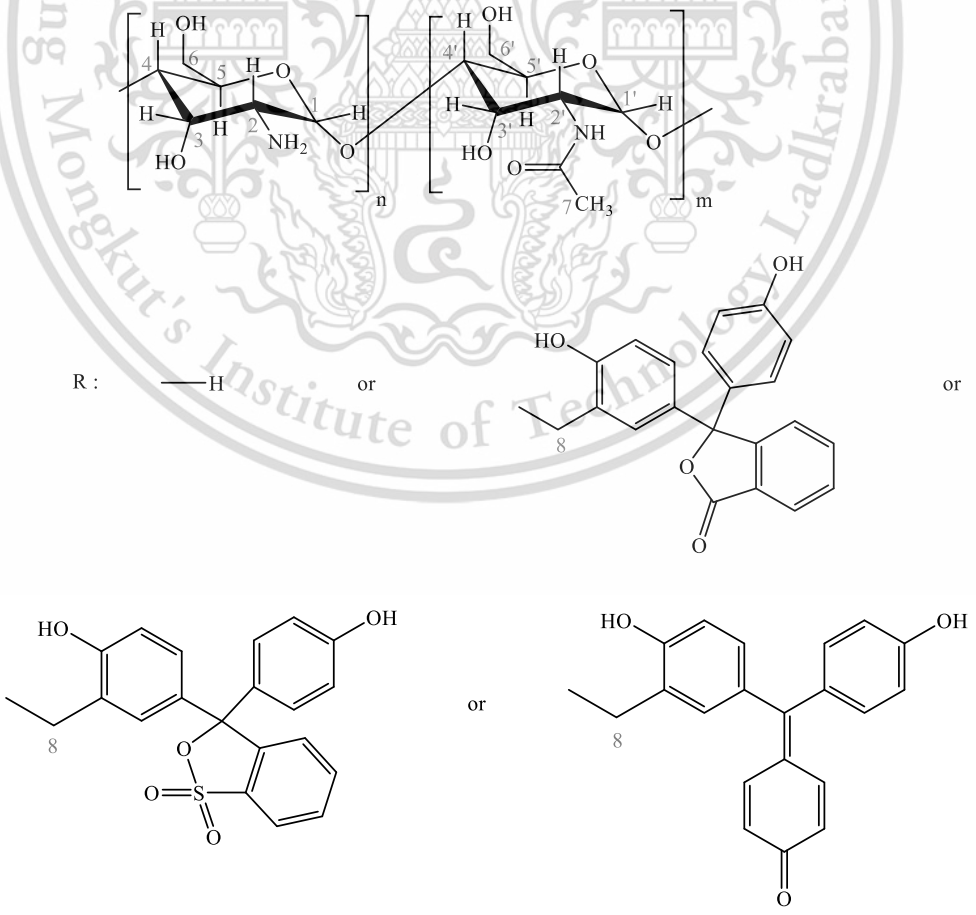

Figure 3.3 Structures of CSPDs

The synthesized WCSPDs, containing the carboxyethyl and dyes groups, were determined the $\%DS_{AA}$ and $\%DS_{dye}$ from the equations 3.2 and 3.3, respectively.

- **UV-vis analysis**

The UV-vis spectra of chitosan and its synthesized derivative solutions (0.05% w/v dissolved in 1% w/v acetic acid solution) were measured between 200-800 nm. To compare with grafting products, the solution containing 0.05% w/v chitosan and 40 μM of free dye was also measured.

- **X-ray Diffraction**

XRD patterns of the samples were analyzed using an X-ray diffractometer, recording over a 2θ of 5–40° with a step size of 0.04° and a step time of 1 s. The crystallinity of samples was calculated by the equation 2.10.

- **Cytotoxicity**

MTT assay was used to determine the cytotoxicity of the derivatives. The extract was made by dissolving 3 mg of sample in 1 ml of DMEM containing 5% FBS. The HaCat and HeLa cells were seeded in a 96-well plate at a density of 6×10^4 cells/mL and incubated at 37°C with 5% CO_2 for 24 h. The culture medium was then removed, and the three replicate extracts were replaced in each well. The cell containing the sample extracts was incubated for 48 h. After that, 10 μl of MTT solution (5 mg/ml) was then added to each well and cultured for 4 h. The purple formazan crystals were dissolved and measured spectrophotometrically at 570 nm with a microplate reader.

3.3.6 Determination of aldehyde contents

The aldehyde content of βCD-DA was determined by the hydroxylamine hydrochloride method [250]. An aldehyde group of the product reacts with hydroxylamine hydrochloride and then releases one hydrochloric acid; it could estimate the aldehyde content by titration against sodium hydroxide. Briefly, 0.1 g βCD-DA was dissolved in 25 mL hydroxylamine hydrochloride (0.25 M) for 2 h at room temperature. Potentiometric titration with a standard NaOH solution at 0.1 M was used to determine the amount of HCl in the mixed solution. When the solution

pH reached 5.0, the titration was terminated. The consumed volume of NaOH solution was determined by the peak value of the differentiated titration curve. The aldehyde content of βCD-DA from the volumes of sodium hydroxide used in the titration by equation 3.4.

$$[CHO] = \frac{V_{NaOH} \times c}{m} \quad (3.4)$$

where *[CHO]* (mmol/g) is the aldehyde content of βCD-DA, V_{NaOH} (mL) is the peak value of differential curve, *c* (mol/L) is the NaOH concentration, and *m* (g) is the weight of βCD-DA.

3.3.7 Preparation of CSPDs-based films

The synthesized CSPDs were utilized to fabricate colorimetric pH-sensitive (CPS) films by blending them with chitosan. Solutions of 1% w/v CSPDs and chitosan were prepared separately by dissolving them in a 1% w/v acetic acid solution. The CSPD solutions were then added to the chitosan solution at a CS:CSPDs weight ratio of 95:5. The mixture was thoroughly stirred at room temperature overnight, cast into Petri dishes, and dried at 60°C. To neutralize the acidic nature of the films, the dried films were immersed in 1 M NaOH and subsequently washed with distilled water until reaching a pH of approximately 7-8. Finally, the films were dried in an oven at 60°C. The films containing CSPDs, namely CS-g-PHP (P1), CS-g-PR, and CS-g-RA, were labeled as CPS-PHP, CPS-PR, and CPS-RA, respectively.

3.3.8 pH-induced color change of the CSPDs-based films

To assess the color changes of the films in response to pH, the prepared films were immersed in various buffer solutions ranging from pH 4 to 12 for 30 min. Subsequently, the films were subjected to absorbance measurements using a UV-Vis spectrometer, scanning the wavelength range of 200-800 nm. Additionally, the color properties of the films were evaluated using a colorimeter based on the CIE-LAB system. The color difference (*ΔE*) between different pH conditions was calculated using equation 3.5.

$$\Delta E = \sqrt{(\Delta L)^2 + (\Delta a)^2 + (\Delta b)^2} \quad (3.5)$$

where ΔL, Δa, and Δb are the differences in related parameters between samples. Each sample was measured in triplicate.

The color stability of the films was investigated by measuring the color of the immersed films over time. UV-Vis was also used to detect the leached dyes in the immersing solutions.

3.3.9 Preparation of WCSPDs-based hydrogel films

Hydrogel films were prepared using a combination of CECS, PR-AA, SA, PAM, and βCD-DA. The process involved dissolving 2% w/v of CECS, PR-AA, and SA in distilled water at 70°C, as well as dissolving 1% w/v of PAM at 90°C. These polymer solutions were then homogeneously mixed in different volume ratios according to Table 3.4. After allowing the mixture to mix overnight, a 2.5% w/v solution of βCD-DA in distilled water was added to the polymer mixture. After 30 minutes, a 3% w/v GDL solution was added to the mixture with continuous stirring, and the resulting mixture was poured into Petri dishes. The gels obtained from the mixture were subsequently dried in an oven at 40°C. The specific composition of the polymers used can be found in Table 3.4. In the case of drug-loaded films, DCF (0.1 g) was added to the βCD-DA solution before combining it with the film mixtures.

3.3.10 Testing and characterization of WCSPDs-based hydrogels

- **Morphology**

The films were fractured in liquid nitrogen and sections of them were coated in gold before being observed and photographed by SEM to examine the morphology of the cross-sections.

- **Swelling behavior and solid remain**

The degree of swelling and solid remains of the films were gravimetrically determined. The weighed films (size of 2×2 cm^2) were immersed in 50 mL buffer solution (pH 5.5, 7.4, and 8.5) at 37°C. The film was weighed again at a predetermined time. The degree of swelling was calculated by equation 3.6. The solid remain was calculated using equation 3.7 after drying the film at equilibrium.

$$Swelling\ degree\ (\%) = \left[\frac{M_s - M_i}{M_i}\right] \times 100 \quad (3.6)$$

$$Solid\ remain\ (\%) = \left[\frac{M_d}{M_i}\right] \times 100 \quad (3.7)$$

where M_s is the mass of the swollen film, M_i is the mass of initial dried film, and M_d is the dry mass of film after immersing.

Table 3.4 Polymer compositions in the WCSPD-based hydrogel films

Formulations	CECS (mL)	PR-AA (mL)	SA (mL)	PAM (mL)	βCD-DA (mL)	GDL (mL)
Non-crosslinked film	30	-	30	20	-	-
Blend-CD	30	-	30	20	20	-
PEC1	15	-	45	20	-	4
PEC2	30	-	30	20	-	4
PEC3	45	-	15	20	-	4
PEC1-CD	15	-	45	20	20	4
PEC2-CD	30	-	30	20	20	4
PEC3-CD	45	-	15	20	20	4
PEC1(PR)-CD	10	5	45	20	20	4
PEC2(PR)-CD	25	5	30	20	20	4
PEC3(PR)-CD	40	5	15	20	20	4

- ***Coloring properties of the films***

To evaluate the color changes of the films in response to different pH levels, the prepared films were immersed in buffer solutions spanning a pH range of 4 to 10 for 3 h. The color properties of the films were then analyzed using a colorimeter, based on the CIE-LAB system.

- ***In vitro* drug release behavior**

To simulate the drug release of the dressing to the skin, DCF-loaded films were released from one side of the film. The film was cut into 2×2 cm^2 squares and

enclosed with a polypropylene board. At 37°C, the sample was floated onto 100 ml of buffer solution (pH 5.5, 7.4, and 8.5), with the film side facing down to the medium's surface. At the time specified, 0.2 mL of the medium was examined and replaced with fresh medium. The amount of released drug was determined from the absorbance at 276 nm in a UV–Vis spectrophotometer, calibrated with standard calibration curve of DCF. Furthermore, the data was fitted to zero order, first order, Higuchi, and Korsmeyer-Peppas kinetic models in order to determine the mechanism of film release [287]. The kinetic models were written in the form of equations 3.8-3.11.

Zero order model: $Q = kt + Q_0$ (3.8)

First order model: $Q = Q_0 e^{kt}$ (3.9)

Higuchi model: $Q = kt^{0.5}$ (3.10)

Korsmeyer-Peppas model: $Q = kt^n$ (3.11)

where Q represents the amount of drug release at time t, Q_0 is the initial drug released amount, k is the rate constant, and n is the release exponent indicative the drug transport mechanism.

- ***Mechanical properties of the films***

The mechanical properties of the films were evaluated using a universal testing machine (LR5K, Lloyd Instrument, UK) in accordance with ASTM D-882 standard at room temperature. Prior to testing, the films were conditioned at 100% relative humidity (RH) for 2 days. Rectangular samples with dimensions of 10 mm × 70 mm and a gauge length of 50 mm were prepared. The samples were subjected to tensile testing at a constant crosshead speed of 50 mm/min using a 100 N load cell. Five replicates were tested, and the average values of tensile strength, elongation at break, and Young's Modulus (at 0 and 2% strain) were determined.

- **Cytotoxicity of the films**

The cytotoxicity of CECS, PR-AA, and PR-AA-based films was evaluated using the MTT assay on human skin fibroblast cells. Confluent monolayers of the cells were prepared in a 96-well plate at a concentration of 1×10^5 cells/mL in Dulbecco's minimal essential medium (DMEM) and incubated at 37°C with 5% CO_2 for 24 h prior to the experiment. The culture medium was then removed, and the cells were treated with replicate solutions of the samples. Following a 24-h incubation period, the cells were stained with MTT to assess cell viability. After incubation for 2 h, the resulting purple formazan crystals were dissolved using DMSO, and the absorbance was measured at 570 nm using a microplate reader. Three replicates of each sample were performed to ensure reliable results.

Chapter 4
Main results and discussion

4.1 Synthesis and characterization of chitosan-based polymeric dyes (CSPDs)

Chitosan (CS) is a cationic polysaccharide that is biocompatible and biodegradable, making it a suitable choice for bio-based polymeric dyes. Moreover, CS contains amino groups that can be easily modified, which enables the creation of functional materials. In this study, CSPDs were synthesized using the Mannich reaction of CS and pH-sensitive dyes containing free ortho positions, i.e., phenolphthalein, phenol red, and rosolic acid. The resulting products were characterized structurally using various techniques such as FTIR, NMR, UV-vis, and XRD. Their solubility and coloring properties were also investigated.

4.1.1 Chitosan-grafted phenolphthalein (CS-g-PHP)

Phenolphthalein (PHP) is a triphenylmethane dye that has two phenol groups capable of reacting with formaldehyde and an amine compound to produce an aminomethyl group *via* the Mannich reaction at the ortho position of the phenol group. In this case, CS can act as an amino group for the Mannich reaction because it contains primary amino groups and can function similarly to a secondary amine that does not have an oxazine ring in its structure [10]. Figure 4.1 shows the chemical scheme for the synthesis of CS-g-PHP. *N, N*-dimethylformamide (DMF) was used as a solvent for PHP to achieve a homogeneous reaction. The resulting products were dissolved in acetic acid and freeze-dried for purification. Four products with varying feed ratios were examined to evaluate the reactivity of the reagent in this reaction (see section 3.3.2).

4.1.1.1 FTIR analysis

The FTIR spectra of CS, CS/PHP mixture, and CS-g-PHPs are shown in Figure 4.2. The characteristic bands of CS were in the range of 3200 to 3500 cm^{-1}, which corresponded to the combination of N-H and O-H group stretching vibrations. Stretch variation bands of 2920 and 2874 cm^{-1} were produced by the $-CH_2$ and $-CH_3$ bonds,

respectively. The peaks at 1651, 1602, and 1324 cm^{-1} were assigned to C=O stretching (amide I), N-H bending (amide II), and C-N stretching (amide III) [288]. Peaks at 1423, 1383, and 1084 cm^{-1} were attributed to $-CH_2$ and $-CH_3$ bending, and C-O stretching, respectively. The spectra for CS-g-PHPs were in the same range as CS, but slight shifts in the peaks of the hydroxyl and amino groups were observed. Additionally, a new peak at about 1748 cm^{-1}, caused by C=O stretching in the lactone group of PHP [289], was observed in the spectra. In comparison to the spectrum of the CS/PHP mixture, the C=O stretching peak of pure PHP was observed at 1737 cm^{-1} [290], indicating that physically mixing CS and PHP had no effect on the structure of PHP. Therefore, the significant shifts at the C=O stretching peak of CS-g-PHPs may indicate the successful grafting of PHP onto the CS backbone. The intensities of C=O (1748 cm^{-1}) and C-O (1264 cm^{-1}) peaks of phenol groups in the CS-g-PHPs spectra increased with an increase in the amounts of formaldehyde and PHP, indicating an increase in the PHP moiety in the products.

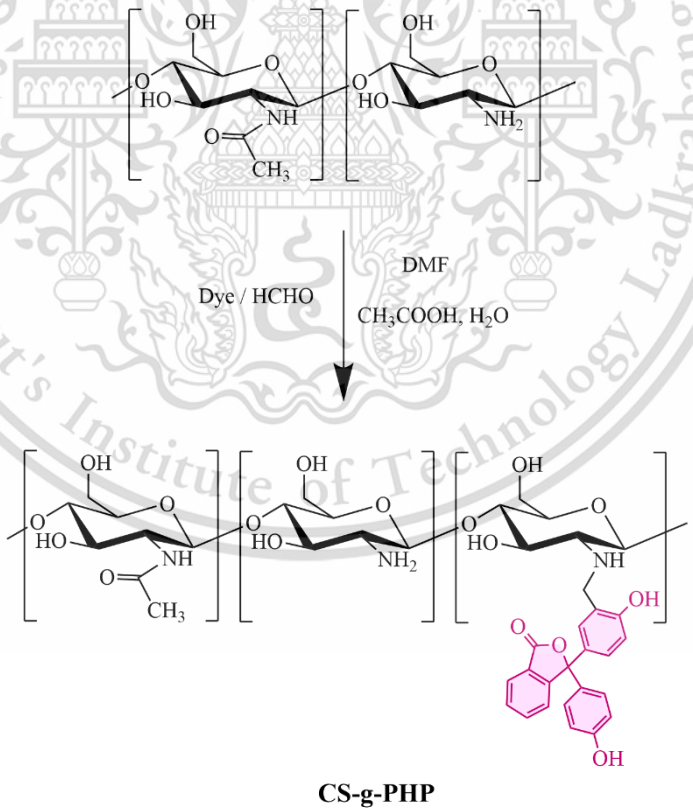

CS-g-PHP

Figure 4.1 Synthesis of CS-g-PHP

4.1.1.2 ^{1}H NMR analysis

The ^{1}H NMR spectra of CS and CS-g-PHPs are shown in Figure 4.3. The characteristic peaks of CS were observed at 1.9, 3.0, and 3.4-3.8 ppm, corresponding to H_7 of N-acetyl glucosamine units, H_2 of glucosamine units, and H_3-H_6 of glucosamine units, as well as $H_{2'}$-$H_{6'}$ of N-acetyl glucosamine units, respectively. In comparison to the CS spectra, new peaks in the range of 6.7-7.9 ppm were detected in all CS-g-PHPs spectra, which were assigned to the aromatic protons of PHP. The result confirmed the successful introduction of PHP into CS. The integral area of these peaks increased with an increase in the feed ratios, reflecting an increase in %DS. %DS was calculated by the proportional integral area of H_7 and H_{Ar} and was found to be 2.4% for CS-g-PHP (F1), 8.5% for CS-g-PHP (F2), 10.8% for CS-g-PHP (F3), and 18.3% for CS-g-PHP (F4).

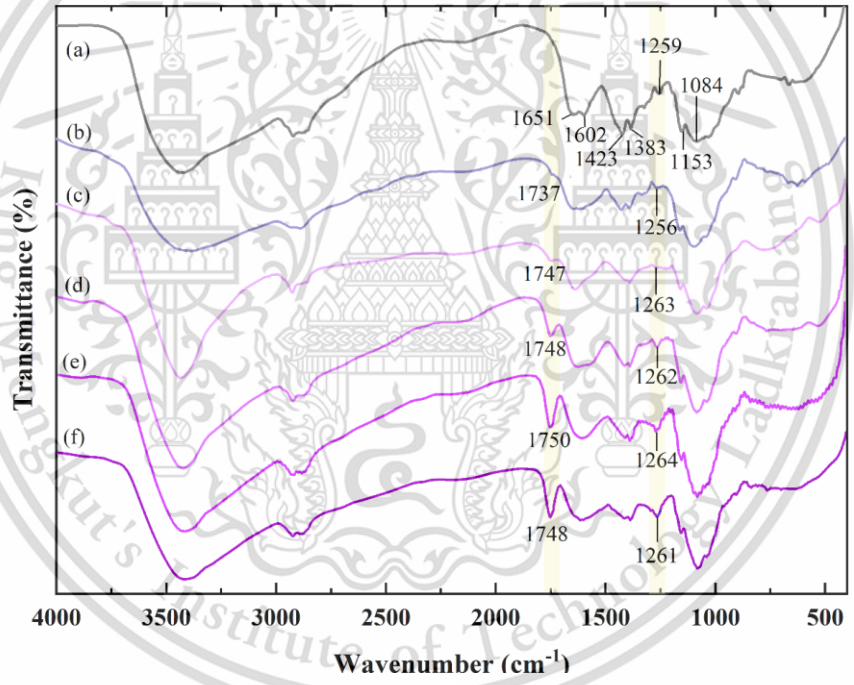

Figure 4.2 FTIR spectra of (a) CS, (b) CS/PHP mixture, (c) CS-g-PHP (F1), (d) CS-g-PHP (F2), (e) CS-g-PHP (F3), and (f) CS-g-PHP (F4)

4.1.1.3 UV-vis analysis

Figure 4.4 illustrates the UV-vis spectra of CS, CS mixed with PHP, and CS-g-PHPs dissolved in 1% acetic acid solution. The absorption peak at 276 nm was observed in the spectrum of CS-g-PHPs, indicating the presence of PHP in acid solution. In contrast, no absorption peak was detected in the CS spectrum, suggesting the

absence of PHP on CS. The absorption intensity was observed to increase with an increase in the feed ratio of formaldehyde and PHP. Additionally, the absorption peak was found to be shifted compared to CS mixed with PHP at 285 nm. This indicated that the Mannich reaction affected the PHP moiety in modified CS, further confirming the success of the reaction.

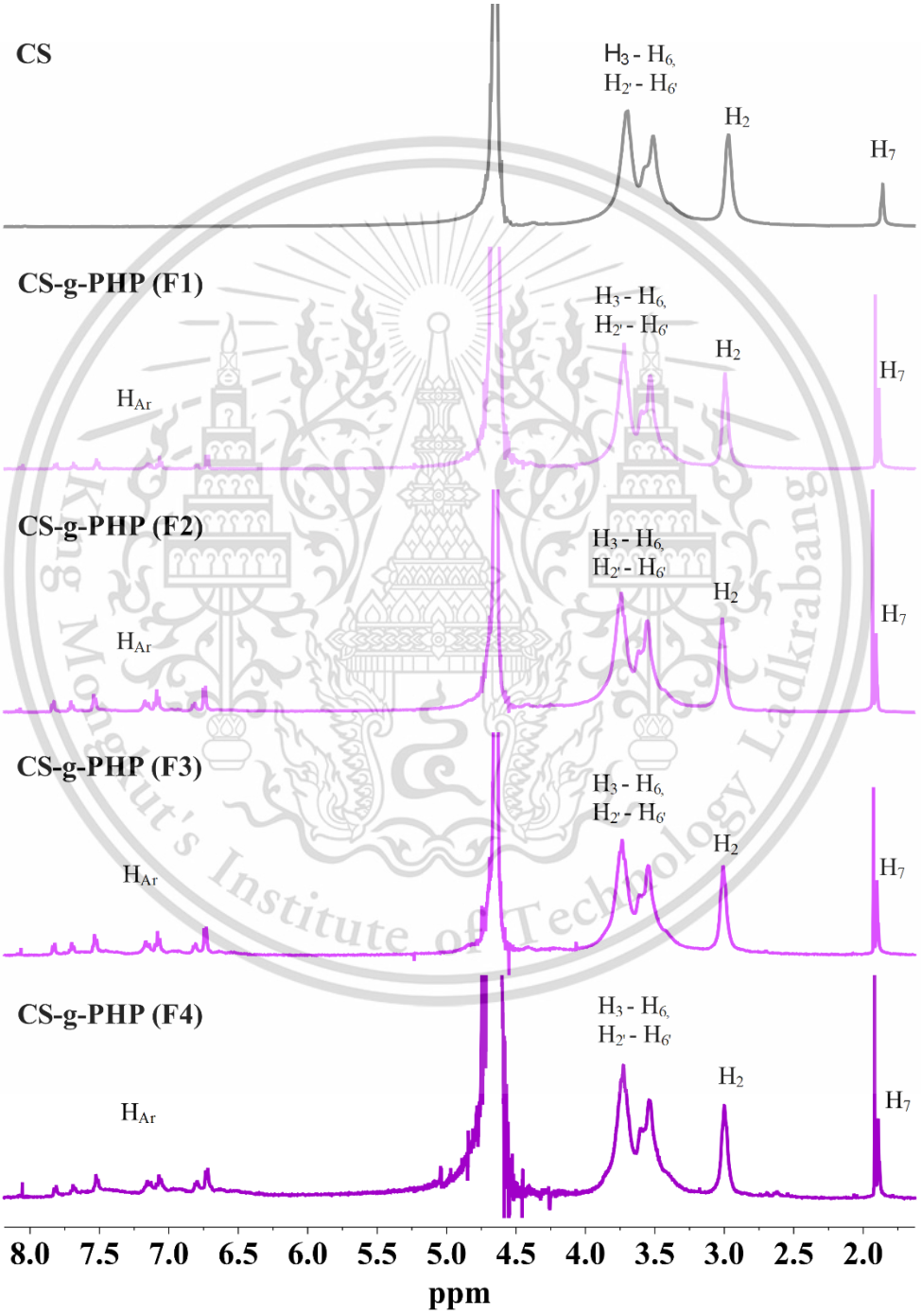

Figure 4.3 ^{1}H NMR spectra of CS and CS-g-PHPs

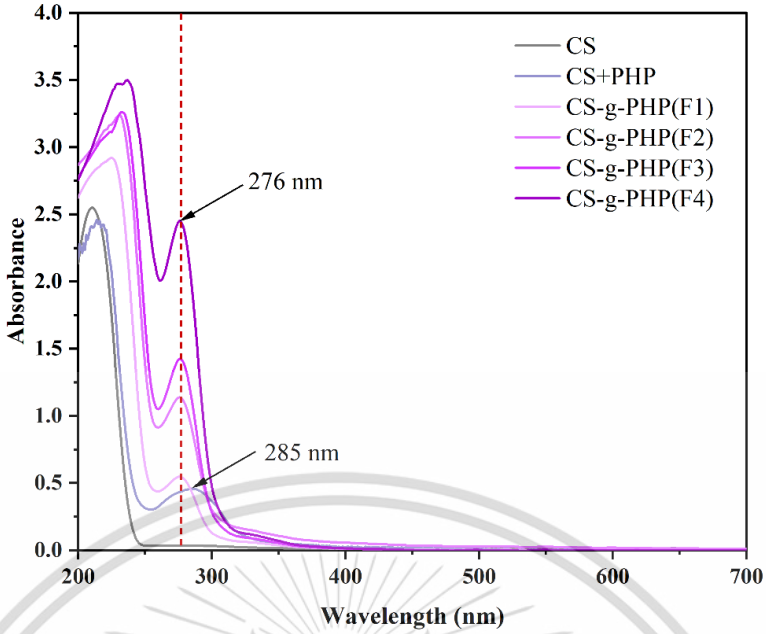

Figure 4.4 UV-vis spectra of CS, CS+PHP, and CS-g-PHPs in 1% acetic acid

4.1.1.4 Solubility

Table 4.1 presents the solubility of CS and CS-g-PHPs under different conditions. It is well known that CS is soluble in acidic solutions due to protonation of its amino groups. Similarly, CS-g-PHPs were found to be soluble in acidic solvents with a pH of less than 5, such as 0.1 M HCl solution, 1% acetic acid solution (w/v), and 1% citric acid solution (w/v). However, the dissolution of CS-g-PHPs with a high DS was difficult, especially for CS-g-PHP (F4) compared to CS. This could be attributed to the formaldehyde-induced crosslinking of the CS backbone. The formaldehyde can react with two amino groups of CS through Schiff base reaction [291, 292]. PHP possesses four ortho positions that can also react with formaldehyde and CS. Thus, CS could be crosslinked through methylene and methylene-PHP-methylene bridges, as shown in Figure 4.5.

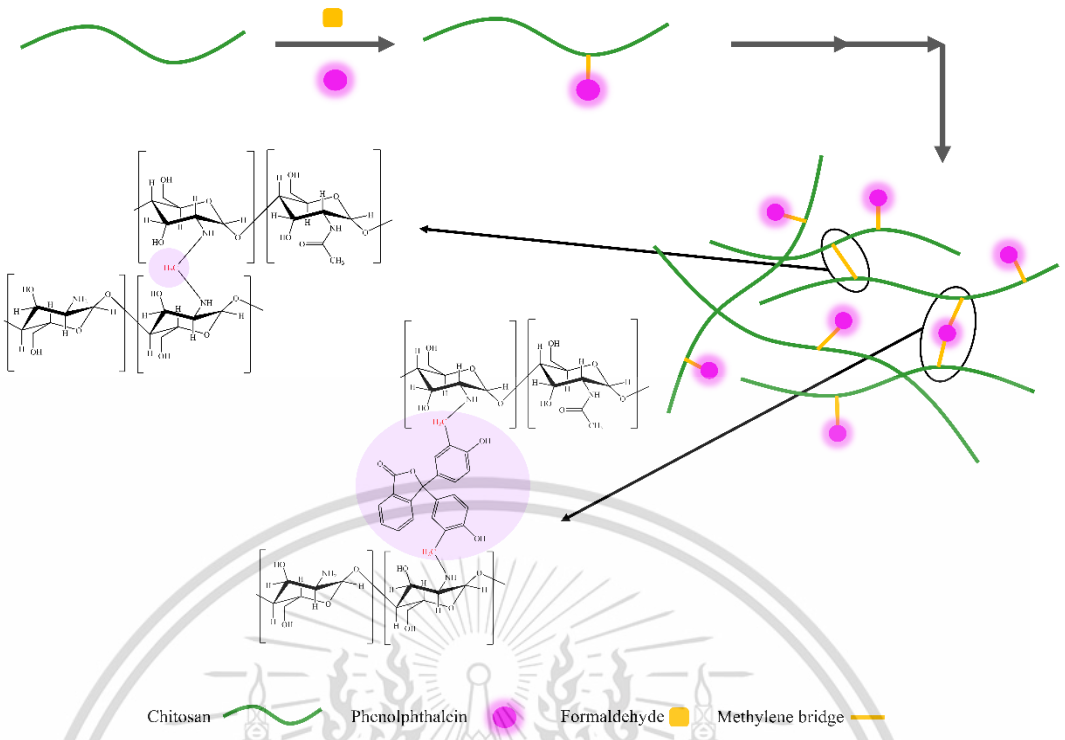

Figure 4.5 Proposed formation of crosslinking between CS, formaldehyde, and PHP *via* the Mannich reaction

Table 4.1 The solubility of CS and CS-g-PHPs

Sample	Solvents										
	0.1 M HCl	1% citric acid	1% acetic acid	1.5 M LiOH		1.5 M KOH		1.5 M NaOH		LiOH/Urea[a]	
				RT[b]	Heating[c]	RT[b]	Heating[c]	RT[b]	Heating[c]	Freeze-thawing[d]	Heating[e]
CS	Soluble	Soluble	Soluble	Insoluble	Insoluble	Insoluble	Insoluble	Insoluble	Insoluble	Soluble	Form gel
CS-g-PHP (F1)	Soluble	Soluble	Soluble	Swell	Swell	Swell	Swell	Swell	Swell	Soluble	Soluble
CS-g-PHP (F2)	Soluble	Soluble	Soluble	Swell	Swell	Swell	Swell	Swell	Swell	Soluble	Soluble
CS-g-PHP (F3)	Soluble	Soluble	Soluble	Swell	Partially soluble	Swell	Partially soluble	Swell	Partially soluble	Soluble	Soluble
CS-g-PHP (F4)	Soluble	Soluble	Soluble	Partially soluble	Soluble	Partially soluble	Soluble	Partially soluble	Soluble	Soluble	Soluble

[a] The alkali/urea system was composed of 4.8 wt% LiOH and 8.0 wt% urea.

[b] The mixture was kept at room temperature for 24 h.

[c] After b process, the mixture was heated up to 70°C for 3 h.

[d] The mixture was frozen at -40°C and thawed at room temperature twice.

[e] After d process, the mixture was then heated up to 70°C for 1 h.

The CS-g-PHPs were observed to disintegrate in alkaline environments (1.5M LiOH, 1.5M NaOH, and 1.5M KOH solutions), as indicated in Table 4.1. The derivative with the highest DS (CS-g-PHP (F4)) was found to be partially soluble after 24 h at room temperature and completely soluble after 3 h at 70°C. In contrast, CS-g-PHP (F3) was only partially soluble after 3 h at 70°C, while CS-g-PHP (F1) and CS-g-PHP (F2) were swollen. This demonstrated that the solubility of CS was affected by the PHP moiety, which caused electrostatic repulsion of carboxylate ions due to lactone ring opening in alkaline conditions (form III and IV – see Figure 4.6). Additionally, the dissolution rate of CS-g-PHP (F4) in 1.5M LiOH solution was slightly faster than that of the other derivatives, possibly due to the smaller size of Li^+ ions, which allowed for greater penetration into the polymers.

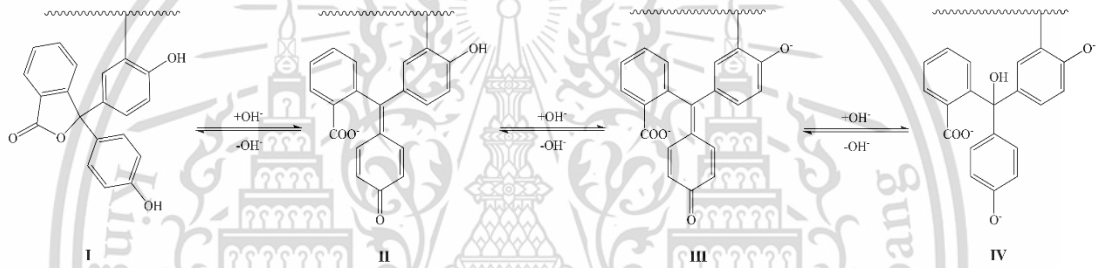

Figure 4.6 Structure changes of PHP

In recent years, a freezing-thawing technique using an aqueous alkali/urea solution has been used to dissolve CS, which resulted in a more stable solution than when acetic acid was used as the solvent [85]. To dissolve CS and CS-g-PHPs, they were dispersed in a LiOH/urea solvent and subjected to the freezing-thawing method. Although the CS derivatives were dissolved in this system similar to CS, the solution's color was pink or dark pink (depending on DS) due to a structural change in PHP in alkaline conditions (refer to Figure 4.7 (a-e)). When heated to high temperatures (70°C), CS in an alkali/urea system forms a gel rapidly due to the inclusion complex between CS and alkali/urea breaking and simultaneously forming inter/intramolecular hydrogen bond among the CS chains [88, 293], as shown in Figure 4.7 (f). However, CS-g-PHPs did not gel and instead resulted in a darker pink solution, as shown in Figure 4.7 (g-j). It was hypothesized that electrostatic repulsion between charged sites ($-COO^-$) decreased the possibility of hydrogen bond formation and gelation. In an alkali/urea system under strong basic conditions, the observed pink color of the solution suggests

the formation of form IV rather than form III. As the temperature increases, the less stable form IV reverts to the more stable form III (darker pink color), resulting in a temperature-induced color change. Similar temperature-induced color changes have been reported in previous studies on PHP [294, 295]. These results suggest that CS-g-PHPs can be dissolved in a variety of conditions, including acidic medium, strong basic medium (pH > 14), and alkali/urea system. In addition, when they were dissolved in an alkali/urea mixture, they displayed thermally sensitive properties.

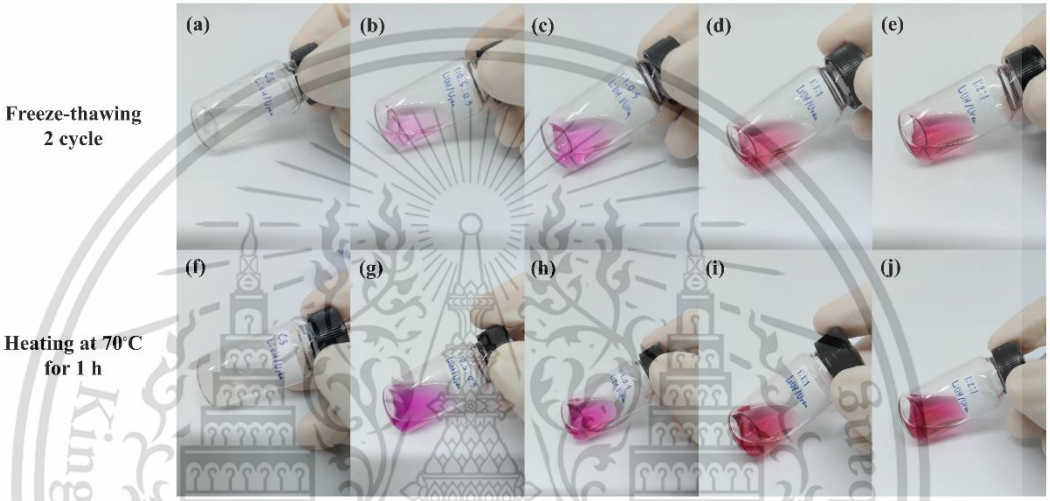

Figure 4.7 CS, CS-g-PHP (F1), CS-g-PHP (F2), CS-g-PHP (F3) and CS-g-PHP (F4) in LiOH/urea solution after freeze-thawing process (a-e) and then treated by heating at 70°C for 1 h (f-j)

4.1.2 Chitosan-grafted phenol red and chitosan-grafted rosolic acid (CS-g-PR and CS-g-RA)

Similar to PHP, PR and RA contain two phenol groups with free ortho positions, making them suitable reagents for the Mannich reaction of CS. The synthesis of CS-g-PR and CS-g-RA followed the same approach as CS-g-PHP, as shown in Figure 4.8. However, when using the same feed ratios of CS-g-PHPs, gelation occurred during the reaction due to crosslinking of the CS mainchain, producing insoluble products (see Figure 4.9). This may be because the sulfonate of PR can interact with the ammonium groups of CS, immobilizing a large amount of PR on the CS structure and facilitating the crosslinking reaction. In the case of RA, even though its structure had no charge in acidic solution, its symmetrical phenol group allowed for attacking at all four ortho positions, resulting in gelation of the entire reaction before the completion of the

reaction period. To overcome this issue, a low feed ratio of CS:formaldehyde:dye (1:0.1:0.5) was employed for these syntheses. Notably, due to the presence of acid residues from the previous section's purification and their tendency to form a gel in the dialysis tube, obstructing the diffusion of residues, these derivatives required reprecipitation in a basic solution and washing until the filtrate was colorless.

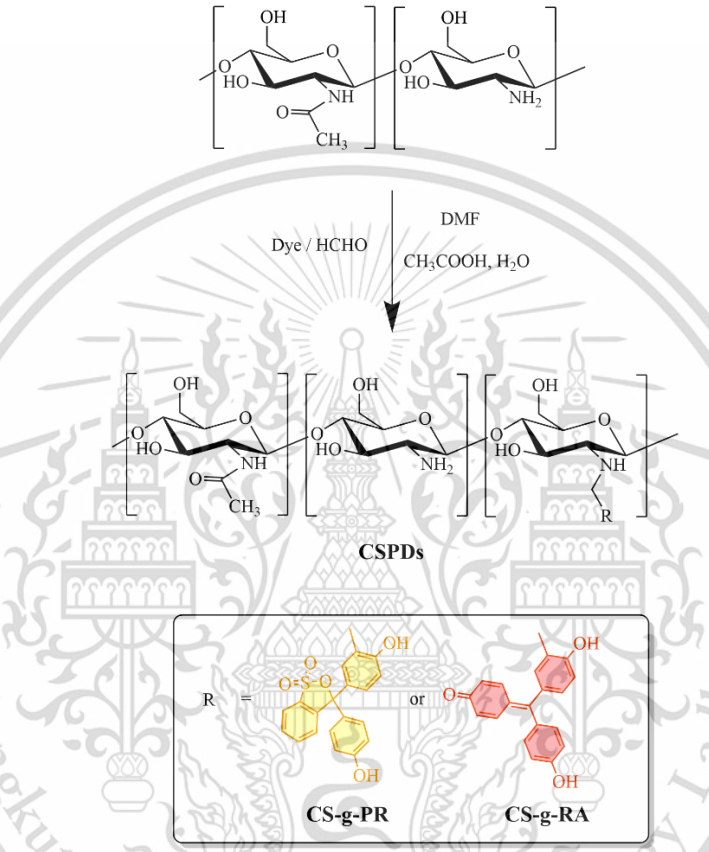

Figure 4.8 Synthesis of CS-g-PR and CS-g-RA

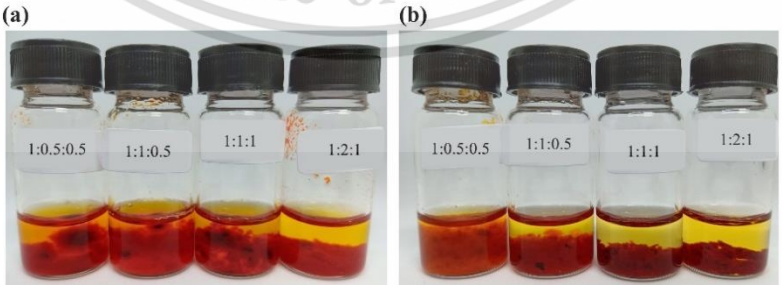

Figure 4.9 Insoluble products: (a) CS-g-PR and (b) CS-g-RA, in 1% w/v acetic acid (The label is feed ratio of amino groups of CS: formaldehyde: dye.)

4.1.2.1 FTIR analysis

Figure 4.10 displays the FTIR spectra of CS, CS-g-PR, and CS-g-RA. In comparison to the CS spectrum, a new peak at 1343 cm^{-1} corresponding to the S=O asymmetric stretching of sulfonate groups was observed in the CS-g-PR spectrum. On the other hand, the CS-g-RA spectrum showed a peak at 1335 cm^{-1}, which was attributed to the O-H bending vibration of phenol groups. In both polymeric dye spectra, a broader peak at ~1500-1650 cm^{-1} and a shoulder at ~1455 cm^{-1} were observed, indicating the C=C stretching of the dye aromatic rings. This study confirms the potential presence of dyes in CS.

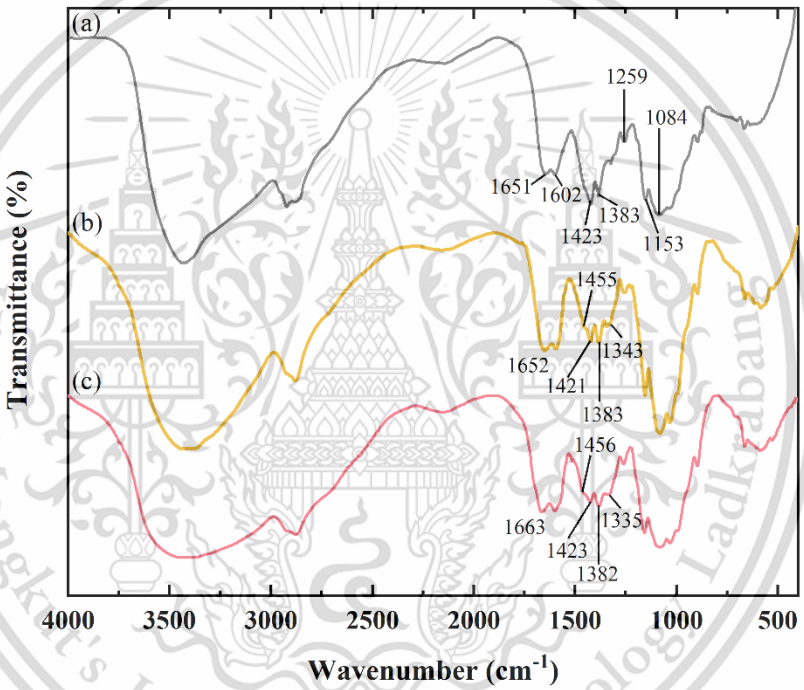

Figure 4.10 FTIR spectra of (a) CS, (b) CS-g-PR, (c) CS-g-RA

4.1.2.2 ^{1}H NMR analysis

Figure 4.11 illustrates the ^{1}H-NMR spectra of CS-g-PR and CS-g-RA. New peaks at 6.5-8.1 ppm for CS-g-PR and 6.6.-7.6 ppm for CS-g-RA were observed, assigned to protons of the aromatic rings for the dyes, compared to the CS spectra. This confirms the hypothesis that the CS-based dyes underwent modification through the Mannich reaction. Additionally, the reprecipitation process caused a reduction in the acetic acid peak at around 2.0 ppm, although a small peak was still present in the spectra. The %DS was calculated based on the proportional integral area of H_7 and H_{Ar}, and was found to be 3.4% for CS-g-PR and 2.3% for CS-g-RA.

To confirm the presence of methylene bridges in all CSPDs, 2D HSQC NMR was used. However, obtaining a higher grafted dye amount at higher concentrations was difficult due to the high molecular weight and possible partial crosslinking of CS. No new methylene peak, including aromatic peaks, was identified in the 2D HSQC spectra (data not shown). Nonetheless, the reaction was carried out with low molecular weight CS (Mw = 9000) and PR at a high feed ratio (1:2:1) as in Arnat's work (unpublished result). The resulting DS was rather high (18.2%), indicating that PR can be more effectively grafted onto short-chain CS. The DEPT-edited HSQC spectrum in Figure 4.12 shows the detection of a new methylene cross-peak at a correlation of 4.75 (^{1}H)-48.56 (^{13}C) ppm, confirming the occurrence of methylene bridges from the Mannich reaction.

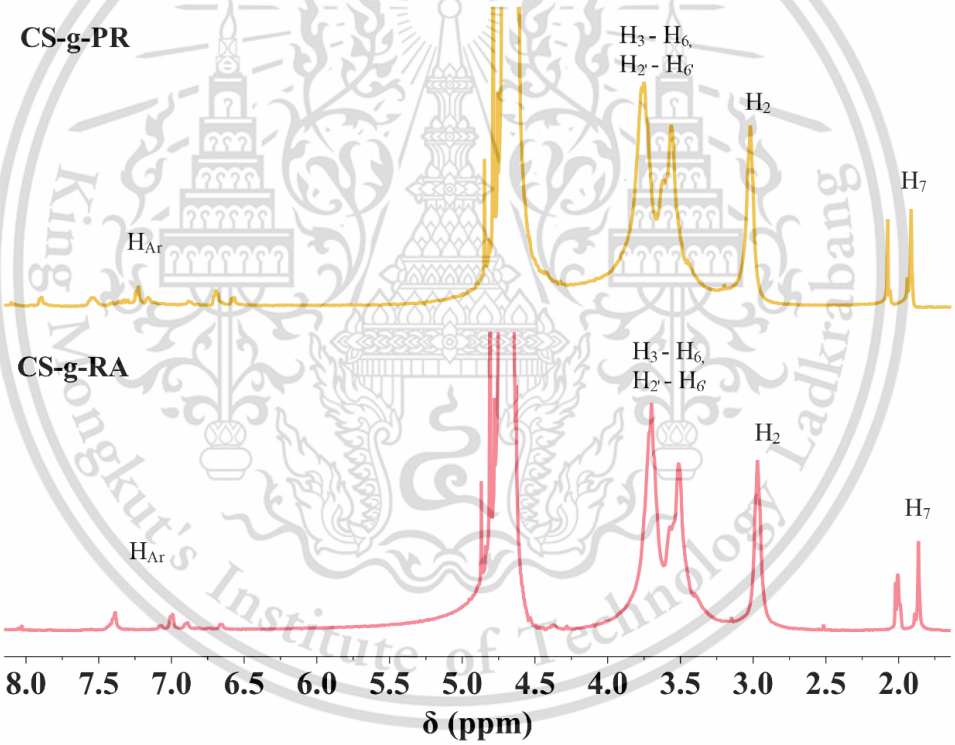

Figure 4.11 ^{1}H NMR spectra of CS-g-PR and CS-g-RA

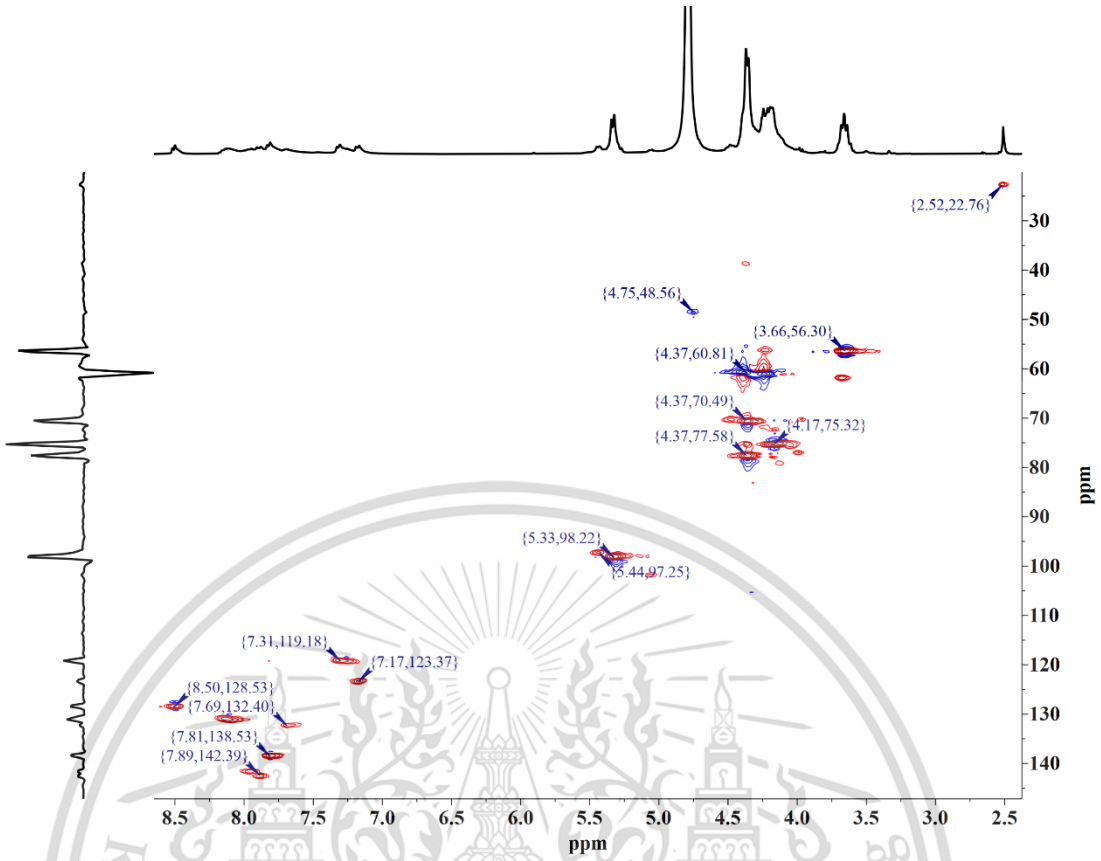

Figure 4.12 DEPT-edited HSQC spectrum of low molecular weight CS-g-PR (%DS=18.2%) at 70°C, 400 MHz. Cross-peaks shown in red correspond to CH and CH_3 groups, blue represents CH_2 groups.

4.1.2.3 UV-vis analysis

Figure 4.13 shows the UV-vis spectra of CS, CS-g-PR, and CS-g-RA dissolved in 1% w/v acetic acid. The characteristic absorption peaks at 445 nm for CS-g-PR and 485 nm for CS-g-RA were observed, whereas no absorption peak was detected for CS. The peaks of CS mixed with PR or RA solutions were found at 433 nm and 475 nm, respectively, indicating red shifts after modification and color changes of the solutions (see insets). This result confirmed the successful grafting of PR or RA onto the CS backbone chain through the Mannich reaction. It also indicated the presence of new auxochrome groups on the dye molecules, resulting in modified structural characteristics and bathochromic shifts [282, 296].

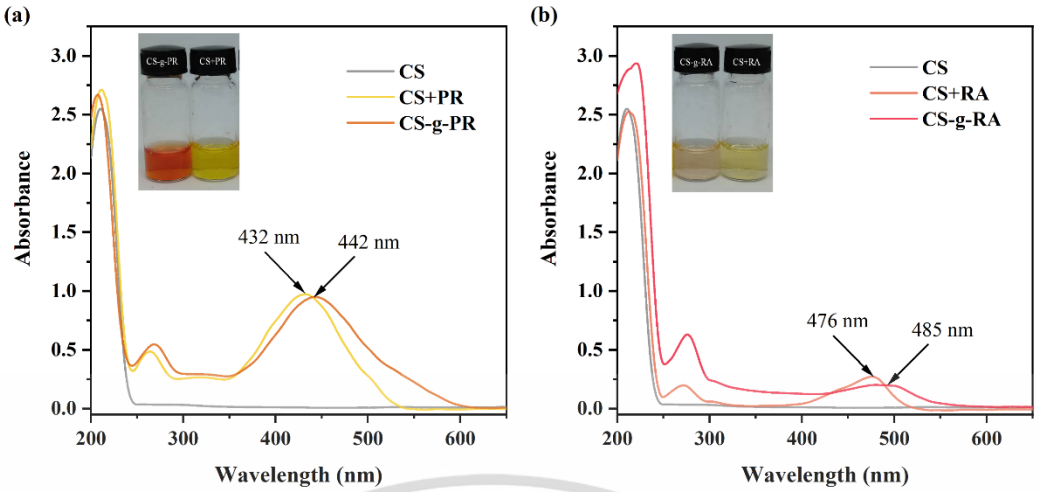

Figure 4.13 UV-vis spectra of (a) CS-g-PR and (b) CS-g-RA in 1% acetic acid

4.1.2.4 XRD patterns

Figure 4.14 presents the XRD patterns of CS and CSPDs. The XRD pattern of CS exhibited three distinct peaks at 2θ = 10.7°, 20.1° and 22.1°, corresponding to (020), (200), and (220) planes of hydrated CS [297]. It was observed that the intensity of the characteristic peaks (2θ = 10.7° and 22.1°) of CS decreased significantly on the CSPDs patterns, indicating successful modifications. This result was consistent for CS-g-PHP (P1), which was purified using reprecipitation, as well as for CS-g-PR and CS-g-RA. The relative crystallinity index (compared to CS) was calculated to be 98.2% for CS-g-PHP (P1), 95.0% for CS-g-PR, and 90.6% for CS-g-RA. It was found that the relative crystallinity index of CSPDs was slightly decreased compared to neat CS, indicating that the modification did not significantly affect the crystalline nature of CS.

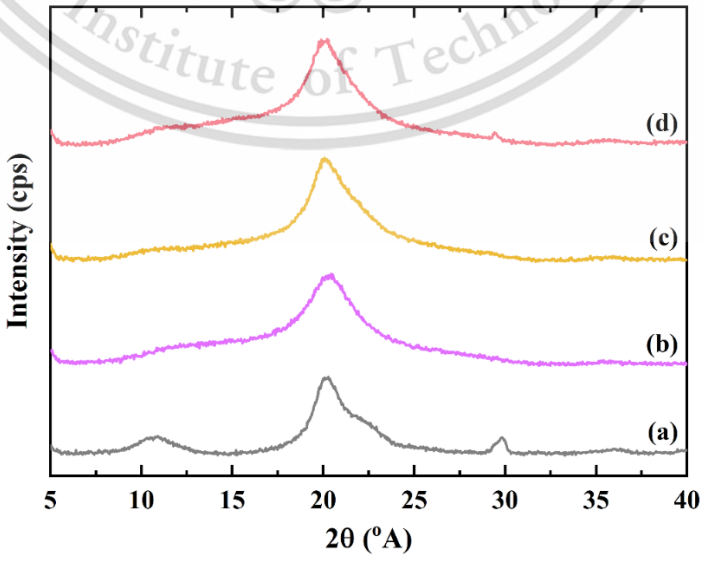

Figure 4.14 XRD patterns of (a) CS, (b) CS-g-PHP (P1), (c) CS-g-PR, and (d) CS-g-RA

4.1.2.5 Solubility

Figure 4.15 illustrates the solubility of CS and CSPDs in water at various pH values, as determined by percentage transmittance (%T). It was found that CS had high %T (~99%) in the pH range of 2-6 and started to form an insoluble form at pH > 6.2. When pH > 6.5, %T remained constant at ~34%, indicating that CS became insoluble, which corresponds to the pKa of CS (~6.3). For CSPDs, they showed a similar trend to CS, suggesting that the attached dye moiety did not significantly affect the solubility.

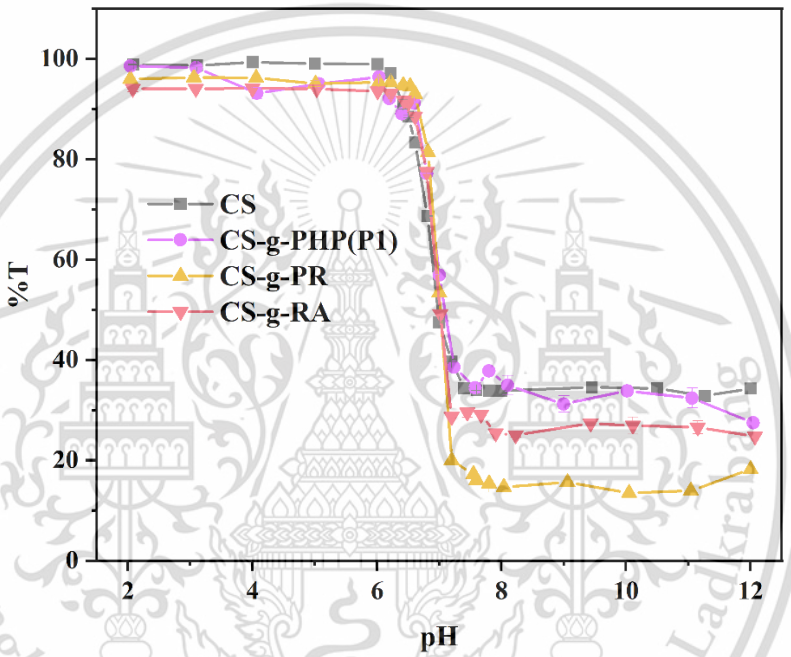

Figure 4.15 Water solubility of CS and CSPDs

4.1.2.6 Cytotoxicity of CSPDs

PHP was previously used as a laxative [298] and to treat amyloid-associated diseases [299], but it is no longer used in medical applications due to its long-term carcinogenic activity [272, 273]. PR has been utilized as a pH indicator for cell culture and hydrogen peroxide detection and has shown no toxicity to mammalian cells [300]. However, PR has been found to be toxic to HeLa cells in the presence of carbon nanoparticles due to their ability to deliver PR into cells, resulting in cell death [301]. RA, on the other hand, has no effect on the toxicity of vascular endothelial cells and can strongly induce heme oxygenase-1 (HO-1) [302]. Since these dyes were grafted onto CS, it was expected that they would exhibit low toxicity, which is a benefit of

polymeric dyes. However, some chemical residues may be harmful to cells. To assess the cytotoxicity of the polymeric dyes to HaCat and HeLa cells as an *in vitro* model, the MTT assay was performed. Figure 4.16 showed that the cell viability of CS and CSPDs to both cells was above 80%, indicating non-toxicity. Additionally, CS-g-PHP (P1) and CS-g-RA demonstrated cell viability greater than 100%, implying cell proliferation in the medium.

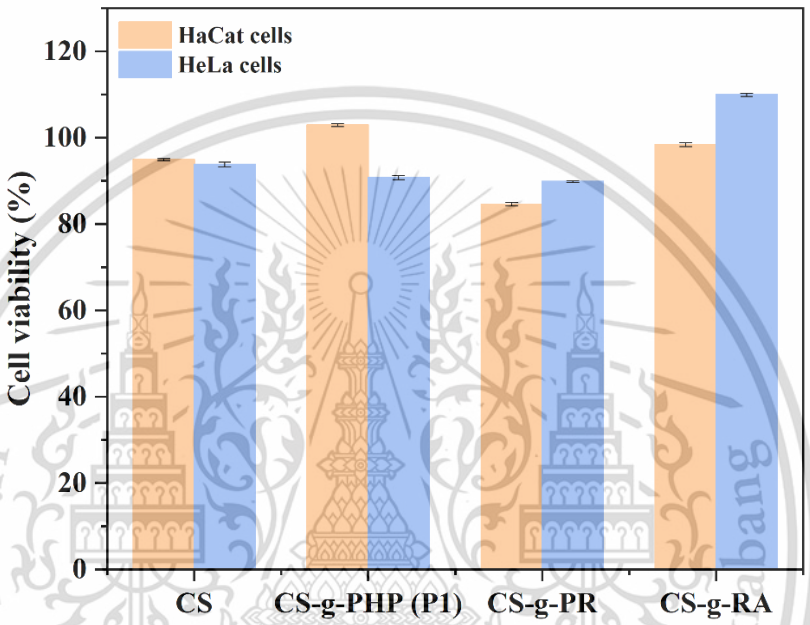

Figure 4.16 Cell viability of CS and CSPDs

4.1.3 Coloring properties of CSPDs

Figure 4.17 illustrates the color change of CS-g-PHP (F2) in various pH buffer solutions. The color was observed to change to pale pink at pH 8.6 and turn deep pink in the pH range of 10.4-11.6. At pH 13.0-14.0, the color faded, but not as much as the PHP solution (Figure 4.18). The changes in color can be explained by the deprotonation of the PHP moiety to form the pink conjugated quinonoid structure (II and III). In strongly alkaline conditions, the structure changed from conjugated quinonoid structure (III) to the colorless non-conjugated carbinol structure (IV) [303]. Notably, the color of CS-g-PHP (F2) remained pink even after several weeks of immersion in various pH solutions without any dye leaching, confirming the covalent dye attachment onto CS by the Mannich reaction. This reaction did not affect the chromophore of the PHP moieties. Moreover, the color dynamic range was shifted

compared to the free PHP, indicating that the new methylene bridge affected the color change of the PHP moiety [267].

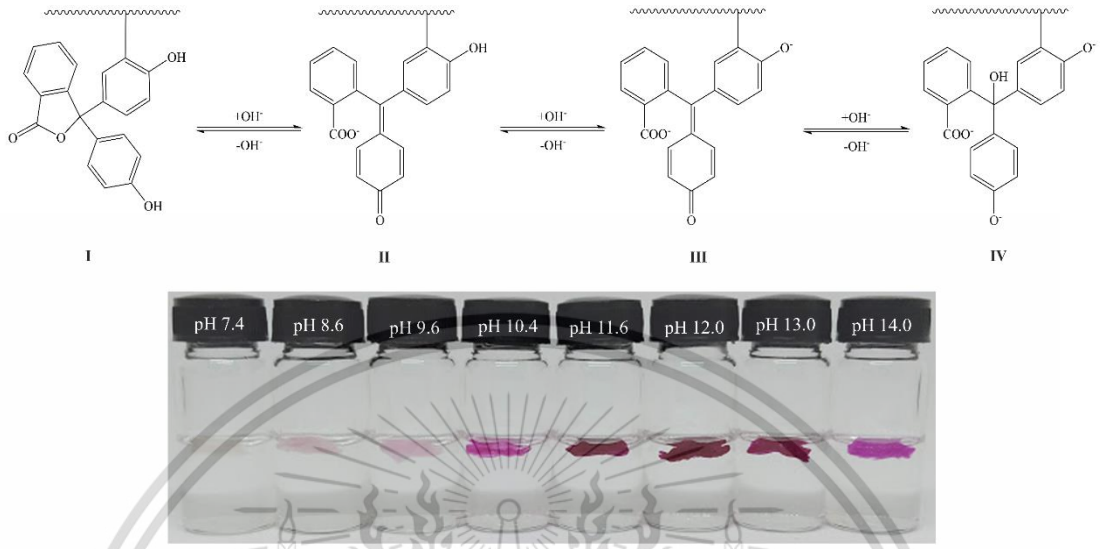

Figure 4.17 Color change of CS-g-PHP (F2) with different pH buffer solutions

Figure 4.18 Color change of PHP with different pH buffer solutions

Due to the spongy form of the CS-g-PHP (F1-F4) and the powder form of CS-g-PHP (P1), CS-g-PR, and CS-g-RA, it was challenging to study their color properties using UV-vis spectra and color parameters. To address this issue, CSPDs were prepared in a 1% solution dissolved in 1% acetic acid and blended with a 1% CS solution to form a film. CS-g-PHP (P1) was selected as the representative for CS-g-PHPs. The resulting smooth and transparent colored CPS-PHP, CPS-PR, and CPS-RA films, prepared by CS-

g-PHP (P1), CS-g-PR, and CS-g-RA, respectively, are shown in Figure 4.19. SEM images of all films indicated a homogenous cross-section, suggesting that the CSPDs had good compatibility with neat CS.

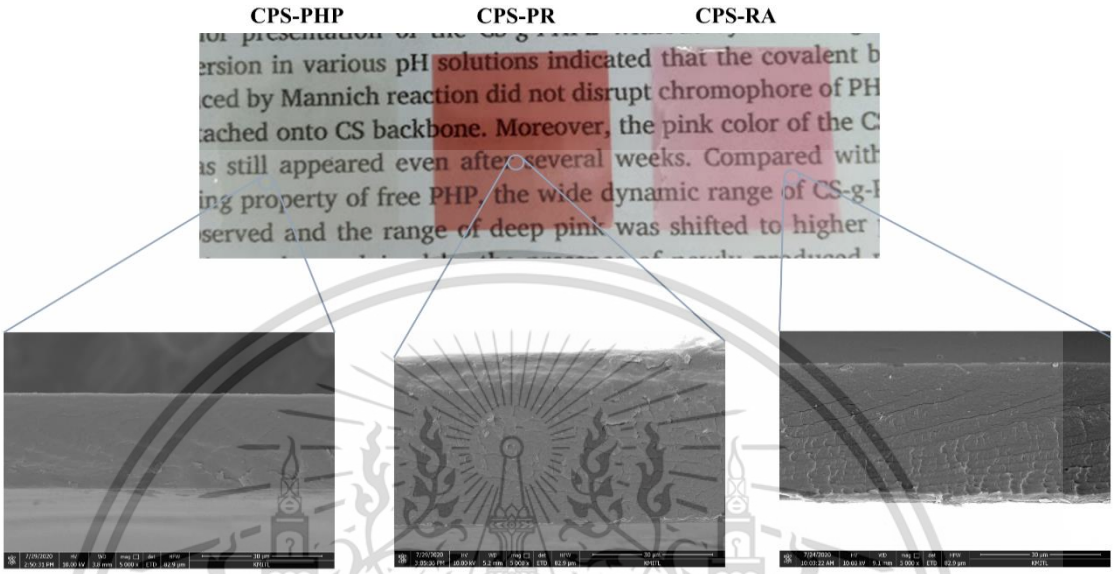

Figure 4.19 Appearances and cross-section images of CPS-PHP, CPS-PR, and CPS-RA films

The color response of CPS films (CPS-PHP, CPS-PR, and CPS-RA) was evaluated using UV-vis spectrometry and colorimetry after immersion in buffer solutions. The UV-vis spectra of CPS-PHP films immersed in various pH media are shown in Figure 4.20a, which displayed an absorption peak at 566 nm when subjected to a solution with pH > 10, corresponding to the open lactone ring of the PHP moiety. However, despite the fact that CS-g-PHP can change color when its pH is greater than 8.6, as demonstrated in Figure 4.17, no peak of CPS-PHP was observed. This could be due to the small amount of CS-g-PHP present in the film. In Figure 4.21a, the CPS-PR film exhibited a maximum absorption peak at 445 nm when immersed in a pH 4 solution. As the pH increased, the peak gradually decreased and disappeared after pH 9, while the intensity of the peak at 572 nm increased from pH 4 to 12. This can be attributed to the removal of a proton from protonated PR (HPR^-) to form PR^{2-} [304]. The CPS-RA film, as shown in Figure 4.22a, exhibited a distinct absorption peak at 542 nm when immersed in pH > 7. This peak corresponds to the ionization of protonated RA (H_2RA)

to RA^{2-} [305]. The CSPDs in CPS films displayed bathochromic shifts and a wide range of color change when compared to the free dye spectra (Figure 4.20b, Figure 4.21b, and Figure 4.22b). Moreover, the sigmoidal plots showed a significant shift in the apparent pKa value of the films (Figure 4.23). The apparent pKa values of CPS-PHP, CPS-PR, and CPS-RA were found to be 11.21, 8.37, and 8.14, respectively, which were higher than the pKa values of the corresponding free dyes (9.10 for PHP, 7.90 for PR, and 6.98 for RA) [279]. This can be explained by the presence of new methylene groups in the grafted dyes, which behave as electron donors and make it difficult for the hydroxyl groups to deprotonate, resulting in a shift of the color change region and apparent pKa values to higher pH values. This is similar to what is observed in other dyes such as cresol red, xylenol blue, and thymol blue [306].

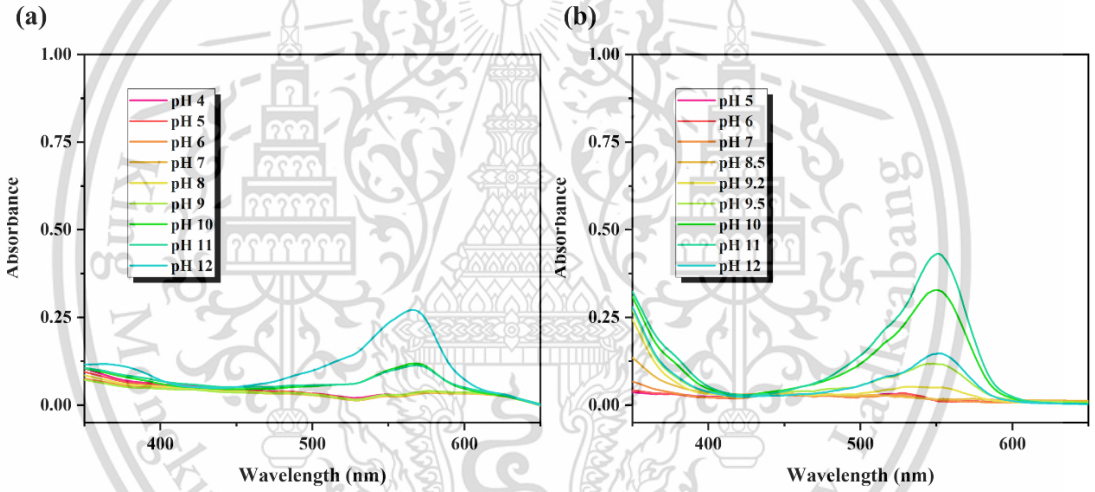

Figure 4.20 UV-vis spectra of (a) CPS-PHP and (b) PHP solution at different pH values

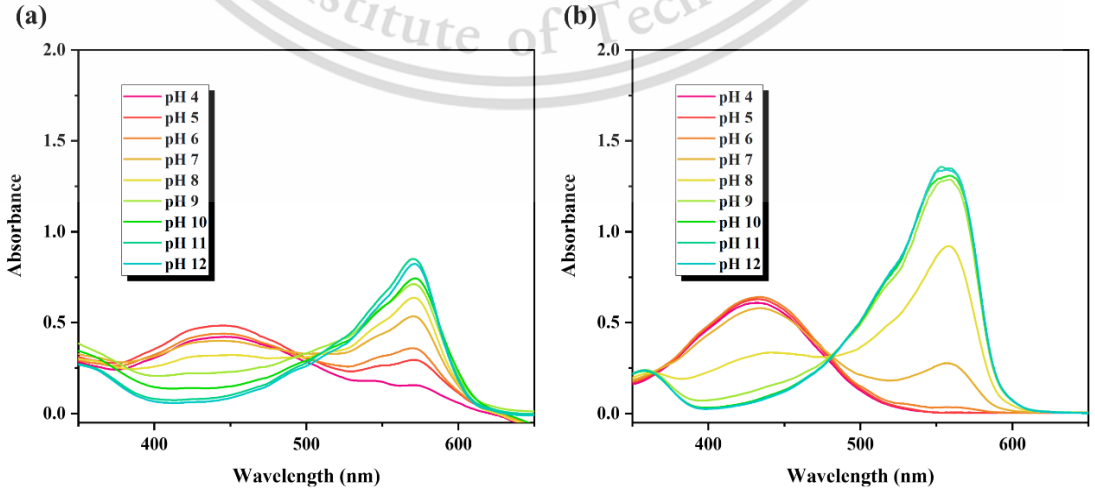

Figure 4.21 UV-vis spectra of (a) CPS-PR and (b) PR solution at different pH values

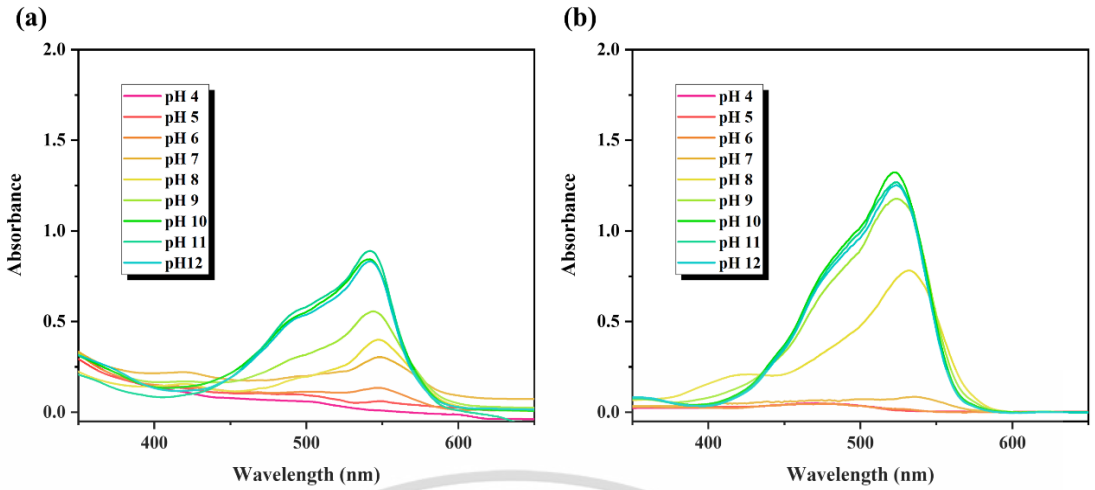

Figure 4.22 UV-vis spectra of (a) CPS-RA and (b) RA solution at different pH values

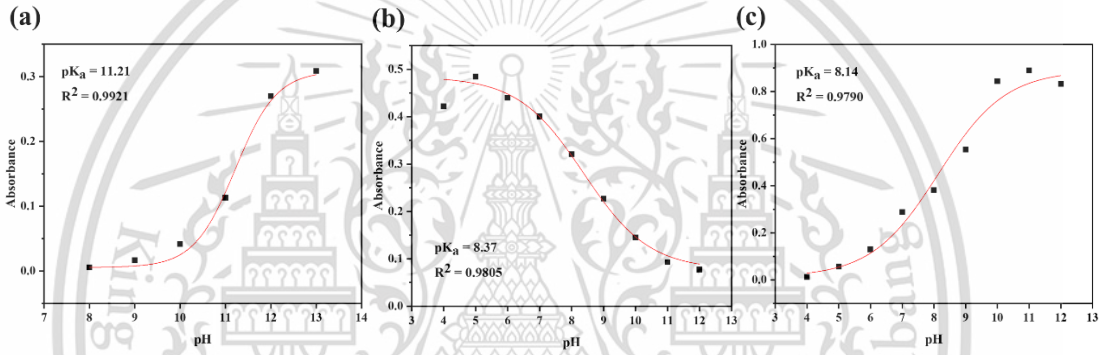

Figure 4.23 Sigmoidal plot of CPS-PHP (a), CPS-PR (b), and CPS-RA (c) films as a function of pH values

Figures 4.24-4.26 illustrate the color parameters and digital images of CPS films exposed to buffer solutions at various pH values. The CIE-LAB system uses *L* to represent pure black (0) and pure white (100), *a* for green (-) and red (+), and *b* for blue (-) and yellow (+). The CPS-PHP films turned pinkish purple at pH 10 and dark purple at pH 12, resulting in an increase in the *a* value from 19.03 to 52.29 and a decrease in the *b* value from -25.82 to -44.49, indicating an increase in red and blue shades. The CPS-PR films initially showed a pale orange color at pH 4, which gradually turned into red and purple shades at pH 8 and 10, respectively. As the pH increased, the *a* value increased from 26.02 to 50.14, indicating a stronger red color, while the *b* value decreased from 21.36 to -37.15, indicating a shift from yellow to blue shades. The CPS-RA films exhibited a change in color from light yellow to red within the pH range of 4-9, becoming more intensely red at pH values higher than 9. The *L* value of the films decreased from 83.40 to 57.98 with increasing pH, indicating lower brightness.

Moreover, the *a* value of the films significantly increased from 6.97 to 60.73, while the *b* value remained close to zero and slightly decreased, indicating a dominant red color.

The CPS films showed a noticeable increase in total color differences (*ΔE*) after immersion, with values greater than 5 when compared to the films before soaking. This suggests that these color changes can be easily perceived by the naked eye. These findings demonstrate that the synthesized CPSDs have potential as pH-indicative colorants for pH-sensing materials.

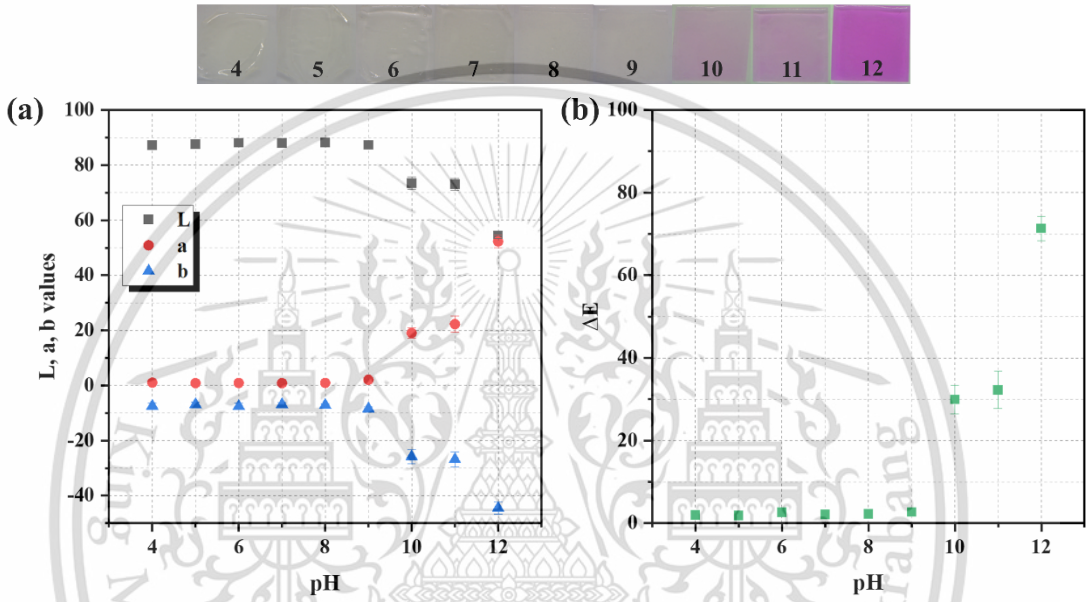

Figure 4.24 Color changes and color parameters of CPS-PHP

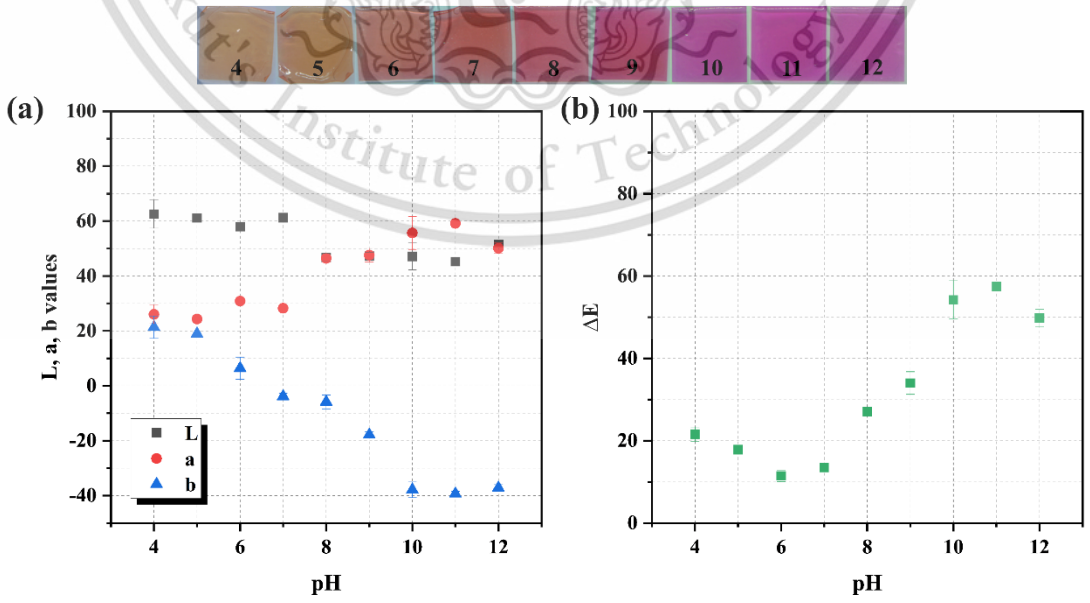

Figure 4.25 Color changes and color parameters of CPS-PR

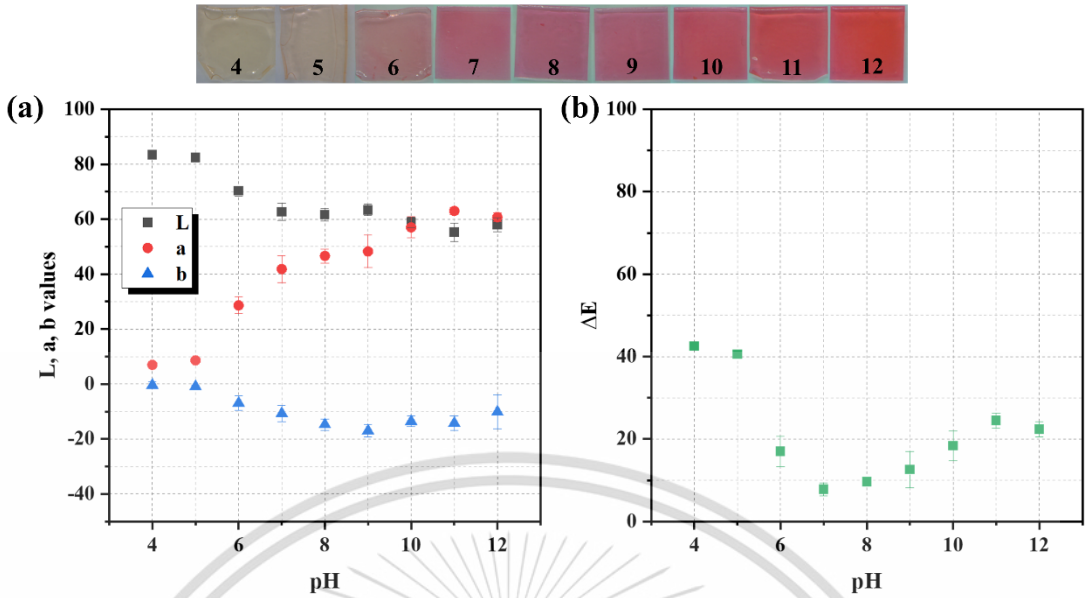

Figure 4.26 Color changes and color parameters of CPS-RA

The color stability of CPS films was tested by immersing them in different media (DI water, pH buffer 4, pH buffer 7.4, and pH buffer 10). As shown in Figure 4.27, the results indicated that the *ΔE* values (compared to the films before immersion) of all films remained constant over time at room temperature under light, indicating that the films were able to maintain their color in each medium for at least two months. Furthermore, UV-vis spectra of the solutions used for immersing the films were analyzed (see Figure 4.28). No absorption peaks corresponding to leaching dyes were detected, which confirmed that the covalent grafting of dyes onto CS prevented the release or degradation of the film color. This demonstrated that the CSPDs in CS films had excellent color stability and leaching resistance in different environments, making them ideal for use as indicative colorants in pH-sensing materials.

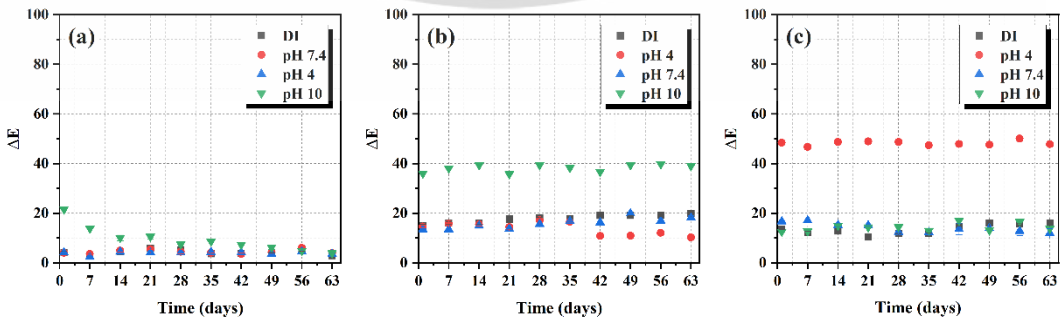

Figure 4.27 Color difference of (a) CPS-PHP, (b) CPS-PR, and (C) CPS-RA films in various media as a function of time

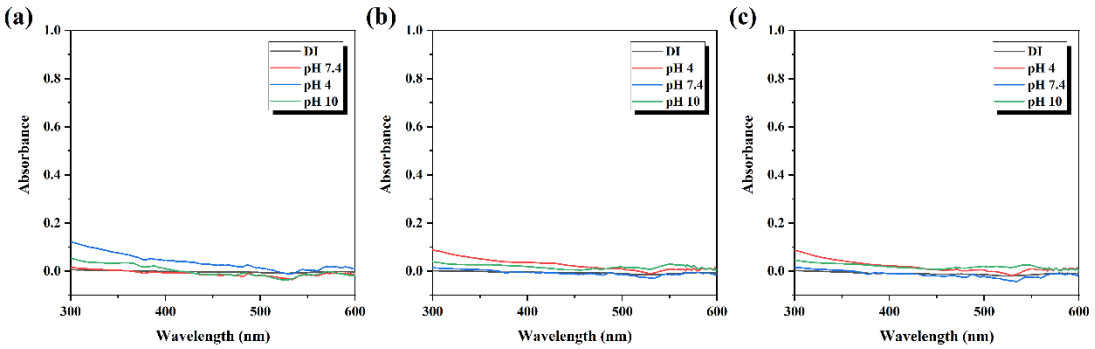

Figure 4.28 UV-vis spectra of solution in which (a) CPS-PHP, (b) CPS-PR, (c) CPS-RA films were immersed for 24 h

4.2 Synthesis and characterization of water- soluble chitosan-based polymeric dyes (WCSPDs)

Despite the potential use of CSPDs in pH-sensing applications, their use has been limited by the need for acid or strong alkali systems for dissolution, which can leave toxic residues in the final materials. Additionally, blending CSPDs with nonionic or anionic polymers under mild conditions can be challenging. Therefore, modifying CSPDs to improve their water-solubility is an attractive solution to this problem.

In this study, two methods were used to synthesize water-soluble CSPDs (WCSPDs). The first method involved modifying CS to obtain water-soluble carboxyethyl chitosan (CECS) by the Michael reaction, which was then reacted with dyes using the Mannich reaction. The reaction pathway is shown in Figure 4.29. However, CECS was not able to react with PR because it formed bulk solid after the addition of the PR solution. This phenomenon could be attributed to the electrostatic interactions between the negatively charged PR resulting from the sulfone ring opening and the positively charged CS units present in CECS. It is notable that CECS is soluble in distilled water, unlike CS, which requires 1% acetic acid for dissolution during the reaction. Consequently, the pH conditions of the reaction influenced the structural behavior of PR, causing the sulfone ring to open in neutral pH and close in acidic solutions.

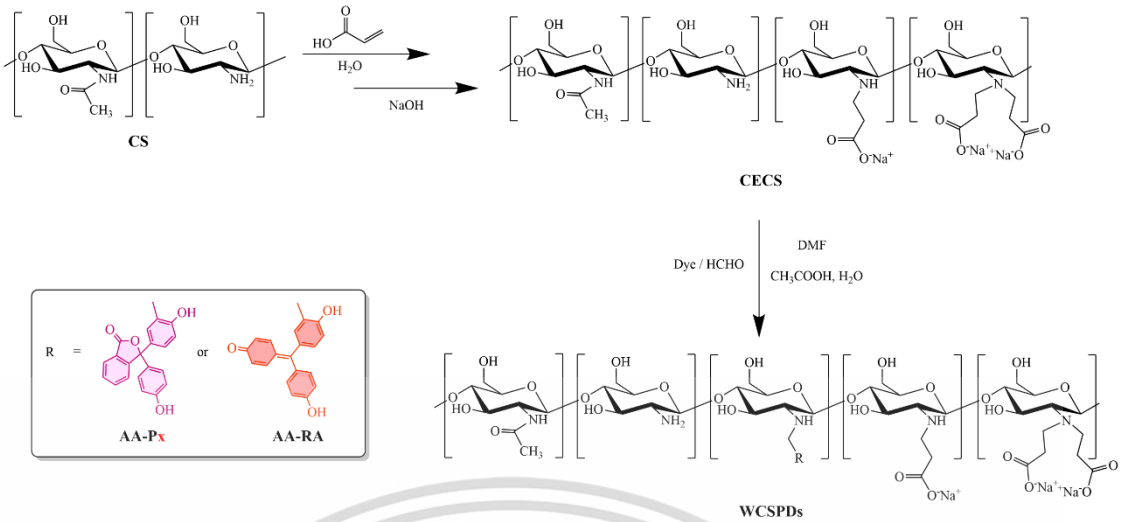

Figure 4.29 Synthesis of WCSPDs by CECS pathway

Figure 4.30 illustrates the ^{1}H NMR spectra of CS, CECS, and WCSPDs synthesized using the first method. The CECS spectra showed two new peaks at 2.30 and 3.00 ppm corresponding to new ethyl groups (H_b and H_a), while H_2 shifted to 2.64 ppm compared to the spectra of CS. These peaks were confirmed by HSQC and DEPT spectra in Figure 4.31 and Figure 4.32. The new H_b peak was correlated with a strong peak at 36.9 ppm in ^{13}C NMR, while the H_a peak was split into two cross-peaks (representing the proton in GlcNHR or GlcNR$_2$ units) and correlated with a strong peak at 45.0 ppm in ^{13}C NMR. The DEPT-135 spectra confirmed these peaks to be new ethyl groups on the CS structure. Upon further modification with dyes, new aromatic protons were detected at 6.7-7.9 ppm for AA-P1 and 6.6-7.7 ppm for AA-RA, indicating the presence of dyes in the final products. The %DS of carboxyethyl groups of CECS was 47.5%, while the %DS$_{DYE}$ was 0.5% for AA-P1 and 0.2% for AA-RA.

The ^{1}H NMR spectra of AA-Px synthesized at different feed ratios were shown in Figure 4.33. Although the aromatic protons were observed in all spectra, their integral areas did not increase significantly with increasing feed ratios in comparison to CS-g-PHPs. The %DS$_{DYE}$ values were calculated to be 0.5% for AA-P1, 0.95% for AA-P2, 0.8% for AA-P3, and 1.2% for AA-P4, which indicated that the grafting of dyes may be obstructed by the new carboxyethyl groups.

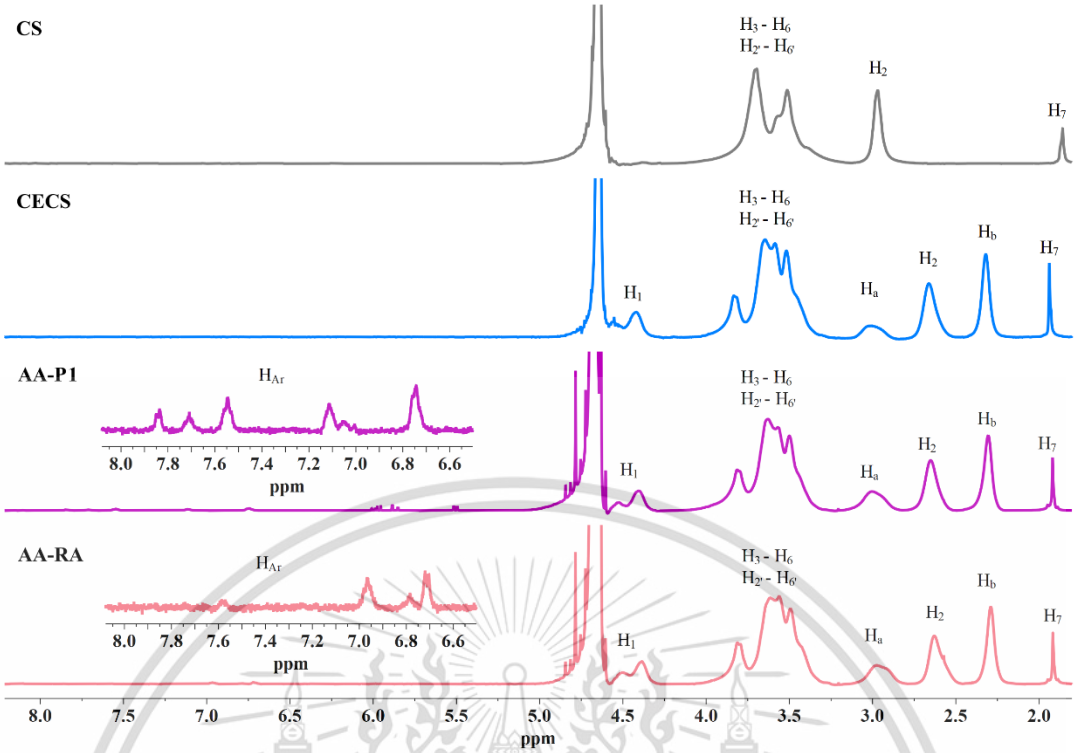

Figure 4.30 ^{1}H NMR spectra of CS, CECS, AA-P1, and AA-RA

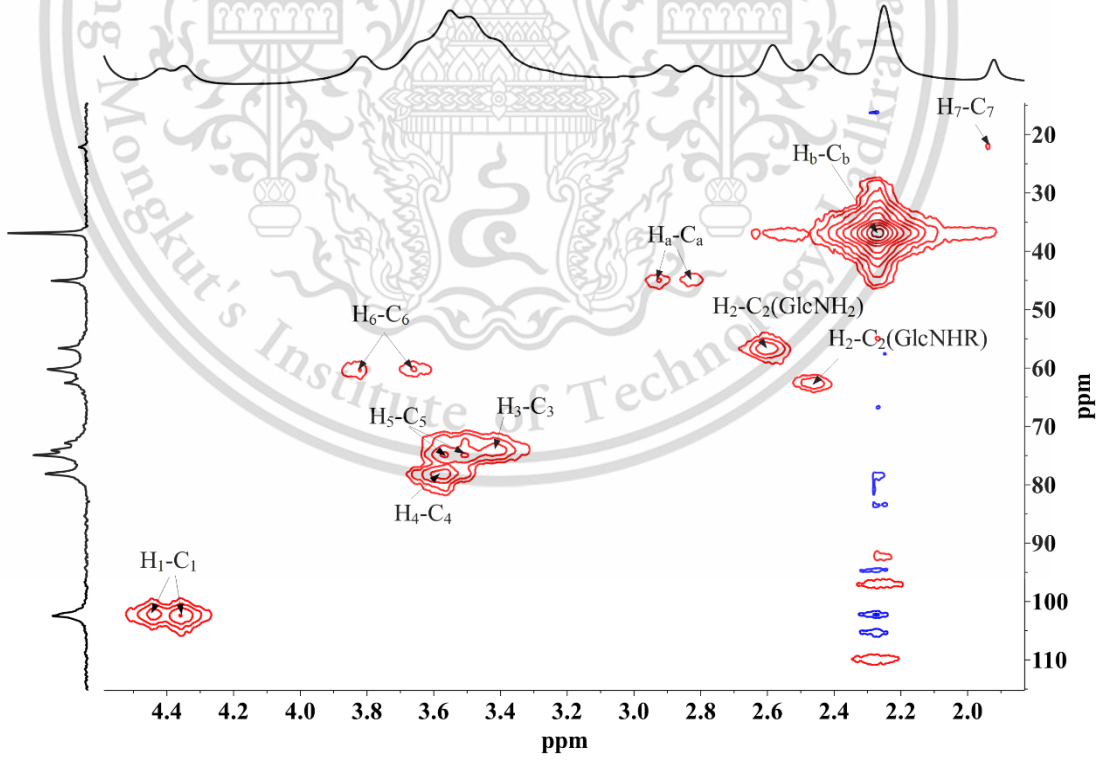

Figure 4.31 HSQC NMR spectra of CECS

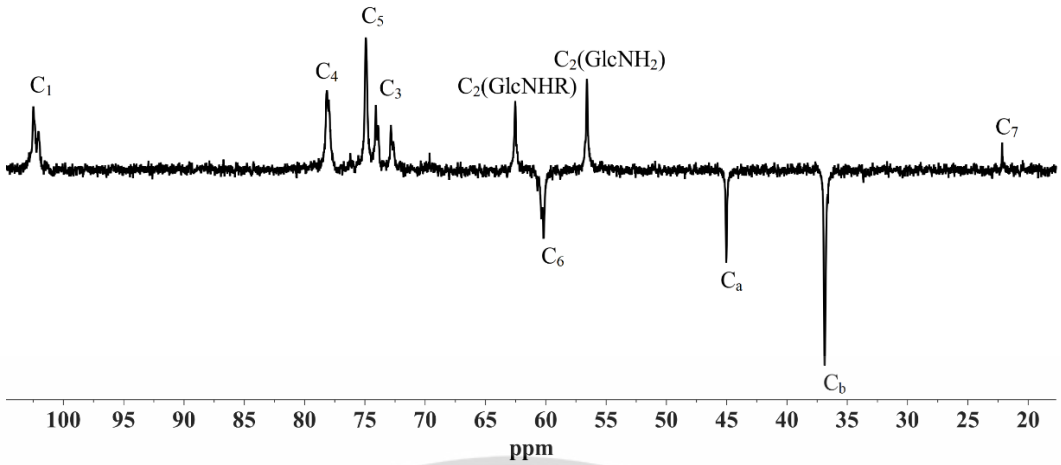

Figure 4.32 ^{13}C DEPT NMR spectra of CECS

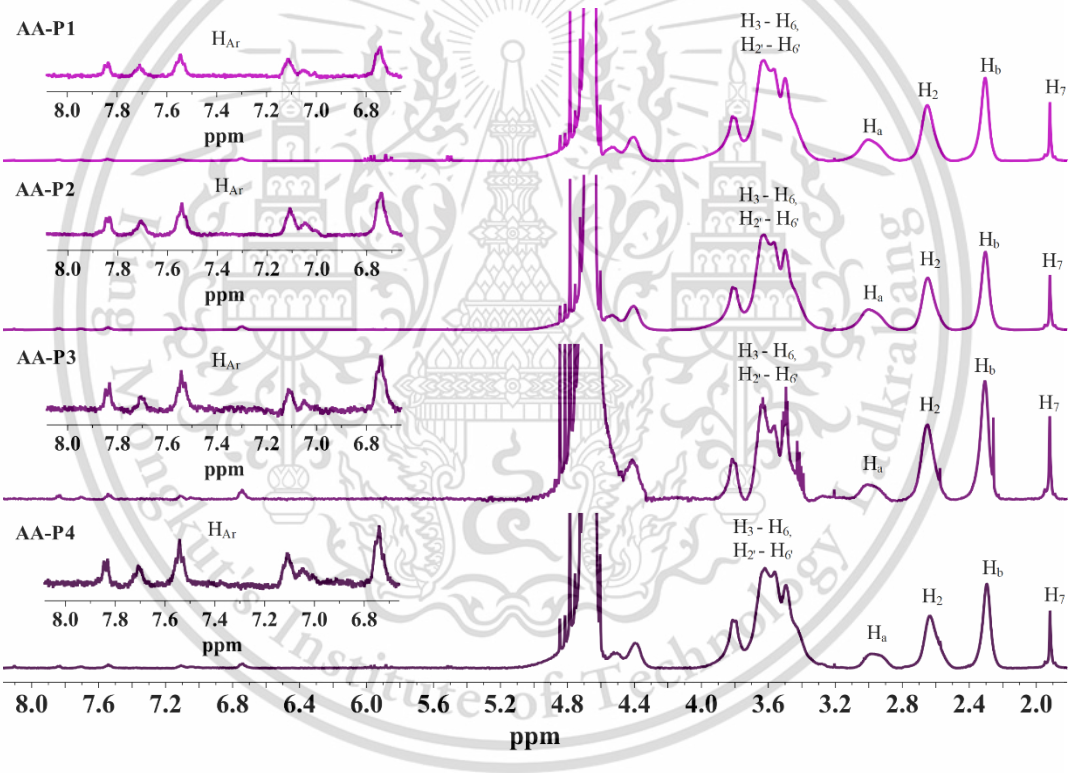

Figure 4.33 ^{1}H NMR spectra of AA-Px

In the second method, carboxyethylation of CSPDs was achieved through the Michael reaction with acrylic acid, as depicted in Figure 4.34. Among the CS-g-PHPs, CS-g-PHP (P1) was selected for this reaction due to its similar %DS to CS-g-PR and CS-g-RA. The reaction was performed at mild conditions (60°C for 2 days) and yielded successful modification of all CSPDs to produce WCSPDs (P1-AA, PR-AA, and RA-AA).

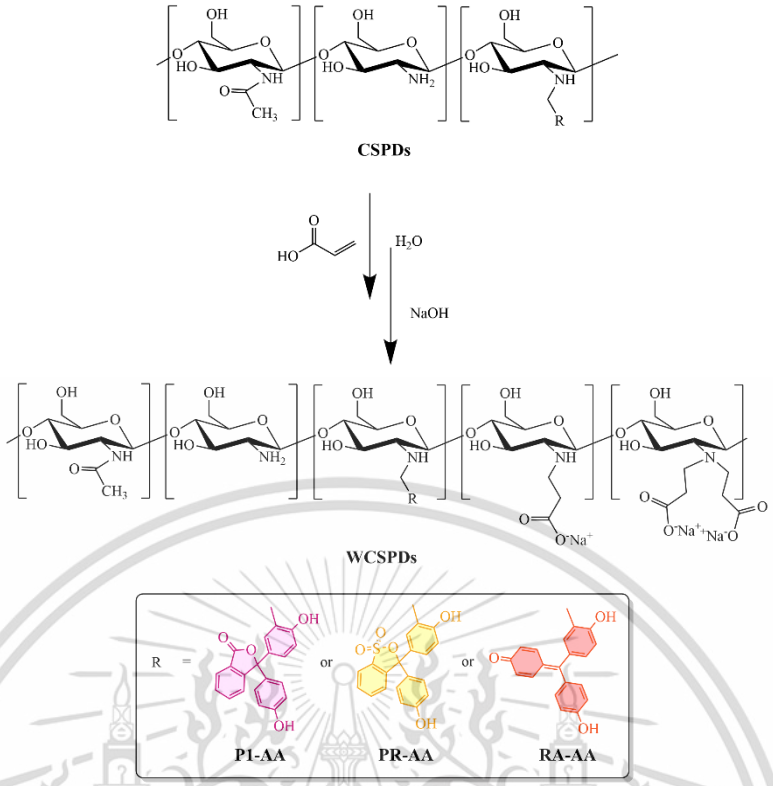

Figure 4.34 Synthesis of WCSPDs by carboxyethylation of CSPDs

4.2.1 FTIR analysis

The FTIR spectra of CECS and WCSPDs are displayed in Figure 4.35. Compared to the CS spectra, two new peaks at 1569 and 1408 cm^{-1} were observed in CECS and WCSPDs, corresponding to the asymmetrical and symmetrical stretching of COO^-. This confirms the success of the reaction [307]. Regarding the characteristic peaks of the dyes, the C=O stretching of the lactone group of PHPs was found at 1743 cm^{-1} in P1-AA, while no remarkable peaks were observed in PR-AA and RA-AA due to low dye substitution.

4.2.2 ^{1}H NMR analysis

Figure 4.36 illustrates the ^{1}H-NMR spectra of the derivatives. Compared to the CECS spectra, two new -CH_2 peaks were found in all WCSPDs at 2.9 and 2.3 ppm, assigned to H_a and H_b, respectively. This was confirmed in the DEPT-ed-HSQC NMR spectra as well (Figure 4.37-Figure 4.39), which indicated the successful modification of CSPDs through the Michael reaction. The dye and carboxyethyl group substitution degrees on WCSPDs were 2.4% and 59.0% for P1-AA, 2.4% and 36.4% for PR-AA, and

0.7% and 51.4% for RA-AA, respectively. This level of substitution was deemed sufficient for improving water solubility.

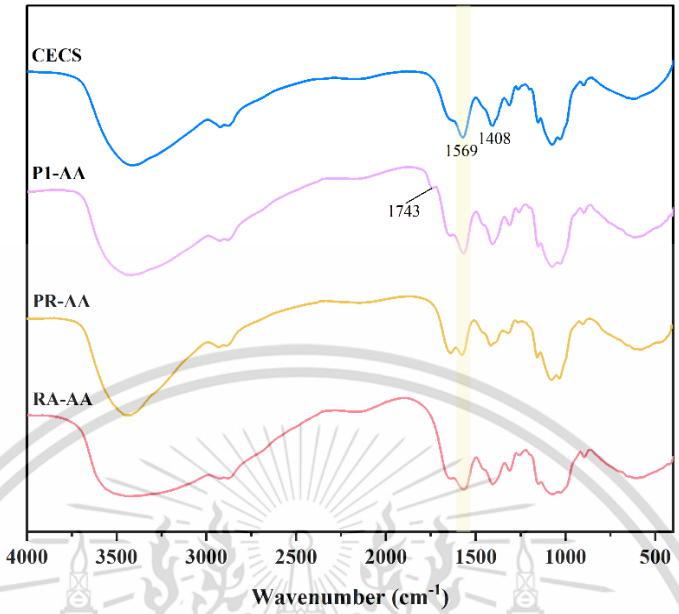

Figure 4.35 FTIR spectra of CECS, P1-AA, PR-AA, and RA-AA

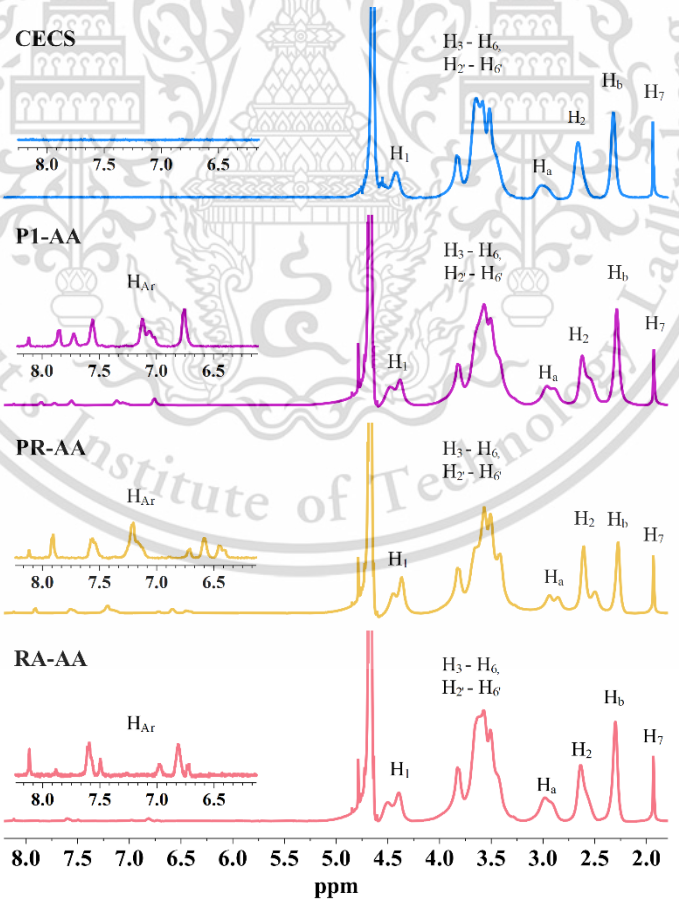

Figure 4.36 ^{1}H NMR spectra of CECS, P1-AA, PR-AA, and RA-AA

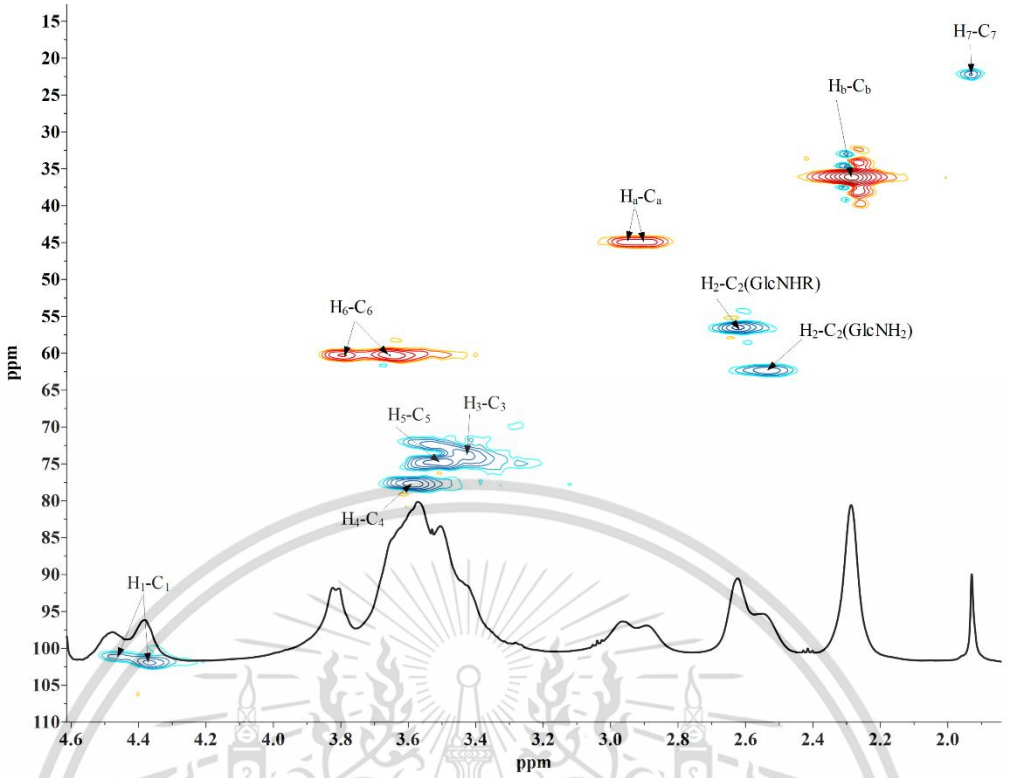

Figure 4.37 DEPT-edited HSQC spectrum of P1-AA at 20°C, 600 MHz. Cross-peaks shown in blue correspond to CH and CH_3 groups, red represents CH_2 groups.

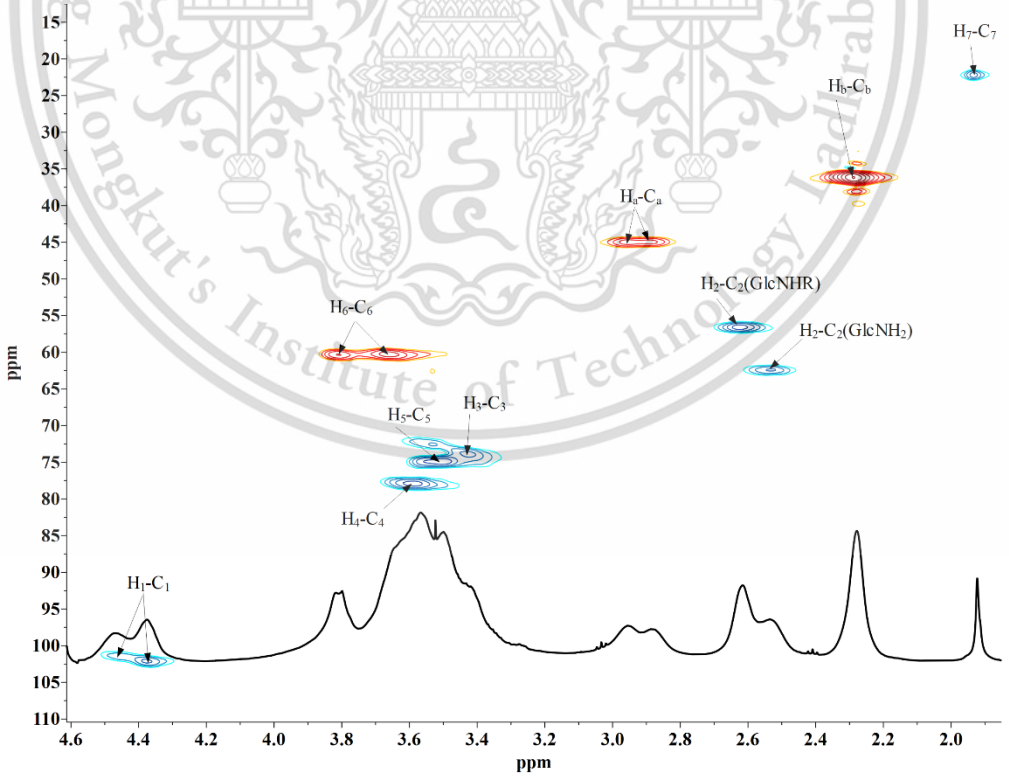

Figure 4.38 DEPT-edited HSQC spectrum of PR-AA at 20°C, 600 MHz. Cross-peaks shown in blue correspond to CH and CH_3 groups, red represents CH_2 groups.

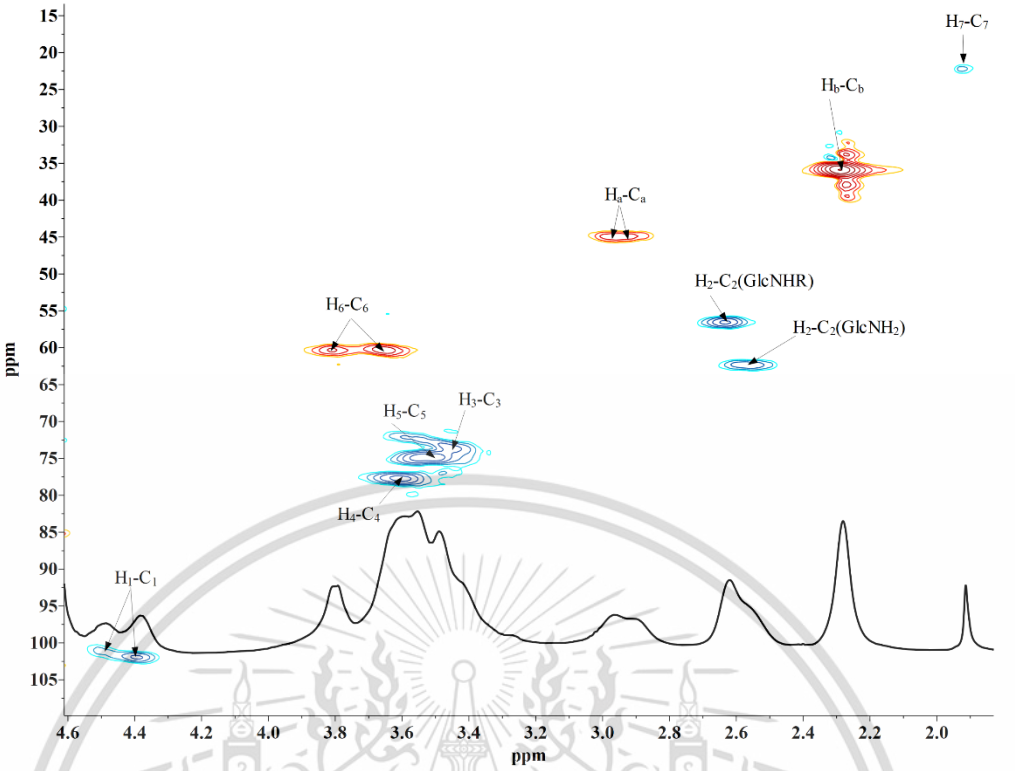

Figure 4.39 DEPT-edited HSQC spectrum of RA-AA at 20°C, 600 MHz. Cross-peaks shown in blue correspond to CH and CH_3 groups, red represents CH_2 groups.

4.2.3 UV-vis analysis

UV-vis spectra of WCSPDs in pH 10 buffer solution are shown in Figure 4.40. The spectra of all WCSPDs were clearly shifted to higher wavelengths compared to the original dyes. Specifically, the shift was from 550 to 559 nm for P1-AA, from 559 to 569 nm for PR-AA, and from 525 to 536 nm for RA-AA. In contrast, CECS showed no absorption. This shift could be attributed to the addition of a new alkyl group to the dye molecules, which directly influences their absorption [306]. This result confirms that the Mannich reaction successfully grafted dye onto CS and that further modification with the Michael reaction had no effect on the attached dyes.

4.2.4 Solubility

The solubility of CECS and WCSPDs in water at different pH values was measured as a percentage transmittance and is shown in Figure 4.41. The results revealed that the solubility of CECS decreased as the pH exceeded 6.5, reaching its lowest point at pH 6.8 before becoming more soluble at higher pH values. This was attributed to the amphoteric nature of CS, which had an isoelectric point at pH 6.8

due to the addition of carboxyethyl groups. On the other hand, WCSPDs had a broader range of poor solubility, with the solubility starting to decrease when the pH exceeded 6.4 and becoming completely soluble when the pH exceeded 7.8. This was due to the partial crosslinking caused by the Mannich reaction, resulting in larger molecules that hindered the deprotonation of their structures. These findings confirmed that WCSPDs have good water solubility over a wide pH range after the carboxylethylation step, as reported by several studies [307-309].

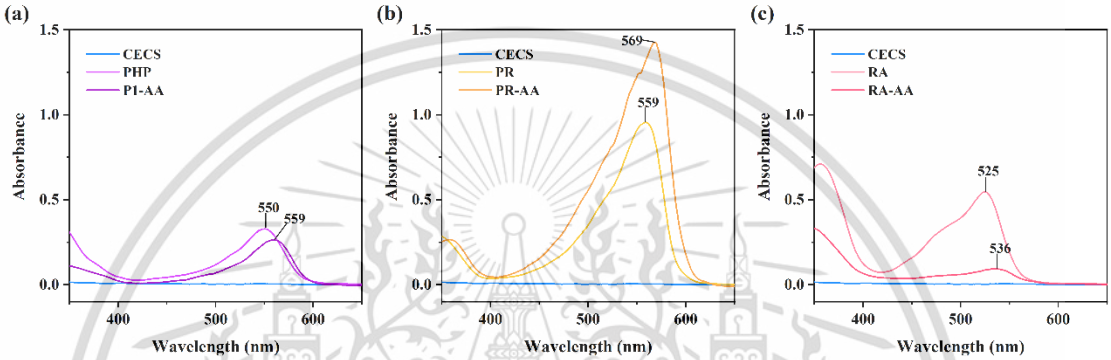

Figure 4.40 UV-vis spectra of WCSPDs compared with original dyes and CECS: CS-PHP-AA (a), CS-PR-AA (b) and CS-RA-AA (c)

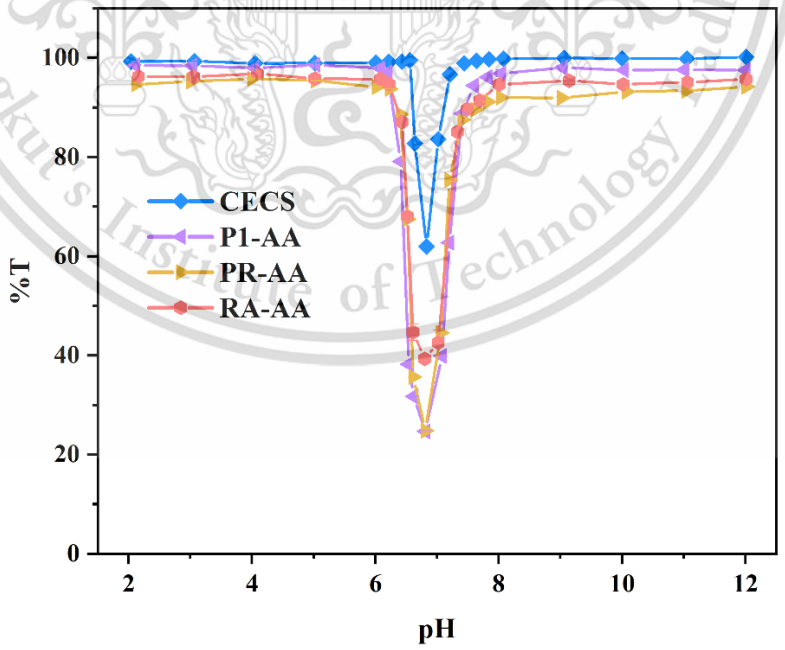

Figure 4.41 Water solubility of CECS and WCSPDs

4.2.5 XRD patterns

Figure 4.42 shows the XRD patterns of CECS and WCSPDs. Compared to CS, CECS and WCSPDs displayed broad XRD peaks at 2θ = 21.3°, indicating an increase in the amorphous phase. Furthermore, the decreased relative crystallinity index values of CECS (70.4%), CS-PHP-AA (67.8%), CS-PR-AA (55.3%), and CS-RA-AA (54.5%) indicated that crystallinity was significantly reduced after carboxyethylation with acrylic acid. This interruption in the formation of inter- and intramolecular hydrogen bonds in the CS structure led to improved water solubility.

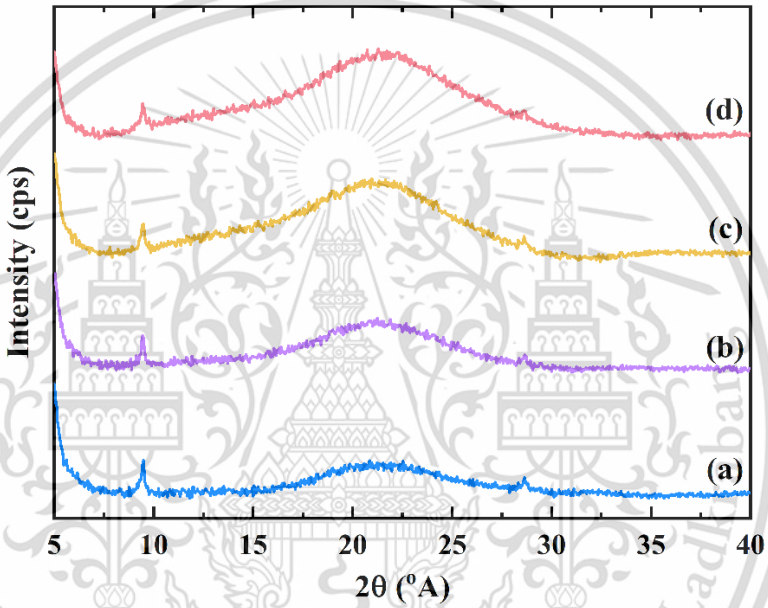

Figure 4.42 XRD patterns of (a) CECS, (b) P1-AA, (c) PR-AA, and (d) RA-AA

4.2.6 Coloring properties of WCSPDs

As mentioned earlier, WCSPDs can be dissolved in a wide range of pH values and exhibit different colors depending on the pH. This indicated that the carboxyethylation process did not affect the dye structures or their color-changing properties. Figure 4.43 illustrates the UV-vis spectra and color changes of P1-AA at various pH levels. The dye appeared pink at pH 9 and gradually turned to dark pink as the pH increased, with a corresponding increase in intensity at 559 nm. This can be attributed to the opening of the lactone ring, which leads to the formation of a conjugated quinonoid structure due to deprotonation [303].

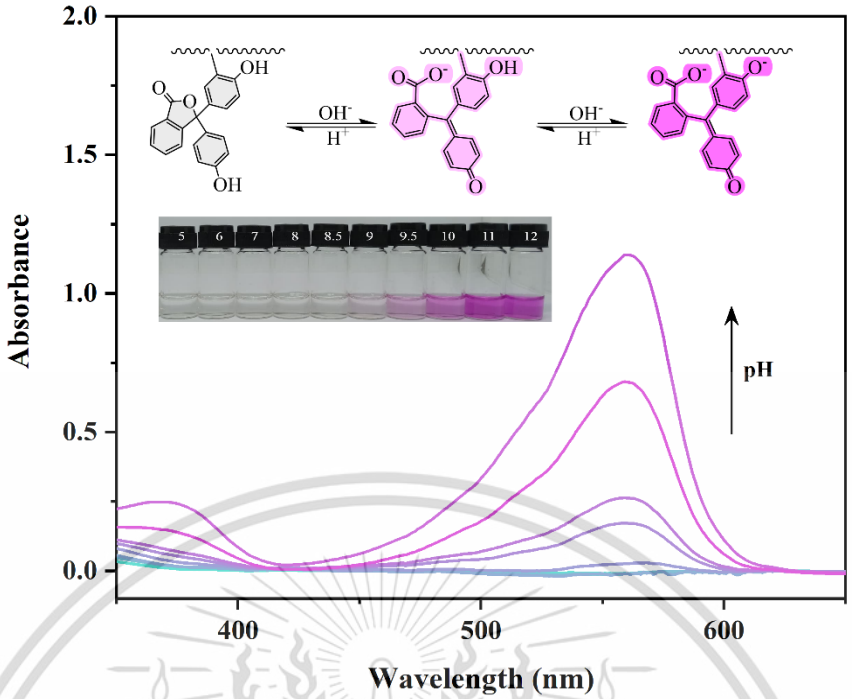

Figure 4.43 UV-vis spectra of P1-AA in different pHs

In addition to its pH-sensitive color changes, PHP also responds to β-cyclodextrin (βCD), a cyclic oligosaccharide that can form inclusion complexes with guest molecules, including PHP. When PHP is ionized in basic solution with βCD (pH 10), the lactone ring closes while the phenolic groups are ionized, resulting in a colorless solution [303, 310]. On the other hand, PR and RA do not show this ability [311]. Therefore, modified CS with PHP moieties could exhibit a response to βCD similar to the PHP molecule. Figure 4.44 shows a decrease in the intensity of PHP and P1-AA in buffer solutions (pH 10) after adding various concentrations of βCD (pH 10). The binding constants were calculated from Scott's plot (see inset) and were found to be 17429 M^{-1} for PHP and 5563 M^{-1} for P1-AA. The lower binding constant of P1-AA with βCD can be attributed to the steric effects of the polymer chain, which wraps around βCD and prevents complexation with PHP [310, 312]. Additionally, the linearity confirmed the formation of a 1:1 complex of PHP moiety and βCD. These findings suggest that grafted PHP on the CS chain can behave as PHP molecules, opening up possibilities for designing sensing materials and serving as crosslinking points in functional materials.

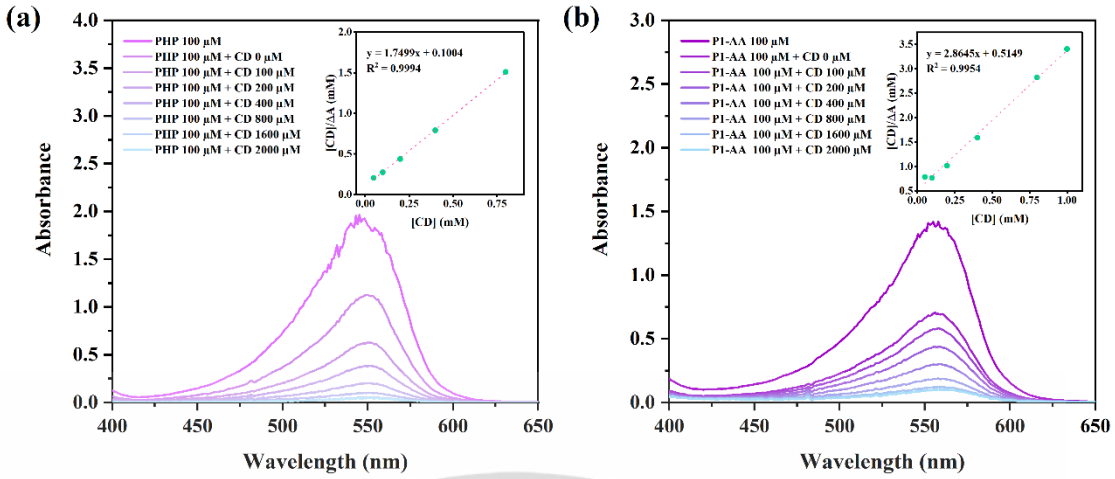

Figure 4.44 UV-vis spectra of buffer (a) PHP and (b) P1-AA (pH 10) with different concentrations of βCD, inset is Scott's plot with regression equation for binding constant determination.

Figure 4.45 demonstrates that PR-AA exhibits two peak changes: a decrease in intensity at 445 nm and an increase in intensity at 569 nm, leading to a color change from orange at pH 4 to red (pH 6.5-8) and to purple (pH 9-12), respectively. These changes are attributed to the proton dissociation of the PR structure.

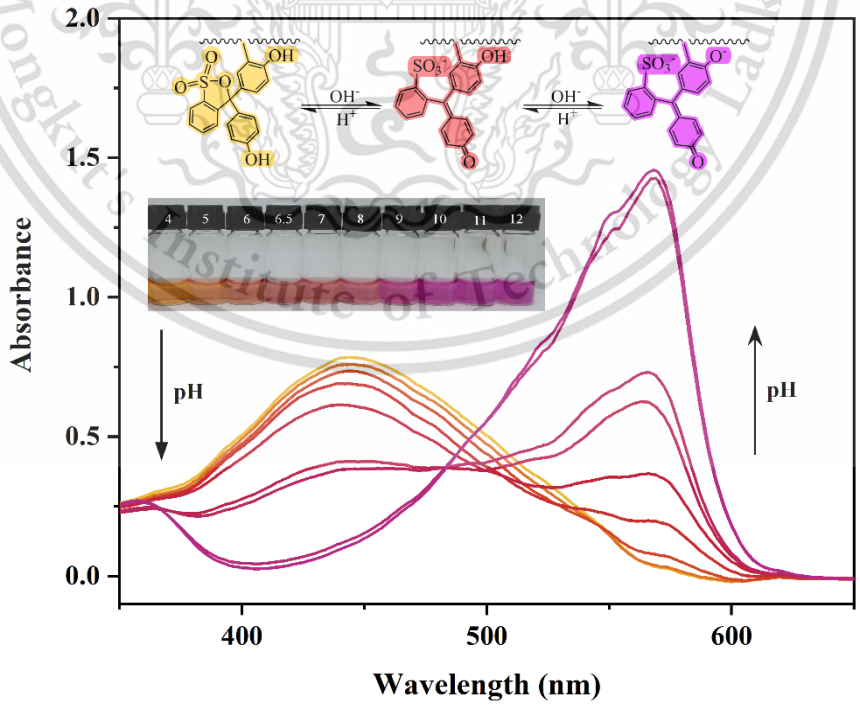

Figure 4.45 UV-vis spectra of PR-AA in different pHs

Figure 4.46 illustrates that the intensity of RA-AA increased at 542 nm as the pH increased from 5 to 10, resulting in a color change from pale yellow to pale pink due to the ionization form of protonated RA. However, the color intensity of RA-AA was found to be rather low due to the low degree of substitution (0.7%). Although the %DS of CS-g-RA was higher (1.8%), it decreased after carboxyethylation. It is possible that the RA moiety could be degraded in strong basic conditions (during the pH adjustment to 10-12 before dialysis).

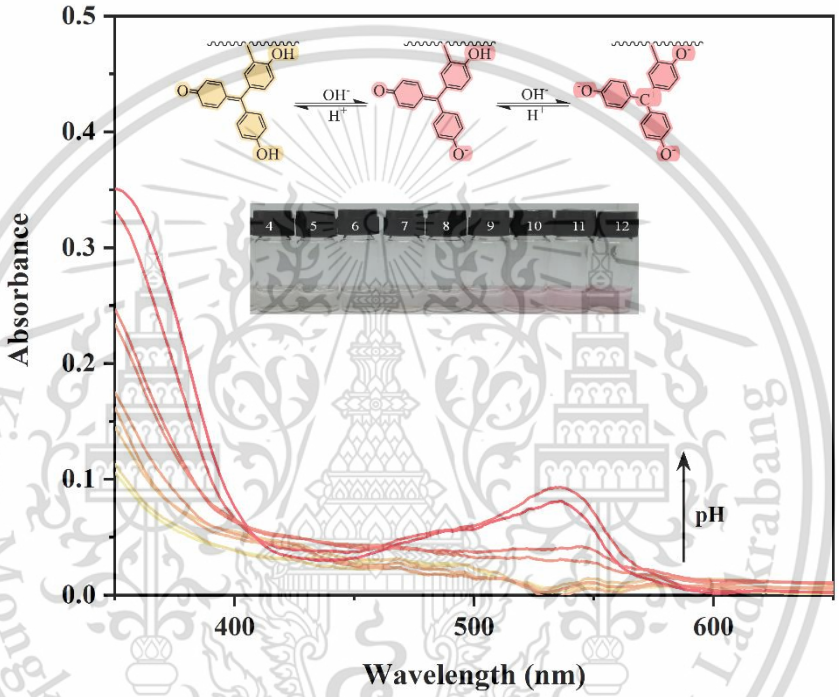

Figure 4.46 UV-vis spectra of RA-AA in different pHs

The pKa values of WCSPDs were estimated using non-linear curve fitting method and the sigmoidal plots shown in Figure 4.47. P1-AA, PR-AA, and RA-AA showed pKa values of 9.95, 7.93, and 8.29 respectively, all higher than those of their corresponding free dyes (9.1 for PHP, 7.90 for PR, and 6.98 for RA [279]). It was noted that the resulting pKa values were different from CSPDs in CPS films even though they were synthesized from CSPDs. It is possible that the different dye content in the samples resulted in a change in the trend of maximum intensity.

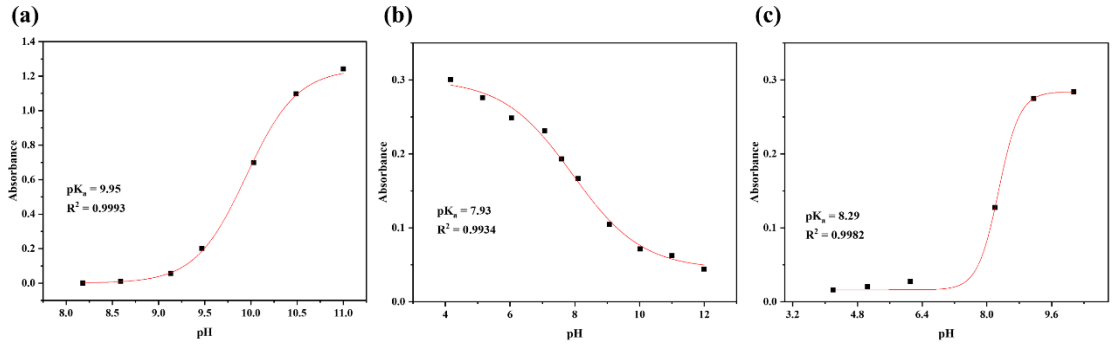

Figure 4.47 Sigmoidal plot of P1-AA (a), PR-AA (b), and RA-AA (c) solutions as a function of pH values

Chemical modification has been employed to enhance the water solubility of CS and its derivatives. These water-soluble CS derivatives offer ease of use without the need for acidic conditions and have been utilized in the fabrication of various materials. They can be combined with nonionic or anionic polymers under neutral conditions without unintended gelation. Moreover, they exhibit desirable properties such as biocompatibility, biodegradability, and antimicrobial activities [288, 307], making them promise for applications in biomaterials and other functional materials [13, 94, 186, 249, 255].

Colored CS derivatives have also garnered attention for their potential applications, such as alkaline fuel cells [313] and as edible colorants in the food industry [6, 7]. In the case of WCSPDs with pH-sensitive properties, they hold potential as pH-sensing materials in food packaging and medical fields. They can be employed to monitor food spoilage caused by basic volatiles released from animal proteins over time, leading to a shift towards higher pH values [314, 315]. Additionally, in the context of food, glucose fermentation can result in the production of ethanol, organic acids, and other microbial byproducts like CO_2, lactic acid, and acetic acid, which can lower the pH of food samples [316]. They can also be developed for biomedical applications, including monitoring wound healing [317, 318]. The pH value at the wound site is closely related to the condition of the wound. Normal skin typically has a slightly acidic pH range of 4-6, whereas chronic wounds and bacterial infections create an alkaline environment with a pH range of 7-9 [19, 20]. Furthermore, there has been report on the functionalization of cellulose nanofiber mats for alcohol consumption detection [319]. This study demonstrated the ability to detect changes

in saliva pH, where a decrease from the normal pH of 7.4 to 4.7 was observed with an increase in alcohol consumption level. Therefore, as mentioned earlier, PR-AA and RA-AA show potential for the suggested applications due to their pH sensing capabilities. Although the pH range of P1-AA may not be suitable for monitoring food freshness or health status, it can be tailored for other functional materials such as colorimetric biodetection [271] and corrosion sensing coatings [270], which require color changes within PHP's pH range. Additionally, the complexation ability of the PHP moiety in P1-AA allows it to serve as a dynamic crosslinking point with CD for the development of multifunctional hydrogels [276].

4.3 Applications of WCSPDs

After synthesizing and characterizing WCSPDs, they were utilized to create materials for the proposed applications. In this section, PR-AA was incorporated into a film mixture to develop pH-indicative hydrogel films for wound dressing applications. On the other hand, the applications of WCSPDs containing PHP and RA moieties were summarized based on the results obtained from published works.

4.3.1 Smart wound dressing (based on PR-AA)

To produce pH-indicative hydrogel films for smart wound dressings, PR-AA was chosen due to its ability to undergo color changes within the pH range of physiological fluids, such as the exudate from the wound bed. The formulation involved blending PR-AA with CECS, SA, and PAM, with βCD-DA serving as a covalent crosslinker. The aldehyde groups of βCD-DA formed imine bonds with the free amine groups of PR-AA and CECS. GDL was also added to create a weak acid environment in the film formulations, promoting electrostatic interactions between the protonated amine groups and the carboxylate group of SA. βCD-DA was synthesized through oxidation with sodium periodate for 0.5 h, resulting in an aldehyde content of 1.69 mmol/g. The preparation of the films is illustrated in Figure 4.48.

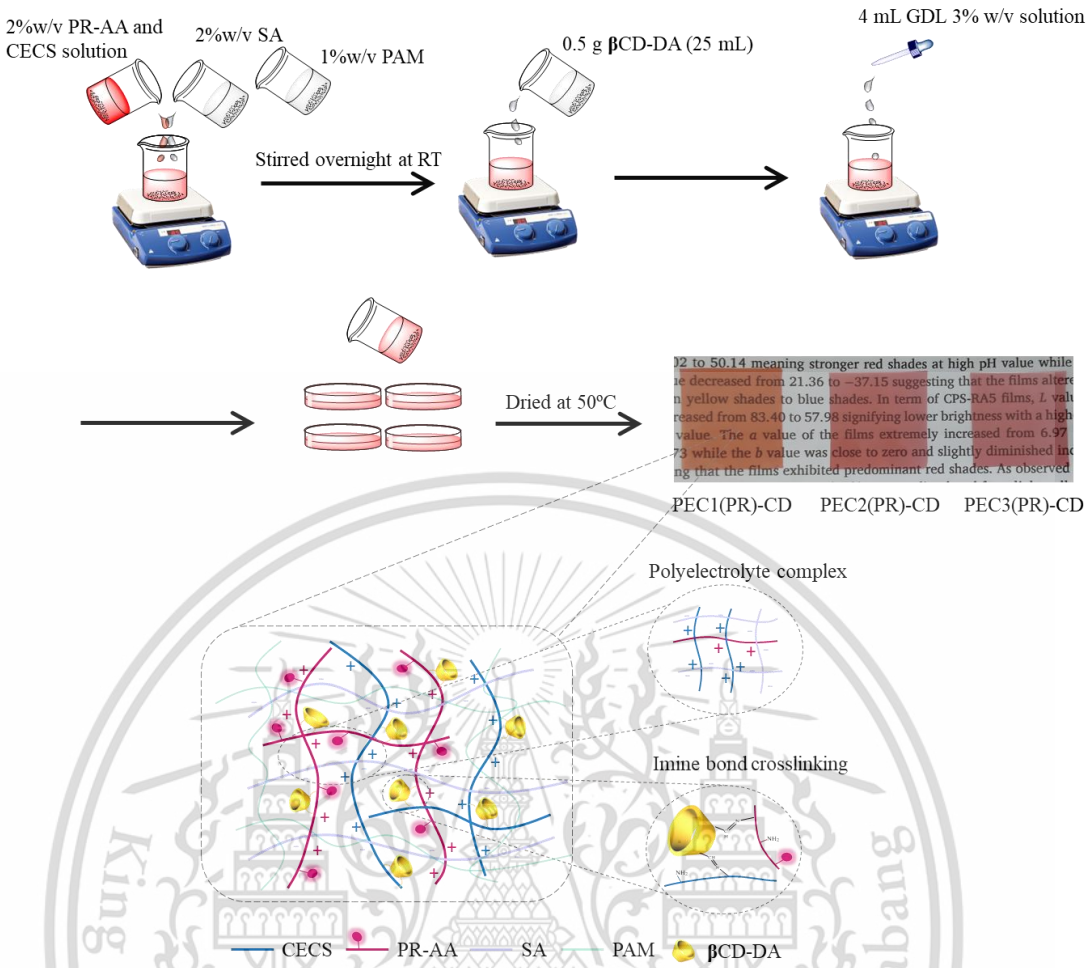

Figure 4.48 Preparation of pH-indicative hydrogel films for smart wound dressings

4.3.1.1 Morphology

Figure 4.49 displays cross-section SEM images of the film crosslinked with GDL, and the film crosslinked with both βCD-DA and GDL, using different ratios of CECS (and PR-AA) to SA. It was observed that the films without βCD-DA (PEC1, PEC2, PEC3) exhibited cracks along the cross-section of the film. This could be attributed to the high glycerol content (40% w/w) in the films, causing them to shrink during the dehydration process [320]. However, the films crosslinked with both βCD-DA and GDL (PEC1(PR)-CD, PEC2(PR)-CD, and PEC3(PR)-CD) showed significantly fewer cracks compared to the films without βCD-DA, suggesting that the addition of βCD-DA, along with PR-AA, could reduce the effect of shrinkage.

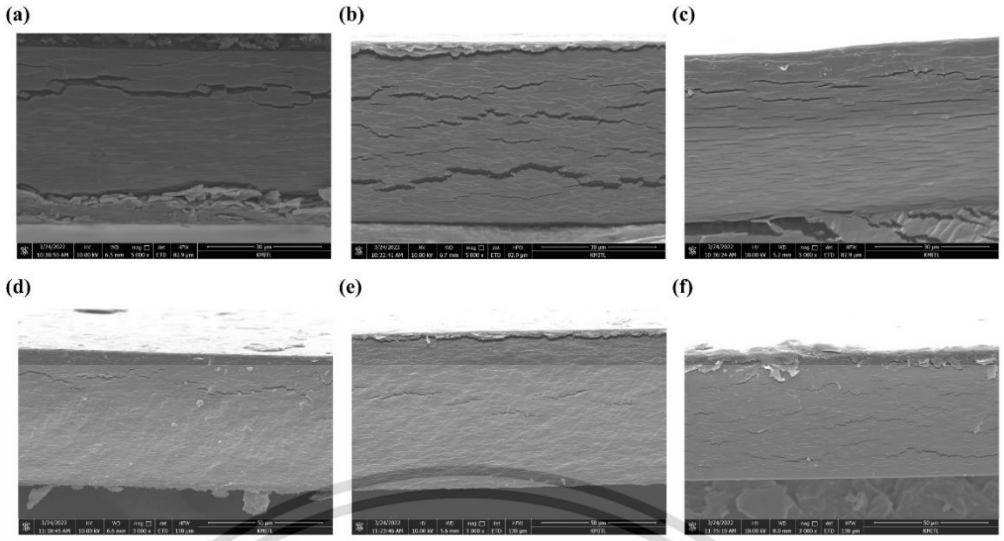

Figure 4.49 SEM micrographs of cross-section of (a) PEC1, (b) PEC2, (c) PEC3, (d) PEC1(PR)-CD, (e) PEC2(PR)-CD, and (f) PEC3(PR)-CD

4.3.1.2 Swelling behavior and solid remain

The swelling degree of the films with and without crosslinking, immersed in buffer pH solutions (pH 5.5, 7.4, and 8.5), is presented in Figure 4.50. These pH solutions were used to represent pH changes in wound exudate as a function of wound status [19]. The non-crosslinked films (Figure 4.50(a)), with an equal content of CECS and SA, initially exhibited a high swelling degree after 5 min of immersion, followed by a rapid decrease until reaching a constant value around 30 min, indicating film dissolution. It is worth noting that the swelling degree at pH 5.5, after reaching equilibrium, was higher than those at pH 7.4 and 8.5, suggesting the presence of some crosslinking between CECS and SA. In weak acidic conditions, the protonation of amine groups in CECS allows for electrostatic interaction with carboxyl groups in SA, leading to the formation of a polyelectrolyte complex [239].

For the films crosslinked with βCD-DA (Blend-CD, Figure 4.50(b)), similar swelling profiles were observed at pH 7.4 and 8.5, with the highest swelling degree at 120 min being 867% and 855% respectively, followed by a slight decrease before reaching equilibrium. This can be attributed to the covalent crosslinking with βCD-DA, which forms imine bonds between the amine groups of CECS and the aldehyde groups of βCD-DA. However, a lower swelling profile was observed at pH 5.5, indicating the effect of acidic conditions enabling the formation of a polyelectrolyte complex. The

formation of the polyelectrolyte complex increased the crosslinking points in the film, resulting in a lower swelling degree.

The films crosslinked with GDL at the same CECS/SA ratio (PEC2 film), compared to the non-crosslinked film and βCD-DA-crosslinked film (Figure 4.50d) exhibited distinct swelling profiles depending on the pH values. At pH 7.4, the films reached a swelling degree of 974% at equilibrium after 3 h of immersion. At pH 5.5, the films reached a swelling degree of 455% at equilibrium after 2 h of immersion, indicating the formation of a polyelectrolyte complex under low pH conditions. However, at pH 8.5, they reached the highest swelling degree of 1454% after 90 min of immersion, followed by a significant decrease to 317% after 24 h. This suggests that the films deteriorated in the basic condition. The basic buffer solution reduced the acidity within the film, resulting in the damage of crosslinking points and ultimately leading to the dissolution of the film. When considering the ratio of CECS to SA in PEC1, PEC2, and PEC3 films, similar swelling profiles were observed based on pH changes, but different values were observed depending on the ratios. At pH 7.4, higher swelling profiles were found in PEC2 and PEC3 films compared to PEC1 film. This can be attributed to an increase in CECS content and a decrease in SA content, resulting in fewer crosslinking points and thus a higher swelling degree. At pH 5.5, the swelling profiles reached equilibrium after 90 min of immersion. The swelling degree of PEC2 and PEC3 films at equilibrium was lower than that of PEC1 film, indicating that films with higher CECS content could undergo further crosslinking at pH 5.5, resulting in higher crosslinking points and a lower swelling degree.

The swelling profiles of films with double crosslinking (GDL and βCD-DA) were presented in Figure 4.50(f-h). It was observed that these films exhibited lower swelling profiles compared to the films with only GDL crosslinking (PEC1, PEC2, and PEC3 films). This can be attributed to the additional crosslinking provided by βCD-DA, which reduces the overall swelling degree of the films. Furthermore, the effect of polyelectrolyte complexation at pH 5.5 was observed in PEC2-CD and PEC3-CD films, as indicated by the constant equilibrium profiles at 460% and 303%, respectively. In the case of the films with PR-AA (Figure 4.50(i-k)), the swelling profiles were similar to the films without PR-AA, but with lower swelling profiles. This may be because PR-AA could undergo partial crosslinking through the Mannich reaction, which could reduce the overall swelling behavior of the films. Additionally, it was observed that increasing

the CECS (and PR-AA) content led to a decrease in swelling degree across all pH values. This suggested that films with higher CECS (and PR-AA) content provided more amine groups that could be crosslinked by βCD-DA, resulting in an increased crosslinking density within the films.

The solid remains of all films are shown in Figure 4.51. The non-crosslinked films exhibited solid remains of 4.8% and 5.5% at pH 7.4 and 8.5, respectively, indicating their dissolution at these pH values. This also confirmed the presence of crosslinking at pH 5.5, as evidenced by the remaining solid remain of 40.9%. The addition of βCD-DA resulted in higher solid remain compared to the non-crosslinked film, confirming the crosslinking provided by βCD-DA. The films crosslinked with GDL exhibited higher solid remain than the non-crosslinked film and the film crosslinked with βCD-DA, especially at pH 5.5 and 7.4. However, at pH 8.5, the solid remain of PEC1 and PEC2 films was significantly low, indicating that these films could be dissolved at this pH, which corresponds to the results of swelling degree.

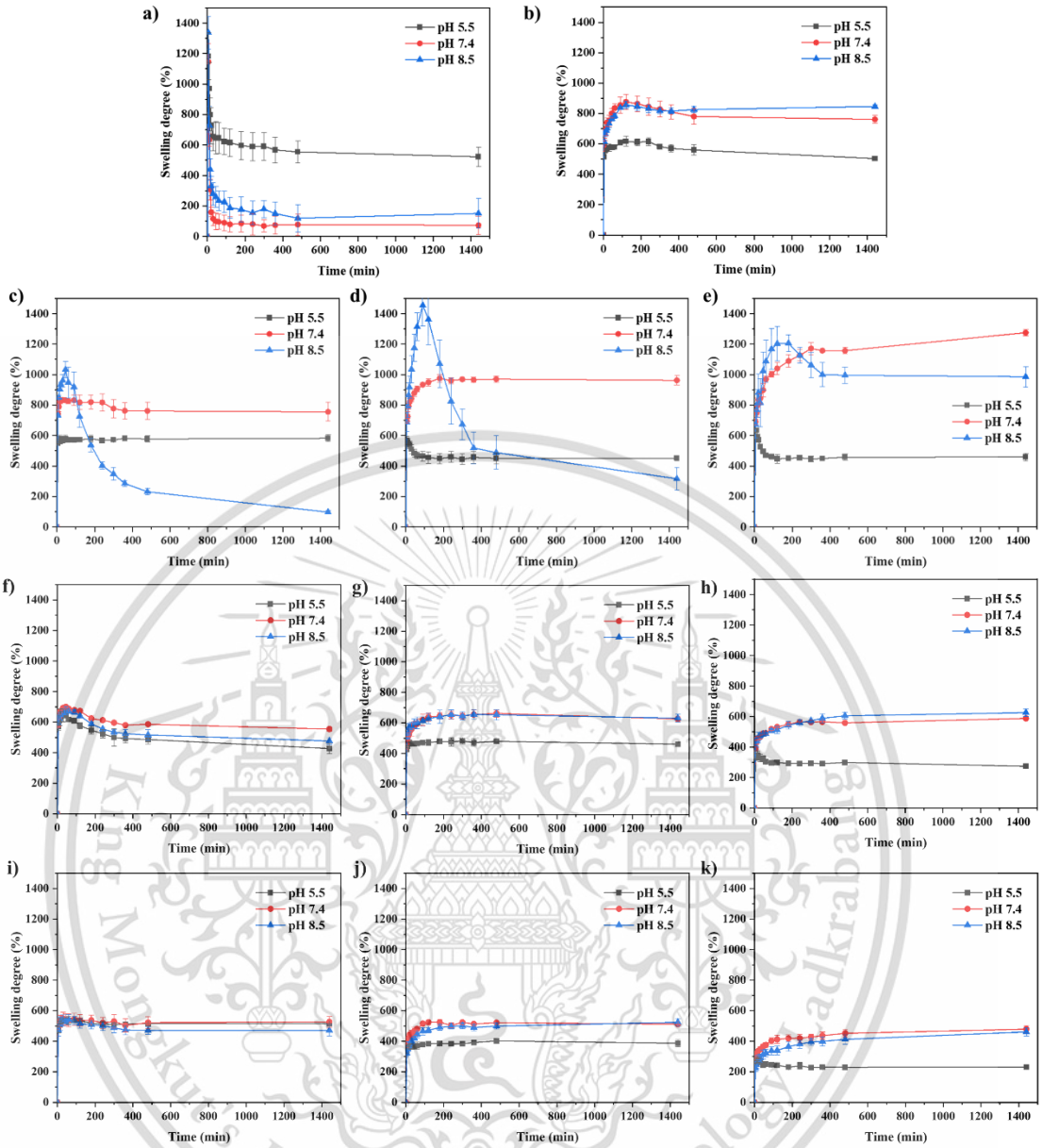

Figure 4.50 Swelling behavior of (a) Non-crosslink, (b) Blend-CD, (c) PEC1, (d) PEC2, (e) PEC3, (f) PEC1-CD, (g) PEC2-CD, (h) PEC3-CD, (i) PEC1(PR)-CD, (j) PEC2(PR)-CD, and (k) PEC3(PR)-CD films

In the case of the double crosslinked films (PEC1-CD, PEC2-CD, and PEC3-CD films), they showed lower solid remain than the films crosslinked with GDL at pH 5.5 and 7.4, while the solid remain at pH 8.5 was higher than that of the films crosslinked with GDL. This was because the crosslinking provided by βCD-DA reduced the possibility of crosslinking from GDL, as well as the formation of polyelectrolyte complex upon immersion at pH 5.5. However, the double crosslinked films maintained

their stability when immersed in pH 8.5, as evidenced by the higher solid remain at this pH. The films incorporating PR-AA (PEC1(PR)-CD, PEC2(PR)-CD, and PEC3(PR)-CD films) followed a similar trend to the films without PR-AA regarding solid remain. It is worth noting that the solid remains of all films remained below 70% due to the removal of glycerol during immersion.

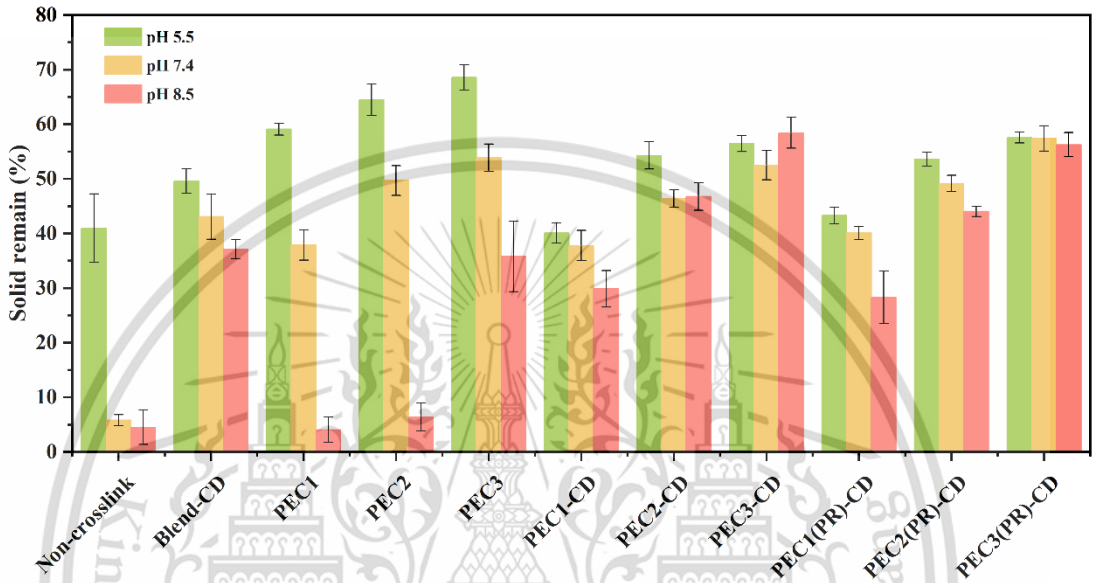

Figure 4.51 Solid remain of the films

4.3.1.3 Coloring properties of the films

The films, incorporating PR-AA with pH-dependent coloring properties, were immersed in buffer solutions with varying pH values, and their color parameters were measured (Figure 4.52). The films exhibited a noticeable color transition, ranging from orange to red and ultimately to purple, as the pH increased from 4 to 10. The color parameters of the films provided interesting insights. PEC1(PR)-CD, PEC2(PR)-CD, and PEC3(PR)-CD films showed an increase in the *a* values from 26.05 to 56.25, 34.26 to 52.56, and 29.15 to 49.54, respectively, indicating a shift towards reddish shades. Conversely, the *b* values decreased from 47.67 to -18.39, 45.34 to -15.76, and 37.89 to -20.99 for PEC1(PR)-CD, PEC2(PR)-CD, and PEC3(PR)-CD films, respectively, signifying a transition from yellow to blue shades. It is noteworthy that the *a* and *b* values of PEC2(PR)-CD and PEC3(PR)-CD films were closely clustered within the pH range of 4-6, resulting in darker orange shades that were difficult to differentiate. This phenomenon can be attributed to the higher CECS content in these films compared to PEC1(PR)-CD,

providing more amine groups available for protonation under acidic conditions. As a result, the protonation of the PR moieties was relatively reduced, leading to less distinct color variations. However, it was important to highlight that the films still exhibited distinguishable shades within the pH range of 4-10, which aligns with the monitoring requirements for wound status. Thus, these films hold potential as smart wound dressings.

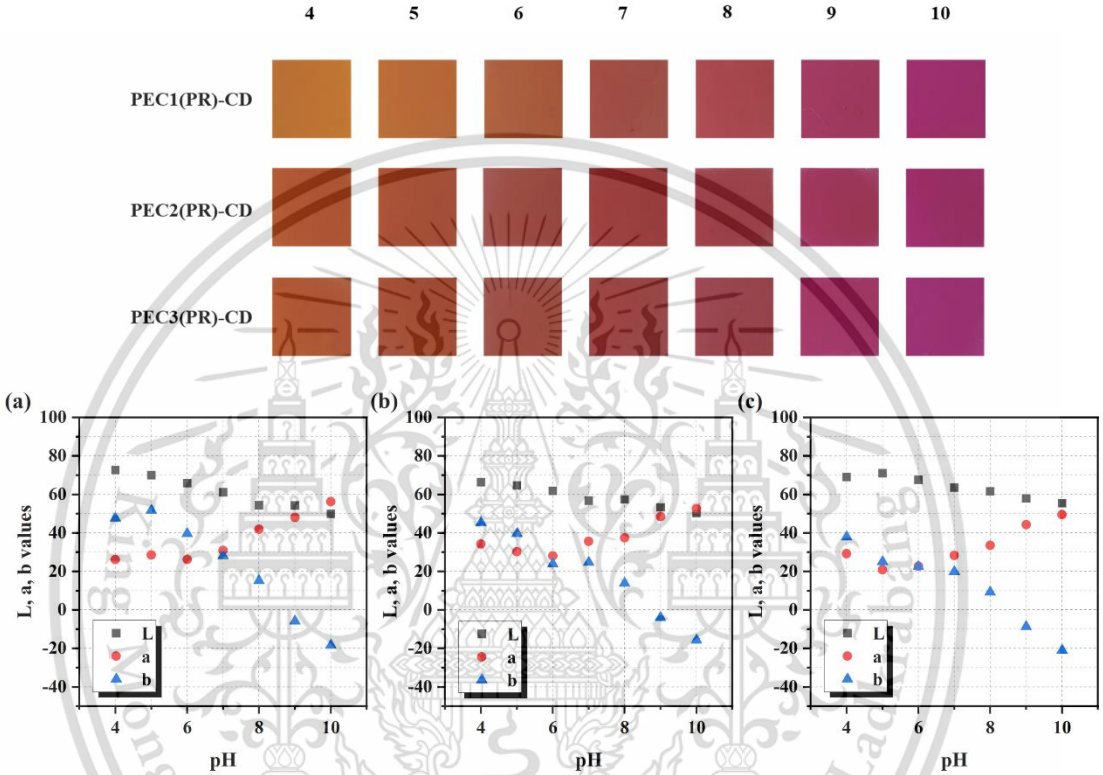

Figure 4.52 Coloring properties of the double crosslinked films with PR-AA and their color parameters: (a) PEC1(PR)-CD, (b) PEC2(PR)-CD, and (c) PEC3(PR)-CD

4.3.1.4 *In vitro* drug release studies

To develop an effective smart wound dressing, drug release capability plays a crucial role in promoting faster wound recovery. Thus, *in vitro* drug release studies were conducted using diclofenac sodium salt (DCF) as a model drug. It is worth noting that there have been reports on the formation of inclusion complexes between CD and DCF [321-323]. Therefore, it was anticipated that DCF would have the ability to form complexes with βCD-DA, enhancing its release properties from the films. The cross-sectional images of the DCF-loaded films, shown in Figure 4.53, demonstrated a homogeneous cross-section without any evidence of drug crystallization. This

observation confirmed the successful incorporation of DCF within the films and supports the potential for controlled drug release.

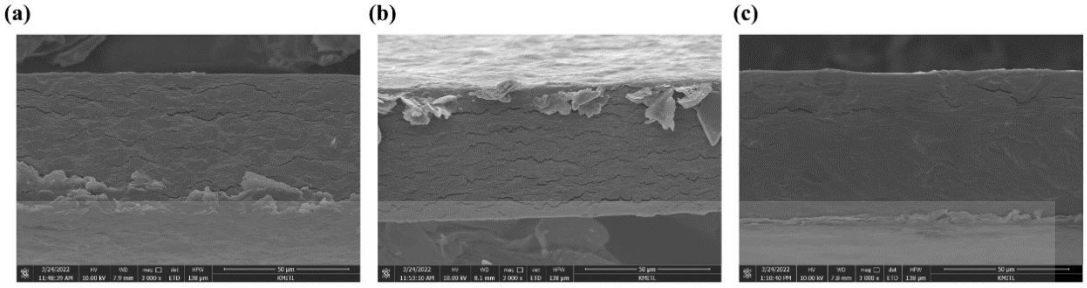

Figure 4.53 SEM micrographs of cross-section of DCF loaded films: (a) PEC1(PR)-CD/DCF, (b) PEC2(PR)-CD/DCF, and (c) PEC3(PR)-CD/DCF

Figure 4.54 presents the *in vitro* drug release profiles of the DCF-loaded films in different pH buffer solutions. At pH 5.5, the films displayed varying release rates, with drug releases of 60.7%, 80.9%, and 86.0% for PEC1(PR)-CD, PEC2(PR)-CD, and PEC3(PR)-CD films, respectively, within 3 h. Complete release was achieved within 24 h. This difference can be attributed to the varying CECS/SA ratios in the films. Specifically, the PEC1(PR)-CD film demonstrated a slower drug release compared to PEC2(PR)-CD and PEC3(PR)-CD films, indicating a delay in drug release. This delay could be attributed to the formation of hydrogen bonds between DCF and SA in the acidic environment, particularly in the case of PEC1(PR)-CD film, which had the highest SA content. However, at pH 7.4 and 8.5, all films exhibited a similar release trend. This can be explained by the reduction in electrostatic interactions within the films due to the deprotonation of ammonium groups in CECS and PR-AA as the pH increased. Consequently, the effect of CECS/SA ratios on the release of DCF became less significant. It is important to note that at pH 8.5, the PEC3(PR)-CD film demonstrated a slightly lower release rate. This can be attributed to its higher crosslinking density, as evidenced by its lower swelling profile in Figure 4.50(k), which resulted in a delay in the drug release.

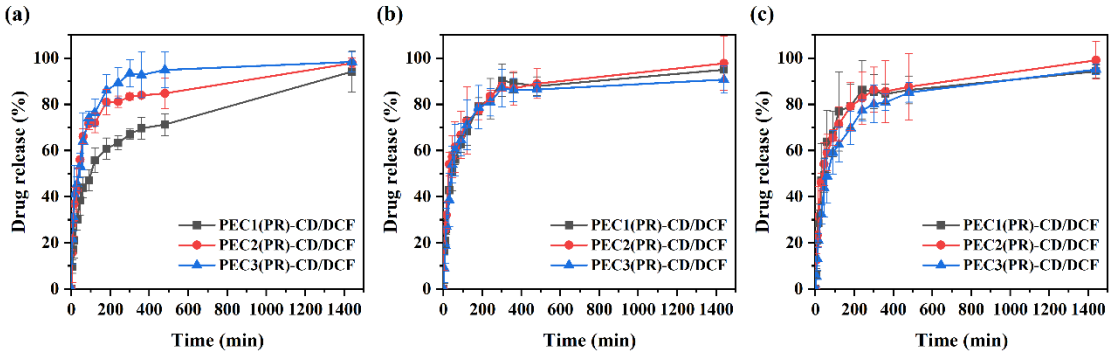

Figure 4.54 Drug release profiles of the films released in (a) pH 5.5, (b) pH 7.4, and (c) pH 8.5 buffer solutions

4.3.1.5 Drug release kinetics

The drug release profiles depicted in Figure 4.54 were analyzed using various mathematical models, such as zero order, first order, Higuchi, and Korsmeyer–Peppas models, to assess the kinetics of drug release. The model with the highest correlation coefficient (R^2) was chosen as the most suitable for each film. Detailed kinetic parameters obtained from the fitting of the mathematical models can be found in Appendix G, where the kinetics were divided into the initial 80% and the final 20% of drug release. Table 4.2 provides an overview of the best fitting kinetic parameters for the DCF-loaded films in different pH solutions.

For the PEC1(PR)-CD film at pH 5.5, the drug release profile demonstrated a good fit with the Higuchi model for the initial 80% release, indicating a slow diffusion of DCF from the film without significant swelling or dissolution effects. However, for the final 20% release, both the first order and Higuchi models provided a good fit, suggesting that the drug release rate depended on the remaining amount of drug in the film. At pH 7.4, the film exhibited a good fit to the Korsmeyer–Peppas model with anomalous transport (n=0.5061) for the initial 80% release. This implied a combination of diffusion and erosion of the film, which could be attributed to a decrease in crosslinking density as the pH increased. For pH 8.5, the film showed a good fit with the Higuchi model for the initial 80% release. This indicated that the drug dissolved rapidly within the film in comparison to its diffusion, suggesting a loss of interactions between DCF and the polymer matrix. As a result, a higher drug release was observed compared to the releases at pH 5.5 and 7.4.

The PEC2(PR)-CD film exhibited a good fit with the Korsmeyer–Peppas model for the initial 80% release in all pH solutions, although with different release exponents (n). At pH 5.5, the film demonstrated Quasi-Fickian diffusion (n=0.4372), indicating that the drug diffused from a non-swellable film that was crosslinked at low pH, resulting in a lower swelling degree. For the final 20% release, the film followed the zero-order model, suggesting that the drug release was independent of drug concentration. At pH 7.4 and 8.5, the film showed anomalous transport (n=0.5030-0.5137), implying a decrease in crosslinking density as the pH increased. This allowed for drug diffusion and relaxation mechanisms to play a role in the release process.

At pH 5.5, the PEC3(PR)-CD film exhibited a good fit with the Korsmeyer–Peppas model for the initial 80% release, displaying Quasi-Fickian diffusion (n=0.3767). This suggested a similar drug diffusion mechanism from the crosslinked film as observed in PEC2(PR)-CD at pH 5.5. At pH 7.4 and 8.5, the PEC3(PR)-CD film demonstrated a good fit with the Higuchi model, indicating a slow release of the drug from a film with negligible swelling. This could be attributed to the high covalent crosslinking density in the film. It is worth noting that for the final 20% release, most samples exhibited a good fit with the first-order model. This was likely because a significant amount of the drug was already released, causing the release rate to depend on the remaining drug concentration.

Table 4.2 Best fitting kinetic parameters for the drug-loaded films selected from several mathematical kinetic models

Film samples	pH	Kinetic model at 80% release	R^2	Release exponent, n (Korsmeyer-Peppas model)	Kinetic model at 20% release	R^2
PEC1(PR)-CD/DCF	5.5	Higuchi model	0.9843	-	First order	0.9943
					Higuchi model	0.9939
	7.4	Korsmeyer-Peppas model	0.9832	0.5061	First order	0.7893
	8.5	Higuchi model	0.9508	-	First order	0.9558
PEC2(PR)-CD/DCF	5.5	Korsmeyer-Peppas model	0.9424	0.4372	Zero order	0.9924
	7.4	Korsmeyer-Peppas model	0.9757	0.5137	First order	0.9730
	8.5	Korsmeyer-Peppas model	0.9432	0.5030	First order	0.9886
PEC3(PR)-CD/DCF	5.5	Korsmeyer-Peppas model	0.9772	0.3767	First order	0.9438
	7.4	Higuchi model	0.9633	-	First order	0.7216
	8.5	Higuchi model	0.9529	-	First order	0.9946

4.3.1.6 Mechanical properties

Figure 4.55 illustrates the tensile strength, elongation at the break, and Young's modulus of the films after being conditioned at 100% relative humidity (RH) for 2 days. The films crosslinked with GDL (PEC1, PEC2, and PEC3 films) exhibited tensile strengths ranging from 6.5 to 11.3 MPa and elongation at the break ranging from 18.4% to 28.5%. In contrast, the double crosslinked films with PR-AA (PEC1(PR)-CD, PEC2(PR)-CD, and PEC3(PR)-CD films) showed higher tensile strengths, ranging from 11.2 to 16.6 MPa. However, the elongation at the break of the double crosslinked films with PR-AA decreased to a range of 7.6 to 14.7%. This corresponded with the higher Young's modulus values of the double crosslinked films with PR-AA, indicating that the crosslinking with βCD-DA had a significant effect on the film properties. It is worth noting that typical tensile strength values for artificial skin range from 2.5 to 16 MPa [324]. On the basis of these results, it may be concluded that the films have the potential to be used in wound dressing applications.

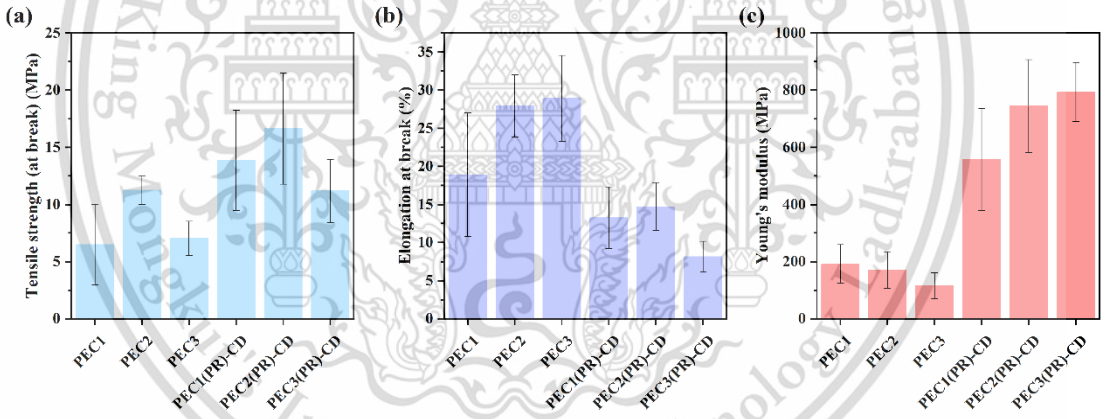

Figure 4.55 Mechanical properties of the films: (a) tensile strength, (b) elongation at break, and (c) Young's modulus

4.3.1.7 Cytotoxicity

Table 4.3 displays the average percentage of cell viability on human skin fibroblasts as measured by the MTT assay. The results revealed that the viability of cells treated with all films, including those with CECS and PR-AA, was close to 100%. This indicates that the films are safe and compatible with cells. Moreover, for a material to be considered biocompatible, the percentage of viable cells should exceed

70% [325]. Therefore, it can be concluded that the films are non-toxic and have the potential to be used as pH-sensing wound dressings while maintaining biocompatibility.

Table 4.3 Cell viability on human skin fibroblasts of the films

Sample	Cell viability
CECS	98.9±0.4
PR-AA	99.0±0.4
PEC1(PR)-CD	98.5±0.8
PEC2(PR)-CD	98.8±0.6
PEC3(PR)-CD	98.5±0.3

4.3.2 Stimuli-responsive and self-healing hydrogels (based on AA-PHP)

In the study published in [326], AA-PHP (CECS-g-PHP) was utilized to develop dual-crosslinked hydrogels with stimuli-responsive properties. These hydrogels employed imine linkages and host-guest interactions, as depicted in Figure 4.56. CECS-g-PHP acted as a guest polymer, forming complexes with hexamethylenediamine modified β-cyclodextrin (β-CD-HDA) as the host molecule. Oxidized sodium alginate (OSA) was introduced to enable crosslinking *via* imine linkages with available amino groups. The resulting hydrogels exhibited pH-responsive behavior, accompanied by a change in color that signified the participation of PHP in CECS-g-PHP, both in pH responsiveness and complexation within the β-CD-HDA cavity. The complexation was confirmed by the fading of the pink color hydrogel at pH 10. Additionally, the hydrogels demonstrated injectability and self-healing properties, with a recovery rate exceeding 80% within 4 hours. They also displayed reversible sol-gel transitions in response to different pH levels and the presence of sodium dodecyl sulfate (SDS) as a competitive guest. Overall, these dual-crosslinked hydrogels, with their pH and stimuli responsiveness, hold substantial potential as versatile biomaterials for various biomedical applications.

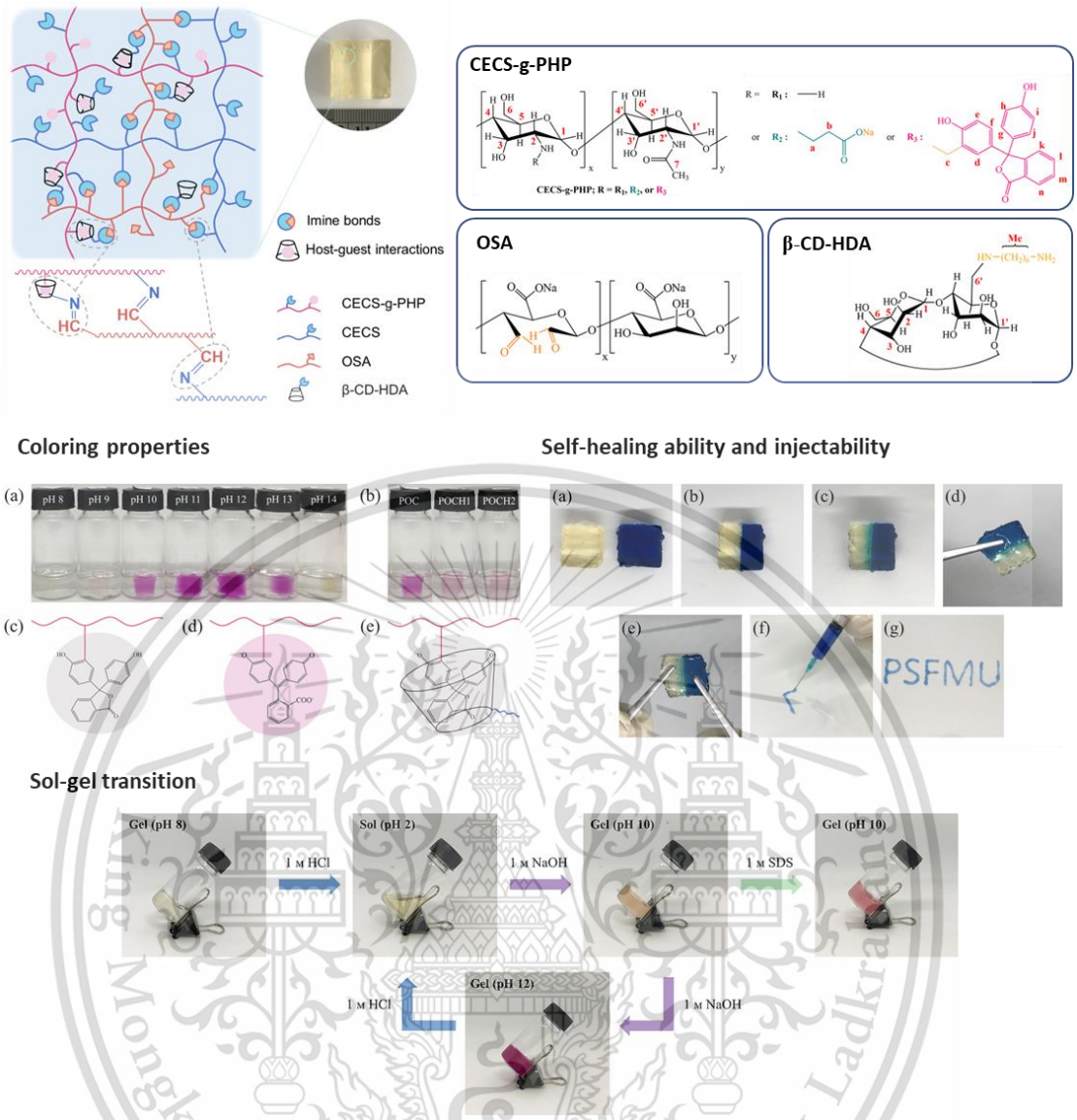

Figure 4.56 Overview of stimuli-responsive, self-healing, and injectable hydrogels based on AA-P2, modified from [326]

4.3.3 Intelligent food packaging films (based on AA-RA)

In the study published in [327], AA-RA (referred to as CECS-g-RA) was used to prepare a film by blending it with CECS, OSA, and poly(vinyl alcohol) (PVA). The aldehyde groups of OSA formed imine bonds with the amino groups of CECS and CECS-g-RA. Additionally, hydrogen bonds were formed between the oxygen-containing groups of the four compounds, resulting in the formation of a double-crosslinked film as depicted in Figure 4.57. The films exhibited distinct color changes, turning yellow at pH 4-5 and transitioning to orange and pink at pH 6-14. Furthermore, the films displayed sensitivity to NH_3 vapor, leading to a color change from yellow to pink.

Moreover, the film was applied for monitoring fish spoilage, where it exhibited color changes that could be observed by the naked eye, indicating its ability to sense volatile nitrogenous compounds released during fish spoilage. These findings demonstrate the potential of the film for intelligent food packaging applications, particularly in the detection of fish freshness.

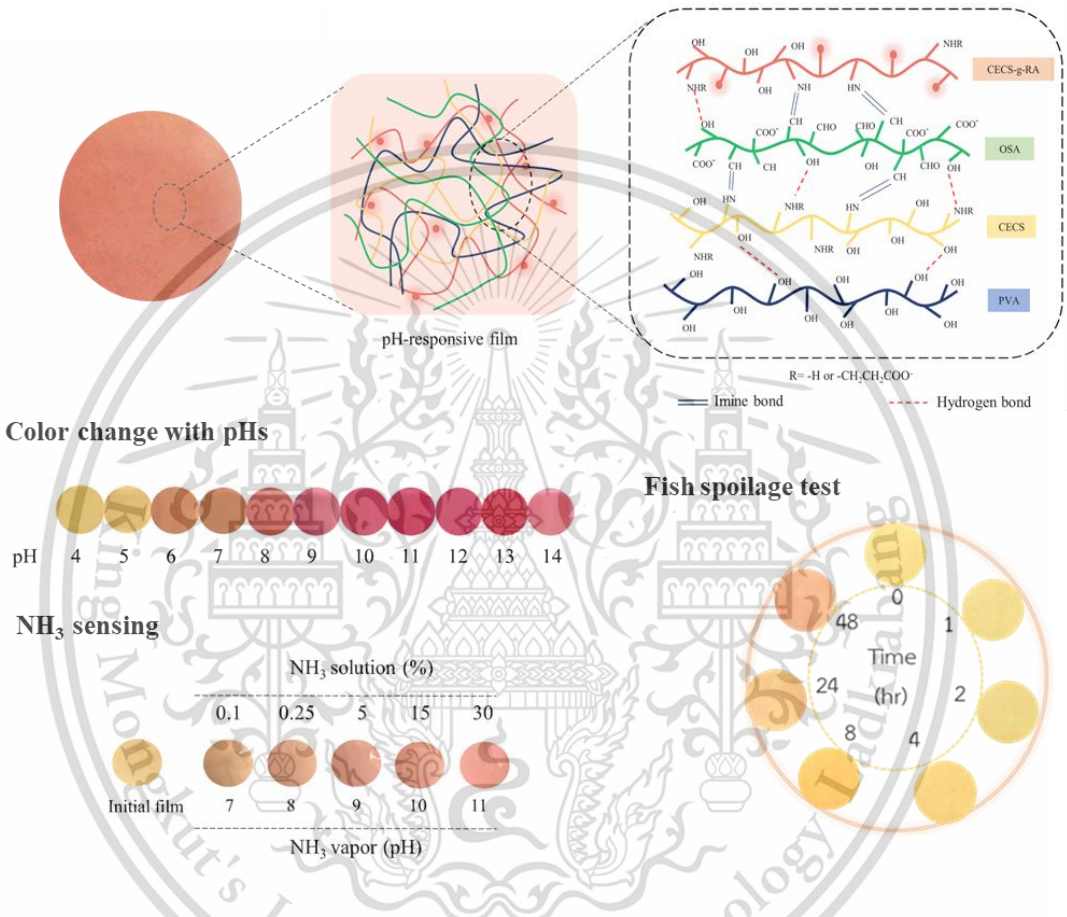

Figure 4.57 Overview of pH-indicative films based on AA-RA for intelligent food packaging, modified from [327]

Chapter 5
Conclusions and suggestions

5.1 Conclusions

In this study, chitosan-based polymeric dyes (CSPDs) were successfully synthesized using the Mannich reaction. The reagents used for the synthesis were phenolphthalein (PHP), phenol red (PR), and rosolic acid (RA), which possess free ortho positions on their phenol groups. The structures of the synthesized derivatives were confirmed through FTIR, NMR, UV-vis, and XRD analyses. The %DS of CS-g-PHPs varied within a wide range (2.4-18.3%) depending on the formaldehyde and PHP contents. Solubility tests demonstrated that CS-g-PHPs dissolved in acidic and strong alkaline conditions, as well as in an alkaline/urea system. Unlike CS, they did not form gels when subjected to heating in the alkaline/urea system, indicating the influence of PHP moieties on their solubility. Furthermore, the CS-g-PHPs exhibited thermally sensitive properties in an alkali/urea mixture.

To synthesize CS-g-PR and CS-g-RA, a lower feed ratio of CS to formaldehyde to dye (1:0.1:0.5) was used to prevent the formation of insoluble products. The resulting %DS was determined to be 3.4% for CS-g-PR and 2.3% for CS-g-RA. The derivatives, including CS-g-PHP (P1) which was purified using the same method, exhibited a crystalline phase with a slightly decreased crystallinity index (CI). This finding indicated that the modification did not have a significant impact on the crystalline nature of CS, which is consistent with the pH-dependent solubility results. Furthermore, all derivatives demonstrated non-toxicity towards HaCat and HeLa cells, suggesting their potential for biocompatible applications.

CSPDs were used to create films to study their color properties. The initially colorless CPS-PHP films exhibited a pink color when the pH was above 10. The CPS-PR films underwent a color transformation, ranging from orange to red to purple, as the pH increased from 4 to 10. Similarly, the CPS-RA films changed from a light-yellow color to red, with a stronger red shade observed at pH values above 9. UV-vis analysis revealed that the films exhibited a red shift compared to their free dye, indicating the presence of new auxochrome groups on the dye molecules. Additionally, the films demonstrated high resistance to dye leaching, indicating that the dyes were covalently

attached to the CS matrix. These findings suggest that these films have great potential for pH sensing applications.

To enhance the water solubility of CSPDs, two methods were used to prepare water-soluble CSPDs (WCSPDs). The first method involved attaching the dyes to carboxyethyl chitosan (CECS), a water-soluble form of chitosan, through the Mannich reaction. However, this method could not be used for phenol red (PR) attachment, and the dye substitutions were limited due to the hindrance caused by the carboxyethyl groups. Therefore, this method was not suitable for the desired function. The second method involved carboxyethylation of CSPDs using the Michael reaction. Successful reactions were confirmed for P1-AA, PR-AA, and RA-AA through FTIR, NMR, UV-vis, and XRD techniques. These derivatives exhibited solubility across a wide pH range, similar to CECS. In terms of coloring properties, they showed color changes similar to CSPDs in the form of CPS films, but in solution form. This resulted in calculated pKa values different from those obtained from the CPS films. Notably, P1-AA demonstrated the ability to form complexes with cyclodextrin, making it suitable as a guest polymer. These findings indicate that WCSPDs, which are soluble in neutral pH and can easily mix with nonionic or anionic polymers, have potential applications in the design of pH-sensing biomaterials and multifunctional biomaterials.

In the application of WCSPDs, specifically PR-AA, hydrogel films were prepared by combining it with SA and PAM. The covalent crosslinker used was βCD-DA, and GDL was incorporated as an acid donor for electrostatic crosslinking. The covalent crosslinking with βCD-DA contributed to the stability of the films, ensuring the maintenance of solid remains. The incorporation of GDL as an acid donor for electrostatic crosslinking resulted in the formation of polyelectrolyte complexes within the film matrix. This led to the films being stable at pH 5.5, exhibiting increased swelling at pH 7.4, and mostly dissolving at pH 8.5. The ratio of CECS to SA played a significant role in determining the swelling degree of the films. Films with higher CECS content exhibited a higher swelling degree at pH 7.4 but a lower swelling degree at pH 5.5. Furthermore, films with double crosslinking showed lower swelling degrees compared to those with single crosslinking. Increasing the CECS content resulted in a decrease in the swelling degree due to the additional crosslinking provided by βCD-DA. The presence of PR-AA in the films not only contributed to lower swelling degrees but also induced color changes from orange to purple, resembling the original color

of PR-AA. These films exhibited discrimination shades in the pH range of 4-10, making them suitable for pH-sensing applications. When DCF was incorporated as a model drug into the hydrogel films, a significant delay in the release rate was observed, particularly in the PEC1(PR)-CD/DCF film at pH 5.5. This highlights the influence of DCF and the composition of the films, specifically the ratio of CECS (and PR-AA) to SA, on the drug release profiles in different buffer pH solutions. Additionally, the mechanical properties of the films were within the applicable range for artificial skin, and they were found to be non-toxic to human skin fibroblast cells. These findings collectively demonstrate the potential of films containing PR-AA as a pH-indicative polymer for wound status monitoring applications.

Furthermore, WCSPDs, including those containing PHP or RA moieties, have been successfully applied in the design of functional materials for various purposes, as demonstrated in published works. These applications encompass the development of hydrogels with multifunctional responsiveness and pH-responsive films for monitoring fish freshness. In summary, this research demonstrates the synthesis of polymeric dyes based on CS, effectively combining the advantageous properties of CS and pH-indicative dyes. With their low toxicity and pH-dependent coloring properties, these derivatives exhibit great potential in the fields of pH sensing and stimuli-responsive materials.

5.2 Suggestions

Although CS is expected to exhibit antimicrobial resistance due to its amino groups, these derivatives did not display such a feature. This discrepancy could be attributed to the long molecular weight of CS. To address this issue, a potential solution would be to use lower molecular weight CS or incorporate additional reaction steps, such as quaternization, to increase the positively charged effects and enhance the antimicrobial activity against microorganisms.

The use of CS with a long molecular weight in this study limited the %DS to prevent the formation of insoluble crosslinking products. To address this limitation, the use of short-chain CS could be considered. However, it is important to note that the mechanical properties and leaching resistance of the materials may be affected and should be carefully considered during the design and fabrication process.

While the derivatives can be visually detected by the naked eye, distinguishing small pH differences can be challenging. To overcome this limitation, color detection using smartphone applications could be employed. By capturing the color changes of the materials with a smartphone camera, specialized software or apps can analyze and quantify the color variations, allowing more accurate and precise pH measurements.

References

[1] Fleischmann, C. Lievenbrück, M. and Ritter, H. 2015. "Polymers and Dyes: Developments and Applications." *Polymers.* 7(4): 717-746.

[2] Chansri, P. Wanno, B. Keawwangchai, S. Tuntulani, T. Pulpoka, B. and Kaewtong, C. 2020. "Spray coating thin polymeric sensor films for Au3+." *Journal of Applied Polymer Science.* 137(2): 48273.

[3] Ding, L. Li, X. Hu, L. Zhang, Y. Jiang, Y. Mao, Z. Xu, H. Wang, B. Feng, X. and Sui, X. 2020. "A naked-eye detection polyvinyl alcohol/cellulose-based pH sensor for intelligent packaging." *Carbohydrate Polymers.* 233: 115859.

[4] Promphet, N. Rattanawaleedirojn, P. Siralertmukul, K. Soatthiyanon, N. Potiyaraj, P. Thanawattano, C. Hinestroza, J P. and Rodthongkum, N. 2019. "Non-invasive textile based colorimetric sensor for the simultaneous detection of sweat pH and lactate." *Talanta.* 192: 424-430.

[5] Mirani, B. Pagan, E. Currie, B. Siddiqui, M A. Hosseinzadeh, R. Mostafalu, P. Zhang, Y S. Ghahary, A. and Akbari, M. 2017. "An Advanced Multifunctional Hydrogel-Based Dressing for Wound Monitoring and Drug Delivery." *Advanced Healthcare Materials.* 6(19): 1700718.

[6] Lv, D. Cui, J. Wang, Y. Zhu, G. Zhang, M. and Li, X. 2017. "Synthesis and color properties of novel polymeric dyes based on grafting of anthraquinone derivatives onto O-carboxymethyl chitosan." *RSC Advances.* 7(53): 33494-33501.

[7] Lv, D. Zhang, M. Cui, J. Lu, J. and Li, W. 2016. "Grafting of edible colorants onto O-carboxymethyl chitosan: preparation, characterization and anti-reduction property evaluation." *New Journal of Chemistry.* 40(4): 3363-3369.

[8] Chawla, S. Kanatt, S. and Sharma, A. 2014. "Chitosan." *Polysaccharides bioactivity and biotechnology. Springer, Cham.* 219-246.

[9] Schoolaert, E. Steyaert, I. Vancoillie, G. Geltmeyer, J. Lava, K. Hoogenboom, R. and De Clerck, K. 2016. "Blend electrospinning of dye-functionalized chitosan and poly(**ε**-caprolactone): towards biocompatible pH-sensors." *Journal of Materials Chemistry B.* 4(26): 4507-4516.

[10] Omura, Y. Taruno, Y. Irisa, Y. Morimoto, M. Saimoto, H. and Shigemasa, Y. 2001. "Regioselective Mannich reaction of phenolic compounds and its application to the synthesis of new chitosan derivatives." *Tetrahedron Letters.* 42(41): 7273-7275.

[11] Morimoto, M. Nakajima, T. Ishikura, M. Shigemasa, Y. Ifuku, S. and Saimoto, H. 2012. "Synthesis of organosoluble chitosan derivatives with polyphenolic side chains." *Carbohydrate Polymers.* 90(3): 1259-1264.

[12] Hossein Beyki, M. Shemirani, F. and Shirkhodaie, M. 2016. "Aqueous Co(II) adsorption using 8-hydroxyquinoline anchored γ-Fe2O3@chitosan with Co(II) as imprinted ions." *International Journal of Biological Macromolecules.* 87: 375-384.

[13] Yu, S. Du, J. Zheng, Y. and Yan, L. 2007. "Synthesis and characterization of carboxymethyl chitosan containing functional ultraviolet absorber substituent." *Journal of Applied Polymer Science.* 106(6): 4098-4103.

[14] Sashiwa, H. Yamamori, N. Ichinose, Y. Sunamoto, J. and Aiba, S-i. 2003. "Chemical Modification of Chitosan, 17." *Macromolecular Bioscience.* 3(5): 231-233.

[15] Ma, G. Yang, D. Zhou, Y. Xiao, M. Kennedy, J F. and Nie, J. 2008. "Preparation and characterization of water-soluble N-alkylated chitosan." *Carbohydrate Polymers.* 74(1): 121-126.

[16] Qu, J. Zhao, X. Ma, P X. and Guo, B. 2017. "pH-responsive self-healing injectable hydrogel based on N-carboxyethyl chitosan for hepatocellular carcinoma therapy." *Acta Biomater.* 58: 168-180.

[17] Jiang, H. Wang, Y. Huang, Q. Li, Y. Xu, C. Zhu, K. and Chen, W. 2005. "Biodegradable hyaluronic acid/n-carboxyethyl chitosan/protein ternary complexes as implantable carriers for controlled protein release." *Macromol Biosci.* 5(12): 1226-1233.

[18] Yang, S. Dong, Q. Yang, H. Liu, X. Gu, S. Zhou, Y. and Xu, W. 2016. "N-carboxyethyl chitosan fibers prepared as potential use in tissue engineering." *International Journal of Biological Macromolecules.* 82: 1018-1022.

[19] Ono, S. Imai, R. Ida, Y. Shibata, D. Komiya, T. and Matsumura, H. 2015. "Increased wound pH as an indicator of local wound infection in second degree burns." *Burns.* 41(4): 820-824.

[20] Qin, M. Guo, H. Dai, Z. Yan, X. and Ning, X. 2019. "Advances in flexible and wearable pH sensors for wound healing monitoring." *Journal of Semiconductors.* 40(11): 111607.

[21] Cabane, E. Zhang, X. Langowska, K. Palivan, C G. and Meier, W. 2012. "Stimuli-responsive polymers and their applications in nanomedicine." *Biointerphases.* 7(1-4): 9.

[22] Wang, D. Green, M D. Chen, K. Daengngam, C. and Kotsuchibashi, Y. 2016. "Stimuli-Responsive Polymers: Design, Synthesis, Characterization, and Applications." *International Journal of Polymer Science.* 2016: 6480259.

[23] Cao, Z-Q. and Wang, G-J. 2016. "Multi-Stimuli-Responsive Polymer Materials: Particles, Films, and Bulk Gels." *The Chemical Record.* 16(3): 1398-1435.

[24] Sun, X. Agate, S. Salem, K S. Lucia, L. and Pal, L. 2021. "Hydrogel-Based Sensor Networks: Compositions, Properties, and Applications—A Review." *ACS Applied Bio Materials.* 4(1): 140-162.

[25] Zhang, L. Xu, T. and Lin, Z. 2006. "Controlled release of ionic drug through the positively charged temperature-responsive membranes." *Journal of Membrane Science.* 281(1): 491-499.

[26] Liu, Y. Meng, L. Lu, X. Zhang, L. and He, Y. 2008. "Thermo and pH sensitive fluorescent polymer sensor for metal cations in aqueous solution." *Polymers for Advanced Technologies.* 19(2): 137-143.

[27] Suwa, K. Morishita, K. Kishida, A. and Akashi, M. 1997. "Synthesis and functionalities of poly(N-vinylalkylamide). V. Control of a lower critical solution temperature of poly(N-vinylalkylamide)." *Journal of Polymer Science Part A: Polymer Chemistry.* 35(15): 3087-3094.

[28] Na, K. Lee, K H. Lee, D H. and Bae, Y H. 2006. "Biodegradable thermo-sensitive nanoparticles from poly(l-lactic acid)/poly(ethylene glycol) alternating multi-block copolymer for potential anti-cancer drug carrier." *European Journal of Pharmaceutical Sciences.* 27(2): 115-122.

[29] Sosnik, A. and Cohn, D. 2004. "Ethoxysilane-capped PEO–PPO–PEO triblocks: a new family of reverse thermo-responsive polymers." *Biomaterials.* 25(14): 2851-2858.

[30] Lee, K W. Yoon, J J. Lee, J H. Kim, S Y. Jung, H J. Kim, S J. Joh, J W. Lee, H H. Lee, D S. and Lee, S K. 2004. "Sustained release of vascular endothelial growth

factor from calcium-induced alginate hydrogels reinforced by heparin and chitosan." *Transplantation Proceedings.* 36(8): 2464-2465.

[31] El-Sherbiny, I M. Khalil, I A. and Ali, I H. 2018. "Updates on Stimuli-Responsive Polymers: Synthesis Approaches and Features." 129-146. in Thakur, V K. and Thakur, M K. **Polymer Gels: Science and Fundamentals**. Singapore: Springer Singapore.

[32] Roggan, A. Friebel, M. Doerschel, K. Hahn, A. and Mueller, G. 1999. "Optical properties of circulating human blood in the wavelength range 400-2500 nm." *Journal of Biomedical Optics.* 4(1).

[33] Ichimura, K. Oh, S-K. and Nakagawa, M. 2000. "Light-Driven Motion of Liquids on a Photoresponsive Surface." *Science.* 288(5471): 1624-1626.

[34] Ichimura, K. Suzuki, Y. Seki, T. Hosoki, A. and Aoki, K. 1988. "Reversible change in alignment mode of nematic liquid crystals regulated photochemically by command surfaces modified with an azobenzene monolayer." *Langmuir.* 4(5): 1214-1216.

[35] Wang, S. Song, Y. and Jiang, L. 2007. "Photoresponsive surfaces with controllable wettability." *Journal of Photochemistry and Photobiology C: Photochemistry Reviews.* 8(1): 18-29.

[36] Jeong, Y J. Yoo, E J. Kim, L H. Park, S. Jang, J. Kim, S H. Lee, S W. and Park, C E. 2016. "Light-responsive spiropyran based polymer thin films for use in organic field-effect transistor memories." *Journal of Materials Chemistry C.* 4(23): 5398-5406.

[37] Jiang, X. Lavender, C A. Woodcock, J W. and Zhao, B. 2008. "Multiple Micellization and Dissociation Transitions of Thermo- and Light-Sensitive Poly(ethylene oxide)-b-poly(ethoxytri(ethylene glycol) acrylate-co-o-nitrobenzyl acrylate) in Water." *Macromolecules.* 41(7): 2632-2643.

[38] Li, Y. Jia, X. Gao, M. He, H. Kuang, G. and Wei, Y. 2010. "Photoresponsive nanocarriers based on PAMAM dendrimers with a o-nitrobenzyl shell." *Journal of Polymer Science Part A: Polymer Chemistry.* 48(3): 551-557.

[39] Dissemond, J. Witthoff, M. Brauns, T C. Haberer, D. and Goos, M. 2003. "[pH values in chronic wounds. Evaluation during modern wound therapy]." *Der Hautarzt; Zeitschrift fur Dermatologie, Venerologie, und verwandte Gebiete.* 54(10): 959-965.

[40] Rofstad, E K. Mathiesen, B. Kindem, K. and Galappathi, K. 2006. "Acidic Extracellular pH Promotes Experimental Metastasis of Human Melanoma Cells in Athymic Nude Mice." *Cancer Research.* 66(13): 6699-6707.

[41] Abdelaal, M Y. Abdel-Razik, E A. Abdel-Bary, E M. and El-Sherbiny, I M. 2007. "Chitosan-based interpolymeric pH-responsive hydrogels for in vitro drug release." *Journal of Applied Polymer Science.* 103(5): 2864-2874.

[42] Kurisawa, M. and Yui, N. 1998. "Gelatin/dextran intelligent hydrogels for drug delivery: Dual-stimuli-responsive degradation in relation to miscibility in interpenetrating polymer networks." *Macromolecular Chemistry and Physics.* 199(8): 1547-1554.

[43] Park, H-Y. Song, I-H. Kim, J-H. and Kim, W-S. 1998. "Preparation of thermally denatured albumin gel and its pH-sensitive swelling." *International Journal of Pharmaceutics.* 175(2): 231-236.

[44] Lee, J W. Kim, S Y. Kim, S S. Lee, Y M. Lee, K H. and Kim, S J. 1999. "Synthesis and characteristics of interpenetrating polymer network hydrogel composed of chitosan and poly(acrylic acid)." *Journal of Applied Polymer Science.* 73(1): 113-120.

[45] Cerritelli, S. Velluto, D. and Hubbell, J A. 2007. "PEG-SS-PPS: Reduction-Sensitive Disulfide Block Copolymer Vesicles for Intracellular Drug Delivery." *Biomacromolecules.* 8(6): 1966-1972.

[46] Yoshida, R. Yamaguchi, T. and Kokufuta, E. 1999. "New intelligent polymer gels: a self-oscillating gel with pacemaking and actuating functions." *Journal of Artificial Organs.* 2(2): 135-140.

[47] Qiu, Y. and Park, K. 2001. "Environment-sensitive hydrogels for drug delivery." *Advanced Drug Delivery Reviews.* 53(3): 321-339.

[48] Chaterji, S. Kwon, I K. and Park, K. 2007. "Smart polymeric gels: Redefining the limits of biomedical devices." *Progress in Polymer Science.* 32(8): 1083-1122.

[49] Wei, M. Gao, Y. Li, X. and Serpe, M J. 2017. "Stimuli-responsive polymers and their applications." *Polymer Chemistry.* 8(1): 127-143.

[50] Ozmen, E Y. Sezgin, M. Yilmaz, A. and Yilmaz, M. 2008. "Synthesis of β-cyclodextrin and starch based polymers for sorption of azo dyes from aqueous solutions." *Bioresource Technology.* 99(3): 526-531.

[51] Crini, G. 2008. "Kinetic and equilibrium studies on the removal of cationic dyes from aqueous solution by adsorption onto a cyclodextrin polymer." *Dyes and Pigments.* 77(2): 415-426.

[52] Donati, F. Pucci, A. and Ruggeri, G. 2009. "Temperature and chemical environment effects on the aggregation extent of water soluble perylene dye into vinyl alcohol-containing polymers." *Physical Chemistry Chemical Physics.* 11(29): 6276-6282.

[53] Ciardelli, F. Ruggeri, G. and Pucci, A. 2013. "Dye-containing polymers: methods for preparation of mechanochromic materials." *Chemical Society Reviews.* 42(3): 857-870.

[54] Donati, F. Pucci, A. Cappelli, C. Mennucci, B. and Ruggeri, G. 2008. "Modulation of the Optical Response of Polyethylene Films Containing Luminescent Perylene Chromophores." *The Journal of Physical Chemistry B.* 112(12): 3668-3679.

[55] Traeger, H. Kiebala, D J. Weder, C. and Schrettl, S. 2021. "From Molecules to Polymers—Harnessing Inter- and Intramolecular Interactions to Create Mechanochromic Materials." *Macromolecular Rapid Communications.* 42(1): 2000573.

[56] Retzmann, N. Maatz, G. and Ritter, H. 2014. "Host–guest-driven color change in water: influence of cyclodextrin on the structure of a copper complex of poly((4-hydroxy-3-(pyridin-3-yldiazenyl)phenethyl)methacrylamide-co-dimethylacrylamide)." *Beilstein Journal of Organic Chemistry.* 10: 2480-2483.

[57] Irie, M. and Kungwatchakun, D. 1984. "Photoresponsive polymers. Mechanochemistry of polyacrylamide gels having triphenylmethane leuco derivatives." *Die Makromolekulare Chemie, Rapid Communications.* 5(12): 829-832.

[58] Shiba, M. Hiramasu, H. Nakano, H. Kawano, Y. Shigeri, Y. and Kondo, T. 1973. "Synthesis of High Polymers with a Light Absorption Band in the Visible Region by Interfacial Polycondensation Reaction." *Polymer Journal.* 4(4): 366-371.

[59] Gao, N. and Zhang, S. 2013. "Phenolphthalein-based cardo poly(arylene ether sulfone): Preparation and application to separation membranes." *Journal of Applied Polymer Science.* 128(1): 1-12.

[60] Yu, Y. Wang, J. Wang, Y. Pan, W. Liu, C. Liu, P. Liang, L. Xu, C. and Liu, Y. 2020. "Polyethyleneimine-functionalized phenolphthalein-based cardo poly(ether ether ketone) membrane for CO2 separation." *Journal of Industrial and Engineering Chemistry.* 83: 20-28.

[61] Li, S. Wang, H. and Tao, M. 2014. "Synthesis and characterization of a new reactive hyperbranched polyphosphate ester, and its modification on benzoxazine-bisoxazoline resins." *Designed Monomers and Polymers.* 17(7): 693-699.

[62] Kiskan, B. Antonietti, M. and Weber, J. 2012. "Teaching New Tricks to an Old Indicator: pH-Switchable, Photoactive Microporous Polymer Networks from Phenolphthalein with Tunable CO2 Adsorption Power." *Macromolecules.* 45(3): 1356-1361.

[63] Dawson, D J. Gless, R D. and Wingard, R E. 1976. "Poly(vinylamine hydrochloride). Synthesis and utilization for the preparation of water-soluble polymeric dyes." *Journal of the American Chemical Society.* 98(19): 5996-6000.

[64] Dawson, D J. Otteson, K M. Wang, P C. and Wingard, R E. 1978. "Soluble Functional Polymers. 2. Utilization of Water-Insoluble Chromophores in Water-Soluble Polymeric Dyes." *Macromolecules.* 11(2): 320-324.

[65] Weil, T. Abdalla, M A. Jatzke, C. Hengstler, J. and Müllen, K. 2005. "Water-Soluble Rylene Dyes as High-Performance Colorants for the Staining of Cells." *Biomacromolecules.* 6(1): 68-79.

[66] Ebbesen, M F. Bienk, K. Deleuran, B W. and Howard, K A. 2014. "Extended blood circulation and joint accumulation of a p(HPMA-co-AzMA)-based nanoconjugate in a murine model of rheumatoid arthritis." *Molecular and Cellular Therapies.* 2(1): 29.

[67] Ebbesen, M F. Schaffert, D H. Crowley, M L. Oupický, D. and Howard, K A. 2013. "Synthesis of click-reactive HPMA copolymers using RAFT polymerization for drug delivery applications." *Journal of Polymer Science Part A: Polymer Chemistry.* 51(23): 5091-5099.

[68] Dollendorf, C. Kreth, S K. Choi, S W. and Ritter, H. 2013. "Polymerization of novel methacrylated anthraquinone dyes." *Beilstein Journal of Organic Chemistry.* 9: 453-459.

[69] Bicker, K L. Wiskur, S L. and Lavigne, J J. 2011. "Colorimetric Sensor Design." 275-295. in **Chemosensors**.

[70] Nopwinyuwong, A. Trevanich, S. and Suppakul, P. 2010. "Development of a novel colorimetric indicator label for monitoring freshness of intermediate-moisture dessert spoilage." *Talanta.* 81(3): 1126-1132.

[71] Nandi, L G. Nicoleti, C R. Bellettini, I C. and Machado, V G. 2014. "Optical Chemosensor for the Detection of Cyanide in Water Based On Ethyl(hydroxyethyl)cellulose Functionalized with Brooker's Merocyanine." *Analytical Chemistry.* 86(10): 4653-4656.

[72] Yoon, J. Chae, S K. and Kim, J-M. 2007. "Colorimetric Sensors for Volatile Organic Compounds (VOCs) Based on Conjugated Polymer-Embedded Electrospun Fibers." *Journal of the American Chemical Society.* 129(11): 3038-3039.

[73] Yoon, J. Jung, Y-S. and Kim, J-M. 2009. "A Combinatorial Approach for Colorimetric Differentiation of Organic Solvents Based on Conjugated Polymer-Embedded Electrospun Fibers." *Advanced Functional Materials.* 19(2): 209-214.

[74] Senthamizhan, A. Celebioglu, A. Bayir, S. Gorur, M. Doganci, E. Yilmaz, F. and Uyar, T. 2015. "Highly Fluorescent Pyrene-Functional Polystyrene Copolymer Nanofibers for Enhanced Sensing Performance of TNT." *ACS Applied Materials & Interfaces.* 7(38): 21038-21046.

[75] Jeon, C H. Lee, J. Ahn, S J. and Ha, T H. 2013. "Solvent effect and amine interference on colorimetric changes of azobenzene-conjugated dithiaazadioxo crown ether mercury sensor." *Tetrahedron Letters.* 54(50): 6841-6847.

[76] Cui, W. Wang, L. Xiang, G. Zhou, L. An, X. and Cao, D. 2015. "A colorimetric and fluorescence "turn-off" chemosensor for the detection of silver ion based on a conjugated polymer containing 2,3-di(pyridin-2-yl)quinoxaline." *Sensors and Actuators B: Chemical.* 207: 281-290.

[77] Alves, N M. and Mano, J F. 2008. "Chitosan derivatives obtained by chemical modifications for biomedical and environmental applications." *International Journal of Biological Macromolecules.* 43(5): 401-414.

[78] Muzzarelli, R A. (2013). **Chitin**. Elsevier.

[79] Aljawish, A. Chevalot, I. Jasniewski, J. Scher, J. and Muniglia, L. 2015. "Enzymatic synthesis of chitosan derivatives and their potential applications." *Journal of Molecular Catalysis B: Enzymatic.* 112: 25-39.

[80] Santos, V P. Marques, N S S. Maia, P C S V. Lima, M A B d. Franco, L d O. and Campos-Takaki, G M d. 2020. "Seafood Waste as Attractive Source of Chitin and Chitosan Production and Their Applications." *International Journal of Molecular Sciences.* 21(12): 4290.

[81] Schmitz, C. Auza, L G. Koberidze, D. Rasche, S. Fischer, R. and Bortesi, L. 2019. "Conversion of Chitin to Defined Chitosan Oligomers: Current Status and Future Prospects." *Mar Drugs.* 17(8).

[82] Roy, J C. Salaün, F. Giraud, S. Ferri, A. Chen, G. and Guan, J. 2017. "Solubility of chitin: solvents, solution behaviors and their related mechanisms." *Solubility of polysaccharides.* 10.

[83] Rinaudo, M. 2006. "Chitin and chitosan: properties and applications." *Progress in Polymer Science.* 31(7): 603-632.

[84] Hu, X. Du, Y. Tang, Y. Wang, Q. Feng, T. Yang, J. and Kennedy, J F. 2007. "Solubility and property of chitin in NaOH/urea aqueous solution." *Carbohydrate Polymers.* 70(4): 451-458.

[85] Fan, M. and Hu, Q. 2009. "Chitosan-LiOH-urea aqueous solution—a novel water-based system for chitosan processing." *Carbohydrate Research.* 344(7): 944-947.

[86] Fang, Y. Zhang, R. Duan, B. Liu, M. Lu, A. and Zhang, L. 2017. "Recyclable Universal Solvents for Chitin to Chitosan with Various Degrees of Acetylation and Construction of Robust Hydrogels." *ACS Sustainable Chemistry & Engineering.* 5(3): 2725-2733.

[87] Cai, J. Zhang, L. Chang, C. Cheng, G. Chen, X. and Chu, B. 2007. "Hydrogen-Bond-Induced Inclusion Complex in Aqueous Cellulose/LiOH/Urea Solution at Low Temperature." *Chemphyschem.* 8(10): 1572-1579.

[88] Liu, S. and Li, L. 2018. "Unique gelation of chitosan in an alkali/urea aqueous solution." *Polymer.* 141: 124-131.

[89] Wang, Z. Nie, J. Qin, W. Hu, Q. and Tang, B Z. 2016. "Gelation process visualized by aggregation-induced emission fluorogens." *Nature Communications.* 7(1): 12033.

[90] He, M. Chen, H. Zhang, X. Wang, C. Xu, C. Xue, Y. Wang, J. Zhou, P. and Zhao, Q. 2018. "Construction of novel cellulose/chitosan composite hydrogels and films and their applications." *Cellulose.* 25(3): 1987-1996.

[91] Liu, Q. Dong, Z. Ding, Z. Hu, Z. Yu, D. Hu, Y. Abidi, N. and Li, W. 2018. "Electroresponsive Homogeneous Polyelectrolyte Complex Hydrogels from Naturally Derived Polysaccharides." *ACS Sustainable Chemistry & Engineering.* 6(5): 7052-7063.

[92] Ding, F. Hu, B. Lan, S. and Wang, H. 2020. "Flexographic and screen printing of carboxymethyl chitosan based edible inks for food packaging applications." *Food Packaging and Shelf Life.* 26: 100559.

[93] Yu, H C. Zhang, H. Ren, K. Ying, Z. Zhu, F. Qian, J. Ji, J. Wu, Z L. and Zheng, Q. 2018. "Ultrathin **K**-Carrageenan/Chitosan Hydrogel Films with High Toughness and Antiadhesion Property." *ACS Applied Materials & Interfaces.* 10(10): 9002-9009.

[94] You, J. Xie, S. Cao, J. Ge, H. Xu, M. Zhang, L. and Zhou, J. 2016. "Quaternized Chitosan/Poly(acrylic acid) Polyelectrolyte Complex Hydrogels with Tough, Self-Recovery, and Tunable Mechanical Properties." *Macromolecules.* 49(3): 1049-1059.

[95] Bi, S. Hu, S. Zhou, Z. Kong, M. Liu, Y. Feng, C. Cheng, X. and Chen, X. 2018. "The green and stable dissolving system based on KOH/urea for homogeneous chemical modification of chitosan." *International Journal of Biological Macromolecules.* 120: 1103-1110.

[96] Song, H. Wu, H. Li, S. Tian, H. Li, Y. and Wang, J. 2018. "Homogeneous Synthesis of Cationic Chitosan via New Avenue." *Molecules.* 23(8): 1921.

[97] Cao, J. You, J. Zhang, L. and Zhou, J. 2018. "Homogeneous synthesis and characterization of chitosan ethers prepared in aqueous alkali/urea solutions." *Carbohydrate Polymers.* 185: 138-144.

[98] Li, C. Han, Q. Guan, Y. and Zhang, Y. 2015. "Michael reaction of chitosan with acrylamides in an aqueous alkali–urea solution." *Polymer Bulletin.* 72(8): 2075-2087.

[99] Matica, A. Menghiu, G. and Ostafe, V. 2017. "Biodegradability of chitosan based products." *New Frontiers in Chemistry.* 26(1): 75-86.

[100] Ma, Z. Wang, W. Wu, Y. He, Y. and Wu, T. 2014. "Oxidative Degradation of Chitosan to the Low Molecular Water-Soluble Chitosan over Peroxotungstate as Chemical Scissors." *PLoS One.* 9(6): e100743.

[101] Zhang, H. and Neau, S H. 2001. "In vitro degradation of chitosan by a commercial enzyme preparation: effect of molecular weight and degree of deacetylation." *Biomaterials.* 22(12): 1653-1658.

[102] Laffleur, F. Hintzen, F. Rahmat, D. Shahnaz, G. Millotti, G. and Bernkop-Schnürch, A. 2013. "Enzymatic degradation of thiolated chitosan." *Drug Development and Industrial Pharmacy.* 39(10): 1531-1539.

[103] Dodane, V. and Vilivalam, V D. 1998. "Pharmaceutical applications of chitosan." *Pharmaceutical Science & Technology Today.* 1(6): 246-253.

[104] Schipper, N G. Vårum, K M. and Artursson, P. 1996. "Chitosans as absorption enhancers for poorly absorbable drugs. 1: Influence of molecular weight and degree of acetylation on drug transport across human intestinal epithelial (Caco-2) cells." *Pharmaceutical Research.* 13(11): 1686-1692.

[105] Chatelet, C. Damour, O. and Domard, A. 2001. "Influence of the degree of acetylation on some biological properties of chitosan films." *Biomaterials.* 22(3): 261-268.

[106] Wedmore, I. McManus, J G. Pusateri, A E. and Holcomb, J B. 2006. "A Special Report on the Chitosan-based Hemostatic Dressing: Experience in Current Combat Operations." *Journal of Trauma and Acute Care Surgery.* 60(3).

[107] Jiang, T. James, R. Kumbar, S G. and Laurencin, C T. 2014. "Chapter 5 - Chitosan as a Biomaterial: Structure, Properties, and Applications in Tissue Engineering and Drug Delivery." 91-113. in Kumbar, S G. Laurencin, C T. and Deng, M. **Natural and Synthetic Biomedical Polymers**. Oxford: Elsevier.

[108] Hosseinnejad, M. and Jafari, S M. 2016. "Evaluation of different factors affecting antimicrobial properties of chitosan." *International Journal of Biological Macromolecules.* 85: 467-475.

[109] Ziani, K. Fernández-Pan, I. Royo, M. and Maté, J I. 2009. "Antifungal activity of films and solutions based on chitosan against typical seed fungi." *Food Hydrocolloids.* 23(8): 2309-2314.

[110] TSAI, G-J. WU, Z-Y. and SU, W-H. 2000. "Antibacterial Activity of a Chitooligosaccharide Mixture Prepared by Cellulase Digestion of Shrimp

Chitosan and Its Application to Milk Preservation." *Journal of Food Protection.* 63(6): 747-752.

[111] Abd El-Hack, M E. El-Saadony, M T. Shafi, M E. Zabermawi, N M. Arif, M. Batiha, G E. Khafaga, A F. Abd El-Hakim, Y M. and Al-Sagheer, A A. 2020. "Antimicrobial and antioxidant properties of chitosan and its derivatives and their applications: A review." *International Journal of Biological Macromolecules.* 164: 2726-2744.

[112] Dai, T. Tanaka, M. Huang, Y-Y. and Hamblin, M R. 2011. "Chitosan preparations for wounds and burns: antimicrobial and wound-healing effects." *Expert Review of Anti-infective Therapy.* 9(7): 857-879.

[113] Zou, P. Yang, X. Wang, J. Li, Y. Yu, H. Zhang, Y. and Liu, G. 2016. "Advances in characterisation and biological activities of chitosan and chitosan oligosaccharides." *Food Chemistry.* 190: 1174-1181.

[114] Smith, J. Wood, E. and Dornish, M. 2004. "Effect of chitosan on epithelial cell tight junctions." *Pharmaceutical Research.* 21(1): 43-49.

[115] Rao, S B. and Sharma, C P. 1997. "Use of chitosan as a biomaterial: Studies on its safety and hemostatic potential." *Journal of Biomedical Materials Research.* 34(1): 21-28.

[116] Patrulea, V. Ostafe, V. Borchard, G. and Jordan, O. 2015. "Chitosan as a starting material for wound healing applications." *European Journal of Pharmaceutics and Biopharmaceutics.* 97: 417-426.

[117] Sivashankari, P R. and Prabaharan, M. 2017. "5 - Deacetylation modification techniques of chitin and chitosan." 117-133. in Jennings, J A. and Bumgardner, J D. **Chitosan Based Biomaterials Volume 1**. Woodhead Publishing.

[118] Kasaai, M R. 2009. "Various Methods for Determination of the Degree of N-Acetylation of Chitin and Chitosan: A Review." *Journal of Agricultural and Food Chemistry.* 57(5): 1667-1676.

[119] Jiang, X. Chen, L. and Zhong, W. 2003. "A new linear potentiometric titration method for the determination of deacetylation degree of chitosan." *Carbohydrate Polymers.* 54(4): 457-463.

[120] dos Santos, Z M. Caroni, A L P F. Pereira, M R. da Silva, D R. and Fonseca, J L C. 2009. "Determination of deacetylation degree of chitosan: a comparison

between conductometric titration and CHN elemental analysis." *Carbohydrate Research.* 344(18): 2591-2595.

[121] Dimzon, I K D. and Knepper, T P. 2015. "Degree of deacetylation of chitosan by infrared spectroscopy and partial least squares." *International Journal of Biological Macromolecules.* 72: 939-945.

[122] Baskar, D. and Sampath Kumar, T S. 2009. "Effect of deacetylation time on the preparation, properties and swelling behavior of chitosan films." *Carbohydrate Polymers.* 78(4): 767-772.

[123] Wijesena, R N. Tissera, N. Kannangara, Y Y. Lin, Y. Amaratunga, G A J. and de Silva, K M N. 2015. "A method for top down preparation of chitosan nanoparticles and nanofibers." *Carbohydrate Polymers.* 117: 731-738.

[124] Hussain, M R. Iman, M. and Maji, T K. 2013. "Determination of degree of deacetylation of chitosan and their effect on the release behavior of essential oil from chitosan and chitosan-gelatin complex microcapsules." *International Journal of Advanced Engineering Applications.* 6(4): 4-12.

[125] Czechowska-Biskup, R. Jarosińska, D. Rokita, B. Ulański, P. and Rosiak, J M. 2012. "Determination of degree of deacetylation of chitosan-comparision of methods." *Progress on Chemistry and Application of Chitin and its Derivatives.* 17: 5-20.

[126] Kaya, M. Mujtaba, M. Ehrlich, H. Salaberria, A M. Baran, T. Amemiya, C T. Galli, R. Akyuz, L. Sargin, I. and Labidi, J. 2017. "On chemistry of γ-chitin." *Carbohydrate Polymers.* 176: 177-186.

[127] Kumari, S. and Kishor, R. 2020. "Chapter 1 - Chitin and chitosan: origin, properties, and applications." 1-33. in Gopi, S. Thomas, S. and Pius, A. **Handbook of Chitin and Chitosan**. Elsevier.

[128] Zhang, Y. Xue, C. Xue, Y. Gao, R. and Zhang, X. 2005. "Determination of the degree of deacetylation of chitin and chitosan by X-ray powder diffraction." *Carbohydrate Research.* 340(11): 1914-1917.

[129] Focher, B. Beltrame, P L. Naggi, A. and Torri, G. 1990. "Alkaline N-deacetylation of chitin enhanced by flash treatments. Reaction kinetics and structure modifications." *Carbohydrate Polymers.* 12(4): 405-418.

[130] Klug, H P. and Alexander, L E. 1974. **X-ray diffraction procedures: for polycrystalline and amorphous materials**. 2nd ed. New Jersey : Wiley.

[131] Mourya, V K. and Inamdar, N N. 2008. "Chitosan-modifications and applications: Opportunities galore." *Reactive and Functional Polymers.* 68(6): 1013-1051.

[132] Pokhrel, S. and Yadav, P N. 2019. "Functionalization of chitosan polymer and their applications." *Journal of Macromolecular Science, Part A.* 56(5): 450-475.

[133] Wang, W. Xue, C. and Mao, X. 2020. "Chitosan: Structural modification, biological activity and application." *International Journal of Biological Macromolecules.* 164: 4532-4546.

[134] Thanou, M. Verhoef, J C. and Junginger, H E. 2001. "Oral drug absorption enhancement by chitosan and its derivatives." *Advanced Drug Delivery Reviews.* 52(2): 117-126.

[135] Cano-Cebrián, M J. Zornoza, T. Granero, L. and Polache, A. 2005. "Intestinal absorption enhancement via the paracellular route by fatty acids, chitosans and others: a target for drug delivery." *Curr Drug Deliv.* 2(1): 9-22.

[136] Li, H. Zhang, Z. Bao, X. Xu, G. and Yao, P. 2018. "Fatty acid and quaternary ammonium modified chitosan nanoparticles for insulin delivery." *Colloids and Surfaces B: Biointerfaces.* 170: 136-143.

[137] Li, J. Xie, B. Xia, K. Zhao, C. Li, Y. Li, D. and Han, J. 2018. "Facile synthesis and characterization of cross-linked chitosan quaternary ammonium salt membrane for antibacterial coating of piezoelectric sensors." *International Journal of Biological Macromolecules.* 120: 745-752.

[138] Zhou, Y. Yang, H. Liu, X. Mao, J. Gu, S. and Xu, W. 2013. "Potential of quaternization-functionalized chitosan fiber for wound dressing." *International Journal of Biological Macromolecules.* 52: 327-332.

[139] Mi, X. Vijayaragavan, K S. and Heldt, C L. 2014. "Virus adsorption of water-stable quaternized chitosan nanofibers." *Carbohydrate Research.* 387: 24-29.

[140] Domard, A. Rinaudo, M. and Terrassin, C. 1986. "New method for the quaternization of chitosan." *International Journal of Biological Macromolecules.* 8(2): 105-107.

[141] Domard, A. Gey, C. Rinaudo, M. and Terrassin, C. 1987. "13C and 1H n.m.r. spectroscopy of chitosan and N-trimethyl chloride derivatives." *International Journal of Biological Macromolecules.* 9(4): 233-237.

[142] Sieval, A B. Thanou, M. Kotze´, A F. Verhoef, J C. Brussee, J. and Junginger, H E. 1998. "Preparation and NMR characterization of highly substitutedN-trimethyl chitosan chloride." *Carbohydrate Polymers.* 36(2): 157-165.

[143] Daly, W H. and Manuszak-Guerrini, M A. (2001) Biocidal chitosan derivatives, Google Patents.

[144] Shigemasa, Y. Usui, H. Morimoto, M. Saimoto, H. Okamoto, Y. Minami, S. and Sashiwa, H. 1999. "Chemical modification of chitin and chitosan 1: preparation of partially deacetylated chitin derivatives via a ring-opening reaction with cyclic acid anhydrides in lithium chloride/N,N-dimethylacetamide." *Carbohydrate Polymers.* 39(3): 237-243.

[145] Hirano, S. Yamaguchi, Y. and Kamiya, M. 2002. "Novel N-saturated-fatty-acyl derivatives of chitosan soluble in water and in aqueous acid and alkaline solutions." *Carbohydrate Polymers.* 48(2): 203-207.

[146] Le Tien, C. Lacroix, M. Ispas-Szabo, P. and Mateescu, M-A. 2003. "N-acylated chitosan: hydrophobic matrices for controlled drug release." *Journal of Controlled Release.* 93(1): 1-13.

[147] Sashiwa, H. Kawasaki, N. Nakayama, A. Muraki, E. Yamamoto, N. Zhu, H. Nagano, H. Omura, Y. Saimoto, H. Shigemasa, Y. and Aiba, S. 2002. "Chemical modification of chitosan. 13.(1) Synthesis of organosoluble, palladium adsorbable, and biodegradable chitosan derivatives toward the chemical plating on plastics." *Biomacromolecules.* 3(5): 1120-1125.

[148] Zong, Z. Kimura, Y. Takahashi, M. and Yamane, H. 2000. "Characterization of chemical and solid state structures of acylated chitosans." *Polymer.* 41(3): 899-906.

[149] Hirano, S. Ohe, Y. and Ono, H. 1976. "Selective N-acylation of chitosan." *Carbohydrate Research.* 47(2): 315-320.

[150] Hirano, S. and Yamaguchi, R. 1976. "N-acetylchitosan gel: A polyhydrate of chitin." *Biopolymers.* 15(9): 1685-1691.

[151] Hirano, S. and Moriyasu, T. 1981. "N-(Carboxyacyl)chitosans." *Carbohydrate Research.* 92(2): 323-327.

[152] Sashiwa, H. and Shigemasa, Y. 1999. "Chitosan, a Biodegradable and Biocompatible Polymer." *Carbohydrate Polymers.* 39(2): 127-138.

[153] Hirano, S. and Moriyasu, T. 2004. "Some novel N-(carboxyacyl)chitosan filaments." *Carbohydrate Polymers.* 55(3): 245-248.

[154] Kurita, K. Nishimura, S-I. and Takeda, T. 1990. "N-Hydroxyacylation of Chitosan with Lactones." *Polymer Journal.* 22(5): 429-434.

[155] Piegat, A. Goszczyńska, A. Idzik, T. and Niemczyk, A. 2019. "The Importance of Reaction Conditions on the Chemical Structure of N,O-Acylated Chitosan Derivatives." *Molecules (Basel, Switzerland).* 24(17): 3047.

[156] Sharma, D. and Singh, J. 2017. "Synthesis and Characterization of Fatty Acid Grafted Chitosan Polymer and Their Nanomicelles for Nonviral Gene Delivery Applications." *Bioconjugate Chemistry.* 28(11): 2772-2783.

[157] Medeiros Borsagli, F G L. Carvalho, I C. and Mansur, H S. 2018. "Amino acid-grafted and N-acylated chitosan thiomers: Construction of 3D bio-scaffolds for potential cartilage repair applications." *International Journal of Biological Macromolecules.* 114: 270-282.

[158] Vasnev, V A. Tarasov, A I. Markova, G D. Vinogradova, S V. and Garkusha, O G. 2006. "Synthesis and properties of acylated chitin and chitosan derivatives." *Carbohydrate Polymers.* 64(2): 184-189.

[159] Sashiwa, H. Kawasaki, N. Nakayama, A. Muraki, E. Yamamoto, N. Zhu, H. Nagano, H. Omura, Y. Saimoto, H. Shigemasa, Y. and Aiba, S-i. 2002. "Chemical Modification of Chitosan. 13. Synthesis of Organosoluble, Palladium Adsorbable, and Biodegradable Chitosan Derivatives toward the Chemical Plating on Plastics." *Biomacromolecules.* 3(5): 1120-1125.

[160] Bidgoli, H. Khodadadi, A A. and Mortazavi, Y. 2019. "A hydrophobic/oleophilic chitosan-based sorbent: Toward an effective oil spill remediation technology." *Journal of Environmental Chemical Engineering.* 7(5): 103340.

[161] Al-Remawi, M. 2015. "Application of N-hexoyl chitosan derivatives with high degree of substitution in the preparation of super-disintegrating pharmaceutical matrices." *Journal of Drug Delivery Science and Technology.* 29: 31-41.

[162] Azmy, E A M. Hashem, H E. Mohamed, E A. and Negm, N A. 2019. "Synthesis, characterization, swelling and antimicrobial efficacies of chemically modified chitosan biopolymer." *Journal of Molecular Liquids.* 284: 748-754.

[163] Lang, G. Maresch, G. Wendel, H. Konrad, E. Lenz, H-r. and Titze, J. (1988) Cosmetic compositions based upon N-hydroxypropyl-chitosans, new N-hyroxypropyl-chitosans, as well as processes for the production thereof, Google Patents.

[164] Lang, G. Maresch, G. Lenz, H-r. Konrad, E. Breuer, L. and Hoch, D. (1989) Cosmetic compositions on the basis of alkyl-hydroxypropyl-substituted chitosan derivatives, new chitosan derivatives and processes for the production thereof, Google Patents.

[165] Xie, Y. Liu, X. and Chen, Q. 2007. "Synthesis and characterization of water-soluble chitosan derivate and its antibacterial activity." *Carbohydrate Polymers.* 69(1): 142-147.

[166] Han, J K. Kim, M S. Lee, D S. Kim, Y-S. Park, R-W. Kim, K. and Kwon, I C. 2009. "Evaluation of the anti-tumor effects of paclitaxel-encapsulated pH-sensitive micelles." *Macromolecular Research.* 17(2): 99-103.

[167] Hyung Park, J. Kwon, S. Lee, M. Chung, H. Kim, J-H. Kim, Y-S. Park, R-W. Kim, I-S. Bong Seo, S. Kwon, I C. and Young Jeong, S. 2006. "Self-assembled nanoparticles based on glycol chitosan bearing hydrophobic moieties as carriers for doxorubicin: In vivo biodistribution and anti-tumor activity." *Biomaterials.* 27(1): 119-126.

[168] Park, K. Kim, J-H. Nam, Y S. Lee, S. Nam, H Y. Kim, K. Park, J H. Kim, I-S. Choi, K. Kim, S Y. and Kwon, I C. 2007. "Effect of polymer molecular weight on the tumor targeting characteristics of self-assembled glycol chitosan nanoparticles." *Journal of Controlled Release.* 122(3): 305-314.

[169] Kim, J-H. Kim, Y-S. Kim, S. Park, J H. Kim, K. Choi, K. Chung, H. Jeong, S Y. Park, R-W. Kim, I-S. and Kwon, I C. 2006. "Hydrophobically modified glycol chitosan nanoparticles as carriers for paclitaxel." *Journal of Controlled Release.* 111(1): 228-234.

[170] Kim, J-H. Kim, Y-S. Park, K. Kang, E. Lee, S. Nam, H Y. Kim, K. Park, J H. Chi, D Y. Park, R-W. Kim, I-S. Choi, K. and Chan Kwon, I. 2008. "Self-assembled glycol chitosan nanoparticles for the sustained and prolonged delivery of antiangiogenic small peptide drugs in cancer therapy." *Biomaterials.* 29(12): 1920-1930.

[171] Sang Yoo, H. Eun Lee, J. Chung, H. Chan Kwon, I. and Young Jeong, S. 2005. "Self-assembled nanoparticles containing hydrophobically modified glycol chitosan for gene delivery." *Journal of Controlled Release.* 103(1): 235-243.

[172] Hwang, H-Y. Kim, I-S. Kwon, I C. and Kim, Y-H. 2008. "Tumor targetability and antitumor effect of docetaxel-loaded hydrophobically modified glycol chitosan nanoparticles." *Journal of Controlled Release.* 128(1): 23-31.

[173] Min, K H. Park, K. Kim, Y-S. Bae, S M. Lee, S. Jo, H G. Park, R-W. Kim, I-S. Jeong, S Y. Kim, K. and Kwon, I C. 2008. "Hydrophobically modified glycol chitosan nanoparticles-encapsulated camptothecin enhance the drug stability and tumor targeting in cancer therapy." *Journal of Controlled Release.* 127(3): 208-218.

[174] Kim, J-H. Kim, Y-S. Park, K. Lee, S. Nam, H Y. Min, K H. Jo, H G. Park, J H. Choi, K. Jeong, S Y. Park, R-W. Kim, I-S. Kim, K. and Kwon, I C. 2008. "Antitumor efficacy of cisplatin-loaded glycol chitosan nanoparticles in tumor-bearing mice." *Journal of Controlled Release.* 127(1): 41-49.

[175] Park, J H. Kwon, S. Nam, J-O. Park, R-W. Chung, H. Seo, S B. Kim, I-S. Kwon, I C. and Jeong, S Y. 2004. "Self-assembled nanoparticles based on glycol chitosan bearing 5β-cholanic acid for RGD peptide delivery." *Journal of Controlled Release.* 95(3): 579-588.

[176] Cho, Y W. Kim, Y-S. Kim, I-S. Park, R-W. Oh, S J. Moon, D H. Kim, S Y. and Kwon, I C. 2008. "Tumoral accumulation of long-circulating, self-assembled nanoparticles and its visualization by gamma scintigraphy." *Macromolecular Research.* 16(1): 15-20.

[177] Park, J S. and Cho, Y W. 2007. "In vitro cellular uptake and cytotoxicity of paclitaxel-loaded glycol chitosan self-assembled nanoparticles." *Macromolecular Research.* 15(6): 513-519.

[178] Uchegbu, I F. Sadiq, L. Pardakhty, A. El-Hammadi, M. Gray, A I. Tetley, L. Wang, W. Zinselmeyer, B H. and Schätzlein, A G. 2004. "Gene Transfer with Three Amphiphilic Glycol Chitosans—the Degree of Polymerisation is the Main Controller of Transfection Efficiency." *Journal of Drug Targeting.* 12(8): 527-539.

[179] Park, J S. Han, T H. Lee, K Y. Han, S S. Hwang, J J. Moon, D H. Kim, S Y. and Cho, Y W. 2006. "N-acetyl histidine-conjugated glycol chitosan self-assembled

nanoparticles for intracytoplasmic delivery of drugs: Endocytosis, exocytosis and drug release." *Journal of Controlled Release.* 115(1): 37-45.

[180] Kim, K. Kim, J-H. Kim, S. Chung, H. Choi, K. Kwon, I C. Park, J H. Kim, Y-S. Park, R-W. Kim, I-S. and Jeong, S Y. 2005. "Self-assembled nanoparticles of bile acid-modified glycol chitosans and their applications for cancer therapy." *Macromolecular Research.* 13(3): 167-175.

[181] Ho, D-K. Frisch, S. Biehl, A. Terriac, E. De Rossi, C. Schwarzkopf, K. Lautenschläger, F. Loretz, B. Murgia, X. and Lehr, C-M. 2018. "Farnesylated Glycol Chitosan as a Platform for Drug Delivery: Synthesis, Characterization, and Investigation of Mucus–Particle Interactions." *Biomacromolecules.* 19(8): 3489-3501.

[182] Fei Liu, X. Lin Guan, Y. Zhi Yang, D. Li, Z. and De Yao, K. 2001. "Antibacterial action of chitosan and carboxymethylated chitosan." *Journal of Applied Polymer Science.* 79(7): 1324-1335.

[183] Abreu, F R d. and Campana-Filho, S P. 2005. "Preparation and characterization of carboxymethylchitosan." *Polímeros.* 15: 79-83.

[184] Muzzarelli, R A A. Tanfani, F. Emanuelli, M. and Mariotti, S. 1982. "N-(carboxymethylidene)chitosans and N-(carboxymethyl)chitosans: Novel chelating polyampholytes obtained from chitosan glyoxylate." *Carbohydrate Research.* 107(2): 199-214.

[185] Shariatinia, Z. 2018. "Carboxymethyl chitosan: Properties and biomedical applications." *International Journal of Biological Macromolecules.* 120: 1406-1419.

[186] Li, X. Chen, S. Zhang, B. Li, M. Diao, K. Zhang, Z. Li, J. Xu, Y. Wang, X. and Chen, H. 2012. "In situ injectable nano-composite hydrogel composed of curcumin, N,O-carboxymethyl chitosan and oxidized alginate for wound healing application." *International Journal of Pharmaceutics.* 437(1): 110-119.

[187] Huang, X. Zhang, Y. Zhang, X. Xu, L. Chen, X. and Wei, S. 2013. "Influence of radiation crosslinked carboxymethyl-chitosan/gelatin hydrogel on cutaneous wound healing." *Materials Science and Engineering: C.* 33(8): 4816-4824.

[188] Muzzarelli, R A A. Ramos, V. Stanic, V. Bruno, D. Mattioli-Belmonte, M. Tosi, G. and Giardino, R. 1998. "Osteogenesis promoted by calcium phosphate N,N-dicarboxymethyl chitosan." *Carbohydrate Polymers.* 36(4): 267-276.

[189] Mishra, D. Bhunia, B. Banerjee, I. Datta, P. Dhara, S. and Maiti, T K. 2011. "Enzymatically crosslinked carboxymethyl–chitosan/gelatin/nano-hydroxyapatite injectable gels for in situ bone tissue engineering application." *Materials Science and Engineering: C.* 31(7): 1295-1304.

[190] Vaghani, S S. Patel, M M. and Satish, C S. 2012. "Synthesis and characterization of pH-sensitive hydrogel composed of carboxymethyl chitosan for colon targeted delivery of ornidazole." *Carbohydrate Research.* 347(1): 76-82.

[191] Zheng, H. Zhang, X. Yin, Y. Xiong, F. Gong, X. Zhu, Z. Lu, B. and Xu, P. 2011. "In vitro characterization, and in vivo studies of crosslinked lactosaminated carboxymethyl chitosan nanoparticles." *Carbohydrate Polymers.* 84(3): 1048-1053.

[192] Xie, M. Liu, H-H. Chen, P. Zhang, Z-L. Wang, X-H. Xie, Z-X. Du, Y-M. Pan, B-Q. and Pang, D-W. 2005. "CdSe/ZnS-labeled carboxymethyl chitosan as a bioprobe for live cell imaging." *Chemical Communications.* (44): 5518-5520.

[193] Hawary, D. Motaleb, M. Farag, H. Guirguis, O. and Elsabee, M. 2011. "Water-soluble derivatives of chitosan as a target delivery system of 99mTc to some organs in vivo for nuclear imaging and biodistribution." *Journal of Radioanalytical and Nuclear Chemistry.* 290(3): 557-567.

[194] Muzzarelli, R. Cucchiara, M. and Muzzarelli, C. 2002. "N-Carboxymethyl chitosan in innovative cosmeceutical products." *Journal of applied cosmetology.* 20(3): 201-208.

[195] Jimtaisong, A. and Saewan, N. 2014. "Utilization of carboxymethyl chitosan in cosmetics." *International Journal of Cosmetic Science.* 36(1): 12-21.

[196] Sashiwa, H. Yamamori, N. Ichinose, Y. Sunamoto, J. and Aiba, S-i. 2003. "Michael Reaction of Chitosan with Various Acryl Reagents in Water." *Biomacromolecules.* 4(5): 1250-1254.

[197] Sashiwa, H. Kawasaki, N. Nakayama, A. Muraki, E. Yajima, H. Yamamori, N. Ichinose, Y. Sunamoto, J. and Aiba, S-i. 2003. "Chemical modification of chitosan. Part 15: Synthesis of novel chitosan derivatives by substitution of hydrophilic amine using N-carboxyethylchitosan ethyl ester as an intermediate." *Carbohydrate Research.* 338(6): 557-561.

[198] Bernkop-Schnürch, A. Brandt, U. and Clausen, A. 1999. "Synthesis and in vitro evaluation of chitosan-cysteine conjugates." *Sci Pharm.* 67(4): 197-208.

[199] Kast, C E. and Bernkop-Schnürch, A. 2001. "Thiolated polymers — thiomers: development and in vitro evaluation of chitosan–thioglycolic acid conjugates." *Biomaterials.* 22(17): 2345-2352.

[200] Bernkop-Schnürch, A. Hornof, M. and Zoidl, T. 2003. "Thiolated polymers—thiomers: synthesis and in vitro evaluation of chitosan–2-iminothiolane conjugates." *International Journal of Pharmaceutics.* 260(2): 229-237.

[201] Kafedjiiski, K. Krauland, A H. Hoffer, M H. and Bernkop-Schnürch, A. 2005. "Synthesis and in vitro evaluation of a novel thiolated chitosan." *Biomaterials.* 26(7): 819-826.

[202] Federer, C. Kurpiers, M. and Bernkop-Schnürch, A. 2021. "Thiolated Chitosans: A Multi-talented Class of Polymers for Various Applications." *Biomacromolecules.* 22(1): 24-56.

[203] Millotti, G. Samberger, C. Fröhlich, E. and Bernkop-Schnürch, A. 2009. "Chitosan-graft-6-mercaptonicotinic Acid: Synthesis, Characterization, and Biocompatibility." *Biomacromolecules.* 10(11): 3023-3027.

[204] Huang, R. Du, Y. Yang, J. and Fan, L. 2003. "Influence of functional groups on the in vitro anticoagulant activity of chitosan sulfate." *Carbohydrate Research.* 338(6): 483-489.

[205] Suwan, J. Zhang, Z. Li, B. Vongchan, P. Meepowpan, P. Zhang, F. Mousa, S A. Mousa, S. Premanode, B. Kongtawelert, P. and Linhardt, R J. 2009. "Sulfonation of papain-treated chitosan and its mechanism for anticoagulant activity." *Carbohydrate Research.* 344(10): 1190-1196.

[206] Whistler, R L. and Kosik, M. 1971. "Anticoagulant activity of oxidized and N- and O-sulfated chitosan." *Archives of Biochemistry and Biophysics.* 142(1): 106-110.

[207] Hirano, S. Tanaka, Y. Hasegawa, M. Tobetto, K. and Nishioka, A. 1985. "Effect of sulfated derivatives of chitosan on some blood coagulant factors." *Carbohydrate Research.* 137: 205-215.

[208] Nishimura, S-I. Kai, H. Shinada, K. Yoshida, T. Tokura, S. Kurita, K. Nakashima, H. Yamamoto, N. and Uryu, T. 1998. "Regioselective syntheses of sulfated polysaccharides: specific anti-HIV-1 activity of novel chitin sulfates." *Carbohydrate Research.* 306(3): 427-433.

[209] Xing, R. Yu, H. Liu, S. Zhang, W. Zhang, Q. Li, Z. and Li, P. 2005. "Antioxidant activity of differently regioselective chitosan sulfates in vitro." *Bioorganic & Medicinal Chemistry.* 13(4): 1387-1392.

[210] Vongchan, P. Sajomsang, W. Subyen, D. and Kongtawelert, P. 2002. "Anticoagulant activity of a sulfated chitosan." *Carbohydrate Research.* 337(13): 1239-1242.

[211] Huang, R. Du, Y. Zheng, L. Liu, H. and Fan, L. 2004. "A new approach to chemically modified chitosan sulfates and study of their influences on the inhibition of Escherichia coli and Staphylococcus aureus growth." *Reactive and Functional Polymers.* 59(1): 41-51.

[212] Zhang, C. Ping, Q. Zhang, H. and Shen, J. 2003. "Preparation of N-alkyl-O-sulfate chitosan derivatives and micellar solubilization of taxol." *Carbohydrate Polymers.* 54(2): 137-141.

[213] Zhang, C. Qineng, P. and Zhang, H. 2004. "Self-assembly and characterization of paclitaxel-loaded N-octyl-O-sulfate chitosan micellar system." *Colloids and Surfaces B: Biointerfaces.* 39(1): 69-75.

[214] Berth, G. Voigt, A. Dautzenberg, H. Donath, E. and Möhwald, H. 2002. "Polyelectrolyte Complexes and Layer-by-Layer Capsules from Chitosan/Chitosan Sulfate." *Biomacromolecules.* 3(3): 579-590.

[215] Thanou, M. Henderson, S. Kydonieus, A. and Elson, C. 2007. "N-sulfonato-N,O-carboxymethylchitosan: A novel polymeric absorption enhancer for the oral delivery of macromolecules." *Journal of Controlled Release.* 117(2): 171-178.

[216] Muzzarelli, R A A. 1992. "Modified chitosans carrying sulfonic acid groups." *Carbohydrate Polymers.* 19(4): 231-236.

[217] Nagasawa, K. Tohira, Y. Inoue, Y. and Tanoura, N. 1971. "Reaction between carbohydrates and sulfuric acid: Part I. Depolymerization and sulfation of polysaccharides by sulfuric acid." *Carbohydrate Research.* 18(1): 95-102.

[218] Vikhoreva, G. Bannikova, G. Stolbushkina, P. Panov, A. Drozd, N. Makarov, V. Varlamov, V. and Gal'braikh, L. 2005. "Preparation and anticoagulant activity of a low-molecular-weight sulfated chitosan." *Carbohydrate Polymers.* 62(4): 327-332.

[219] Holme, K R. and Perlin, A S. 1997. "Chitosan N-sulfate. A water-soluble polyelectrolyte." *Carbohydrate Research.* 302(1): 7-12.

[220] Yin, Q. Li, Y. Yin, Q-J. Miao, X. and Jiang, B. 2009. "Synthesis and rheological behavior of a novel N-sulfonate ampholyte chitosan." *Journal of Applied Polymer Science.* 113(5): 3382-3387.

[221] Yao, Z. Zhang, C. Ping, Q. and Yu, L. 2007. "A series of novel chitosan derivatives: Synthesis, characterization and micellar solubilization of paclitaxel." *Carbohydrate Polymers.* 68(4): 781-792.

[222] Jung, B-O. Na, J. and Kim, C H. 2007. "Synthesis of chitosan derivatives with anionic groups and its biocompatibility in vitro." *Journal of Industrial and Engineering Chemistry.* 13(5): 772-776.

[223] Sashiwa, H. and Aiba, S-i. 2004. "Chemically modified chitin and chitosan as biomaterials." *Progress in Polymer Science.* 29(9): 887-908.

[224] Tojima, T. Katsura, H. Nishiki, M. Nishi, N. Tokura, S. and Sakairi, N. 1999. "Chitosan beads with pendant α-cyclodextrin: preparation and inclusion property to nitrophenolates." *Carbohydrate Polymers.* 40(1): 17-22.

[225] Auzély-Velty, R. and Rinaudo, M. 2001. "Chitosan Derivatives Bearing Pendant Cyclodextrin Cavities: Synthesis and Inclusion Performance." *Macromolecules.* 34(11): 3574-3580.

[226] Auzély-Velty, R. and Rinaudo, M. 2002. "New supramolecular assemblies of a cyclodextrin-grafted chitosan through specific complexation." *Macromolecules.* 35(21): 7955-7962.

[227] Venter, J P. Kotzé, A F. Auzély-Velty, R. and Rinaudo, M. 2006. "Synthesis and evaluation of the mucoadhesivity of a CD-chitosan derivative." *International Journal of Pharmaceutics.* 313(1): 36-42.

[228] Tang, X-H. Tan, S-Y. and Wang, Y-T. 2002. "Study of the synthesis of chitosan derivatives containing benzo-21-crown-7 and their adsorption properties for metal ions." *Journal of Applied Polymer Science.* 83(9): 1886-1891.

[229] Li, H-B. Chen, Y-Y. and Liu, S-L. 2003. "Synthesis, characterization, and metal ions adsorption properties of chitosan–calixarenes (I)." *Journal of Applied Polymer Science.* 89(4): 1139-1144.

[230] Hu, Q. and Luo, Y. 2016. "Polyphenol-chitosan conjugates: Synthesis, characterization, and applications." *Carbohydrate Polymers.* 151: 624-639.

[231] Woranuch, S. and Yoksan, R. 2013. "Preparation, characterization and antioxidant property of water-soluble ferulic acid grafted chitosan." *Carbohydrate Polymers.* 96(2): 495-502.

[232] Rui, L. Xie, M. Hu, B. Zhou, L. Saeeduddin, M. and Zeng, X. 2017. "Enhanced solubility and antioxidant activity of chlorogenic acid-chitosan conjugates due to the conjugation of chitosan with chlorogenic acid." *Carbohydrate Polymers.* 170: 206-216.

[233] Nam, S. and Renganathan, V. 2000. "Non-enzymatic reduction of azo dyes by NADH." *Chemosphere.* 40(4): 351-357.

[234] Pellá, M C G. Lima-Tenório, M K. Tenório-Neto, E T. Guilherme, M R. Muniz, E C. and Rubira, A F. 2018. "Chitosan-based hydrogels: From preparation to biomedical applications." *Carbohydrate Polymers.* 196: 233-245.

[235] Xing, G. Shao, L. Du, Y. Tao, H. and Qi, C. 2021. "Citric acid crosslinked chitosan/poly(ethylene oxide) composite nanofibers fabricated by electrospinning and thermal treatment for controlled drug release." *Cellulose.* 28(2): 961-971.

[236] Zhuang, L. Zhi, X. Du, B. and Yuan, S. 2020. "Preparation of Elastic and Antibacterial Chitosan–Citric Membranes with High Oxygen Barrier Ability by in Situ Cross-Linking." *ACS Omega.* 5(2): 1086-1097.

[237] Xu, Y. Li, Y. Chen, Q. Fu, L. Tao, L. and Wei, Y. 2018. "Injectable and Self-Healing Chitosan Hydrogel Based on Imine Bonds: Design and Therapeutic Applications." *International Journal of Molecular Sciences.* 19(8): 2198.

[238] Wu, D. Zhu, L. Li, Y. Zhang, X. Xu, S. Yang, G. and Delair, T. 2020. "Chitosan-based Colloidal Polyelectrolyte Complexes for Drug Delivery: A Review." *Carbohydrate Polymers.* 238: 116126.

[239] Lv, X. Zhang, W. Liu, Y. Zhao, Y. Zhang, J. and Hou, M. 2018. "Hygroscopicity modulation of hydrogels based on carboxymethyl chitosan/Alginate polyelectrolyte complexes and its application as pH-sensitive delivery system." *Carbohydrate Polymers.* 198: 86-93.

[240] Lv, X. Liu, Y. Song, S. Tong, C. Shi, X. Zhao, Y. Zhang, J. and Hou, M. 2019. "Influence of chitosan oligosaccharide on the gelling and wound healing properties of injectable hydrogels based on carboxymethyl chitosan/alginate polyelectrolyte complexes." *Carbohydrate Polymers.* 205: 312-321.

[241] Wei, Y. Xie, R. Lin, Y. Xu, Y. Wang, F. Liang, W. and Zhang, J. 2016. "Structure formation in pH-sensitive hydrogels composed of sodium caseinate and N,O-carboxymethyl chitosan." *International Journal of Biological Macromolecules.* 89: 353-359.

[242] Shchipunov, Y. Sarin, S. Kim, I. and Ha, C-S. 2010. "Hydrogels formed through regulated self-organization of gradually charging chitosan in solution of xanthan." *Green Chemistry.* 12(7): 1187-1195.

[243] Hu, X. Yan, L. Wang, Y. and Xu, M. 2020. "Self-assembly of binary oppositely charged polysaccharides into polyelectrolyte complex hydrogel film for facile and efficient Pb2+ removal." *Chemical Engineering Journal.* 388: 124189.

[244] Ahmed, S. Annu. Ali, A. and Sheikh, J. 2018. "A review on chitosan centred scaffolds and their applications in tissue engineering." *International Journal of Biological Macromolecules.* 116: 849-862.

[245] Zhao, H. Liao, J. Wu, F. and Shi, J. 2021. "Mechanical strength improvement of chitosan/hydroxyapatite scaffolds by coating and cross-linking." *Journal of the Mechanical Behavior of Biomedical Materials.* 114: 104169.

[246] El-Aassar, M R. Ibrahim, O M. Fouda, M M G. Fakhry, H. Ajarem, J. Maodaa, S N. Allam, A A. and Hafez, E E. 2021. "Wound dressing of chitosan-based-crosslinked gelatin/ polyvinyl pyrrolidone embedded silver nanoparticles, for targeting multidrug resistance microbes." *Carbohydrate Polymers.* 255: 117484.

[247] Jawad, A H. Abdulhameed, A S. Kashi, E. Yaseen, Z M. Alothman, Z A. and Khan, M R. 2021. "Cross-Linked Chitosan-Glyoxal/Kaolin Clay Composite: Parametric Optimization for Color Removal and COD Reduction of Remazol Brilliant Blue R Dye." *Journal of Polymers and the Environment.*

[248] Gómez-Mascaraque, L G. Méndez, J A. Fernández-Gutiérrez, M. Vázquez, B. and San Román, J. 2014. "Oxidized dextrins as alternative crosslinking agents for polysaccharides: Application to hydrogels of agarose–chitosan." *Acta Biomaterialia.* 10(2): 798-811.

[249] Zhang, H. Qadeer, A. and Chen, W. 2011. "In Situ Gelable Interpenetrating Double Network Hydrogel Formulated from Binary Components: Thiolated Chitosan and Oxidized Dextran." *Biomacromolecules.* 12(5): 1428-1437.

[250] Lou, C. Tian, X. Deng, H. Wang, Y. and Jiang, X. 2020. "Dialdehyde-β-cyclodextrin-crosslinked carboxymethyl chitosan hydrogel for drug release." *Carbohydrate Polymers.* 231: 115678.

[251] Adel, A M. Ibrahim, A A. El-Shafei, A M. and Al-Shemy, M T. 2019. "Inclusion complex of clove oil with chitosan/β-cyclodextrin citrate/oxidized nanocellulose biocomposite for active food packaging." *Food Packaging and Shelf Life.* 20: 100307.

[252] Ngwabebhoh, F A. Zandraa, O. Patwa, R. Saha, N. Capáková, Z. and Saha, P. 2021. "Self-crosslinked chitosan/dialdehyde xanthan gum blended hypromellose hydrogel for the controlled delivery of ampicillin, minocycline and rifampicin." *International Journal of Biological Macromolecules.* 167: 1468-1478.

[253] Huang, J. Deng, Y. Ren, J. Chen, G. Wang, G. Wang, F. and Wu, X. 2018. "Novel in situ forming hydrogel based on xanthan and chitosan re-gelifying in liquids for local drug delivery." *Carbohydrate Polymers.* 186: 54-63.

[254] Chen, F. Tian, M. Zhang, D. Wang, J. Wang, Q. Yu, X. Zhang, X. and Wan, C. 2012. "Preparation and characterization of oxidized alginate covalently cross-linked galactosylated chitosan scaffold for liver tissue engineering." *Materials Science and Engineering: C.* 32(2): 310-320.

[255] Li, X. Kong, X. Zhang, Z. Nan, K. Li, L. Wang, X. and Chen, H. 2012. "Cytotoxicity and biocompatibility evaluation of N,O-carboxymethyl chitosan/oxidized alginate hydrogel for drug delivery application." *International Journal of Biological Macromolecules.* 50(5): 1299-1305.

[256] Chen, X. Fan, M. Tan, H. Ren, B. Yuan, G. Jia, Y. Li, J. Xiong, D. Xing, X. Niu, X. and Hu, X. 2019. "Magnetic and self-healing chitosan-alginate hydrogel encapsulated gelatin microspheres via covalent cross-linking for drug delivery." *Materials Science and Engineering: C.* 101: 619-629.

[257] Xie, W. Gao, Q. Guo, Z. Wang, D. Gao, F. Wang, X. Wei, Y. and Zhao, L. 2017. "Injectable and Self-Healing Thermosensitive Magnetic Hydrogel for Asynchronous Control Release of Doxorubicin and Docetaxel to Treat Triple-Negative Breast Cancer." *ACS Applied Materials & Interfaces.* 9(39): 33660-33673.

[258] Zhang, Y. Tao, L. Li, S. and Wei, Y. 2011. "Synthesis of Multiresponsive and Dynamic Chitosan-Based Hydrogels for Controlled Release of Bioactive Molecules." *Biomacromolecules.* 12(8): 2894-2901.

[259] Cao, L. Cao, B. Lu, C. Wang, G. Yu, L. and Ding, J. 2015. "An injectable hydrogel formed by in situ cross-linking of glycol chitosan and multi-benzaldehyde functionalized PEG analogues for cartilage tissue engineering." *Journal of Materials Chemistry B.* 3(7): 1268-1280.

[260] Wang, S. Liu, J. Zhao, H. and Zhang, F. 2021. "Carboxymethyl chitosan crosslinked β-cyclodextrin containing hydrogen bonded NC QDs nanocomposites to design fluorescence probes for manganese ion (II) sensing." *Materials Science and Engineering: C.* 119: 111556.

[261] Tripodo, G. Trapani, A. Rosato, A. Di Franco, C. Tamma, R. Trapani, G. Ribatti, D. and Mandracchia, D. 2018. "Hydrogels for biomedical applications from glycol chitosan and PEG diglycidyl ether exhibit pro-angiogenic and antibacterial activity." *Carbohydrate Polymers.* 198: 124-130.

[262] Xu, D. Jin, J. Chen, C. and Wen, Z. 2018. "From Nature to Energy Storage: A Novel Sustainable 3D Cross-Linked Chitosan–PEGGE-Based Gel Polymer Electrolyte with Excellent Lithium-Ion Transport Properties for Lithium Batteries." *ACS Applied Materials & Interfaces.* 10(44): 38526-38537.

[263] Pérez-Calderón, J. Santos, M V. and Zaritzky, N. 2020. "Synthesis, characterization and application of cross-linked chitosan/oxalic acid hydrogels to improve azo dye (Reactive Red 195) adsorption." *Reactive and Functional Polymers.* 155: 104699.

[264] Song, Y. Nagai, N. Saijo, S. Kaji, H. Nishizawa, M. and Abe, T. 2018. "In situ formation of injectable chitosan-gelatin hydrogels through double crosslinking for sustained intraocular drug delivery." *Materials Science and Engineering: C.* 88: 1-12.

[265] Asfour, M H. Salama, A A A. and Mohsen, A M. 2021. "Fabrication of all-trans retinoic acid loaded chitosan/tripolyphosphate lipid hybrid nanoparticles as a novel oral delivery approach for management of diabetic nephropathy in rats." *Journal of Pharmaceutical Sciences.*

[266] Kiernan, J A. 2001. "Classification and naming of dyes, stains and fluorochromes." *Biotechnic & Histochemistry.* 76(5-6): 261-278.

[267] Liu, Z. Luo, F. and Chen, T. 2004. "Phenolphthalein immobilized membrane for an optical pH sensor." *Analytica Chimica Acta.* 510(2): 189-194.

[268] Zhang, L. Li, Z. Chang, R. Chen, Y. and Zhang, W. 2009. "Synthesis and characterization of novel phenolphthalein immobilized halochromic fiber." *Reactive and Functional Polymers.* 69(4): 234-239.

[269] Chang, C-F. and Chen, J-W. 2006. "The experimental investigation of concrete carbonation depth." *Cement and Concrete Research.* 36(9): 1760-1767.

[270] Galvão, T L P. Sousa, I. Wilhelm, M. Carneiro, J. Opršal, J. Kukačková, H. Špaček, V. Maia, F. Gomes, J R B. Tedim, J. and Ferreira, M G S. 2018. "Improving the functionality and performance of AA2024 corrosion sensing coatings with nanocontainers." *Chemical Engineering Journal.* 341: 526-538.

[271] Kim, S. and Sikes, H D. 2018. "Phenolphthalein-Conjugated Hydrogel Formation under Visible-Light Irradiation for Reducing Variability of Colorimetric Biodetection." *ACS Applied Bio Materials.* 1(2): 216-220.

[272] Dunnick, J K. and Hailey, J R. 1996. "Phenolphthalein exposure causes multiple carcinogenic effects in experimental model systems." *Cancer Research.* 56(21): 4922-4926.

[273] Okamura, M. Kashida, Y. Watanabe, T. Yasuhara, K. Onodera, H. Hirose, M. Usui, T. Tamaoki, N. and Mitsumori, K. 2003. "Lack of susceptibility of heterozygous p53-knockout CBA and CIEA mice to phenolphthalein in a 6-month carcinogenicity study." *Toxicology.* 185(1): 17-22.

[274] Taguchi, K. 1986. "Transient binding of phenolphthalein-.beta.-cyclodextrin complex: an example of induced geometrical distortion." *Journal of the American Chemical Society.* 108(10): 2705-2709.

[275] Goel, A. and Nene, S N. 1995. "Modifications in the Phenolphthalein Method for Spectrophotometric Estimation of Beta Cyclodextrin." *Starch - Stärke.* 47(10): 399-400.

[276] Takashima, Y. Yonekura, K. Koyanagi, K. Iwaso, K. Nakahata, M. Yamaguchi, H. and Harada, A. 2017. "Multifunctional Stimuli-Responsive Supramolecular Materials with Stretching, Coloring, and Self-Healing Properties Functionalized via Host–Guest Interactions." *Macromolecules.* 50(11): 4144-4150.

[277] Tillu, V H. Dumbre, D K. Borate, H B. Wakharkar, R D. and Choudhary, V R. 2012. "Solvent-Free One-Pot Synthesis of Sulfonephthaleins from Saccharin and Phenols." *Synthetic Communications.* 42(8): 1101-1107.

[278] Welshons, W V. Wolf, M F. Murphy, C S. and Jordan, V C. 1988. "Estrogenic activity of phenol red." *Molecular and Cellular Endocrinology.* 57(3): 169-178.

[279] Sabnis, R W. (2007). **Handbook of acid-base indicators**. CRC Press.

[280] El-Nahhal, I M. Livage, J. Zourab, S M. Kodeh, F S. and Al swearky, A. 2015. "Entrapment of phenol red (PR) pH indicator into sol–gel matrix in presence of some surfactants." *Journal of Sol-Gel Science and Technology.* 75(2): 313-322.

[281] Wang, E. Chow, K-F. Kwan, V. Chin, T. Wong, C. and Bocarsly, A. 2003. "Fast and long term optical sensors for pH based on sol–gels." *Analytica Chimica Acta.* 495(1): 45-50.

[282] Liu, Z. Liu, J. and Chen, T. 2005. "Phenol red immobilized PVA membrane for an optical pH sensor with two determination ranges and long-term stability." *Sensors and Actuators B: Chemical.* 107(1): 311-316.

[283] Liu, L. Li, X. Nagao, M. Elias, A L. Narain, R. and Chung, H-J. 2017. "A pH-Indicating Colorimetric Tough Hydrogel Patch towards Applications in a Substrate for Smart Wound Dressings." *Polymers.* 9(11): 558.

[284] Gondima, C. Palhares, M. Santos, P. Sousa, R. Junqueira, R. and Souza, S. 2021. "Detection of Acid Neutralizers in Fraudulent Milk: Full Validation of a Classical Qualitative Method." *Quimica Nova.*

[285] Morsy, M K. Zór, K. Kostesha, N. Alstrøm, T S. Heiskanen, A. El-Tanahi, H. Sharoba, A. Papkovsky, D. Larsen, J. Khalaf, H. Jakobsen, M H. and Emnéus, J. 2016. "Development and validation of a colorimetric sensor array for fish spoilage monitoring." *Food Control.* 60: 346-352.

[286] Lee, J W. Lee, J-S. and Chang, Y-T. 2006. "Colorimetric Identification of Carbohydrates by a pH Indicator/pH Change Inducer Ensemble." *Angewandte Chemie International Edition.* 45(39): 6485-6487.

[287] Bruschi, M L. 2015. **Strategies to Modify the Drug Release from Pharmaceutical Systems**. Cambridge : Woodhead Publishing.

[288] Lim, S-H. and Hudson, S M. 2004. "Synthesis and antimicrobial activity of a water-soluble chitosan derivative with a fiber-reactive group." *Carbohydrate Research.* 339(2): 313-319.

[289] Hamad, N S. 2010. "Synthesis of Phenolphthalein-formaldehyde resin and study of it's antibacterial activity." *Journal of Basrah Researches (Sciences).* 36(1A): 94-102.

[290] Kunimoto, K-K. Sugiura, H. Kato, T. Senda, H. Kuwae, A. and Hanai, K. 2001. "Molecular structure and vibrational spectra of phenolphthalein and its dianion." *Spectrochimica Acta Part A: Molecular and Biomolecular Spectroscopy.* 57(2): 265-271.

[291] Berezin, A S. Ishmetova, R I. Rusinov, G L. and Skorik, Y A. 2014. "Tetrazole derivatives of chitosan: synthetic approaches and evaluation of toxicity." *Russian Chemical Bulletin.* 63(7): 1624-1632.

[292] Singh, A. Narvi, S S. Dutta, P K. and Pandey, N D. 2006. "External stimuli response on a novel chitosan hydrogel crosslinked with formaldehyde." *Bulletin of Materials Science.* 29(3): 233-238.

[293] Sun, Y. Li, Y. Nie, J. Wang, Z. and Hu, Q. 2013. "High-strength Chitosan Hydrogels Prepared from LiOH/Urea Solvent System." *Chemistry Letters.* 42(8): 838-840.

[294] Baron, M G. and Elie, M. 2003. "Temperature sensing using reversible thermochromic polymeric films." *Sensors and Actuators B: Chemical.* 90(1-3): 271-275.

[295] Mills, A. and Lepre, A. 1999. "Development of novel thermochromic plastic films for optical temperature sensing." *The Analyst.* 124(5): 685-689.

[296] Luo, F-L. Liu, Z-H. Chen, T-L. and Gong, B-L. 2006. "Cross-linked Polyvinyl Alcohol pH Sensitive Membrane Immobilized with Phenol Red for Optical pH Sensors." *Chinese Journal of Chemistry.* 24(3): 341-344.

[297] Baklagina, Y G. Klechkovskaya, V V. Kononova, S V. Petrova, V A. Poshina, D N. Orekhov, A S. and Skorik, Y A. 2018. "Polymorphic Modifications of Chitosan." *Crystallography Reports.* 63(3): 303-313.

[298] Abramowitz, E W. 1950. "Phenolphthalein today: A critical review." *The American Journal of Digestive Diseases.* 17(3): 79-82.

[299] Gazit, E. and Porat, Y. 2005. "PCT Int. Appl. WO 2005027901, 2005." page 349074. in Chem. Abstr.

[300] Morgan, A. Babu, D. Reiz, B. Whittal, R. Suh, L Y K. and Siraki, A G. 2019. "Caution for the routine use of phenol red – It is more than just a pH indicator." *Chemico-Biological Interactions.* 310: 108739.

[301] Zhu, Y. Zhang, X. Zhu, J. Zhao, Q. Li, Y. Li, W. Fan, C. and Huang, Q. 2012. "Cytotoxicity of phenol red in toxicity assays for carbon nanoparticles." *International Journal of Molecular Sciences.* 13(10): 12336-12348.

[302] Foresti, R. Hoque, M. Monti, D. Green, C J. and Motterlini, R. 2005. "Differential activation of heme oxygenase-1 by chalcones and rosolic acid in endothelial cells." *Journal of Pharmacology and Experimental Therapeutics.* 312(2): 686-693.

[303] Tamura, Z. Abe, S. Ito, K. and MAEDA, M. 1996. "Spectrophotometric analysis of the relationship between dissociation and coloration, and of the structural formulas of phenolphthalein in aqueous solution." *Analytical Sciences.* 12(6): 927-930.

[304] Tamura, Z. and Maeda, M. 1997. "Differences between phthaleins and sulfonphthaleins." *Yakugaku zasshi: Journal of the Pharmaceutical Society of Japan.* 117(10-11): 764-770.

[305] Shokrollahi, A. Gohari, M. and Ebrahimi, F. 2018. "Determination of Acidity Constants of p-Rosolic acid and Bromoxylenol Blue by Solution Scanometric Method." *Analytical and Bioanalytical Chemistry Research.* 5(1): 67-79.

[306] De Meyer, T. Hemelsoet, K. Van Speybroeck, V. and De Clerck, K. 2014. "Substituent effects on absorption spectra of pH indicators: An experimental and computational study of sulfonphthaleine dyes." *Dyes and Pigments.* 102: 241-250.

[307] Ibrahim, H M. Mostafa, M. and Kandile, N G. 2020. "Potential use of N-carboxyethylchitosan in biomedical applications: Preparation, characterization, biological properties." *International Journal of Biological Macromolecules.* 149: 664-671.

[308] Huang, J. Xie, H. Hu, S. Xie, T. Gong, J. Jiang, C. Ge, Q. Wu, Y. Liu, S. Cui, Y. Mao, J. and Mei, L. 2015. "Preparation, Characterization, and Biochemical Activities

of N-(2-Carboxyethyl)chitosan from Squid Pens." *Journal of Agricultural and Food Chemistry.* 63(9): 2464-2471.

[309] Huaytragul, J. Chalitangkoon, J. Monvisade, P. and Chotsaeng, N. 2021. "Enhancing chitosan solubility in alcohol: water mixtures for film-forming systems releasing with turmeric extracts." *Journal of the Taiwan Institute of Chemical Engineers.* 123: 293-301.

[310] Vishwakarma, N K. Patel, V K. Hira, S K. Ramesh, K. Srivastava, P. Mitra, K. Singh, S. Chattopadhyay, D. Maiti, P. and Misra, N. 2015. "Tadpole-shaped β-cyclodextrin-tagged poly (N-vinylpyrrolidone): synthesis, characterization and studies of its complexation with phenolphthalein and anti tumor activities." *RSC Advances.* 5(20): 15547-15558.

[311] Buvári, Á. Barcza, L. and Kajtár, M. 1988. "Complex formation of phenolphthalein and some related compounds with β-cyclodextrin." *Journal of the Chemical Society, Perkin Transactions 2.* (9): 1687-1690.

[312] Trellenkamp, T. and Ritter, H. 2010. "Poly(N-vinylpyrrolidone) Bearing Covalently Attached Cyclodextrin via Click-Chemistry: Synthesis, Characterization, and Complexation Behavior with Phenolphthalein." *Macromolecules.* 43(13): 5538-5543.

[313] Zhou, T. He, X. Song, F. and Xie, K. 2016. "Chitosan modified by polymeric reactive dyes containing quanternary ammonium groups as a novel anion exchange membrane for alkaline fuel cells." *Int. J. Electrochem. Sci.* 11: 590-608.

[314] Liu, X. Chen, K. Wang, J. Wang, Y. Tang, Y. Gao, X. Zhu, L. Li, X. and Li, J. 2020. "An on-package colorimetric sensing label based on a sol-gel matrix for fish freshness monitoring." *Food Chemistry.* 307: 125580.

[315] Sun, G. Chi, W. Zhang, C. Xu, S. Li, J. and Wang, L. 2019. "Developing a green film with pH-sensitivity and antioxidant activity based on κ-carrageenan and hydroxypropyl methylcellulose incorporating Prunus maackii juice." *Food Hydrocolloids.* 94: 345-353.

[316] Priyadarshi, R. Ezati, P. and Rhim, J-W. 2021. "Recent Advances in Intelligent Food Packaging Applications Using Natural Food Colorants." *ACS Food Science & Technology.* 1(2): 124-138.

[317] Pakolpakçıl, A. Osman, B. Özer, E T. Şahan, Y. Becerir, B. Göktalay, G. and Karaca, E. 2020. "Halochromic composite nanofibrous mat for wound healing monitoring." *Materials Research Express.* 6(12): 1250c1253.

[318] Zepon, K M. Martins, M M. Marques, M S. Heckler, J M. Dal Pont Morisso, F. Moreira, M G. Ziulkoski, A L. and Kanis, L A. 2019. "Smart wound dressing based on κ–carrageenan/locust bean gum/cranberry extract for monitoring bacterial infections." *Carbohydrate Polymers.* 206: 362-370.

[319] Devarayan, K. and Kim, B-S. 2015. "Reversible and universal pH sensing cellulose nanofibers for health monitor." *Sensors and Actuators B: Chemical.* 209: 281-286.

[320] Liu, F. Chiou, B-S. Avena-Bustillos, R J. Zhang, Y. Li, Y. McHugh, T H. and Zhong, F. 2017. "Study of combined effects of glycerol and transglutaminase on properties of gelatin films." *Food Hydrocolloids.* 65: 1-9.

[321] Arancibia, J A. and Escandar, G M. 1999. "Complexation study of diclofenac with β-cyclodextrin and spectrofluorimetric determination." *Analyst.* 124(12): 1833-1838.

[322] Li, S. Tang, Y. Zhang, X. Dou, Y. and Shen, X. 2019. "Preparation and characterization of diclofenac sodium β-cyclodextrin inclusion complex eye drops." *Journal of Inclusion Phenomena and Macrocyclic Chemistry.* 94: 85-94.

[323] Das, S. and Subuddhi, U. 2015. "Studies on the complexation of diclofenac sodium with β–cyclodextrin: Influence of method of preparation." *Journal of Molecular Structure.* 1099: 482-489.

[324] Silver, F H. 1994. "Wound dressings and skin replacement." 46-91. in **Biomaterials, medical devices and tissue engineering: An integrated approach**. Springer.

[325] Sousa, J M. Vieira, A C C. Costa, M P. Rizzo, M S. Chaves, L L. Braz, E M A. Bezerra, R D S. Leal, R C. Barreto, H M. Osajima, J A. and Silva-Filho, E C. 2022. "Chitosan grafted with maleic anhydride and ethylenediamine: Preparation, characterization, computational study, antibacterial and cytotoxic properties." *Materials Chemistry and Physics.* 287: 126301.

[326] Savetsakulanont, J. Chalitangkoon, J. and Monvisade, P. 2021. "Stimuli-Responsive, Self-Healing, and Injectable Hydrogels with Dual-Crosslinked

Design from Phenolphthalein-Grafted N-Carboxyethyl Chitosan." *Macromolecular Materials and Engineering.* 306(10): 2100287.

[327] Buakaew, J. Chalitangkoon, J. and Monvisade, P. 2021. "pH-responsive films from chitosan-based/poly(vinyl alcohol)/oxidized alginate for intelligent packaging." page 51-56. in The International Polymer Conference of Thailand (PCT-11). Thailand.

Appendices

Appendix A: Characterization of βCD-DA

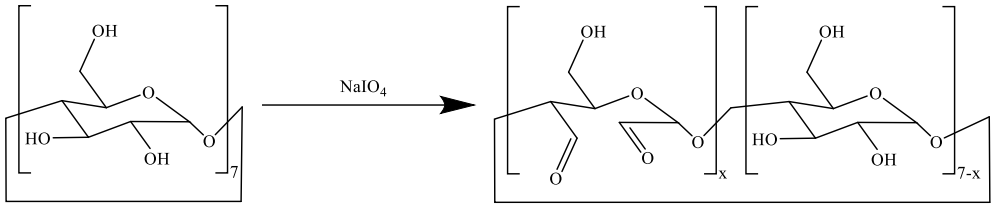

Figure A-1 Synthesis of βCD-DA

Determination of aldehyde contents

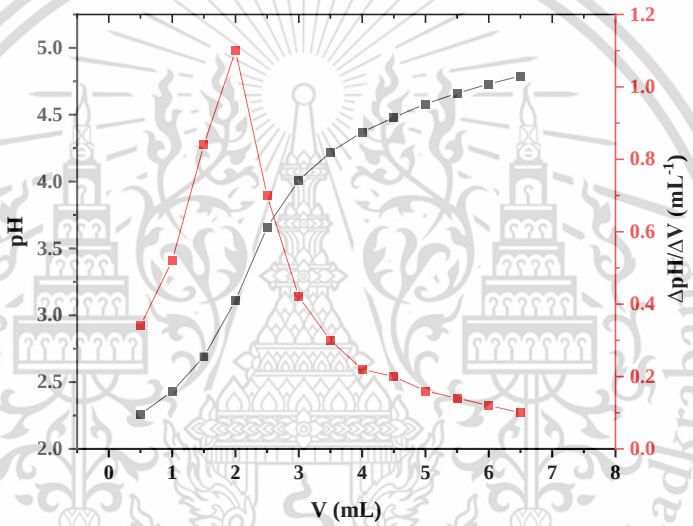

Figure A-2 Potentiometric titration curve and first derivative the titration curve of βCD-DA titrated with hydroxylamine hydrochloride

From the first derivative curve, the volume of NaOH solution used was 1.8 mL.

$$[CHO]=\frac{1.8ml\times0.0957M}{0.1017g}$$

$$=1.69\ mmol/g$$

Therefore, the aldehyde content of βCD-DA was 1.69 mmol/g.

Appendix B: Swelling behavior

Table B-1 Swelling behavior of the non-crosslinked films at 37°C

Time (min)	Swelling degree (%)		
	pH 5.5	pH 7.4	pH 8.5
0	0±0	0±0	0±0
5	1182±154	1145±117	1337±106
10	971±172	634±42	729±125
15	799±109	309±68	439±70
20	727±121	159±30	331±63
30	655±94	115±45	279±73
45	647±105	99±55	259±69
60	645±102	96±48	234±63
90	622±86	90±51	226±71
120	615±92	79±50	188±68
180	596±93	86±54	177±83
240	589±93	81±70	155±77
300	592±91	69±39	179±56
360	567±83	74±59	150±75
480	555±73	78±70	120±89
1440	522±63	74±59	151±99

Table B-2 Swelling behavior of the Blend-CD films at 37°C

Time (min)	Swelling degree (%)		
	pH 5.5	pH 7.4	pH 8.5
0	0±0	0±0	0±0
5	514±10	593±43	613±15
10	556±15	677±55	666±17
15	572±25	700±45	689±6
20	569±19	741±29	703±19
30	575±25	752±35	734±25
45	576±15	801±31	765±15
60	578±13	836±29	785±18
90	607±14	855±52	837±7
120	616±33	877±49	856±23
180	611±22	864±51	846±29
240	615±26	845±57	831±25
300	582±18	829±52	817±17
360	570±24	810±47	816±19
480	559±35	780±51	825±21
1440	504±16	761±26	846±9

Table B-3 Swelling behavior of the PEC1 films at 37°C

Time (min)	Swelling degree (%)		
	pH 5.5	pH 7.4	pH 8.5
0	0±0	0±0	0±0
5	550±6	742±19	732±8
10	565±10	790±31	850±14
15	575±27	823±7	903±6
20	570±27	829±21	936±14
30	566±3	833±17	960±41
45	578±23	832±15	1033±53
60	570±2	826±18	948±102
90	572±17	831±33	919±99
120	573±15	818±47	726±71
180	580±24	819±46	538±45
240	568±14	817±56	403±24
300	572±11	777±59	348±41
360	581±8	763±51	286±19
480	578±21	762±56	232±21
1440	582±23	755±61	97±13

Table B-4 Swelling behavior of the PEC2 films at 37°C

Time (min)	Swelling degree (%)		
	pH 5.5	pH 7.4	pH 8.5
0	0±0	0±0	0±0
5	569±27	697±14	689±63
10	557±27	725±33	795±75
15	541±22	793±18	864±81
20	537±24	820±26	916±73
30	511±30	843±20	1035±88
45	483±26	880±23	1175±88
60	470±23	905±19	1314±91
90	466±32	934±13	1454±135
120	456±36	950±24	1362±165
180	449±34	975±25	1071±155
240	459±36	961±20	826±152
300	445±33	969±12	673±102
360	457±39	966±16	519±105
480	450±35	970±20	488±110
1440	452±15	962±30	317±75

Table B-5 Swelling behavior of the PEC3 films at 37°C

Time (min)	Swelling degree (%)		
	pH 5.5	**pH 7.4**	**pH 8.5**
0	0±0	0±0	0±0
5	634±9	691±19	672±a
10	634±14	747±23	769±102
15	594±15	798±47	811±90
20	570±9	834±36	882±121
30	527±13	843±33	816±159
45	497±17	898±44	1024±125
60	469±13	969±19	1087±139
90	462±16	1002±19	1169±134
120	447±29	1040±41	1203±114
180	450±14	1089±40	1206±56
240	454±14	1127±37	1127±52
300	447±19	1171±38	1063±82
360	449±13	1157±9	1000±78
480	459±21	1157±21	996±53
1440	459±23	1275±20	986±67

Table B-6 Swelling behavior of the PEC1-CD films at 37°C

Time (min)	Swelling degree (%)		
	pH 5.5	**pH 7.4**	**pH 8.5**
0	0±0	0±0	0±0
5	572±25	581±5	591±2
10	610±35	635±15	623±15
15	633±53	669±6	652±16
20	637±31	674±6	660±26
30	643±42	692±9	659±30
45	643±40	700±7	675±28
60	618±16	688±6	670±12
90	608±17	678±14	665±16
120	576±20	673±9	641±4
180	547±26	623±22	588±12
240	524±26	612±10	555±15
300	499±56	596±12	534±18
360	493±28	580±0	524±29
480	486±29	586±9	516±34
1440	427±35	554±13	476±24

Table B-7 Swelling behavior of the PEC2-CD films at 37°C

Time (min)	Swelling degree (%)		
	pH 5.5	**pH 7.4**	**pH 8.5**
0	0±0	0±0	0±0
5	425±12	457±28	510±16
10	447±2	498±15	532±22
15	462±10	520±13	568±27
20	470±19	542±17	570±26
30	462±5	559±43	579±25
45	464±16	585±24	597±30
60	466±2	596±32	601±39
90	470±10	621±36	613±33
120	471±19	639±26	629±34
180	478±9	646±22	641±43
240	475±28	651±25	655±31
300	483±21	645±19	646±26
360	471±25	655±31	655±32
480	479±11	662±24	653±34
1440	461±6	626±18	631±25

Table B-8 Swelling behavior of the PEC3-CD films at 37ºC

Time (min)	Swelling degree (%)		
	pH 5.5	**pH 7.4**	**pH 8.5**
0	0±0	0±0	0±0
5	327±7	389±11	411±29
10	340±15	428±11	446±22
15	346±28	455±9	452±23
20	337±22	459±10	462±34
30	328±24	466±9	476±16
45	324±20	489±5	484±4
60	304±14	492±12	487±10
90	296±12	519±10	508±14
120	298±9	532±0	513±24
180	293±14	549±7	543±26
240	292±8	564±0	560±22
300	294±7	564±9	573±19
360	291±10	565±3	589±30
480	299±3	559±8	605±22
1440	274±7	588±10	626±25

Table B-9 Swelling behavior of the PEC1(PR)-CD films at 37°C

Time (min)	Swelling degree (%)		
	pH 5.5	pH 7.4	pH 8.5
0	0±0	0±0	0±0
5	482±26	497±21	472±37
10	513±19	527±25	506±45
15	530±14	531±39	515±45
20	536±15	540±31	527±29
30	533±5	549±41	537±36
45	535±17	542±37	534±19
60	538±26	538±41	541±34
90	537±5	543±39	537±26
120	535±5	536±37	515±31
180	518±15	537±33	509±29
240	515±10	520±36	502±32
300	509±11	530±44	488±32
360	512±11	504±43	473±30
480	516±3	522±38	471±25
1440	516±2	527±36	471±37

Table B-10 Swelling behavior of the PEC2(PR)-CD films at 37°C

Time (min)	Swelling degree (%)		
	pH 5.5	pH 7.4	pH 8.5
0	0±0	0±0	0±0
5	341±19	382±22	322±20
10	361±10	405±15	349±21
15	364±12	423±9	369±28
20	373±8	443±12	383±15
30	366±18	449±22	401±20
45	365±11	466±25	419±15
60	372±23	480±16	445±23
90	379±1	516±12	465±23
120	384±8	524±14	471±17
180	384±7	525±20	491±20
240	384±10	504±17	497±17
300	383±16	524±13	502±19
360	392±5	513±10	490±21
480	403±7	522±8	499±20
1440	387±22	512±1	524±24

Table B-11 Swelling behavior of the PEC3(PR)-CD films at 37°C

Time (min)	Swelling degree (%)		
	pH 5.5	pH 7.4	pH 8.5
0	0±0	0±0	0±0
5	262±7	295±8	224±22
10	277±6	312±14	247±21
15	283±10	325±12	275±27
20	277±14	337±11	281±28
30	266±19	347±17	290±26
45	243±15	366±14	312±29
60	250±13	376±15	322±24
90	246±13	403±19	337±26
120	243±12	412±26	340±29
180	231±10	419±24	365±30
240	239±22	420±26	381±27
300	227±3	428±19	396±23
360	231±4	437±24	400±30
480	230±14	452±22	412±30
1440	230±10	479±21	461±27

Appendix C: Solid remains

Table C-1 Solid remains of the films for 24 h at 37°C

Samples	Solid remains (%)		
	pH 5.5	pH 7.4	pH 8.5
Non-crosslink	41±6	6±1	4±3
Blend-CD	50±2	43±4	37±2
PEC1	59±1	38±3	4±2
PEC2	64±3	50±3	6±3
PEC3	69±2	54±3	36±6
PEC1-CD	40±2	38±3	30±3
PEC2-CD	54±3	46±2	47±3
PEC3-CD	56±1	52±3	58±3
PEC1(PR)-CD	43±2	40±1	28±5
PEC2(PR)-CD	54±1	49±1	44±1
PEC3(PR)-CD	58±1	57±2	56±2

Appendix D: Color parameters

Table D-1 Color parameters of the CPS-PHP in various pH solutions

pH	*L*	*a*	*b*	*ΔE*
4	87.2±1.3	1.0±0.5	-7.5±1.1	2.0±0.8
5	87.6±0.8	0.8±0.5	-6.9±1.0	1.9±0.3
6	88.1±0.9	0.9±0.8	-7.5±1.1	2.6±0.6
7	88.0±0.5	0.9±0.3	-6.9±0.7	2.1±0.2
8	88.2±0.5	0.9±0.1	-7.1±0.5	2.2±0.6
9	87.3±0.7	2.1±0.3	-8.4±0.7	2.7±0.4
10	73.5±2.3	19±2.0	-25.8±2.6	29.9±3.5
11	73.1±2.2	22.3±2.9	-26.8±2.7	32.3±4.5
12	54.4±1.1	52.3±2.2	-44.5±2.1	71.3±2.9

Table D-2 Color parameters of the CPS-PR in various pH solutions

pH	*L*	*a*	*b*	*ΔE*
4	62.5±5.1	26.0±3.3	21.4±4.1	21.6±1.7
5	61.2±1.0	24.3±1.2	19.0±0.7	17.9±0.7
6	58.0±0.8	30.8±1.0	6.4±4.0	11.5±1.4
7	61.3±0.2	28.2±0.8	-3.8±1.2	13.5±0.9
8	46.8±1.5	46.4±1.3	-5.9±2.6	27.1±0.6
9	47.3±1.4	47.6±2.5	-17.8±1.0	34.0±2.8
10	47.1±4.9	55.7±6.0	-37.8±2.8	54.2±4.7
11	45.3±0.4	59.1±0.3	-39.3±0.8	57.5±0.4
12	51.4±1.4	50.1±1.9	-37.2±1.2	49.8±2.1

Table D-3 Color parameters of the CPS-RA in various pH solutions

pH	*L*	*a*	*b*	*ΔE*
4	83.4±0.5	7.0±0.9	-0.4±1.3	42.5±1.0
5	82.4±0.4	8.6±1.1	-0.9±0.6	40.5±0.8
6	70.2±1.7	28.6±3.1	-6.9±2.8	17.0±3.7
7	62.7±3.1	41.9±4.9	-10.7±2.9	7.8±1.6
8	61.6±2.3	46.6±2.5	-14.7±2.0	9.6±0.9
9	63.4±2.1	48.3±5.9	-17.0±2.3	12.6±4.4
10	58.8±1.8	57.0±3.8	-13.6±1.9	18.4±3.6
11	55.2±3.3	63.0±1.3	-14.3±2.7	24.5±1.9
12	58.0±2.5	60.7±1.5	-10.1±6.1	22.3±1.9

Table D-4 Color difference (*ΔE*) of the CPS-PHP films immersed in various solutions as a function of storage time

Time (Day)	DI	pH 7.4	pH 4	pH 10
1	4.2±0.5	4.1±0.3	4.3±0	21.5±0
7	3.0±0.4	3.6±0.4	2.4±0.2	13.9±0.1
14	4.6±0.9	4.9±0.6	4.5±0.8	10.2±1.3
21	5.9±1.4	5.5±0.2	4.2±0.3	10.6±1.1
28	5.2±1.1	4.5±0.9	4.2±0.2	7.5±0.8
35	3.7±0.2	4.0±0.1	4.3±0.1	8.7±1.1
42	3.7±0.3	3.6±0.3	4.2±0.9	7.3±0.7
49	4.1±0.1	4.3±0.6	3.6±0.2	6.3±1.0
56	5.6±0.9	6.0±0.5	4.6±0.2	4.9±0.5
63	3.0±0.2	3.9±0.2	3.6±0.2	3.9±0.2

Table D-5 Color difference (*ΔE*) of the CPS-PR films immersed in various solutions as a function of storage time

Time (Day)	DI	pH 7.4	pH 4	pH 10
1	14.9±0.6	13.5±0.2	14.7±0.5	36±0.6
7	16.0±0.6	13.5±0.4	15.8±0.4	38.1±0.4
14	16.0±0.4	15.0±0.1	15.6±0.8	39.4±0.3
21	17.6±0.5	13.8±0.3	14.4±1.0	35.8±0.4
28	18.1±0.2	15.6±0.3	17.2±0.7	39.4±0
35	17.8±0	16.9±0.1	16.6±0.2	38.3±0.1
42	19.1±0.3	16.3±0.7	10.8±0.4	36.7±0.2
49	19.1±0.1	20.0±0	10.9±0.7	39.4±0.1
56	19.2±0.5	16.9±0.2	12.1±0.1	39.8±0.6
63	20.0±0.4	18.3±0.7	10.3±0.4	39.0±0.2

Table D-6 Color difference (*ΔE*) of the CPS-RA films immersed in various solutions as a function of storage time

Time (Day)	DI	pH 7.4	pH 4	pH 10
1	13.7±0.3	16.7±0.2	48.4±0.7	12.6±0
7	12.3±0.5	17.2±0.2	46.7±0.9	12.7±0.2
14	12.8±0.4	15.2±0.7	48.7±0.5	15.0±0.2
21	10.4±0.3	15.1±0.3	48.9±0.3	14.4±0
28	11.8±0.1	12.5±0.2	48.7±0.4	14.4±0
35	12.0±0	12.3±1.0	47.4±1.0	13.0±0.3
42	14.5±0.3	13.6±2.4	47.9±0.4	17.0±0.6
49	16.1±0.3	13.9±1.7	47.6±1	13.1±0.1
56	15.6±0.4	12.8±1.9	50.0±0.9	16.6±0.1
63	16.1±0.3	12.0±1.8	47.9±1.0	13.8±0.3

Table D-7 Color parameters of the PEC1(PR)-CD in various pH solutions

pH	*L*	*a*	*b*
4	72.7±0.1	26.1±0.1	47.7±0.1
5	70.0±0.1	28.5±0.2	51.7±0.1
6	65.8±0.2	26.2±0.2	39.7±0.3
7	61.1±0.1	30.9±0.3	28.2±0.2
8	54.4±0.1	41.9±0.4	15.2±0.3
9	54.2±0.2	48.0±0.4	-5.8±0.1
10	49.9±0	56.2±0.1	-18.4±0.1

Table D-8 Color parameters of the PEC2(PR)-CD in various pH solutions

pH	*L*	*a*	*b*
4	66.3±0.2	34.3±0.3	45.3±0.3
5	64.6±0	30.2±0.1	39.7±0.1
6	61.8±0.2	28.1±0.1	23.8±0.2
7	56.8±0.1	35.6±0.2	24.7±0.2
8	57.4±0.1	37.4±0.4	13.8±1.6
9	53.2±0.1	48.5±0.3	-4.0±0.1
10	50.3±1.3	52.6±2.4	-15.8±0.8

Table D-9 Color parameters of the PEC3(PR)-CD in various pH solutions

pH	*L*	*a*	*b*
4	69.0±0.3	29.2±0.5	37.9±0.3
5	71.0±0.1	20.9±0.2	25.1±0.2
6	67.6±0.2	22.7±0.3	22.6±0.2
7	63.5±0.3	28.3±0.4	19.9±0.4
8	61.6±0.1	33.5±0.3	9.3±0.3
9	57.9±0.3	44.3±0.6	-8.6±0.3
10	55.5±0.2	49.5±0.4	-21.0±0.2

Appendix E: Calibration curves

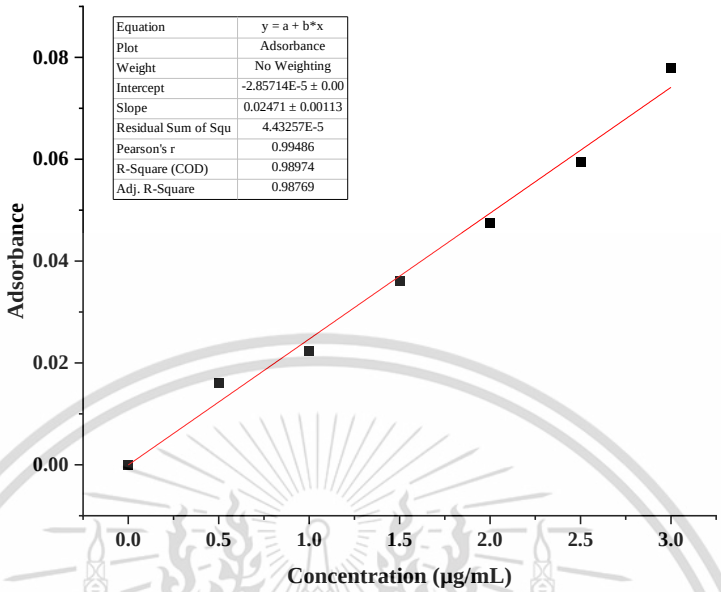

Figure E-1 Calibration curve of DCF in pH 5.5

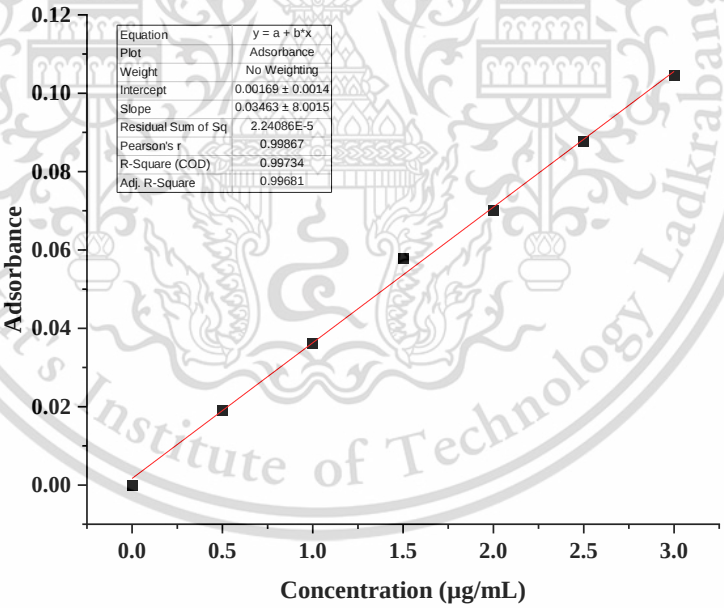

Figure E-2 Calibration curve of DCF in pH 7.4

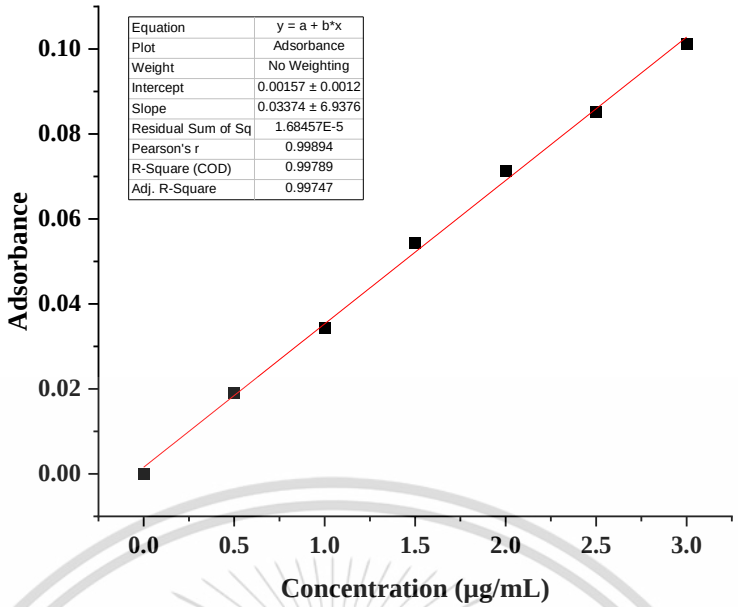

Figure E-3 Calibration curve of DCF in pH 8.5

Appendix F: Drug release behavior

Table F-1 Drug release behavior of the PEC1(PR)-CD/DCF in different pH solutions at 37°C

Time (min)	Drug release (%)		
	pH 5.5	pH 7.4	pH 8.5
0	0±0	0±0	0±0
5	9.6±2.9	16.3±13.9	6.7±2.1
10	17.0±0.7	20.9±2.9	20.9±13.1
15	21.1±7.8	25.8±2.1	28.5±8.2
30	30.0±4.6	42.8±1.7	47.1±15.9
45	38.4±6.6	50.9±8.4	49.3±7.4
60	43.8±4.5	56.0±2.2	63.8±13.4
90	47.1±4.6	62.7±3.6	67.0±9.8
120	55.7±5.4	68.2±6.0	76.8±17.1
180	60.7±4.6	79.1±3.6	79.2±9.4
240	63.3±3.1	82.4±8.7	86.2±12.8
300	67.0±2.2	90.3±6.9	85.5±7.5
360	69.6±4.7	89.3±4.4	84.5±4.2
480	71.2±4.7	87.8±4.0	86.2±6.0
1440	94.1±8.8	95.0±0.8	94.3±2.8

Table F-2 Drug release behavior of the PEC2(PR)-CD/DCF in different pH solutions at 37°C

Time (min)	Drug release (%)		
	pH 5.5	pH 7.4	pH 8.5
0	0±0	0±0	0±0
5	15.6±12.8	18.5±10.3	12.5±2.7
10	28.4±5.6	25.7±6.6	23.4±1.5
15	36.8±7.2	32±5.8	31.4±13.0
30	42.7±9.5	54±5.1	46.2±3.8
45	56.0±0.8	57.2±9	54.1±9.4
60	66.1±3.2	61.4±11.1	59.1±7.9
90	71.5±2.5	66.7±10.2	65.5±3.3
120	71.9±4.2	72.9±14.5	71.3±7.4
180	80.9±5.5	77.0±3.6	79.1±10.4
240	81.1±2.5	83.5±2.4	82.7±11.2
300	83.3±1.4	87.5±1.9	86.3±9.8
360	83.9±0.7	86.8±7.4	85.6±13.4
480	84.7±6.5	88.9±6.5	87.5±14.4
1440	97.8±2.1	97.7±11.7	99.1±8.1

Table F-3 Drug release behavior of the PEC3(PR)-CD/DCF in different pH solutions at 37°C

Time (min)	Drug release (%)		
	pH 5.5	pH 7.4	pH 8.5
0	0±0	0±0	0±0
5	21.6±10.9	8.8±6.2	5.4±4.4
10	31.0±5.9	18.7±7.8	13.1±4.8
15	41.1±12.4	27.0±8.0	20.9±2.9
30	45.5±3.1	38.6±11.5	32.4±4.2
45	53.3±5.3	53.9±7.9	43.7±12.6
60	63.9±12.4	60.0±11.0	48.9±11.5
90	74.1±2.9	64.5±7.0	59.1±9.5
120	76.3±6.0	71.1±10.8	62.5±7.6
180	86.0±6.9	78.7±9.4	69.6±7.2
240	89.2±6.8	80.8±6	77.3±4.6
300	93.4±5.9	87.0±8.1	80.1±8.1
360	92.7±9.9	86.1±5	80.8±3.6
480	94.8±7.8	86.3±2.9	85.1±4.2
1440	98.3±4.4	90.7±6.0	95.1±2.3

Appendix G: Drug release kinetics

Table G-1 Results of fitting kinetic parameters for DCF release from the films

Film samples	pH	Kinetic model at 80% release	Slope	Intercept	R^2	Kinetic model at 20% release	Slope	Intercept	R^2
PEC1(PR)-CD/DCF	5.5	Zero order	18.7840	14.9780	0.8273	Zero order	1.4578	59.3150	0.9897
		First order	-0.1314	1.9335	0.9098	First order	-0.0398	1.7339	0.9943
		Higuchi model	38.2510	8.7083	0.9843	Higuchi model	10.3780	43.1040	0.9939
		Korsmeyer-Peppas model	0.5046	1.6021	0.9741	Korsmeyer-Peppas model	0.2181	1.6688	0.9869
	7.4	Zero order	23.6780	20.3710	0.8172	Zero order	0.4286	84.9140	0.6110
		First order	-0.2131	1.9148	0.9488	First order	-0.0212	1.2101	0.7893
		Higuchi model	44.7630	6.4801	0.9647	Higuchi model	3.1158	79.961	0.6399
		Korsmeyer-Peppas model	0.5061	1.7426	0.9832	Korsmeyer-Peppas model	0.0593	1.8969	0.6539
	8.5	Zero order	25.6790	20.1790	0.7688	Zero order	0.4605	82.9860	0.9384
		First order	-0.2369	1.9103	0.8994	First order	-0.0212	1.2778	0.9558
		Higuchi model	54.3320	10.1230	0.9508	Higuchi model	3.2022	78.084	0.8991
		Korsmeyer-Peppas model	0.6318	1.7333	0.8852	Korsmeyer-Peppas model	0.0571	1.8910	0.8275
PEC2(PR)-CD/DCF	5.5	Zero order	23.6910	25.069	0.7454	Zero order	0.7976	78.6560	0.9924
		First order	-0.2281	1.8809	0.8941	First order	-0.0473	1.4914	0.9887
		Higuchi model	44.3420	12.0930	0.9212	Higuchi model	5.6536	69.8560	0.9881
		Korsmeyer-Peppas model	0.4372	1.7638	0.9424	Korsmeyer-Peppas model	0.1037	1.8439	0.9681
	7.4	Zero order	22.2390	25.972	0.7075	Zero order	0.6217	83.0510	0.9404
		First order	-0.2027	1.8688	0.8548	First order	-0.0439	1.3986	0.9730
		Higuchi model	41.3910	14.2730	0.8957	Higuchi model	4.4630	76.0300	0.9604
		Korsmeyer-Peppas model	0.5137	1.8239	0.9757	Korsmeyer-Peppas model	0.1348	1.8247	0.9037

Table G-1 Results of fitting kinetic parameters for DCF release from the films (continued)

Film samples	pH	Kinetic model at 80% release	Slope	Intercept	R^2	Kinetic model at 20% release	Slope	Intercept	R^2
PEC2(PR)-CD/DCF	8.5	Zero order	23.7590	22.281	0.7724	Zero order	0.7511	81.1710	0.9730
		First order	-0.2172	1.8992	0.9207	First order	-0.0639	1.5211	0.9886
		Higuchi model	45.1920	8.2962	0.9368	Higuchi model	5.3280	72.8010	0.9792
		Korsmeyer-Peppas model	0.5030	1.7073	0.9443	Korsmeyer-Peppas model	0.1121	1.8144	0.8686
PEC3(PR)-CD/DCF	5.5	Zero order	24.3900	26.7330	0.7826	Zero order	0.3466	90.4270	0.7482
		First order	-0.2649	1.8849	0.9524	First order	-0.0361	1.0069	0.9438
		Higuchi model	44.3090	14.6900	0.9641	Higuchi model	2.5524	86.3280	0.8040
		Korsmeyer-Peppas model	0.3767	1.7828	0.9772	Korsmeyer-Peppas model	0.0467	1.9307	0.8510
	7.4	Zero order	25.0590	18.9480	0.7935	Zero order	0.3296	83.0990	0.6011
		First order	-0.2229	1.9189	0.9235	First order	-0.0114	1.2358	0.7216
		Higuchi model	52.5670	9.3742	0.9633	Higuchi model	2.4294	79.1940	0.6469
		Korsmeyer-Peppas model	0.5909	1.7158	0.9384	Korsmeyer-Peppas model	0.0487	1.8927	0.6831
	8.5	Zero order	23.1770	14.119	0.8265	Zero order	0.8161	76.0050	0.9457
		First order	-0.1774	1.9412	0.9215	First order	-0.0325	1.4664	0.9946
		Higuchi model	45.9950	-2.0971	0.9529	Higuchi model	5.8897	66.6990	0.9761
		Korsmeyer-Peppas model	0.6899	1.6388	0.9354	Korsmeyer-Peppas model	0.1144	1.8216	0.9912

Appendix H: Mechanical properties

Table H-1 Tensile strength, Elongation at break, and Young's modulus of the films

Samples	Tensile strength (at break) (MPa)	Elongation at break (%)	Young's modulus (MPa)
PEC1	6.5±3.6	18.9±8.1	191.6±67.3
PEC2	11.3±1.3	27.9±4.1	170.1±64.0
PEC3	7.0±1.5	28.9±5.6	115.1±45.8
PEC1(PR)-CD	13.9±4.4	13.2±4.1	557.2±178.0
PEC2(PR)-CD	16.6±4.9	14.7±3.2	744.6±162.0
PEC3(PR)-CD	11.2±2.8	8.1±2.0	792.5±102.1

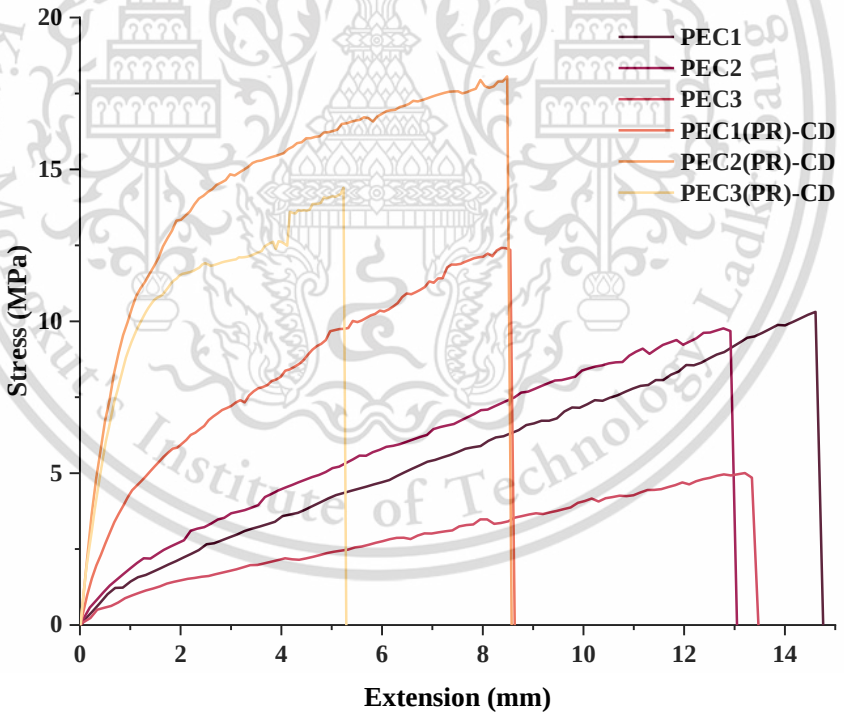

Figure H-1 Stress-strain curves of the films

Author biography

Name	Miss Jongjit Chalitangkoon
Date of Birth	19 March 1995
Address	874/83 Charansanitwong 57, Bangkok, Thailand 10700
Education	(2016) Bachelor of Science in industrial chemistry GPA: 3.72 (King Mongkut's Institute of Technology Ladkrabang, School of Science)
Scholarship	Scholarship from the Royal Golden Jubilee Ph.D Program, Thailand research fund Canada-ASEAN Scholarships and Educational Exchanges for Development (SEED)

Academic Publications

1. Sakboriboon, Y., Chalitangkoon, J., & Monvisade, P. (2023). Improving the fluorescence of carbon dots through boron and silver doping: A single-step microwave synthesis approach. Biointerface Research in Applied Chemistry. (Accepted)
2. Chalitangkoon, J., Ronte, A., & Monvisade, P. (2023). Carboxyethylation of chitosan-based polymeric dyes for potential pH-sensing applications. Journal of the Taiwan Institute of Chemical Engineers, 149, 105001.
3. Chittratan, P., Chalitangkoon, J., Wongsariya, K., Mathaweesansurn, A., Detsri, E., & Monvisade, P. (2022). New Chitosan-Grafted Thymol Coated on Gold Nanoparticles for Control of Cariogenic Bacteria in the Oral Cavity. *ACS Omega*, 7, 26582−26590.
4. Jarupatnadech, T., Chalitangkoon, J., & Monvisade, P. (2022). Colorimetric oxygen indicator films based on β-cyclodextrin grafted chitosan/montmorillonite with redox system for intelligent food packaging. *Packaging Technology and Science*, *35*, 515-525.
5. Weerawan, N., Chalitangkoon, J., & Monvisade, P. (2022). Self-healing hydrogels based on sodium carboxymethyl cellulose/

poly(Vinyl alcohol) reinforced with montmorillonite. *Biointerface Research in Applied Chemistry*, *12(4)*, 4770–4779.

6. Savetsakulanont, J., Chalitangkoon, J., & Monvisade, P. (2021). Stimuli-Responsive, Self-Healing, and Injectable Hydrogels with Dual-Crosslinked Design from Phenolphthalein-Grafted N-Carboxyethyl Chitosan. *Macromolecular Materials and Engineering*, 2100287.

7. Huaytragul, J., Chalitangkoon, J., Monvisade, P., & Chotsaeng, N. (2021). Enhancing chitosan solubility in alcohol: water mixtures for film-forming systems releasing with turmeric extracts. *Journal of the Taiwan Institute of Chemical Engineers*, *123*, 293-301.

8. Chalitangkoon, J., & Monvisade, P. (2021). Synthesis of chitosan-based polymeric dyes as colorimetric pH-sensing materials: Potential for food and biomedical applications. *Carbohydrate Polymers, 260,* 117836.

9. Chalitangkoon, J., Wongkittisin, M., & Monvisade, P. (2020). Silver loaded hydroxyethylacryl chitosan/sodium alginate hydrogel films for controlled drug release wound dressings. *International journal of biological macromolecules, 159*, 194-203.

10. Chalitangkoon, J., & Monvisade, P. (2019). Dual pH/thermal-dependent coloring polymeric dye through Mannich reaction of chitosan: Synthesis and characterization. *Carbohydrate polymers, 223*, 115049.

Conferences

1. Chalitangkoon, J., Moreira, R., Monvisade, P., & Foster, J. 2022. “Synthesis and Characterization of pH-sensitive Fluorescent Cellulose Nanocrystals for Ratiometric Fluorescence Probe.” in **The International Polymer Conference of Thailand (PCT-13)**. (Poster presentation)

2.Ronte, A., Chalitangkoon, J., Foster, J., & Monvisade, P. 2022. “Facile Fabrication of pH-responsive Screen-printed Label from Phenol Red-grafted Chitosan for Intelligent Food Packaging

Applications" in **The International Polymer Conference of Thailand (PCT-13)**. (Poster presentation)

3. Chalitangkoon, J., & Monvisade, P. 2022. "Synthesis and characterization of chitosan-based water-soluble polymeric dyes." in **Pure And Applied Chemistry International Conference 2022 (PACCON 2022)**. (Poster presentation)

4. Ronte, A., Chalitangkoon, J., Phoonperm, K., Meakrangsimun, A., & Monvisade, P. 2022. "pH-responsive waterborne inks based on poly(vinyl acetate), fatty acid-modified poly(vinyl alcohol) and dye-grafted chitosan for food freshness detection." in **Pure And Applied Chemistry International Conference 2022 (PACCON 2022)**. (Poster presentation)

5. Sakboriboon, Y., Chalitangkoon, J., & Monvisade, P. 2022. "One step microwave-assisted green synthesis of highly fluorescent carbon dots." in **Pure And Applied Chemistry International Conference 2022 (PACCON 2022)**. (Poster presentation)

6. Chittratan, P., Chalitangkoon, J., Wongsariya, K., Detsri, E., & Monvisade, P. 2022. "Design and characterization of chitosan-grafted-thymol on gold nanoparticles for antimicrobial activities." in **Pure And Applied Chemistry International Conference 2022 (PACCON 2022)**. (Oral presentation)

7. Chalitangkoon, J., & Monvisade, P. 2021. "Dye-grafted chitosan derivatives as pH-indicative materials for biomedical applications." in **The 2021 National RGJ and RRI Conferences**. (Online presentation)

8. Buakaew, J., Chalitangkoon, J., & Monvisade, P. 2021. "pH-responsive Films from Chitosan-based/poly(vinyl alcohol)/Oxidized Alginate for Intelligent Packaging." in **The International Polymer Conference of Thailand (PCT-11)**. (Online presentation)

9. Jarupatnadech, T., Chalitangkoon, J., & Monvisade, P. 2021. "The Effect of Glucose on Chitosan/methylene-blue Oxygen Indicator Films." in **The International Polymer Conference of Thailand (PCT-11)**. (Online presentation)

10. Weerawan, N., Monvisade, P., & Chalitangkoon, J. 2021. “Effect of Montmorillonite on Self-healing Properties of Sodium Carboxymethyl Cellulose/poly(vinyl alcohol) Hydrogel.” in **The International Polymer Conference of Thailand (PCT-11)**. (Online presentation)